DE GRUYTER

REFERENCE

Tharwat F. Tadros

HANDBOOK OF COLLOID AND INTERFACE SCIENCE

VOLUME 1: BASIC PRINCIPLES OF INTERFACE SCIENCE AND COLLOID STABILITY

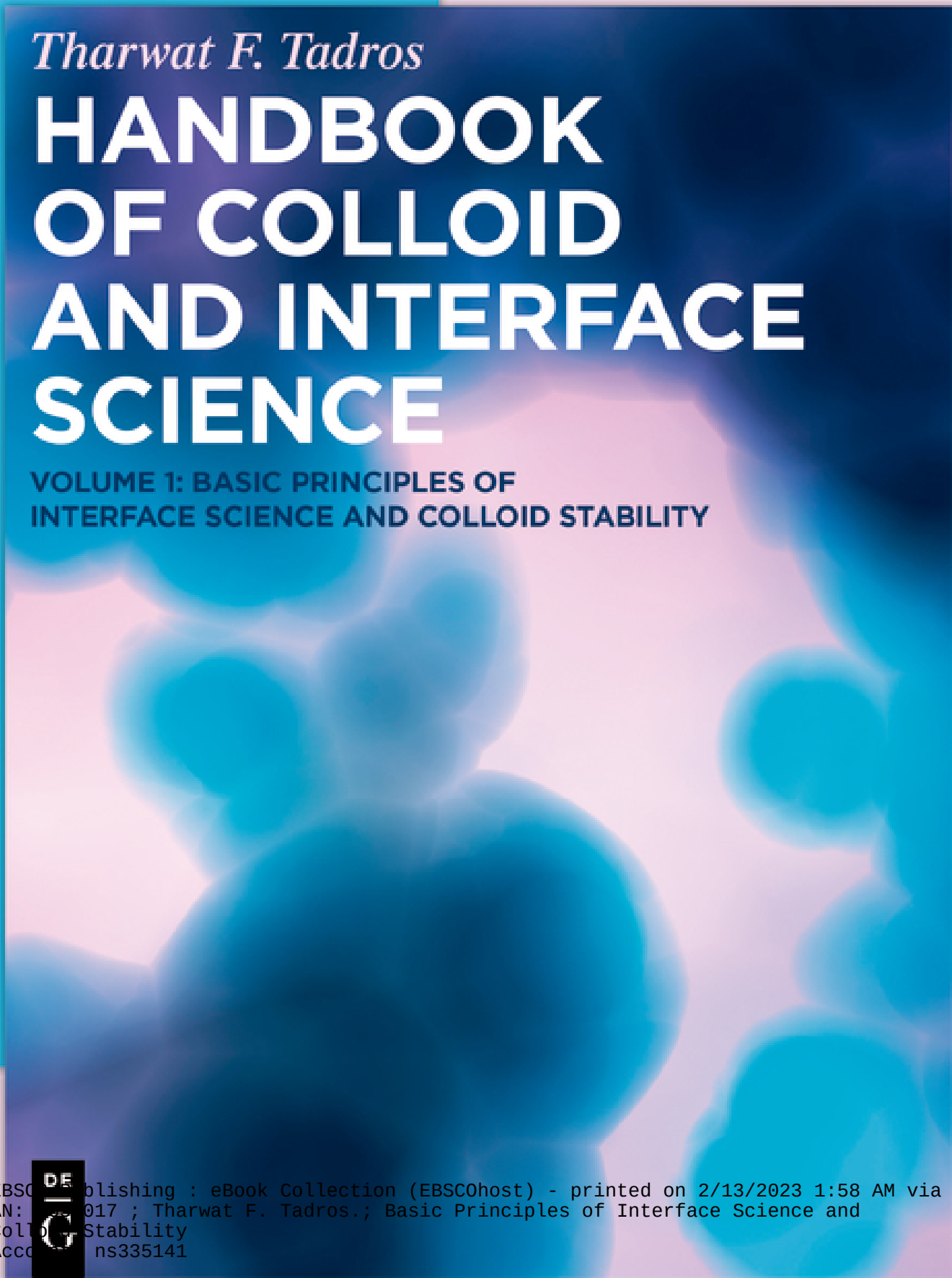

Tharwat F. Tadros

Handbook of Colloid and Interface Science

De Gruyter Reference

Also of Interest

Handbook of Colloid and Interface Science.
Volume 2: Basic Principles of Dispersions
Tadros, 2017
ISBN 978-3-11-053991-2, e-ISBN 978-3-11-054195-3

Handbook of Colloid and Interface Science.
Volume 3: Industrial Applications:
Pharmaceuticals, Cosmetics and Personal Care
Tadros, 2018
ISBN 978-3-11-055409-0, e-ISBN 978-3-11-055525-7

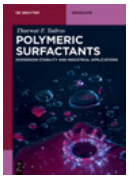

Polymeric Surfactants.
Dispersion Stability and Industrial Applications
Tadros, 2017
ISBN 978-3-11-048722-0, e-ISBN 978-3-11-048728-2

Suspension Concentrates.
Preparation, Stability and Industrial Applications
Tadros, 2017
ISBN 978-3-11-048678-0, e-ISBN 978-3-11-048687-2

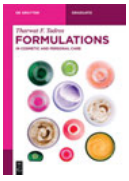

Formulations.
In Cosmetic and Personal Care
Tadros, 2016
ISBN 978-3-11-045236-5, e-ISBN 978-3-11-045238-9

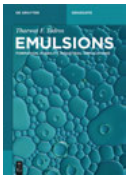

Emulsions.
Formation, Stability, Industrial Applications
Tadros, 2016
ISBN 978-3-11-045217-4, e-ISBN 978-3-11-045224-2

Tharwat F. Tadros

Handbook of Colloid and Interface Science

Volume 1:
Basic Principles of Interface Science and Colloid Stability

DE GRUYTER

Author
Prof. Tharwat F. Tadros
89 Nash Grove Lane
Workingham RG40 4HE
Berkshire, UK
tharwattadros3@gmail.com

ISBN 978-3-11-053990-5
e-ISBN (PDF) 978-3-11-054089-5
e-ISBN (EPUB) 978-3-11-053993-6
Set-ISBN 978-3-11-054090-1

Library of Congress Cataloging-in-Publication Data
A CIP catalog record for this book has been applied for at the Library of Congress.

Bibliographic information published by the Deutsche Nationalbibliothek
The Deutsche Nationalbibliothek lists this publication in the Deutsche Nationalbibliografie; detailed bibliographic data are available on the Internet at http://dnb.dnb.de.

Cover image: satori13/iStock/Getty Images Plus
Typesetting: PTP-Berlin, Protago-TEX-Production GmbH, Berlin
Printing and binding: CPI Books GmbH, Leck
♾ Printed on acid-free paper
Printed in Germany

www.degruyter.com

Preface

The word "colloid" was first coined by Thomas Graham in 1861 who borrowed the word from the Greek word "kolla" meaning glue-like. Colloidal particles possess characteristic properties between those of true solution (with molecules that can diffuse through membranes) and suspensions that can sometimes be easily observed by the naked eye. The best definition of colloids is perhaps "systems in which a significant proportion of the molecules lie in or are associated with interfacial regions". Simple considerations suggest that the lowest limit for colloids (whereby one can distinguish between molecules in the interfacial region and the bulk) is 1 nm. The upper limit for colloidal dispersions lies in the region of 1000 nm (1 μm), whereby a significant proportion of the total molecules lie at the interface. An important class of colloids are produced by self-assembly of surfactants that form micelles with dimensions in the colloid range.

In all disperse systems such as suspensions, emulsions, foams, etc., the structure of the interfacial region determines its colloidal properties. For convenience, I will list the topics of colloid and interface science under two main headings: disperse systems and interfacial phenomena. This subdivision does not imply any separation for the following reasons: All disperse systems involve an interface and many interfacial phenomena are precursors for formation of disperse systems, e.g. nucleation and growth, emulsification, etc. The main objectives of Volume 1 of the present handbook is to cover the following topics: The basic principles that are involved in interfacial phenomena as well as the formation of colloidal dispersions and their stabilization, surfactants and polymer adsorption at various interfaces The colloid stability/instability of any disperse system is determined by the property of the interfacial region. In actual fact, colloid and interface science are one individual subject.

The field of colloid and interface science has no boundary since chemists, physicists, engineers, biologists, mathematicians can all be engaged in the field. For successful applications in industry, multidisciplinary teams are required. Understanding the basic principles of colloid and interface science will enable industry to develop many complex systems in a shorter period of time. Most colloidal systems used in industry are multiphase and complex formulations. They may contain more than one disperse phase, e.g. suspension/emulsion systems (suspoemulsions).

Chapter 2 deals with origin of charge in colloidal systems and structure of the electrical double layer. A great variety of processes occur to produce a surface charge, e.g. surface ions that have such a high affinity to the surface of the particles that they may be taken as part of the surface, isomorphic substitution which occurs in clay minerals, specific adsorption of ions that have non-electrostatic affinity to the surface, e.g. bivalent cations on oxides, cationic and anionic surfactants on most surfaces can also produce a surface charge. Chapter 2 also deals with the structure of the electrical double layer, namely the diffuse double layer due to Gouy and Chapman and its modification by Stern and Graham who considered the role of specifically adsorbed

https://doi.org/10.1515/9783110540895-001

ions near the surface. The most common methods for investigating double layers in disperse systems are described to obtain the surface charge as a function of surface potential at different electrolyte concentrations and types.

Chapter 3 deals with electrokinetic phenomena and the concept of zeta potential. Electrokinetic effects arise when one of the two phases is caused to move tangentially past the second phase. The tangential motion can be caused by an electric field, forcing a liquid into a capillary, forcing a liquid into a plug of particles or by a gravitational field on the particles. This leads to four different types of electrokinetic phenomena, namely electrophoresis, electro-osmosis, streaming potential and sedimentation potential. In this chapter, only electrophoresis will be discussed since this is the most commonly used method for dispersions, allowing one to measure the particle mobility which can be converted to the zeta potential using theoretical treatments. The various theoretical treatments that can be applied to convert particle mobility to zeta potential are described. This is followed by a section on the methods that can be applied for measurement of particle mobility and zeta potential for various colloidal systems.

Chapter 4 describes the double layer repulsion between colloidal particles. The origin of electrostatic interactions is due to the double layer overlap that occurs when the surface-to-surface distance becomes smaller than twice the double layer thickness. One of the most important features of double layers is their strong dependence on the concentration of indifferent electrolytes. An increase in electrolyte concentration causes a reduction in the diffuse double layer potential and compression of the double layer, i.e. reduction of the Debye length. Both of these effects affect the colloid stability of lyophobic colloids. The theoretical analysis of interaction between particles containing double layers is described for the case of constant potential and constant charge. The effect of increasing electrolyte concentration, valency of counterions and Stern potential is described at a fundamental level.

Chapter 5 deals with van der Waals attraction between colloidal particles. The interaction between two particles can in general be considered in terms of the potential energy or the work required to separate them from a centre-to-centre distance r to some large distance apart. There are generally two approaches for describing the van der Waals attraction between macroscopic bodies such as colloidal particles, emulsion droplets, etc. The first approach considers the London–van der Waals attraction to be the sum of the forces acting between isolated molecules. This approach, referred to as the microscopic approach, was suggested by de Boer and Hamaker. The second approach, developed by Lifshitz et al., is based on the correlation between electric fluctuations of two macroscopic bodies. It is referred to as the macroscopic approach. Both approaches are described in this chapter.

Chapter 6 gives a thorough description of the theory of colloid stability due to Deryaguin, Landau, Verwey, Overbeek (DLVO theory). The DLVO theory is based on the combination of electrostatic repulsion and van der Waals attraction at various separation distances between the particles or droplets. This results in an energy–distance curve containing a shallow attractive minimum (weak attraction) at long separation

distances between the particles, a deep attractive minimum at short separation distances and an energy maximum (energy barrier) at intermediate distances. The dependency of the energy maximum on electrolyte concentration, electrolyte valency and zeta potential is described to distinguish between stable and unstable (flocculated) dispersions.

Chapter 7 describes the flocculation of colloidal dispersions. The mechanism of aggregation is described in terms of the DLVO theory which predicts the process of aggregation on addition of electrolytes with different valencies. The kinetics of flocculation is described for two cases: Fast flocculation in the absence of an energy barrier and slow flocculation in the presence of an energy barrier. The theory of fast flocculation kinetics, due to Smoluchowski, is described and this is followed by the theory of slow flocculation, due to Fuchs and definition of the stability ratio W (ratio of fast flocculation rate to slow flocculation rate). The dependency of W on electrolyte concentration C for uni–uni (1 : 1) and bi–bi (2 : 2) electrolyte is described. log W–log C curves are established and this allows one to define the critical flocculation (coagulation) concentration and its dependency on electrolyte valency. A section is given over to the process of (reversible) flocculation as well as orthokinetic (in the presence of shear) flocculation.

Chapter 8 describes association colloids mostly produced by surfactant molecules. It starts with a section on the general classification of surfactant molecules: anionic, cationic, zwitterionic and nonionic. A section is devoted to polymeric surfactants and their structure. The physical chemistry of surfactant solutions is described at a fundamental level, illustrating the abrupt changes at a critical concentration (critical micelle concentration, cmc) due to the aggregation of the molecules into micelles. The dependency of the cmc on the surfactant structure is described. This is followed by a section on the solubility-temperature relationship for ionic and nonionic surfactants. The kinetics and thermodynamic aspects of micelle formation are described to illustrate the spontaneous formation of micelles. The driving force of micelle formation is described in terms of the balance between enthalpy and entropy of the process.

Chapter 9 deals with the process of surfactant adsorption at the liquid/liquid interface. It starts with a thermodynamic definition of interfacial tension by application of the second law of thermodynamics. Two approaches are described for the process of surfactant adsorption at liquid interfaces. The first approach treats the process as one of equilibrium and by application of the second law of thermodynamics one can relate the variation of interfacial tension with surfactant concentration to the amount of surfactant adsorption at the liquid/liquid interface. This allows one to obtain the area per surfactant molecule at the interface and its dependence on the orientation of the molecule. The second approach for surfactant adsorption considers the molecules to produce a layer at the interface which produces a surface pressure. This approach allows one to obtain the orientation of the surfactant molecules by following the change in surface pressure with surfactant concentration.

Chapter 10 describes the adsorption of surfactants at the solid/liquid interface. It emphasizes the reversibility of adsorption and the possibility of application of thermodynamics. Four systems are considered: ionic surfactants on hydrophobic and hydrophilic surfaces, nonionic surfactants on hydrophobic and hydrophilic surfactants. It shows that the adsorption of both ionic and nonionic surfactants on hydrophobic surfaces is governed by hydrophobic bonding between the alkyl chain and the nonpolar surface; charge interactions play a minor role. The adsorption of ionic and nonionic surfactants on hydrophilic surfaces is governed by the polar interaction between the surfactant head group and the charged or polar surface. The adsorption of ionic surfactants on hydrophobic surfaces can be described by the Stern–Langmuir equation at low surface coverage. At high surface coverage, lateral interaction between the surfactant molecules on the solid surface must be taken into account. Using the Stern–Langmuir equation, one can define the free energy of adsorption which contains several contributions, e.g. surfactant/surfactant interaction, surfactant/surface interaction and head group/surface interaction. The experimental technique for determining the adsorption isotherm is described and some examples are given to show the effect of surfactant structure and nature of the surface. The adsorption of ionic surfactants on charged surfaces (with opposite charge) shows a very rapid increase above a critical concentration which is attributed to the formation of hemimicelles. Several types of adsorption isotherms are described for the adsorption of nonionic surfactants on nonpolar and polar surfaces. These isotherms are analysed in terms of the structure of the surfactant molecules on the surface.

Chapter 11 describes the solution properties of polymers and polymeric surfactants. It starts with the Flory–Huggins theory that describes the free energy of random coils in terms of the entropy and enthalpy contributions to the free energy. Equations are given for the end-to-end distance and radius of gyration of the random coil. Modification of the Flory–Huggins theory is described for block and graft copolymers. Particular attention is given to the association of block and graft copolymers that gives association structures similar to surfactant micelles. The techniques that can be applied to investigate the solution properties of polymers and polymeric surfactants are described.

Chapter 12 describes the process of adsorption of polymers at the solid/liquid interface. It emphasizes the complexity of the adsorption process that must take into consideration the conformation of the polymer chains at the solid/liquid interface. Several classes of polymers are considered, namely random coils, “blocky copolymers” (that contain short blocks with high affinity to the surface), block and graft copolymers. The importance of a minimum adsorption energy per segment attached, that is required to counteract the entropy loss due to adsorption, is clearly illustrated. The theories of polymer adsorption are described with particular reference to the step-weighted random walk approach and the scaling concepts. The experimental techniques used to obtain the various adsorption parameters are described.

Chapter 13 deals with the process of steric stabilization. It starts with describing the interaction between particles or droplets containing polymer layers. This interaction could result in overlap and/or compression of the adsorbed layer, both of which result in an increase in the segment density in the overlap. The repulsion is described in terms of the unfavourable mixing of the polymer chain and the loss of entropy of the chains on considerable overlap. Unfavourable mixing results in a positive free energy of repulsion providing the chains are in good solvent conditions. Equations are derived to obtain the mixing free energy illustrating the importance of the Flory–Huggins interaction parameter. Equations are also given for the entropy loss (that is described as elastic interaction). Combining the mixing elastic terms gives the total steric interaction, which when combined with the van der Waals attraction gives energy–distance curves with only one shallow minimum (at separation distances close to twice the adsorbed layer thickness), but when the surface-surface separation distance become smaller than twice the adsorbed layer thickness a sharp increase in repulsion is obtained and this is the origin of steric stabilization. The criteria of effective steric stabilization are described.

Chapter 14 describes the different flocculation mechanisms of sterically stabilized dispersions. The first mechanism, referred to as weak and reversible flocculation, occurs when the energy minimum in the energy–distance curve is sufficiently deep (few kT units, where k is the Boltzmann constant and T is the absolute temperature) for sufficient attraction to occur. The dependency of the depth of the minimum on the colloidal dispersion volume fraction is described. The second type of flocculation, referred to as incipient flocculation, is strong and irreversible. The conditions for incipient flocculation, in particular the solvency of the medium for the chains, are described. A definition is given for the onset of incipient flocculation that is determined by the Flory–Huggins interaction parameter. The correlation between the flocculation point and the theta conditions for the chains is described. The third type of flocculation, referred to as depletion flocculation, occurs on the addition of "free", nonadsorbing polymer to the dispersion. The parameters that determine depletion flocculation are described at a fundamental level. The fourth type of flocculation, described as bridging flocculation, is obtained when there is not sufficient polymer to cover the particles. The various parameters that determine bridging flocculation are described. The fifth type of flocculation occurs when charged polymers with opposite sign to that of the particles are added to the colloidal dispersion.

This handbook (Vol. 1) gives a comprehensive fundamental analysis of interface science and colloid stability. It would be valuable for graduate students requiring knowledge of the subject as well as research workers who are engaged in the field. It will also be extremely valuable for industrial chemists and chemical engineers who are engaged in formulation of various disperse systems. It will also provide the formulation chemist with a fundamental approach on how to arrive at a required state of a colloidal dispersion and how to maintain the ease of its application.

April 2017 Tharwat Tadros

Contents

1 Introduction

1.1 Colloidal dispersions

The word "colloid" was first coined by Thomas Graham [1] in 1861 who borrowed the word from the Greek word "kolla" meaning glue-like. Colloidal particles possess characteristic properties between those of true solutions (with molecules that can diffuse through membranes) and suspensions that can sometimes be easily observed by the naked eye. Clearly colloidal particles are unable to diffuse through membranes and when dispersed in a liquid medium they form a heterogeneous (two-phase) system that can scatter light. The best definition of colloids is perhaps "systems in which a significant proportion of the molecules lie in or are associated with interfacial regions". Simple considerations suggest that the lowest limit for colloids (whereby one can distinguish between molecules in the interfacial region and the bulk) is 1 nm. The upper limit for colloidal dispersions lies in the region of 1000 nm (1 μm), whereby a significant proportion of the total molecules lie at the interface. Unfortunately, the exact range of colloid size is difficult to ascertain in an exact manner. For that reason Ostwald [2] described colloids as "the world of neglected dimensions".

Colloidal particles are too small to be observed with ordinary optical microscopy. However, it was possible to demonstrate their existence using the technique of ultramicroscopic illumination first employed by Zsigmondy [3] in 1903. This is due to the fact that colloidal particles scatter light. The technique, known as dark field microscopy, works provided the refractive index of the particles is very much different from that of the medium so that sufficient light is scattered from them to be seen [4]. A schematic representation of the slit ultramicroscopic is shown in Fig. 1.1.

To visualize colloidal particles both scanning electron microscopy (SEM) and transmission electron microscopy (TEM) are effectively used with a resolution down to 5 nm for TEM. For metallic colloids (such as gold sols), a drop of the dispersion is deposited on a TEM grid, dried and observed directly in the microscope. The images, which are a two-dimensional representation, are captured on film or digitally and from

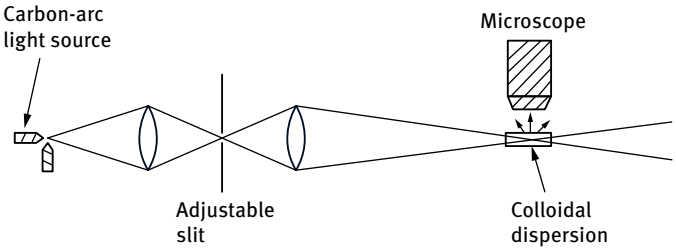

Fig. 1.1: Schematic representation of the slit ultramicroscope [5].

https://doi.org/10.1515/9783110540895-002

these the size distribution is determined using an image analyser. For colloids such as organic polymers, proteins and biocolloids that can be damaged by the electron beam, a carbon or gold replica is prepared that is floated off the sample and observed in the microscope instead of the colloid. Many other techniques can be used for measuring the size of colloidal particles, of which light scattering is perhaps the most convenient to use. Both static (elastic) and dynamic (quasi-elastic) light scattering methods can be applied and these will be described in detail in Chapter 12, Vol. 2.

It should be mentioned that colloidal particles are not always spherical and many other shapes are encountered in practice, e.g. ellipsoids, rods, discs, etc. Measurement of particle size and shape distribution is essential since these determine many of the properties of the colloidal dispersion, such as its flow characteristics (rheology), solubility rate, stability, appearance of the dispersion , processing, etc. The particles are described as monodisperse if they are of the same size, otherwise they are polydisperse. It is therefore important to determine the particle size distribution and polydispersity index as will be discussed in detail in Chapter 12, Vol. 2.

As mentioned above, a colloidal dispersion is a two-phase system in which one phase (the disperse phase) is dispersed in a second continuous phase (the dispersion medium). The disperse phase can be solid, liquid or gas and the same applies for the dispersion medium. On this basis one can distinguish several classes of colloidal dispersions as shown in Tab. 1.1.

Tab. 1.1: Classes of colloidal dispersions.

Solid	Liquid	Suspension
Liquid	Liquid	Emulsion
Gas	Liquid	Foam
Liquid	Gas	Aerosol
Liquid	Solid	Gel
Solid	Gas	Smoke
Solid	Solid	Composite

Several examples of dispersion classes can be quoted. One of the earliest colloidal dispersions of the solid/liquid type is colloidal gold which was used in the fourth and fifth century BC by ancient Egyptians and Chinese to make ruby glass and for colouring ceramics [4]. Michael Faraday [6] prepared the first pure colloidal gold dispersion by reducing a solution of gold chloride with phosphorous. He recognized the colour of the dispersion was due to the small size of the gold particles. Nowadays such small sized particles covering the size range 1–100 nm are referred to as nanoparticles. The early work of Brown on the random drifting of dispersed particles induced by thermal energy (referred to as Brownian motion) was given a theoretical treatment by Einstein [7]. Brownian motion of colloidal particles and the resultant dynamics are unique and important characteristics of colloidal systems [4].

A good example of naturally occurring colloid of the liquid/liquid type is milk, which consists of fat droplets dispersed in aqueous medium that also contains casein micelles which are also colloidal in nature. When milk is first obtained from cows, the fat droplets may exceed 1 μm and this results in creaming of these droplets. However, when milk is homogenized (using high pressure homogenizers) the fat droplets are subdivided into submicron droplets (nanodroplets) and this prevents the process of creaming.

An example of gas/liquid system (foam) is the beer head. When beer is poured into a glass one observes a head of foam and the air bubbles are stabilized by protein present in the beer. Several examples of liquid/gas dispersions (aerosols) can be quoted, such as fog or mist. One of the main applications of aerosols is in pharmacy for oral and topical use. Pharmaceutical aerosols are dosage forms containing therapeutically active ingredients intended for topical administration, introduction into body cavities, or by inhalation via the respiratory tract. The aerosol product consists of two components, namely concentrate containing the active ingredient and propellant(s). The latter provides the internal pressure that forces the product out of the container when the valve is opened and delivers the product in the desired form.

Liquid/solid dispersions or gels are semisolids consisting of a "three-dimensional" network in which the liquid is entrapped. The network can be either suspensions of small particles or large organic molecules (polymers) interpenetrated with liquid. In the first case, the inorganic particles, such as bentonite, form a three-dimensional "house of cards" structure through the gel. This is a true two-phase system. With polymers, either natural or synthetic, the molecules tend to entangle with each other due to their random motion. These systems are actually single phase in the macro-sense; the organic molecules are dissolved in the continuous phase. However, the unique behaviour of polymers, leading to high viscosities and gel formation, makes it possible to consider the gel as a two-phase system on the micro-level; the colloidal polymer molecule and the solvent. Gels find use as delivery systems for oral administration, for topical drugs applied directly to the skin or eye as well as for long acting forms of drugs.

Examples of solid/gas dispersions are smoke and dust as well as particles produced in coal fires and diesel engines. Several examples of solid/solid dispersions can be quoted such as painted glass, pigmented plastics as well as dispersions of silica in plastic to enhance the mechanical properties of the system.

1.2 Self-assembly systems

Certain organic molecules such as surfactants (generally described as amphiphiles) tend to associate in solution above a critical concentration to form aggregate structures (referred to as micelles) with dimensions in the colloid range. A good example is the association of sodium dodecyl sulphate (SDS) at concentrations $\geq 8.1 \times 10^{-3}$ mol

to form spherical micelles [8] as represented in Fig. 1.2. However, the micelles can be of different shapes (rod-shaped or lamellar) but still with one dimension in the colloid range. The different shapes of micelles are illustrated in Fig. 1.3. The size and shape of any micelle is determined by the surfactant structure and the environment. The surfactant structure determines the critical packing parameter of the molecule (the ratio of the cross-sectional area of the hydrocarbon chain to that of the head group). The head group cross-sectional area is determined by the size of that group which in turn is determined by electrolyte addition. For example, a spherical micelle may change to a rod-shaped one on addition of electrolyte.

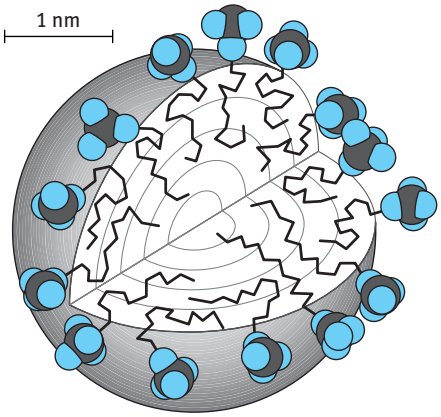

Fig. 1.2: Schematic representation of SDS micelles.

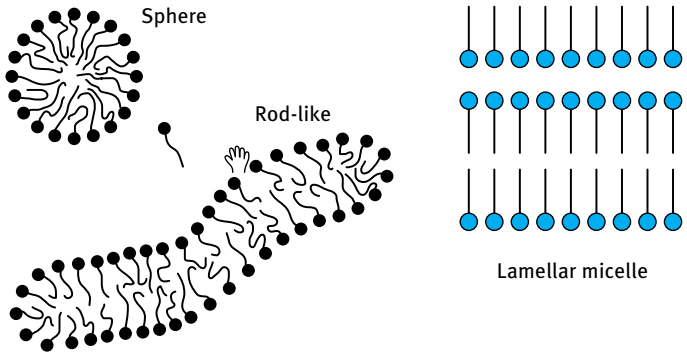

Fig. 1.3: Shape of micelles.

1.3 Interfacial phenomena

In all disperse systems such as suspensions, emulsions, foams, etc., the structure of the interfacial region determines its colloidal properties [9–13]. The larger the interfacial area, i.e. the larger the surface to volume ratio of the particle or droplet, the more important the role of the structure of the interfacial region. For convenience, I will list the topics of colloid and interface science under two main headings, namely disperse systems and interfacial phenomena. This subdivision does not imply any separation for the following reasons: All disperse systems involve an interface and many interfacial phenomena are precursors for formation of disperse systems, e.g. nucleation and growth, emulsification, etc. The main objective of the present book is to cover the following topics: The basic principles that are involved in interfacial phenomena as well as the formation of colloidal dispersions and their stabilization, as well as surfactants and polymer adsorption at various interfaces and interfacial phenomena in wetting, spreading and adhesion.

Several interfacial phenomena may be considered when dealing with colloidal dispersions:

(i) Charge separation and formation of electrical double layers.
(ii) Wetting of powders and the role of surfactants.
(iii) Adsorption of surfactants and polymers at the solid/liquid and liquid/liquid interfaces and the role of the structure of the interfacial region.

The colloid stability/instability of any disperse system is determined by the property of the interfacial region. In actual fact, colloid and interface science are one individual subject. This is particularly the case with charged interfaces that form electrical double layers and those interfaces that contain adsorbed surfactants and/or polymers. With systems containing electrical double layers, repulsion between the particles or droplets takes place as a result of the overlap of double layers. This is particularly the case at low electrolyte concentrations and low valency of the indifferent electrolyte. This double layer repulsion overcomes the van der Waals attraction and at intermediate distances an energy barrier is produced that prevents approach of the particles. This barrier can reach several kT units (where k is the Boltzmann constant and T is the absolute temperature) which becomes much higher than the thermal motion ($\approx kT$) and this prevents particle aggregation (flocculation or coagulation). As the electrolyte concentration is increased, the range and magnitude of the repulsive energy is reduced and at a critical concentration (defined as the critical coagulation concentration, CCC) fast flocculation and irreversible aggregation occur. With adsorbed nonionic surfactants or polymers an adsorbed layer with thickness δ is produced. When the particles or droplets approach to a surface-surface distance $h < 2\delta$, strong repulsion occurs due to the unfavourable mixing of the adsorbed chains when these are in good solvent conditions. This repulsion is referred to as steric interaction and at distances $< 2\delta$ a very sharp increase in repulsion energy occurs when $h < 2\delta$. This

steric repulsion overcomes the van der Waals attraction at $h \approx 2\delta$. The repulsion produced by the presence of adsorbed layers of surfactant or polymers is generally more effective than the electrostatic repulsion produced by overlap of the double layers. The stability is less sensitive to addition of moderate electrolyte concentration, provided the medium remains a good solvent for the chains.

The field of colloid and interface science has no boundary since chemists, physicists, engineers, biologists, mathematicians can all be engaged in the field. For successful applications in industry, multidisciplinary teams are required. Understanding the basic principles of colloid and interface science will enable industry to develop many complex systems in a shorter period of time. Most colloidal systems used in industry are multiphase and complex formulations. They may contain more than one disperse phase, e.g. suspension/emulsion systems (suspoemulsions).

1.4 Outline of the book

Chapter 2 deals with origin of charge in colloidal systems and structure of the electrical double layer. A great variety of processes occur to produce a surface charge [13]: Surface ions that have such a high affinity to the surface of the particles that they may be taken as part of the surface, e.g. Ag^+ and I^- for AgI; ionization of surface groups, e.g. carboxylic groups that are chemically bound to the surface of synthetic latexes. The charge is a function of pH as the degree of dissociation is a function of pH; isomorphic substitution which occurs in clay minerals, with the basic structure of a clay particle consisting of an aluminosilicate layer lattice; specific adsorption of ions that have non-electrostatic affinity to the surface, e.g. bivalent cations on oxides, cationic and anionic surfactants on most surfaces can also produce a surface charge. The second part of Chapter 2 deals with the structure of the electrical double layer, namely the diffuse double layer due to Gouy and Chapman [14, 15] and its modification by Stern and Graham [16, 17] who considered the role of specifically adsorbed ions near the surface. One of the main features of the electrical double layer is its extension in bulk solution (referred to as the double layer thickness) which depends on electrolyte concentration and valency of the counterions and co-ions. The methods that can be applied for investigating the double layer are described. The most common method for investigating double layers in disperse systems is to use titration techniques that can be applied to obtain the surface charge as a function of surface potential at different electrolyte concentrations and types. The titration method was successfully applied for double layer investigations on oxides. The surface charge can be directly determined by titration of an oxide suspension in an aqueous solution of indifferent electrolyte (e.g. KCl).

Chapter 3 deals with electrokinetic phenomena and the concept of zeta potential [18]. Electrokinetic effects are the direct result of charge separation at the interface between two phases, I and II. When one of the phases is a polar liquid like water, its dipolar molecules will tend to be oriented in a particular direction at the interface and

this will generate a potential difference. If there are ions or excess electrons in one or both of the phases, or ionogenic groups, there will be a tendency for the electric charges to distribute themselves in a non-uniform way at the interface. This results in the formation of an electrical double layer as described in Chapter 2. Electrokinetic effects arise when one of the two phases is caused to move tangentially past the second phase. The tangential motion can be caused by an electric field, forcing a liquid into a capillary, forcing a liquid into a plug of particles or by a gravitational field on the particles. This leads to four different types of electrokinetic phenomena, namely electrophoresis, electro-osmosis, streaming potential and sedimentation potential. In this chapter, only electrophoresis will be discussed since this is the most commonly used method for dispersions, allowing one to measure the particle mobility which can be converted to the zeta potential using theoretical treatments. The various theoretical treatments that can be applied to convert particle mobility to zeta potential are described. This is followed by a section on the methods that can be applied for measurement of particle mobility and zeta potential for various colloidal systems.

Chapter 4 describes the double layer repulsion between colloidal particles. The origin of electrostatic interactions is due to the double layer overlap that occurs when the surface-to-surface distance becomes smaller than twice the double layer thickness. One of the most important features of double layers is their strong dependence on the concentration of indifferent electrolytes. An increase in electrolyte concentration causes a reduction in the diffuse double layer potential and compression of the double layer, i.e. reduction of the Debye length. Both of these effects affect the colloid stability of lyophobic colloids. The theoretical analysis of interaction between particles containing double layers is described for the case of constant potential and constant charge. The effect of increasing electrolyte concentration, valency of counterions and Stern potential is described at a fundamental level.

Chapter 5 deals with van der Waals attraction between colloidal particles. The interaction between two particles can in general be considered in terms of the potential energy or the work required to separate them from a centre-to-centre distance r to some large distance apart [13]. One must first consider the intermolecular attraction between atoms or molecules: dipole-dipole interaction (Keesom–van der Waals interaction), dipole-induced dipole interaction (Debye–van der Waals interaction), London–van der Waals interaction (dispersion interaction). There are generally two approaches for describing the van der Waals attraction between macroscopic bodies such as colloidal particles, emulsion droplets, etc. The first approach considers the London–van der Waals attraction to be the sum of the forces acting between isolated molecules. This approach, referred to as the microscopic approach, was suggested by de Boer and Hamaker [19, 20]. The second approach, developed by Lifshitz et al. [21], is based on the correlation between electric fluctuations of two macroscopic bodies. It is referred to as the macroscopic approach. Both approaches are described in this chapter

Chapter 6 gives a thorough description of the theory of colloid stability due to Deryaguin, Landau, Verwey, Overbeek (DLVO theory) [22, 23]. The DLVO theory is based on the combination of electrostatic repulsion and van der Waals attraction at various separation distances between the particles. This results in an energy–distance curve containing a shallow attractive minimum (weak attraction) at long separation distances between the particles, a deep attractive minimum at short separation distances and an energy maximum (energy barrier) at intermediate distances. The dependency of the energy maximum on electrolyte concentration, electrolyte valency and zeta potential is described to distinguish between stable and unstable (flocculated) dispersions.

Chapter 7 describes the flocculation of colloidal dispersions. The mechanism of aggregation is described in terms of the DLVO theory which predicts the process of aggregation on addition of electrolytes with different valencies. The kinetics of flocculation is described for two cases: Fast flocculation in the absence of an energy barrier and slow flocculation in the presence of an energy barrier. The theory of fast flocculation kinetics, due to Smoluchowski [24], is described. This is followed by the theory of slow flocculation, due to Fuchs [25] and definition of the stability ratio W (ratio of fast flocculation rate to slow flocculation rate). The dependency of W on electrolyte concentration C for uni–uni (1 : 1) and bi–bi (2 : 2) electrolyte is described. $\log W$–$\log C$ curves are established and this allows one to define the critical flocculation (coagulation) concentration and its dependency on electrolyte valency. A section is given over to the process of (reversible) flocculation as well as orthokinetic (in the presence of shear) flocculation.

Chapter 8 describes association colloids mostly produced by surfactant molecules. It starts with a section on the general classification of surfactant molecules: anionic, cationic, zwitterionic and nonionic. A section is devoted to polymeric surfactants and their structure. The physical chemistry of surfactant solutions is described at a fundamental level, illustrating the abrupt changes at a critical concentration due to the aggregation of the molecules into micelles. The critical concentration is defined as the critical micelle concentration (cmc). The dependency of the cmc on the surfactant structure is described. This is followed by a section on the solubility-temperature relationship for ionic and nonionic surfactants. The kinetics and thermodynamic aspects of micelle formation are described to illustrate the spontaneous formation of micelles. The driving force of micelle formation is described in terms of the balance between enthalpy and entropy of the process.

Chapter 9 deals with the process of surfactant adsorption at the liquid/liquid interface. It starts with a thermodynamic definition of interfacial tension by application of the second law of thermodynamics. Two approaches are described for the process of surfactant adsorption at liquid interfaces. The first approach treats the process as one of equilibrium and by application of the second law of thermodynamics one can relate the variation of interfacial tension with surfactant concentration to the amount of surfactant adsorption at the liquid/liquid interface. This allows one to obtain the

area per surfactant molecule at the interface and its dependence on the orientation of the molecule. The second approach for surfactant adsorption considers the molecules to produce a layer at the interface which produces a surface pressure. This approach allows one to obtain the orientation of the surfactant molecules by following the change in surface pressure with surfactant concentration.

Chapter 10 describes the adsorption of surfactants at the solid/liquid interface. It emphasizes the reversibility of adsorption and the possibility of application of thermodynamics. Four systems are considered: ionic surfactants on hydrophobic and hydrophilic surfaces, nonionic surfactants on hydrophobic and hydrophilic surfactants. It shows that the adsorption of both ionic and nonionic surfactants on hydrophobic surfaces is governed by hydrophobic bonding between the alkyl chain and the nonpolar surface; charge interactions play a minor role. The adsorption of ionic and nonionic surfactants on hydrophilic surfaces is governed by the polar interaction between the surfactant head group and the charged or polar surface. The adsorption of ionic surfactants on hydrophobic surfaces can be described by the Stern–Langmuir equation at low surface coverage. At high surface coverage, lateral interaction between the surfactant molecules on the solid surface must be taken into account. Using the Stern–Langmuir equation, one can define the free energy of adsorption which contains several contributions, e.g. surfactant/surfactant interaction, surfactant/surface interaction and head group/surface interaction. The experimental technique for determining the adsorption isotherm is described and some examples are given to show the effect of surfactant structure and nature of the surface. The adsorption of ionic surfactants on charged surfaces (with opposite charge) shows a very rapid increase above a critical concentration which is attributed to the formation of hemimicelles. Several types of adsorption isotherms are described for the adsorption of nonionic surfactants on nonpolar and polar surfaces. These isotherms are analysed in terms of the structure of the surfactant molecules on the surface.

Chapter 11 describes the solution properties of polymers and polymeric surfactants. It starts with the Flory–Huggins theory that describes the free energy of random coils in terms of the entropy and enthalpy contributions to the free energy. Equations are given for the end-to-end distance and radius of gyration of the random coil. Modification of the Flory–Huggins theory is described for block and graft copolymers. Particular attention is given to the association of block and graft copolymers that gives association structures similar to surfactant micelles. The techniques that can be applied to investigate the solution properties of polymers and polymeric surfactants are described.

Chapter 12 describes the process of adsorption of polymers at the solid/liquid interface. It emphasizes the complexity of the adsorption process that must take into consideration the conformation of the polymer chains at the solid/liquid interface. Several classes of polymers are considered, namely random coil, “blocky copolymers” (that contain short blocks with high affinity to the surface), block and graft copolymers. The importance of a minimum adsorption energy per segment attached, that is

required to counteract the entropy loss due to adsorption, is clearly illustrated. The theories of polymer adsorption are described with particular reference to the step-weighted random walk approach and the scaling concepts. The experimental techniques that are used to obtain the various adsorption parameters are described.

Chapter 13 deals with the process of steric stabilization. It starts with describing the interaction between particles or droplets containing polymer layers. This interaction could result in overlap and/or compression of the adsorbed layer, both of which results in an increase in the segment density in the overlap. The repulsion is described in terms of the unfavourable mixing of the polymer chain and the loss of entropy of the chains on considerable overlap. The unfavourable mixing results in a positive free energy of repulsion providing the chains are in good solvent conditions. Equations are derived to obtain the mixing free energy illustrating the importance of the Flory–Huggins interaction parameter. Equations are also given for the entropy loss (that is described as elastic interaction). Combining the mixing elastic terms gives the total steric interaction, which when combined with the van der Waals attraction gives energy–distance curves with only one shallow minimum (at separation distances close to twice the adsorbed layer thickness), but when the surface-surface separation distance become smaller than twice the adsorbed layer thickness a sharp increase in repulsion is obtained and this is the origin of steric stabilization. The criteria of effective steric stabilization are described.

Chapter 14 describes the different flocculation mechanisms of sterically stabilized dispersions. The first mechanism, referred to as weak and reversible flocculation, occurs when the energy minimum in the energy–distance curve is sufficiently deep (few kT units, where k is the Boltzmann constant and T is the absolute temperature) for sufficient attraction to occur. The dependency of the depth of the minimum on the colloidal dispersion volume fraction is described. The second type of flocculation, referred to as incipient flocculation, is strong and irreversible. The conditions for incipient flocculation, in particular the solvency of the medium for the chains, are described. A definition is given for the onset of incipient flocculation that is determined by the Flory–Huggins interaction parameter. The correlation between the flocculation point and the theta conditions for the chains is described. The third type of flocculation, referred to as depletion flocculation, occurs on the addition of "free", nonadsorbing polymer to the dispersion. The parameters that determine depletion flocculation are described at a fundamental level. The fourth type of flocculation, described as bridging flocculation, is obtained when there is not sufficient polymer to cover the particles. The various parameters that determine bridging flocculation are described. The fifth type of flocculation occurs when charged polymers with opposite sign to that of the particles are added to the colloidal dispersion.

Chapter 1, Vol. 2 describes the flow characteristics (rheology) of colloidal dispersions. It starts with a section on the basic principles of rheology that include steady state (shear stress-shear rate measurements), constant stress (creep measurements), constant strain (stress relaxation measurements) and dynamic (oscillatory) tech-

niques. The various rheological models that are used to describe each technique are described. This is followed by a section on very dilute and moderately concentrated colloidal dispersions (which takes into account the hydrodynamic interaction). The rheology of concentrated colloidal dispersions is then described by considering four different systems. The first is represented by hard-sphere interactions where both repulsion and attraction are screened. The semi-empirical model that can be applied to describe the rheology of hard-sphere dispersions is described. The second system is that of "soft" or electrostatic interaction whereby the rheology of the system is determine by double layer repulsion. The third system is that of sterically stabilized dispersions. The importance of the ratio of adsorbed layer thickness to particle radius is described. The fourth system is that of flocculated dispersions and a distinction can be made between weak and strong flocculation.

Chapter 2, Vol. 2 describes the various processes of wetting, spreading and adhesion. It starts with the equilibrium thermodynamic treatment and Young's equation. The calculation of surface tension and contact angle is described. This is followed by a description of the process of spreading of liquids on surfaces and definition of the Harkins spreading coefficient. The process of contact angle hysteresis and effect of roughness and surface heterogeneity is described. This is followed by a section on the critical surface tension of wetting and the effect of surfactant adsorption. The dynamic process of adsorption and wetting is described.

Chapter 3, Vol. 2 deals with solid/liquid dispersions (suspensions). Both colloidal and non-colloidal, organic and inorganic particles suspended in aqueous and nonaqueous media are described. Particular attention is given to nanosuspensions that cover the size range 1–100 nm. The general methods of preparation and stabilization of dispersions are described. The distinction between colloidal and physical stability is described. This is followed by a section on preparation of suspensions by bottom-up process, namely by nucleation and growth. The thermodynamic theory of nucleation and growth is described at a fundamental level. This is followed by a section on precipitation kinetics and control of particle size distribution. The preparation of suspensions by bottom-down process, namely by breaking of aggregates and agglomerates, dispersion and comminution (milling) is then described. The role of wetting and dispersing agents is described at a fundamental level. This is followed by a section on electrostatic and steric stabilization of suspensions. The Ostwald ripening (crystal growth) of suspensions that results from the difference in solubility between small and large particles is described. This is followed by a section on sedimentation of suspensions and prevention of formation of hard sediments ("clays"). The final part deals with nonaqueous suspensions in both polar and nonpolar liquids.

Chapter 4, Vol. 2 describes the liquid/liquid dispersions (emulsions). It starts with a section on the classification of emulsions based on the nature of the emulsifier and the structure of the system. Special attention is given to nanoemulsions covering the size range 1–100 nm. The general instability problems with emulsions are described. This is followed by a section on the thermodynamics of emulsion formation and break-

down with particular reference to the importance of having a repulsive energy barrier to ensure the kinetic stability of the system. The interaction forces between emulsion droplets are briefly described. This is followed by a description of the mechanism of emulsification and the role of the emulsifier. The various methods that can be applied for emulsification are described with particular reference to the use of high pressure homogenizers. The various methods for selection of emulsifiers are described. The process of creaming/sedimentation of emulsions and its prevention is described. This is followed by sections on flocculation of emulsions and its prevention, Ostwald ripening and its reduction, emulsion coalescence and its prevention and phase inversion.

Chapter 5, Vol. 2 deals with multiple emulsions. It starts with a definition and types of multiple emulsions. The breakdown processes of multiple emulsions are described. This is followed by a section on preparation of multiple emulsions with particular reference to the role of the emulsifiers and the nature of the oil phase. The factors affecting the stability of multiple emulsions are described at a fundamental level. This is followed by a section on the methods that can be applied for characterization of multiple emulsions and their long-term physical stability.

Chapter 6, Vol. 2 deals with gas (air)/liquid dispersions (foams). It starts with the methods of foam preparation and foam structure. The classification of foam stability is described. This is followed by a section on drainage and thinning of foam films. The various theories of foam stability are described. This is followed by a description of foam inhibitors. The physical properties of foams are described and this is followed by a section on the experimental techniques for studying foam structure and stability.

Chapter 7, Vol. 2 describes liquid/solid dispersions or gels. It starts with a definition of a gel and description of the rheological behaviour of a gel. The various classifications of gels are described. It starts with physical gels obtained by polymer chain overlap. Gels produced by associative thickeners are described. This is followed by a section on crosslinked (chemical) gels. The second part of this chapter deals with particulate gels formed by crosslinking of finely divided particles.

Chapter 8, Vol. 2 deals with the subject of polymer colloids (latexes). It starts with a section on the preparation by emulsion polymerization, with particular reference to the theories and the role of the emulsifier. The use of block and graft copolymers in emulsion polymerization is described. This is followed by a section on dispersion polymerization for preparation of nonaqueous polymer latexes. Particular attention is given to the importance of the presence of a "protective colloid" to prevent the flocculation of the resulting latex.

Chapter 9, Vol. 2 describes microemulsions. It starts with the definition of microemulsions, their spontaneous formation and thermodynamic stability. The various theories of microemulsion formation and stability are described, with particular reference to the importance of having an ultra-low interfacial tension. The use of mixed surfactants for preparation of microemulsions is described. The various techniques that can be applied for characterization of microemulsions are described.

Chapter 10, Vol. 2 deals with liposomes and vesicles and their important applications. The various lipids that are used for preparing liposomes and vesicles are described. This is followed by a description of the driving force for formation of vesicles and the importance of the critical packing parameter concept. The enhancement of stability of vesicles by incorporation of block copolymers is described.

Chapter 11, Vol. 2 deals with the process of deposition of particles and their adhesion at interfaces, with particular reference to the role of interparticle interactions. The methods of measurement of particle deposition using rotating disc and cylinder techniques are described. This is followed by applications of particle deposition in hair sprays, hair conditioners, foundation, creams and lotions. The effect of polymers and polyelectrolytes on particle deposition at interfaces is described. This is followed by a section on the effect of nonionic, anionic and cationic polymers on particle deposition. The process of particle-surface adhesion is described with particular reference to the importance of short-range forces and calculation of the force of adhesion. The surface energy approach to adhesion is described. This is followed by the experimental methods for measurement of particle deposition and adhesion. The process of removal of solid dirt and liquid droplets from surfaces is described.

Chapter 12, Vol. 2 deals with the various techniques that can be applied for characterization of colloidal dispersions. It starts with a definition of particle size distribution and polydispersity. Various sections are devoted to the application of optical microscopy, image analysis, confocal laser scanning microscopy, diffraction methods and scanning and electron microscopy. The various scattering techniques that can be applied for determination of particle size and polydispersity index are described with particular reference to time-average and dynamic (quasi-elastic) (photon correlation spectroscopy) light scattering methods. The methods that can be applied to assess creaming or sedimentation, flocculation, Ostwald ripening and coalescence are described in this chapter.

References

[1] Graham T. Philos Trans Royal Soc. 1861;151:183.
[2] Ostwald CWW. An introduction to theoretical and applied colloid chemistry. New York: Wiley, 1917.
[3] Zsigmondy R. Properties of colloids. Nobel Foundation, December 11, 1926.
[4] Ho CC. Colloidal state. In: Tadros T, editor. Encyclopedia of colloid and interface science. Berlin: Springer; 2013.
[5] Shaw DJ. Introduction to colloid science. 4th ed. Oxford: Butterworth Heinemann; 1992.
[6] Faraday M. Philos Trans. 1857;147:145.
[7] Einstein A. Investigations on the theory of Brownian movement. New York: Dover; 1956.
[8] Tadros T. An introduction to surfactants. Berlin: De Gruyter; 2014.
[9] Tadros T. Applied surfactants. Weinheim: Wiley-VCH; 2005.
[10] Tadros T. Dispersion of powders in liquids and stabilisation of suspensions. Weinheim: Wiley-VCH; 2012.

[11] Tadros T, editor. Emulsion formation and stability. Weinheim: Wiley-VCH; 2013.
[12] Tadros T, editor. Encyclopedia of colloid and interface science. Berlin: Springer; 2013.
[13] Tadros T. Interfacial phenomena and colloid stability, Vol. 1. Berlin: De Gruyter; 2015.
[14] Gouy G. J Phys. 1910;9:457; Ann Phys. 1917;7:129.
[15] Chapman DL. Phil Mag. 1913;25:475.
[16] Stern O. Z Electrochem. 1924;30:508.
[17] Grahame DC. Chem Rev. 1947;41;441.
[18] Hunter RJ. Zeta potential in colloid science. London: Academic Press; 1981.
[19] de Boer JH. Trans Faraday Soc. 1936;32:10.
[20] Hamaker HC. Physica. 1937;4:1058.
[21] Lifshitz EM. Soviet Physics JETP. 1956;2:73.
[22] Deryaguin BV, Landau L. Acta Physicochem USSR. 1941;14:633.
[23] Verwey EJW, Overbeek JTG. Theory of stability of lyophobic colloids. Amsterdam: Elsevier; 1948.
[24] von Smoluchowski M. Physik Z. 1916;17:557, 585.
[25] Fuchs N. Z Physik. 1936;89:736.

2 Origin of charge at interfaces and structure of the electrical double layer

2.1 Introduction

Many colloidal dispersions are stabilized against aggregation by electrostatic repulsion between the particles. The particle acquires a surface charge that is compensated by unequal distribution of counterions (with opposite sign to the surface charge) and co-ions (with the same sign as the surface charge) thus producing an electrical double layer. When the particles approach each other to a separation distance that is smaller than twice the double layer extinction, strong repulsion occurs and this overcomes the van der Waals attraction.

In this chapter, I will discuss the origin of charge on surfaces and the structure of the electrical double layer. The methods that can be applied for investigating the double layer structure are also discussed in this chapter. Double layer repulsion and van der Waals attraction will be discussed in detail in Chapters 4 and 5. The combination of van der Waals attraction and double layer repulsion forms the basis of the theory of colloid stability that will be discussed in Chapter 6.

2.2 Origin of charge on surfaces

A great variety of processes occur to produce a surface charge [1–3].

2.2.1 Surface ions

These are ions that have such a high affinity to the surface of the particles that they may be taken as part of the surface, e.g. Ag^+ and I^- for AgI. If silver iodide, that is sparingly soluble in water, is brought into water, dissolution occurs until the concentration of the ionic components in solution corresponds to the solubility product of the compound K_s. The latter $K_s = [Ag^+][I^-] = 10^{-16}$. If the precipitation is produced under conditions which have an excess of I^-, say 1×10^{-4} mol dm^{-3}, one forms a dispersion with negatively charged surface. Using $p[I^-] = \log[I^-]$, the solution has a $p[I^-] = 4$ and then $p[Ag^+] = 12$. In this case the solution of Ag^+ is suppressed with the surface of the particles consisting of I^- species. In contrast, if the precipitation is produced under conditions of excess Ag^+ ions, say 1×10^{-4} mol dm^{-3}, or $p[Ag^+] = 4$, one forms a dispersion that is positively charged with the surface of the particles consisting of Ag^+ ion species. At $p[I^-] = 10.5$ or $p[Ag^+] = 5.5$, the surface populations of the two types are equal and the point of zero charge (pzc) is reached as the net charge is zero.

https://doi.org/10.1515/9783110540895-003

For AgI in a solution of KNO_3, the surface charge σ_0 is given by the following expression,

$$\sigma_0 = F(\Gamma_{Ag^+} - \Gamma_{I^-}) = F\Gamma_{AgNO_3} - \Gamma_{KI}, \tag{2.1}$$

where F is the Faraday constant (96 500 C mol^{-1}) and Γ is the surface excess of ions (mol m^{-2}).

The surface potential ψ_0 can be expressed using the Nernst equation (as for an electrode surface),

$$\psi_0 = \frac{RT}{F} \ln\left(\frac{[Ag^+]}{[Ag^+]_{pzc}}\right), \tag{2.2}$$

where R is the gas constant and T is the absolute temperature. This gives a surface potential of about ±60 mV for a factor of ±10 in the silver ion concentration from that corresponding to the pzc.

2.2.2 Ionization of surface groups

Carboxylic groups that are chemically bound to the surface of synthetic latexes provide an example of this. The charge is a function of pH as the degree of dissociation is a function of pH. Although the pK_a of an isolated –COOH group is pH ≈ 4, this is not the situation with a surface with many –COOH groups in close proximity. The dissociation of one group makes it more difficult for the immediate neighbours to dissociate. This means that the surface has variable pK_a and pH values as high as 9 may be required to ensure dissociation of all surface groups.

Another example where the charge is produced by dissociation is that of oxides which have surface hydroxyl groups. At high pH, these can ionize to give $-O^-$ and at low pH the lone pair of electrons can hold a proton to give $-OH_2^+$. This process can be represented as follows,

$$MOH_2^+ \overset{H^+}{\longleftrightarrow} MOH \overset{OH^-}{\longleftrightarrow} MO^- + H_2O.$$

The surface charge follows from,

$$\sigma_0 = F([MOH_2^+] - [MO^-]) = F(\Gamma_{H^+} - \Gamma_{OH^-}), \tag{2.3}$$

where Γ refers to the surface concentration in moles per unit area.

A schematic representation of the process of charge formation in an oxide is shown in Fig. 2.1 whereby HNO_3 and KOH are used to provide the H^+ and OH^- ions respectively. In this case one may write equation (2.3) as,

$$\sigma_0 = F(\Gamma_{HNO_3} - \Gamma_{KOH}) \tag{2.4}$$

The charge depends on the pH of the solution: Below a certain pH the surface is positive and above a certain pH the surface is negative. At a specific pH ($\Gamma_H = \Gamma_{OH}$) the

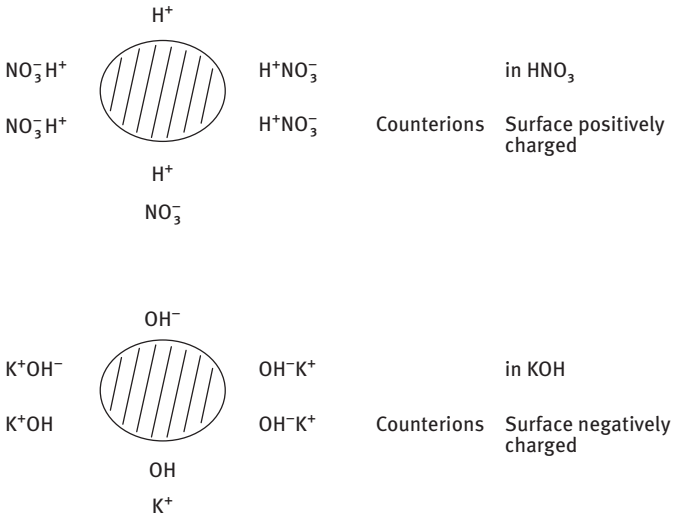

Fig. 2.1: Schematic representation of an oxide surface.

surface is uncharged; this is referred to as the point of zero charge (pzc). The pzc depends on the type of oxide: For an acidic oxide such as silica the pzc is ≈ pH 2–3. For a basic oxide such as alumina pzc is ≈ pH 9. For an amphoteric oxide such as titania the pzc ≈ pH 6. Some typical values of pzc for various oxides are given in Tab. 2.1.

Tab. 2.1: pzc values for some oxides.

Oxide	pzc
SiO_2 (precipitated)	2–3
SiO_2 (quartz)	3.7
SnO_2 (cassiterite)	5–6
TiO_2 (anatase)	6.2
TiO_2 (rutile)	5.7–5.8
RuO_2	5.7
α-Fe_2O_3 (haematite)	8.5–9.5
α-FeO.OH (goethite)	8.4–9.4
ZnO	8.5–9.5
γ-$Al(OH)_3$ (gibbsite)	8–9

2.2.3 Isomorphic substitution

This process occurs in clay minerals, with the basic structure of a clay particle consisting of an aluminosilicate layer lattice. As the clay is formed, it crystallizes with a layer of silicon atoms tetrahedrally coordinated to oxygen atoms, i.e. it forms an SiO_2

layer. The next layer of the lattice is aluminium with octahedrally coordinated oxygen atoms (i.e. an Al_2O_3), some of which are shared with the tetrahedral silica layer. This layer structure is repeated throughout the crystal. With kaolinite a 1 : 1 layer lattice structure is produced, whereas for montmorillonite a 2 : 1 structure, with the alumina layer sandwiched between two silica layers, is formed. A schematic representation of one unit cell of a 2 : 1 layer mineral is shown in Fig. 2.2.

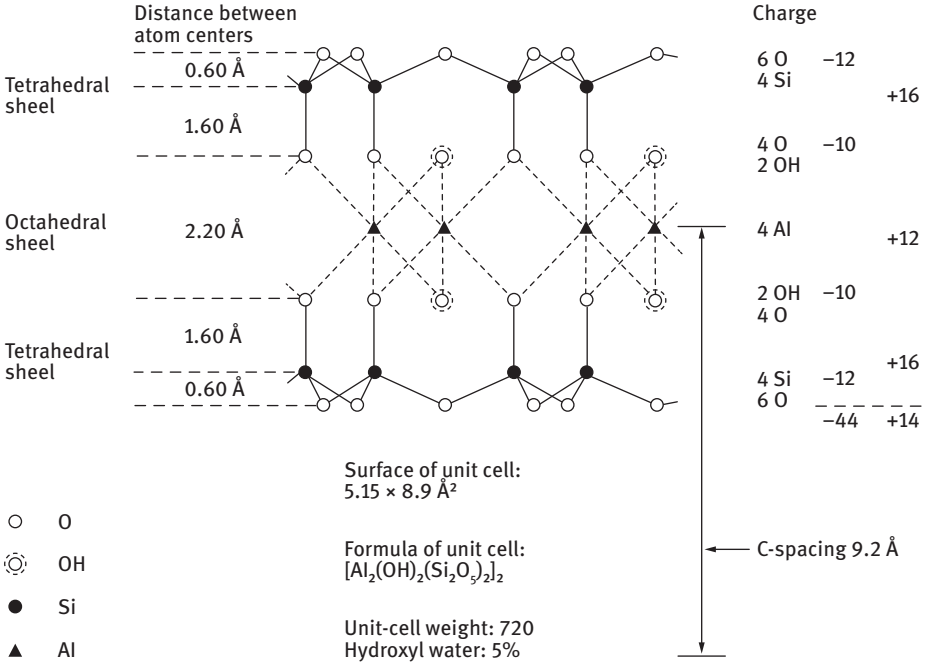

Fig. 2.2: Schematic representation of a 2 : 1 layer of montmorillonite.

During the crystallization process an occasional tetravalent Si atom is substituted by a trivalent Al atom and more frequently a trivalent Al atom is substituted by a bivalent Mg atom. This results in a deficit of positive charges and formation of negative charges, a process referred to as isomorphic substitution. This net negative charge on the surface of the clay particle is balanced by soluble cations (counterions), e.g. Na^+ ions. In the dry state, the counterions are located on the surface of the crystal, whereas in the hydrated state they are in solution near the surface. The 2 : 1 layer lattice clays have a unit cell ≈ 1 nm thick and, on hydration, water penetrates between the layers and the negative charges of the surfaces repel causing the clays to swell. This swelling can result in separation between (original) unit cells of a greater dimension than that of the (original) unit cell. A schematic representation of a clay particle is shown in Fig. 2.3. The surface charge and counterions form the electrical double layer.

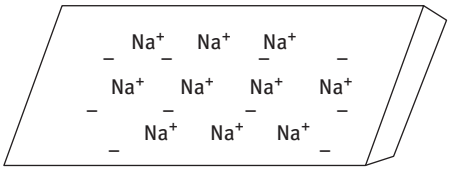

Fig. 2.3: Schematic representation of a clay particle.

2.2.4 Specific adsorption of ions

In some cases, specifically adsorbed ions (that have non-electrostatic affinity to the surface) "enrich" the surface but may not be considered as part of the surface, e.g. bivalent cations on oxides, cationic and anionic surfactants on most surfaces. In particular, ionic surfactants are often added as a component to disperse systems, as wetting and dispersing agents for powders to produce solid/liquid dispersions (suspensions). They are also added for emulsification of oils to produce oil/water emulsions. In most cases the surfactant also acts as a stabilizer for the final suspension or emulsion. By adsorption at the solid/liquid or liquid/liquid interface the surfactant ions produce a charge (negative for anionic surfactants and positive for cationic surfactants) on the surface of the particle or droplet. This charge is compensated by unequal distribution of counterions (with opposite charge to the surface) and co-ions (with the same charge of the surface) forming an electrical double layer. In some cases the charge on the particle or droplet is produced by adsorption of anionic or cationic polyelectrolytes. An example is polyacrylates that are used to disperse many pigments such as titania.

2.3 Structure of the electrical double layer

Two main models for the electrical double were described, namely the diffuse double layer model of Gouy and Chapman [4, 5] and its modification by Stern [6] and Graham [7] who introduced the concept of the nondiffuse part of the double layer resulting from specific adsorption of counterions. Both models are described below.

2.3.1 Diffuse double layer (Gouy and Chapman)

Gouy and Chapman [4, 5] assumed that the charge is smeared out over a plane surface immersed in an electrolyte solution. This surface has a uniform potential ψ_0 and the compensating ions are regarded as point charges immersed in a continuous dielectric medium. The surface charge σ_0 is compensated by unequal distribution of counterions (opposite in charge to the surface) and co-ions (same sign as the surface) which extend to some distance from the surface [4, 5]. The counterion and co-ion concentration n_i near the surface can be related to the value in the bulk n_{i0} using the Boltzmann

distribution principle,

$$n_i = n_{i0} \exp\left[-\frac{Z_i e \psi_x}{kT}\right], \tag{2.5}$$

where Z_i is the valency of the ion i, e is the electronic charge, ψ_x is the potential at a distance x from the surface, k is the Boltzmann constant and T is the absolute temperature. Since the charge on the counterion is always opposite to that of the surface, the exponent in equation (2.5) will always be negative for the counterion concentration and positive for the co-ion concentration. Equation (2.5) shows that the concentration of counterions increases close to the surface (positively adsorbed) whereas the co-ion concentration is reduced near the surface (negative adsorption). Fig. 2.4 shows the local ion concentration profiles according to equation (2.5).

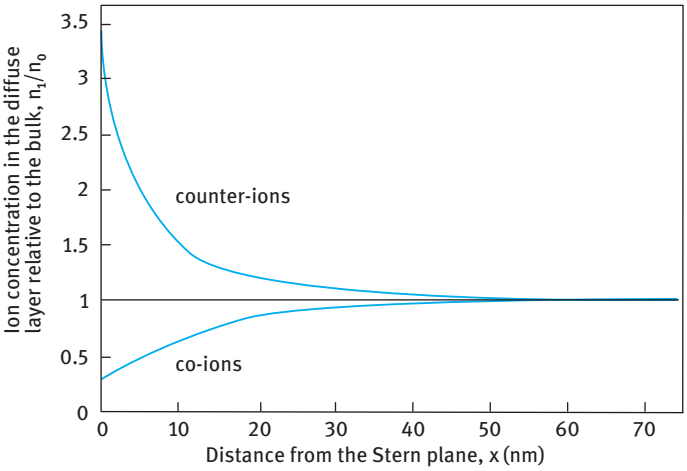

Fig. 2.4: Local ion concentration profiles: $\psi_0 = -30$ mV, in 10^{-3} mol dm^{-3} NaCl.

The number of charges per unit volume, i.e. the space charge density ρ is given by,

$$\rho = \sum_i n_i Z_i e = -2 n_0 Z e \sinh\left[\frac{Z e \psi_x}{kT}\right]. \tag{2.6}$$

Note that $\sinh x = (\exp x - \exp -x)/2$.

A schematic picture of the diffuse double layer according to Gouy [4] and Chapman [5] is shown in Fig. 2.5. The potential decays exponentially with distance x.

Using the Poisson equation one can relate the charge density to the curvature of potential,

$$\nabla^2 \psi(x) = -\frac{\rho}{\varepsilon_0 \varepsilon_r}, \tag{2.7}$$

where ∇^2 is the Laplace operator which for a planer surface is $\mathrm{d}^2\psi/\mathrm{d}x^2$.

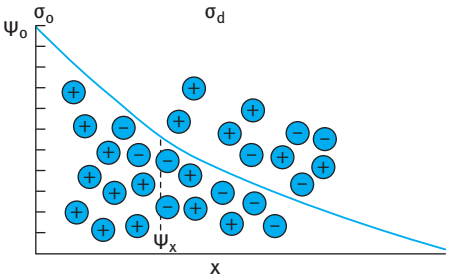

Fig. 2.5: Schematic representation of the diffuse double layer according to Gouy [4] and Chapman [5].

Combining equations (2.6) and (2.7) gives the Poisson–Boltzmann equation for a planer surface,

$$\frac{\mathrm{d}^2\psi}{\mathrm{d}x^2} = \frac{2n_0 Ze}{\varepsilon_0\varepsilon_\mathrm{r}} \sinh\left[\frac{Ze\psi(x)}{kT}\right]. \tag{2.8}$$

ε_r is the permittivity (dielectric constant); 78.6 for water at 25 °C. ε_0 is the permittivity of free space (8.854×10^{-12} F m^{-1}) and n_0 is the number of ions per unit volume of each type present in bulk solution.

Equation (2.8) can be solved by considering the boundary condition: at $x = 0$, $\psi(x) = \psi_0$ and at $x = \infty$, $\psi(x) = 0$ and $\mathrm{d}\psi(x)/\mathrm{d}x = 0$.

For small potentials ($\psi(x) < 25$ mV), $Ze\psi(x)/kT < 1$ and $\sinh x \approx x$ so that equation (2.8) becomes.

$$\frac{\mathrm{d}^2\psi}{\mathrm{d}x^2} \approx \frac{2n_0(Ze)^2}{\varepsilon_0\varepsilon_\mathrm{r}kT}\psi(x). \tag{2.9}$$

Equation (2.9) is the well-known Debye–Huckel approximation whose solution is,

$$\psi = \psi_0 \exp -(\kappa x) \tag{2.10}$$

Note that when $x = 1/\kappa$, $\psi_x = \psi_0/e$; $1/\kappa$ is referred to as the "thickness" of the double layer.

The double layer extension depends on electrolyte concentration and valency of the counterions,

$$\left(\frac{1}{\kappa}\right) = \left(\frac{\varepsilon_\mathrm{r}\varepsilon_0 kT}{2n_0 Z_i^2 e^2}\right). \tag{2.11}$$

The double layer extension increases with decreasing electrolyte concentration. It also depends on the valency of the ions. An expression for $(1/\kappa)$ in terms of the electrolyte ionic strength I is,

$$\left(\frac{1}{\kappa}\right) = \left(\frac{\varepsilon_\mathrm{r}\varepsilon_0 RT}{2000\,\mathrm{F}^2}\right)^{1/2} I^{-1/2} \text{ in m}^{-1} = 0.304 I^{-1/2} \text{ in nm}, \tag{2.12}$$

where

$$I = \sum c_i Z_i^2. \tag{2.13}$$

c_i is the electrolyte concentration in mol dm^{-3}.

Increasing the ionic strength causes a decrease in $(1/\kappa)$, that is referred to as compression of the double layer. The distance $(1/\kappa)$ is referred to as the thickness of the double layer. For example, for KCl in water at 25 °C, $(1/\kappa) = 96.17$ nm at $I = 10^{-5}$ mol dm^{-3}, decreasing to 3.04 nm at $I = 10^{-2}$ mol dm^{-3}. Approximate values of $(1/\kappa)$ for KCl are given in Tab. 2.2.

Tab. 2.2: Approximate values of $(1/\kappa)$ for 1 : 1 electrolyte (KCl).

C (mol dm^{-3})	10^{-5}	10^{-4}	10^{-3}	10^{-2}	10^{-1}
$(1/\kappa)$ (nm)	100	33	10	3.3	1

Equations (2.12) and (2.13) show that $(1/\kappa)$ depends on the valency of the counter- and co-ions. Fig. 2.6 shows the variation of $(1/\kappa)$ with c_i for various electrolytes with different valences of both ions.

At higher potentials (> 25 mV) the solution to equation (2.8) results in,

$$\psi(x) = \frac{2kT}{Ze} \ln\left[\frac{1 + \exp(-\kappa x)\tanh\left(\frac{Ze\psi_0}{4kT}\right)}{1 - \exp(-\kappa x)\tanh\left(\frac{Ze\psi_0}{4kT}\right)}\right]. \tag{2.14}$$

For the case of sufficiently high potential such that $\tanh(x) \approx 1$ at $x \gg 1$ then $\exp(-\kappa x)$ is small and hence at long distances equation (2.14) reduces to,

$$\psi(x) \approx \frac{4kT}{Ze} \tanh\left(\frac{Ze\psi_0}{4kT}\right) \exp(-\kappa x). \tag{2.15}$$

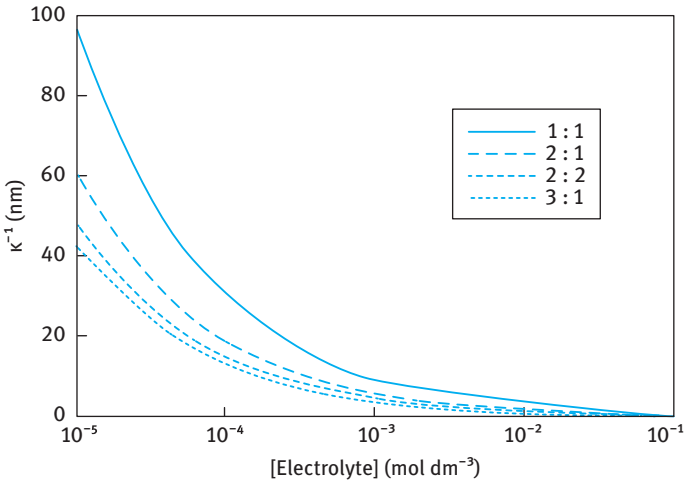

Fig. 2.6: Variation of double layer extension with electrolyte concentration for various valences of ions.

The charge per unit area on the surface σ_0 (surface charge density) must balance that in adjacent solution,

$$\sigma_0 = -\int_0^\infty \rho \, \mathrm{d}x. \tag{2.16}$$

Using equation (2.7),

$$\sigma_0 = \varepsilon_r \varepsilon_0 \int_0^\infty \frac{\mathrm{d}^2\psi}{\mathrm{d}x^2} \, \mathrm{d}x = -\varepsilon_r \varepsilon_0 \left(\frac{\mathrm{d}\psi}{\mathrm{d}x}\right)_{x=0}. \tag{2.17}$$

For symmetrical electrolytes,

$$\frac{\mathrm{d}\psi}{\mathrm{d}x} = -\frac{2\kappa kT}{Ze} \sinh \frac{Ze\psi}{2kT}. \tag{2.18}$$

Combining equations (2.6), (2.17) and (2.18),

$$\sigma_0 = \frac{4n_0 Ze}{\kappa} \sinh \frac{Ze\psi_0}{2kT} = 11.74c^{1/2} \sinh(19.46Z\psi_0) \text{ in } \mu\text{C cm}^{-2} \tag{2.19}$$

for ψ_0 and c in mol dm^{-3}.

For unsymmetrical electrolytes,

$$\sigma_0 = \left\{ 2\varepsilon_r \varepsilon_0 kT \sum_i n_i \left[\exp\left(-\frac{Z_i e\psi_0}{kT} \right) - 1 \right] \right\}^{1/2}. \tag{2.20}$$

For very small potentials,

$$\sigma_0 = \varepsilon_r \varepsilon_0 \kappa \psi_0. \tag{2.21}$$

For spherical particles, the solution of the Poisson–Boltzmann equation (2.8) is only possible at low potentials (i.e. when using the Debye–Huckel approximation). In this case it is usual to use polar coordinates instead of Cartesian coordinates that are used for planer surfaces. The solution of equation (2.8) for a symmetrical electrolyte is,

$$\frac{1}{r^2} \frac{\partial}{\partial r} r^2 \frac{\partial \psi(r)}{\partial r} = \frac{2Zen_0}{\varepsilon_0 \varepsilon_r} \sinh\left[\frac{Ze\psi(r)}{kT} \right], \tag{2.22}$$

where r is the distance from the centre of the particles.

Using the Debye–Huckel approximation, one obtains the diffuse double layer potential $\psi(r)$ as a function of distance for particles with radius a,

$$\psi(r) = \psi_0 \frac{a}{r} \exp[-\kappa(r = a)]. \tag{2.23}$$

The surface charge σ_0 is given by,

$$\sigma_0 = \frac{\varepsilon_0 \varepsilon_r \psi_0 (1 + \kappa a)}{a}. \tag{2.24}$$

For potentials > 25 mV, numerical solutions are available [8, 9].

2.3.2 Stern–Grahame model of the double layer

Stern [6] recognized that the assumption in the Gouy–Chapman theory [4, 5], that the electrolyte ions are regarded as point charges, is unsatisfactory. Also the assumption that the solvent can be treated as a structureless dielectric of constant permittivity is also unsatisfactory. He then introduced the concept of the nondiffuse part of the double layer for specifically adsorbed ions, the rest being diffuse in nature. This is schematically illustrated in Fig. 2.7.

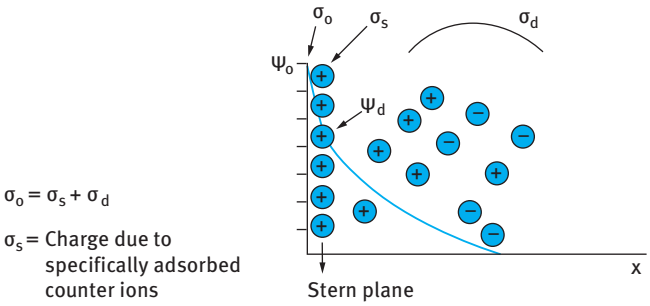

Fig. 2.7: Schematic representation of the double layer according to Stern and Grahame.

The potential drops linearly in the Stern region and then exponentially. Grahame [7] distinguished two types of ions in the Stern plane, physically adsorbed counterions (outer Helmholtz plane – OHP) and chemically adsorbed ions (that lose part of their hydration shell) (inner Helmholtz plane – IHP). The outer Helmholtz plane is considered as the plane of closest approach of hydrated counterions, i.e. the Stern plane. The inner Helmholtz plane is that of specifically adsorbed counterions which may have lost part or their complete hydration shell. The number of these specifically adsorbed ions may exceed the number of surface charges causing a reversal of the sign of the potential as is illustrated in Fig. 2.8 for a positively charged surface with specifically adsorbed anions.

For the specifically adsorbed ions the range of interaction is short, i.e. these ions must reside at the distance of closest approach, possibly within the hydration shell. For the indifferent ions the situation is different and these ions are subjected to an attractive (for the counterions) or repulsive (for the co-ions) potential (energy = $\pm ZF\psi(x)/RT$). The space charge density due to these ions is high near the surface and decreases gradually with distance to its bulk value. Such a layer is the diffuse double layer described by Gouy–Chapman [4, 5]. Generally speaking, a double layer contains a part that is specifically adsorbed and a diffuse part. Because of the finite size of the counterions there is always a charge-free layer near the surface.

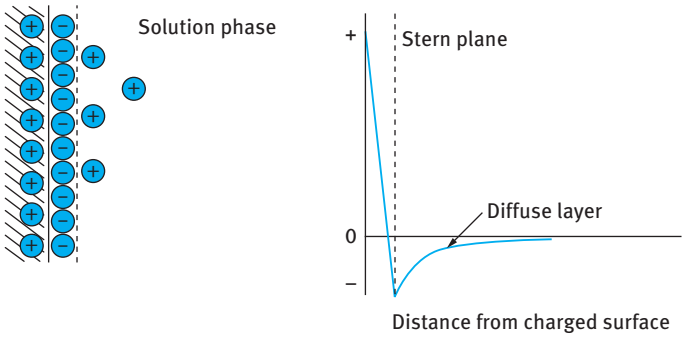

Fig. 2.8: Schematic representation of charge reversal by specifically adsorbed counterions.

A good example to illustrate the role of specific adsorption of the counterions is that of a negative silica surface in the presence of three counterions, namely Li^+, Ca^{2+} and Al^{3+}. This is shown in Fig. 2.9.

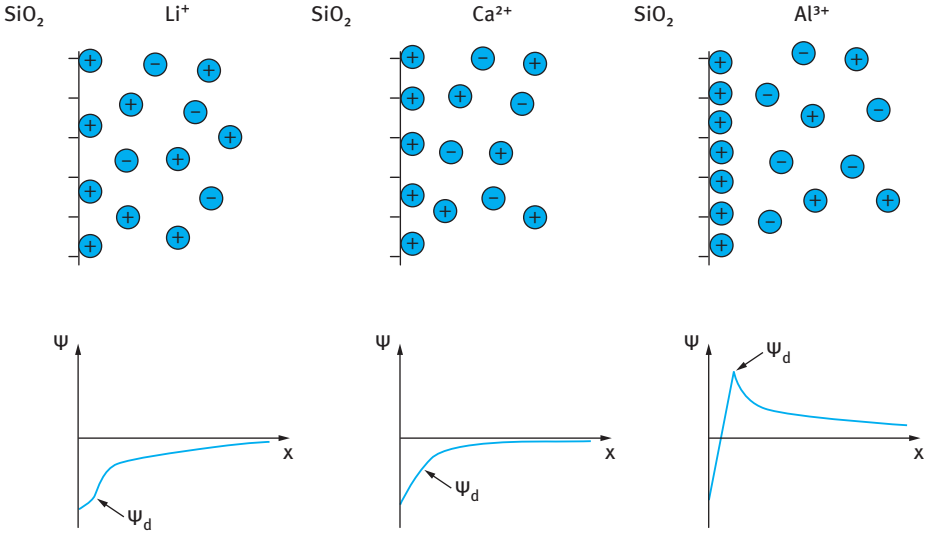

Fig. 2.9: Influence of the nature of counterion on the interaction with a negative silica surface.

The strongly hydrated Li^+ ion is weakly attached to the negative silica surface and is probably located in the OHP. The potential-distance curve shows the location of the Stern potential ψ_d. The bivalent Ca^{2+} ion is more strongly attached and is located closer to the surface in the Stern plane. In contrast, the trivalent Al^{3+} ion is more strongly adsorbed causing charge reversal with ψ_d becoming positive.

Stern [6] considered the first layer of adsorbed ions to interact specifically with the surface through a specific chemical adsorption potential θ. In this picture, the distance of closest approach to the surface is x_1 so that the region $0 \leq x < x_1$ is free of charge. The diffuse part of the double layer starts at a distance x_2 from the surface and for $x > x_2$ the specific interaction forces are negligible. The number of ions in the region $x_1 \leq x < x_2$ can be calculated using a Langmuir isotherm, modified by the incorporation of a Boltzmann factor.

At equilibrium, the number of ions entering the adsorbed layer is equal to the number leaving in unit time. The number entering, n_{ads}, is proportional to the mole fraction of these ions in the bulk, x^{s}, and the area available for adsorption,

$$n_{\text{ads}} = k_1 x^{\text{s}} (N_1 - n_i), \tag{2.25}$$

where k_1 is the rate constant for the adsorption process, N_1 is the total number of adsorption sites and n_i is the number of sites already occupied by adsorbed ions.

The number of ions leaving the adsorbed layer, n_{des}, is given by,

$$n_{\text{des}} = k_2 n_i, \tag{2.26}$$

where k_2 is the rate constant for desorption.

The equilibrium constant for adsorption $K = k_1/k_2$ and from the second law of thermodynamics, the standard free energy of adsorption per ion, ΔG^0_{ads}, is given by,

$$\Delta G^0_{\text{ads}} = -kT \ln K = -kT \ln \frac{k_1}{k_2} \tag{2.27}$$

Combining equations (2.25)–(2.27), the number of adsorbed ions in the Stern layer is given by,

$$n_i = \frac{x^{\text{s}} N_1 \left(\frac{k_1}{k_2}\right)}{1 + x^{\text{s}} \left(\frac{k_1}{k_2}\right)}, \tag{2.28}$$

and the surface charge density, σ_i, is given by,

$$\sigma_i = Z_i e n_i = \frac{Z_i e x^{\text{s}} \exp\left(\frac{-\Delta G^0_{\text{ads}}}{kT}\right)}{1 + x^{\text{s}} \exp\left(\frac{-\Delta G^0_{\text{ads}}}{kT}\right)}. \tag{2.29}$$

Allowing for the possibility of adsorption of both positive and negative ions and expressing $\exp(-\Delta G^0_{\text{ads}}/kT)$ as b, one obtains the following expression for σ_i,

$$\sigma_i = \frac{Z_i e N_1 x^{\text{s}} (b_+ - b_-)}{1 + (b_+ - b_-) x^{\text{s}}}. \tag{2.30}$$

Stern [6] considered the free energy of adsorption to be made up of an electrical contribution, $Z_i e \psi_i$, and a chemical contribution, θ_i. If the specific adsorption is confined to one ion type, then equation (2.30) simplifies to,

$$\sigma_i = Z_{\pm} e N_1 x^{\text{s}} \exp\left[-\frac{(Z_{\pm} e \psi_i + \theta_{\pm})}{kT}\right]. \tag{2.31}$$

2.3.3 Capacitance of the double layer

The dielectric displacement D (assumed to be continuous) in the inner region, $0 < x < x_1$, is given by,

$$D = \varepsilon_1 \varepsilon_0 E = -\varepsilon_1 \varepsilon_0 \frac{\mathrm{d}\psi}{\mathrm{d}x}, \tag{2.32}$$

where ε_1 is the relative permittivity in the inner region and E is the field strength. For $x = 0$, this quantity is equal to the surface charge as defined by equation (2.17).

Integration of equation (2.17) gives,

$$\psi_0 - \psi_i = \frac{\sigma_0 x_1}{\varepsilon_1 \varepsilon_0}. \tag{2.33}$$

Applying the same procedure to the region $x_1 < x < x_2$ (the diffuse part of the double layer),

$$\psi_i - \psi_\mathrm{d} = -\frac{\sigma_d}{\varepsilon_2 \varepsilon_0}(x_2 - x_1). \tag{2.34}$$

The above procedure amounts to treating the inner and diffuse layers as molecular capacitors, characterized by sharp changes of permittivity between successive pairs of plates. The principal effect of introducing the Stern layer is to lower the overall capacitance of the interfacial region, C_T, since the Stern and diffuse layers are in series,

$$\frac{1}{C_\mathrm{T}} = \frac{1}{C_\mathrm{inner}} + \frac{1}{C_\mathrm{diffuse}} \tag{2.35}$$

The diffuse layer capacitance is given by the following expression,

$$C_\mathrm{diffuse} = \frac{\mathrm{d}\sigma_d}{\mathrm{d}\psi_\mathrm{d}} = 228.5 Z c^{1/2} \cosh(19.46 Z \psi_\mathrm{d})\,\mu\mathrm{F\,cm^{-2}}, \tag{2.36}$$

in water at 25 °C, for c in mol dm^{-3} and ψ_d in volts.

Equation (2.36) shows that C_diffuse is very large, except when ψ_d and/or c are very small. This means that C_diffuse does not contribute effectively to C_T. For very dilute solutions near the point of zero charge (pzc), the measured capacitance approaches that given by equation (2.36). However, at higher concentrations and away from the pzc, the much lower value attributable to C_inner is observed. Measurements at the dropping mercury electrode suggest a value for C_inner in aqueous solution in the range 16–30 μF cm^{-2} [7] depending on the metal charge. For a simple molecular condenser this means a value of $x_1/\varepsilon_1\varepsilon_0 \approx 25$ pm in equation (2.33) and $x_2/\varepsilon_2\varepsilon_0 \approx 60$ pm in equation (2.34). This corresponds to values of $x_1 = 0.15$ nm and $\varepsilon_1 = 6$ for the inner Helmholtz plane and $x_2 = 0.6$ nm and $\varepsilon_2 = 20$ for the outer Helmholtz plane.

The difference between ε_1 and ε_2 is due to the very higher field strength in the inner layer when compared to that in the outer layer. The potential drop in the inner layer is often 0.1–1 V and since this occurs across a distance of less than 1 nm the field strengths are $\approx 10^8$–10^9 V m^{-1}. Such high field strengths cause considerable dipole orientation with a consequent reduction in permittivity and a value of $\varepsilon_1 \approx 6$ is assigned

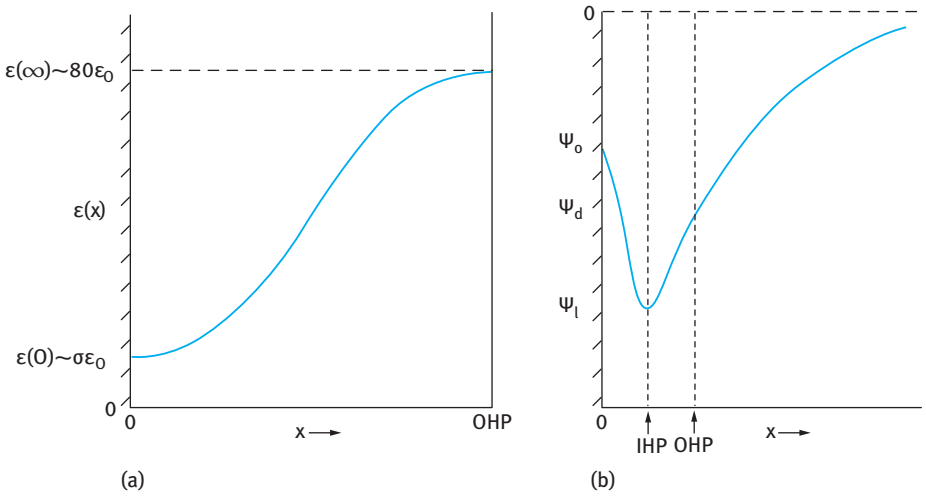

Fig. 2.10: Variation of permittivity (a) and potential (b) with distance for the inner and outer Helmholtz planes.

for the inner region. For the outer region with a thickness >1 nm, the field strength is lower and a somewhat lower level of water organization ε_2 is assigned values in the region of ≈ 20–40. A schematic representation of the variation of permittivity and potential with distance x from the surface is shown in Fig. 2.10.

The specific adsorption of ions in the inner region is described in terms of the discreteness of charge effect as first recognized by Frumkin [10]. The phenomenon is described as the Esin and Markov effect [11] and it refers to the fact that the point of zero charge of the mercury/solution interface, when measured against a reference electrode with liquid junction, depends on electrolyte concentration if the electrolyte is specifically adsorbed. An analogous procedure can be used in colloidal systems [12]. The importance of the discreteness of charge effect can explain a wide variety of effects that cannot be explained using the simple version of the Gouy–Chapman–Stern theory. It also explains the fact that anion-specific adsorption can cause the negative potential of the OHP to pass through a maximum value as the potential ψ_0 is made increasingly negative.

2.4 Double layer investigation

One of the earliest studies of the double layer was carried out using the mercury/electrolyte interface [7]. In the majority of colloidal systems the dispersed particles are insulating and to develop models of ion distribution one needs to use a conducting metal/solution interface. The dropping mercury electrode in aqueous electrolyte represents a model metal/electrolyte system. The interface between liquid mercury

and electrolyte solution is atomically smooth and continual renewal of the surface minimizes contamination. In addition, the mercury/aqueous electrolyte interface is ideally polarizable, i.e. charge carriers are not transferred across the interface, over a wide range of potential differences [13].

The most common method for investigating double layers in disperse systems is to use titration techniques that can be applied to obtain the surface charge as a function of surface potential at different electrolyte concentrations and types. The first established example of such a procedure was obtained using silver iodide sols since the charge determining mechanism is well established. Both stable positive and negative sols can be made and the material is rather inert and insoluble and not particularly sensitive to light. In addition, Ag/AgI electrodes are very stable and the sol can be titrated with Ag^+ and I^- ions while measuring the pAg and pI. Using material balance one can determine the surface concentration of Ag^+ and I^- ions and this allows one to calculate the surface charge σ_0 using equation (2.1). In order to obtain the surface charge per unit area of the interface one needs to know the specific surface area of the AgI sol. The most appropriate procedure for determining the surface area is to measure the expulsion of the co-ions from the increase in its concentration in solution. This is referred to as negative adsorption. The surface potential at each point of titration can be calculated by application of the Nernst equation (2.2). This requires knowledge of the point of zero charge and this can be located from the intersection point of the titration curves at various electrolyte concentrations (in absence of any specific adsorption). One of the earliest set of charge-pAg (or ψ_0) curves for AgI in 1 : 1 electrolytes was obtained by Verwey [14] and de Bruyn [15] as illustrated by Lyklema [16]. This is shown in Fig. 2.11.

To the negative side, σ_0 becomes more negative, and on the positive side it becomes more positive as the electrolyte concentration increases. This is due to better screening of the charge with increasing C_{salt}. However, the increase is far less than predicted by the diffuse double layer theory.

The titration method was successfully applied for double layer investigations on oxides. σ_0 can be directly determined by titration of an oxide suspension in an aqueous solution of indifferent electrolyte (e.g. KCl) using a cell of the type,

$$E_1 \mid \text{oxide suspension} \mid E_2,$$

where E_1 is an electrode reversible to H^+ and OH^- ions, such as a glass electrode, and E_2 is a reference electrode such as Ag–AgCl. A known mass m of solid oxide with a specific surface area A ($m^2\,g^{-1}$) is added to a known volume V of electrolyte solution such as KCl or KNO_3 (assuming there is no specific adsorption of ions) of known concentration (e.g. 10^{-2} mol dm^{-3} KCl or KNO_3) [17] . The initial pH (called pH_0) is noted and the sample is titrated with, say, 10^{-2} mol dm^{-3} NaOH and the volume required to achieve each solution pH might be as shown in Fig. 2.12. A suitable time must elapse after each addition to establish equilibrium with the surface. If on the same diagram one superimposes the titration curve for V ml of KCl or KNO_3 alone, the volume v_1

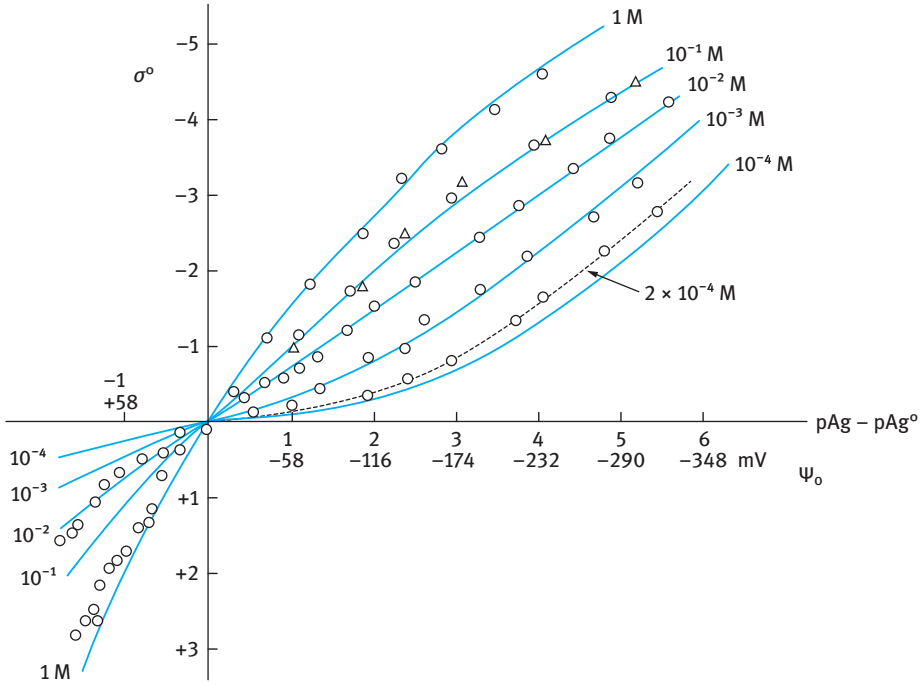

Fig. 2.11: Surface charge–pAg (or ψ_0) for AgI at various 1 : 1 electrolyte concentrations.

(in cm^3) corresponds to the amount of base taken up by the oxide in order to establish equilibrium with a solution of pH = pH_1. The net increase in negative surface charge per unit area is given by,

$$-(\Gamma_+ - \Gamma_-) = \frac{10^{-5} v_1}{mA} \tag{2.37}$$

The quantity obtained from equation (2.37) is the relative amount of OH^- adsorbed at pH_1. If this calculation is repeated for all pH > pH_0 and the comparable data for acid titration are also obtained, a plot of relative charge versus pH can be constructed at various KCl or KNO_3 concentrations as is illustrated in Fig. 2.13 (a). The point at which all three isotherms cross one another can be identified as the pzc because only at that point is the surface charge independent of the supporting electrolyte concentration (assuming there is no specific adsorption). Fig. 2.13 (a) can then be redrawn as 2.13 (b) to give the absolute value of σ_0. This procedure amounts to finding the point at which the Esin–Markovic coefficient β [11] is zero [18],

$$\beta = \left(\frac{\partial \sigma_0}{\partial \mu_s}\right)_{\psi_0} = \left(\frac{\partial \sigma_0}{\partial \mu_s}\right)_{a_i}, \tag{2.38}$$

where a_i is the activity of potential determining ion.

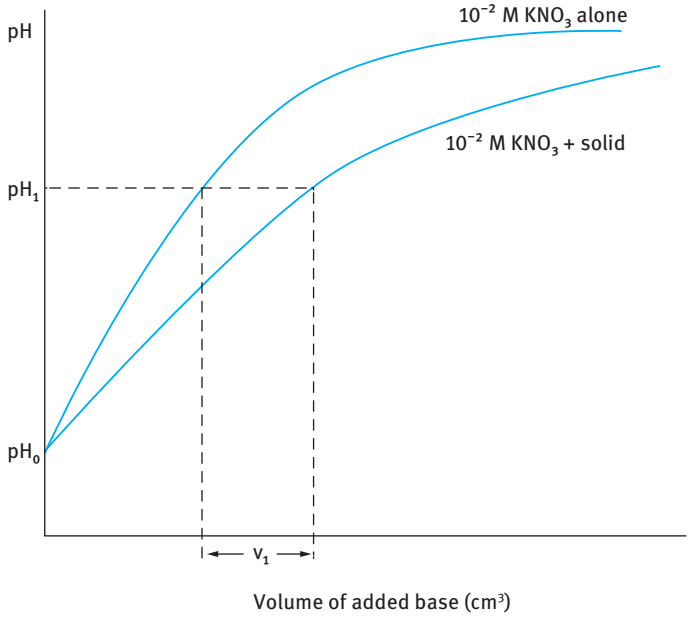

Fig. 2.12: Schematic illustration of potentiometric titration to obtain the surface charge.

The determination of the surface charge density σ_0 (μC cm^{-2}) requires accurate determination of the specific surface area A. The particles are usually irregular in shape and they may undergo Ostwald ripening on standing. This causes problems for determining A from average particle size obtained say by electron microscopy. In addition, most oxide particles are not smooth and this may underestimate the area obtained using gas adsorption and application of the BET equation. Measurement of the surface area using dye adsorption requires knowledge of the effective cross-sectional area of the dye molecule and this may vary from one substrate to another. An appropriate method for measuring the surface area is to measure the expulsion of the co-ions from the increase in their concentration in solution, referred to as negative adsorption [19].

As an illustration, Fig. 2.14 shows the results of σ_0–pH curves for homodisperse haematite sols in the three concentrations of KCl (that is not specifically adsorbed) [20].

It can be seen that at low pH, σ_0 becomes more positive with increasing KCl concentration, whereas at high pH it becomes more negative. At one particular pH (pH = 9.1) σ_0 is independent of KCl concentration. At this pH, $\Gamma_H^+ = \Gamma_{OH}^-$ and this defines the pzc. At pH < pzc, σ_0 is positive since $\Gamma_H^+ > \Gamma_{OH}^-$, whereas at pH > pzc, σ_0 is negative since $\Gamma_H^+ < \Gamma_{OH}^-$.

Most oxides show similar behaviour to that shown in Fig. 2.14. However, this is not the case with precipitated silica which shows different trends as illustrated in Fig. 2.15, where σ_0 is plotted versus pH at four different KCl concentrations [21].

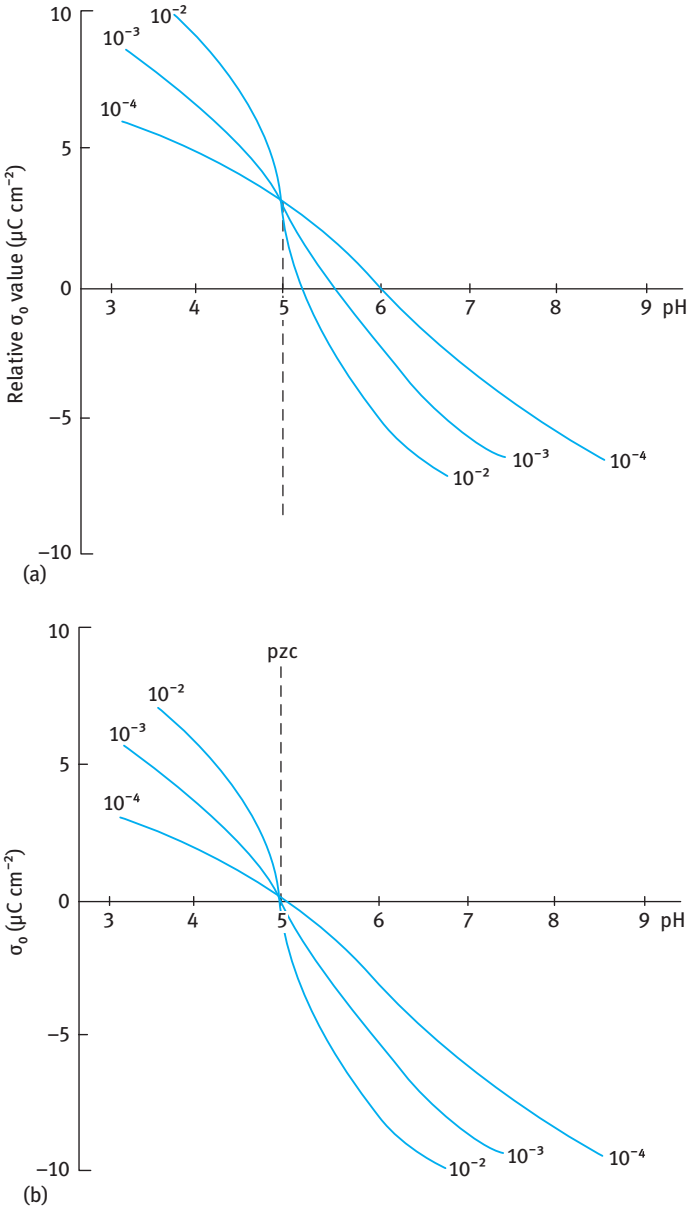

Fig. 2.13: Relative surface charge–pH curves (a) and absolute charge–pH curves (b).

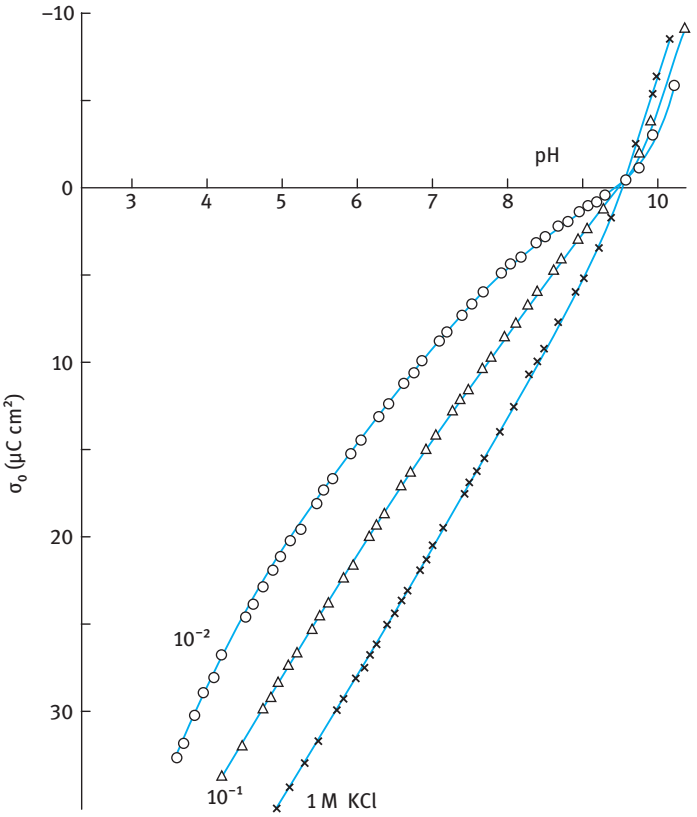

Fig. 2.14: σ_0–pH curves for homodisperse hematite sols in three KCl concentrations.

There is a common intersection point at $pH \approx 3$, i.e. the pzc, indicating absence of specific adsorption of K^+ or Cl^- ions. The charge increases progressively with increasing pH reaching very high values at high pH and electrolyte concentrations. This high surface charge was accounted for by assuming the presence of a porous gel layer on the precipitated silica particles [22]. The basic idea is that H^+ and OH^- ions could penetrate the surface layers of the oxide and react there with amphoteric –OH groups. In this way quite large amounts of surface charge could develop whilst retaining a reasonable separation between the charged groups. At the same time, if counterions are permitted to enter this porous layer, the net electrical potential at the outer edge of the porous layer would be considerably reduced in magnitude.

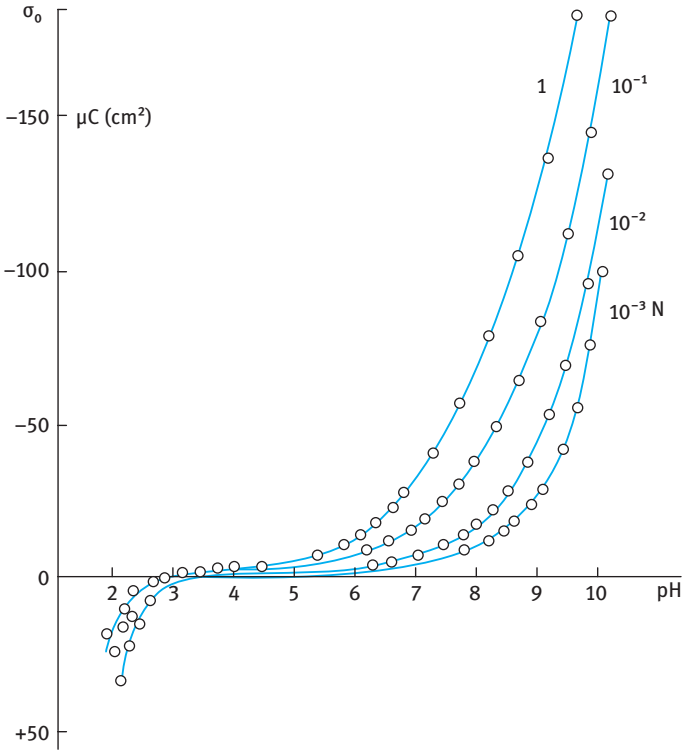

Fig. 2.15: σ_0 versus pH at four different KCl concentrations.

References

[1] Lyklema J. Structure of the solid/liquid interface and the electrical double layer. In: Tadros TF, editor. Solid/liquid dispersions. London: Academic Press; 1987.
[2] Goodwin JW. Colloids and interfaces with surfactants and polymers. London: John Wiley and Sons; 2009.
[3] Tadros T. Dispersions of powders in liquids and stabilisation of suspensions. Weinheim: Wiley-VCH; 2012.
[4] Gouy G. J Phys. 1910;9:457; Ann Phys. 1917;7:129.
[5] Chapman DL. Phil Mag. 1913;25:475.
[6] Stern O. Z Electrochem. 1924;30:508.
[7] Grahame DC. Chem Rev. 1947;41;441.
[8] Loeb AL, Overbeek JTG, Wiersema PH. The electrical double layer around a spherical colloidal particle. Cambridge, MA, USA: MIT Press; 1961.
[9] Ohshima H, Healy TW, White LR. J Colloid Interface Sci. 1982;89:446.
[10] Frumkin AN. Phys Zhur Soviet Union. 1933;4:256.
[11] Esin OA, Markov BF. Zhur Fiz Khim. 1939;13:318.
[12] Lyklema J. J Electroanal Chem. 1972;37:53.
[13] Riley J. In: Cosgrove T, editor. Colloid science. Oxford: Blackwell; 2005.
[14] Verwey EJW. Rec Trav Chim. 1941;60:887.

[15] de Bruyn H. Rec Trav Chim. 1942;61(3):189.
[16] Lyklema J. Fundamentals of interface and colloid science. London: Academic Press; 1995.
[17] Hunter RJ. Zeta potential in colloid science. London: Academic Press; 1981.
[18] Lyklema J. In: Bockris JO'M, Rand DAJ, Welch BJ, editors. Trends in Electrochemistry. New York: Plenum Publishing Corp.; 1977.
[19] Ven den Hul HJ, Lyklema J. J Colloid Sci. 1967;23:500.
[20] Penners NHG. The preparation and stability of monodisperse colloidal haematite (α-Fe_2O_3). PhD thesis. Agricultural University, Wageningen, Netherlands.
[21] Tadros TF, Lyklema J. J Electroanal Chem. 1968;17:267.
[22] Lyklema J. J Electroanal Chem. 1968;18:341.

3 Electrokinetic phenomena and zeta potential

3.1 Introduction

As mentioned in Chapter 2, one of the main characteristics of the electrical double layer is the surface potential ψ_0 which, as will be discussed in Chapter 4, determines the magnitude of the double layer repulsion. Measurement of ψ_0 is only possible for colloidal systems that can be titrated with potential determining ions, such as AgI and oxides. With most colloidal systems that are stabilized by adsorption of surfactant ions this titration procedure is not possible. An indirect method of obtaining information on the surface potential is to apply electrokinetic methods that can be used to obtain the zeta potential that is closely related to ψ_0. As we will see below, ζ can be equated to ψ_0 in particular in the absence of specific adsorption of counterions. In practice, ζ is used in place of ψ_0 for calculating the double layer repulsion.

3.2 Charge separation at interfaces and various electrokinetic effects

Electrokinetic effects are the direct result of charge separation at the interface between two phases I and II. When one of the phases is a polar liquid like water, its dipolar molecules will tend to be oriented in a particular direction at the interface [1] and this will generate a potential difference. If there are ions or excess electrons in one or both of the phases, or ionogenic groups, there will be a tendency for the electric charges to distribute themselves in a non-uniform way at the interface. This results in the formation of an electrical double layer as discussed in detail in Chapter 2. For the present discussion, we need only to simply describe the region between two adjoining surfaces as a simple charge separation with the region near phase I having an excess charge of one sign and the balancing charge being distributed in some way through the adjoining surface regions of phase II. This is illustrated in Fig. 3.1.

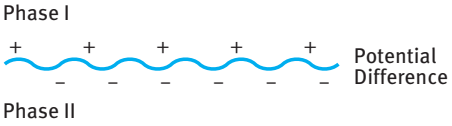

Fig. 3.1: Schematic representation of charge separation at an interface.

https://doi.org/10.1515/9783110540895-004

If the surface of phase I is positively charged, its electrostatic potential will be positive with respect to the bulk phase II. If phase II is a liquid containing ions, then as one moves into phase II, the potential will decreases more or less regularly until it becomes constant in the bulk liquid far from the surface phase I. For aqueous systems, "far from" means a distance greater than 5–200 nm depending on electrolyte concentration.

Consider a negatively charged surface; positive ions (counterions) are attracted to the surface, whereas negative ions (co-ions) are repelled. This is schematically shown in Fig. 3.2. If the surface of phase I is negatively charged, its electrostatic potential will be negative relative to the bulk of phase II. If phase II is a liquid containing dissolved ions, the potential will decrease more or less regularly, until it becomes constant in bulk liquid far from the surface of phase I. As mentioned above, the constant potential is usually reached at a distance in the region of 5–200 nm, depending on electrolyte concentration. In most colloid systems the point *p* shown in Fig. 3.2 is at a distance of about 1–50 nm from the surface.

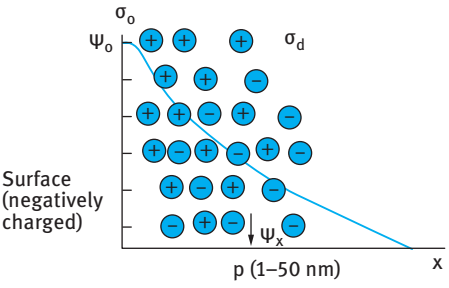

Fig. 3.2: Schematic representation of charge accumulation at an interface.

The accumulation of excess positive ions causes a gradual reduction in the potential from its value ψ_0 at the surface to 0 in bulk solution. At the point p from the surface, one can define a potential ψ_x. As we will see later, the zeta potential is taken at the point of the "shear plane" (which is an imaginary plane from the particle surface at which one of the phases move tangentially past the second phase). The region where the liquid has a negative electrostatic potential will accumulate an excess of positive ions (counterions) and repel negative ions of the electrolyte (co-ions). It is this excess of positive ions that gradually lowers the electrostatic potential (and the electric field) to zero in bulk solution. The arrangement of negative charges on the surface of phase I and the charges in phase II (counterions and co-ions) is referred to as the electrical double layer at the interface as discussed in detail in Chapter 2.

Electrokinetic effects arise when one of the two phases is caused to move tangentially past the second phase. The tangential motion can be caused by electric field, forcing a liquid in a capillary, forcing a liquid in a plug of particles or by gravitational field on the particles. This leads to four different types of electrokinetic phenomena.

3.2.1 Electrophoresis

In electrophoresis, the movement of one phase is induced by the application of an electric field (with a field strength E/l (V m^{-1}), where E is the potential difference applied and l is the distance between the two electrodes. This is schematically illustrated in Fig. 3.3.

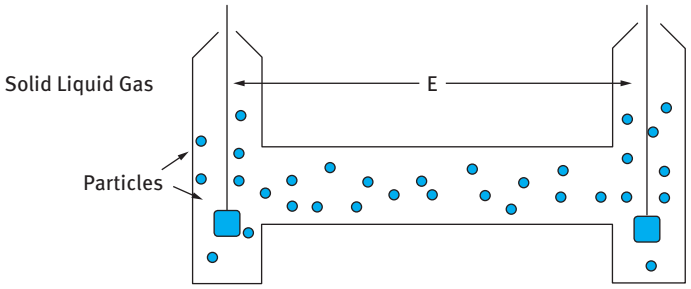

Fig. 3.3: Schematic set-up for electrophoresis.

In electrophoresis, a fluid moves with respect to a solid, liquid or gas surface, i.e. movement of one phase induced by application of an external electric field. One measures the particle velocity v (m s^{-1}) of the particles, droplets or air bubbles from which the electrophoretic mobility u (velocity divided by field strength) can be calculated,

$$u = \frac{v}{(E/l)}\ \mathrm{m^2\ V^{-1}\ s^{-1}}, \tag{3.1}$$

where E is the applied potential and l is the distance between the two electrodes; E/l is the field strength. For example, if the surface charge on the capillary surface is negative, the counterions, which are positive, will move towards the cathode.

3.2.2 Electro-osmosis

In this case, the solid is kept stationary (e.g. a capillary or porous plug), whereas the liquid is allowed to move under the influence of an electric field. The electric field acts on the charges (ions) in the liquid. When these move, they drag liquid with them; one observes movement of the liquid along the capillary from one electrode to the other. For example, if the surface charge on the capillary surface is negative, the counterions, which are positive, will move towards the cathode. Measurement of the velocity of the liquid, or the volume of the liquid transported per unit current flow, gives information on the net surface charge or the electrical potential in the neighbourhood of the wall.

3.2.3 Streaming potential

The liquid is forced through a capillary or a porous plug (containing the particles) under the influence of a pressure gradient. The excess charges near the wall (or the surface of particles in the plug) are carried along by the liquid flow, thus producing an electric field that can be measured by using electrodes and an electrometer.

3.2.4 Sedimentation potential (Dorn effect)

Particles (in a suspension) or droplets (in an emulsion) or gas bubbles in a foam are allowed to settle or rise under the influence of gravity or a centrifugal field. When the particles move (up or down depending on the density difference between the particles and medium), they leave behind their ionic atmosphere. A potential difference (sedimentation potential) develops in the direction of motion. If two electrodes are placed in the sedimentation tube, one can measure a potential difference as a result of charge separation. This is schematically shown in Fig. 3.4.

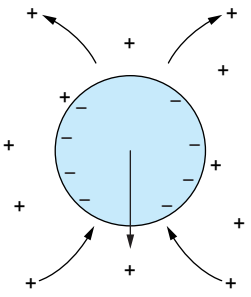

Fig. 3.4: Schematic representation of the current flow which generates the sedimentation potential.

3.3 The surface of shear and the zeta potential

In all electrokinetic phenomena [1], a fluid moves with respect to a solid surface. One needs to derive a relationship between fluid velocity (which varies with distance from the solid) and the electric field in the interfacial region. The main problem in any analysis of electrokinetic phenomena is defining the plane at which the liquid begins to move past the surface of the particle, droplet or air bubble. This is defined as the "shear plane", which is at some distance from the surface. One usually defines an "imaginary" surface close to the particle surface within which the fluid is stationary. The point just outside this imaginary surface is described as the surface of shear and the potential at this point is described as the zeta potential (ζ). A schematic representation of the surface of shear, the surface and zeta potential is shown in Fig. 3.5.

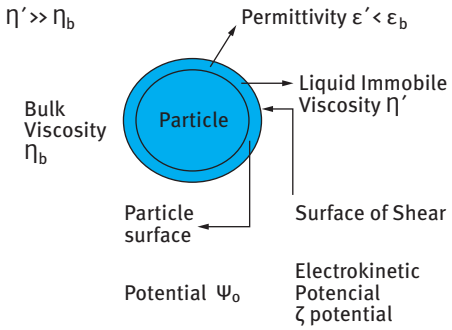

Fig. 3.5: Surface (plane) of shear.

The exact position of the plane of shear is not known; it is usually in the region of few A. In some cases one may equate the shear plane with the Stern plane (the centre of specifically adsorbed ions) although this may be an underestimate of its location. Several layers of liquid may be immobilized at the particle surface (which means that the shear plane is farther apart from the Stern plane). The particle, droplet or air bubble plus its immobile liquid layer form the kinetic unit that moves under the influence of the electric field. The viscosity of the liquid in the immobile sheath around the particles (η') is much larger than the bulk viscosity η. The permittivity of the liquid in this liquid sheath ε' is also lower than the bulk permittivity (due to dielectric saturation in this layer). In the absence of specific adsorption, the assumption is usually made that $\zeta \approx \psi_0$. The latter potential is the value that is commonly used to calculate the repulsive energy between two particles.

3.4 Relationship between zeta potential and potential distribution across the interface

For that purpose it is useful to consider the structure of the electrical double layer. As discussed in Chapter 2, one of the earliest pictures of the double layer is that due to Gouy and Chapman [2, 3], usually referred to as the diffuse double layer concept. In this picture, it was assumed that the charge on the surface is "smeared out" and this charge is compensated by a diffuse layer of counter- and co-ions that extends to a distance from the surface (that depends on electrolyte concentration and valency). A schematic representation of the diffuse double layer for a flat negatively charged surface was shown in Fig. 2.2. In this case the negative surface charge is compensated in bulk solution by unequal distribution of counter- and co-ions (excess counterions and deficit of co-ions).

The surface potential decays exponentially with the distance x from the particle surface. For low potentials ($\psi_0 < 25$ mV), the potential ψ is related to the surface potential ψ_0 by the simple expression,

$$\psi = \psi_0 \exp(-\kappa x), \tag{3.2}$$

where κ is the Debye–Huckel parameter that is related to electrolyte concentration and valency,

$$\kappa^2 = \left(\frac{e^2 \sum n_i^2 z_i^2}{\varepsilon \varepsilon_0 kT} \right), \tag{3.3}$$

where e is the electronic charge, n_i is the number of ions per unit volume, z_i is the valency of each type of ion, ε is the relative permittivity, ε_0 is the permittivity of free space, k is the Boltzmann constant and T is the absolute temperature.

For water at 25 °C,

$$\kappa = 3.88 I^{1/2} \ (\mathrm{nm}^{-1}), \tag{3.4}$$

where I is the ionic strength,

$$I = (1/2) \sum c_i z_i^2, \tag{3.5}$$

where c_i is the concentration of ion i in mol dm^{-3}. Note that the dimension of κ is in reciprocal length and $1/\kappa$ is referred to as the double layer thickness. It is clear from equation (3.2) that when $\kappa = 1/x$, $\psi = \psi_0/e$; $(1/\kappa)$ is referred to as the double layer extension or thickness that depends on c_i and z_i. As an illustration, Tab. 3.1 shows the values of $(1/\kappa)$ for various concentrations of 1 : 1 electrolyte (e.g. NaCl).

Tab. 3.1: Double layer thickness for various concentrations of 1 : 1 electrolyte.

c_i (mol dm^{-3})	$(1/\kappa)$ (nm)
10^{-5}	100
10^{-4}	33
10^{-3}	10
10^{-2}	3.3
10^{-1}	1.0

It can be seen from Tab. 3.1 that as the electrolyte concentration increases, the thickness of the double layer $(1/\kappa)$ decreases. This amounts to compression of the double layer with increasing electrolyte concentration.

As discussed in Chapter 2, Stern [4] introduced the concept of the nondiffuse part of the double layer for specifically adsorbed ions, the rest being diffuse in nature. The potential drops linearly in the Stern region and then exponentially. Grahame [5] distinguished two types of ions in the Stern plane; physically adsorbed counterions,

outer Helmholtz plane, and chemically adsorbed ions (that lose part of their hydration shell), inner Helmholtz plane. The surface potential ψ_0 decays linearly with x until ψ_s (the position of the inner Helmholtz plane) and then ψ_d (the position of the outer Helmholtz plane) and then exponentially with further a decrease in x. One usually equates ψ_d with the zeta potential ζ, although the exact value of ζ cannot be assigned from the above picture since the position of the shear plane is not identified in these double layer theories. Clearly, if there is specific adsorption of counter- or co-ions in the IHP, the above equality is not justified.

A schematic representation of the possible potential and charge distribution at the interface is shown in Fig. 3.6. On oxides, the great majority of counterions (up to 90 %) appear to be between the solid surface and the OHP. With AgI surface, on the other hand, there is usually little or no charge in the IHP in the presence of simple electrolytes like KNO_3.

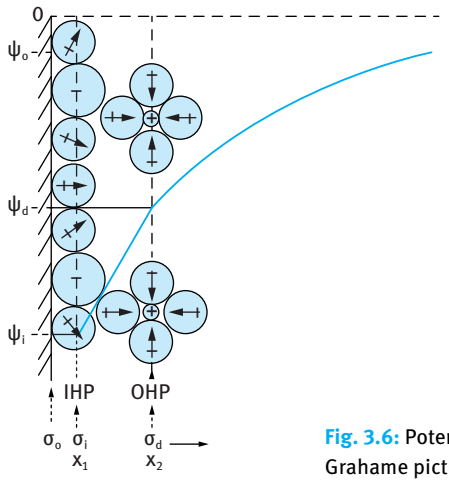

Fig. 3.6: Potential and charge distribution according to Stern–Grahame pictures [4, 5].

Measurement of zeta potential (ζ) is valuable in determining the properties of dispersions. In addition it has many other applications in various fields: electrode kinetics, electro-dialysis, corrosion, adsorption of surfactants and polymers, crystal growth, mineral flotation and particle sedimentation.

Although measurement of particle mobility is fairly simple (particularly with the development of automated instruments), the interpretation of the results is not. The calculation of zeta potential from particle mobility is not straightforward since this depends on the particle size and shape as well as the electrolyte concentration. For simplicity we will assume that the particles are spherical.

3.5 Calculation of zeta potential from particle mobility

3.5.1 Von Smoluchowski (classical) treatment [6]

Von Smoluchowski [6] considered the movement of the liquid adjacent to a flat, charged surface under the influence of an electric field parallel to the surface (i.e. electro-osmotic flow of the liquid). If the surface is negatively charged, there will be a net excess of negative ions in the adjacent liquid and as they move under the influence of the applied field they will draw the liquid along with them. The surface of shear may be taken as a plane parallel to the surface and distance δ from it. The velocity of the liquid in the direction parallel to the wall, v_z, rises from a value of zero at the plane of shear to a maximum value, v_{eo}, at some distance from the wall, after which it remains constant. This is illustrated in Fig. 3.7. v_{eo} is called the electro-osmotic velocity of the liquid. The electrical potential ψ changes from its maximum negative value (ζ) at the shear plane to zero when v_z reaches v_{eo}.

Consider a volume element of area A and thickness dx, as shown in Fig. 3.8. The applied electric force in the z-direction is E_zQ, where E_z is the field strength in the z-direction and Q is the charge density in the volume element that is equal to $\rho A\,\mathrm{d}x$, where ρ is the charge density per unit volume. This electric force is balanced by the hydrodynamic force at the liquid surfaces, i.e.,

$$E_zQ = E_z\rho A\,\mathrm{d}x = \eta_A\left(\frac{\mathrm{d}v_x}{\mathrm{d}x}\right)_x - \eta_A\left(\frac{\mathrm{d}v_x}{\mathrm{d}x}\right)_{x+\mathrm{d}x}. \tag{3.6}$$

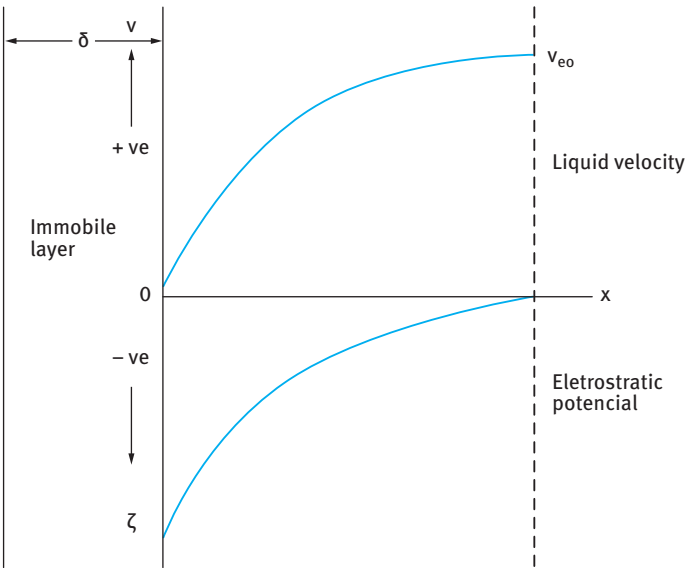

Fig. 3.7: Distribution of electrostatic potential near a charged surface and the resulting electro-osmotic velocity under an applied field.

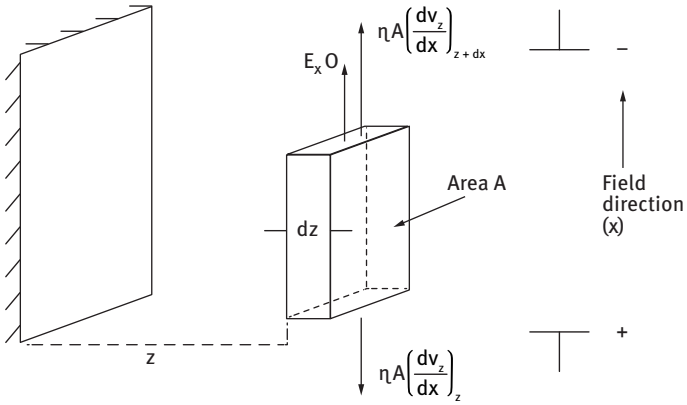

Fig. 3.8: Force on a volume element of a liquid of area A containing charge Q.

Equation (3.6) can be written as,

$$E_z \rho \, \mathrm{d}x = -\eta \left(\frac{\mathrm{d}^2 v_x}{\mathrm{d}x^2} \right) \mathrm{d}x. \tag{3.7}$$

From the Poisson equation,

$$\frac{\mathrm{d}^2 \psi}{\mathrm{d}x^2} = -\frac{\rho}{\varepsilon \varepsilon_0}. \tag{3.8}$$

Combining equations (3.7) and (3.8),

$$E_z \varepsilon \varepsilon \frac{\mathrm{d}^2 \psi}{\mathrm{d}x^2} \, \mathrm{d}x = \eta \frac{\mathrm{d}^2 v_x}{\mathrm{d}x^2} \, \mathrm{d}x. \tag{3.9}$$

Equation (3.9) can be integrated twice from a point from the solid where $\psi = 0$ and $v_z = v_{\mathrm{eo}}$ up to the shear plane where $v_z = 0$ and $\psi = \zeta$, using the fact that for the first integration both $\mathrm{d}\psi/\mathrm{d}x$ and $\mathrm{d}v_x/\mathrm{d}x$ are zero from the surface, i.e.,

$$\frac{v_{\mathrm{eo}}}{E_z} = u_{\mathrm{E}} = -\frac{\varepsilon \varepsilon_0 \zeta}{\eta}, \tag{3.10}$$

where u_{E} is the electro-osmotic mobility. The negative sign indicates that when ζ is negative, the space charge is positive and the liquid flows towards the negative electrode.

In electro-osmotic mobility experiments one usually measures the total volume of liquid transported say in a capillary on application of the electric field. For a capillary with constant cross section with radius r, the volume displaced per unit time, V, is given by,

$$V = \pi r^2 v_{\mathrm{eo}} = \frac{\pi r^2 \varepsilon \varepsilon_0 \zeta E_z}{\eta}. \tag{3.11}$$

The electric current, i, transported by the liquid is given by Ohm's law,

$$\frac{i}{E_z} = \pi r^2 \lambda_0, \tag{3.12}$$

where λ_0 is the electrical conductivity.

Combining equations (3.11) and (3.12),

$$\frac{V}{i} = \frac{\varepsilon \varepsilon_0 \zeta}{\eta \lambda_0}. \tag{3.13}$$

In equation (3.13) the units can be in SI, $\varepsilon_0 = 8.854 \times 10^{-12}\ \mathrm{C\,V^{-1}\,m^{-1}}$, and if ζ is in volts, η in Pa s (N m^{-2} s), V/i is obtained in m^3 C^{-1} or m^3 s^{-1} per ampere of current used.

One may also use mixed units to obtain ζ in mV,

$$\frac{V\ (\mathrm{cm^3\,s^{-1}})}{i\ (\mathrm{mA})} = \frac{8.854 \times 10^{-13} \varepsilon \zeta\ (\mathrm{mV})}{\eta\ (\mathrm{Poise}) \times \lambda_0 (\mathrm{Ohm^{-1}\,cm^{-1}})} \tag{3.14}$$

In equations (3.12)–(3.14), the assumption is made that the current is transported by the bulk liquid, i.e. the contribution from the conductance near the wall or through the solid (surface conductance) is small. However, if the contribution from the surface conductance is significant, the accumulated charge in the double layer may lead to an unusually high conductivity, especially at low electrolyte concentration. In this case, equation (3.12) has to be modified to take into account the surface conductance λ_s,

$$\frac{i}{E_z} = \pi r^2 \lambda_0 + 2\pi r \lambda_s. \tag{3.15}$$

Note that λ_s is in Ohm^{-1}.

Equation (3.13) then becomes,

$$\frac{V}{i} = \frac{\varepsilon_r \varepsilon_0 \zeta}{\eta(\lambda_0 + 2\lambda_s/r)} \tag{3.16}$$

The specific surface conductivity values are of the order of 10^{-9}–10^{-8} for water in glass capillaries so that significant effects on ζ-potential can be expected in 1 mm capillaries at electrolyte concentrations below about $10^{-3.5}$ mol dm^{-3}.

The above treatment can be applied to the electrophoretic motion of a large particle with a thin double layer ($\kappa R \gg 1$). The liquid is regarded as fixed so that the particle moves in the opposite direction from equation (3.10),

$$u = \frac{\varepsilon_r \varepsilon_0 \zeta}{\eta}. \tag{3.17}$$

u_E is the electrophoretic mobility (Smoluchowski equation). For water at 25 °C, ε_r is the relative permittivity of the medium; 78.6, ε_0 is the permittivity of free space; 8.85×10^{-12} F m^{-1} and η is the viscosity of the medium; 8.9×10^{-4},

$$\zeta = 1.282 \times 10^6 u. \tag{3.18}$$

u is expressed in m^2 V^{-1} s^{-1} and ζ in Volts.

Equation (3.17) applies to the case where the particle radius R is much larger than the double layer thickness $(1/\kappa)$, i.e. $\kappa R \gg 1$. This is generally the case for particles that are greater than 0.5 µm (when the 1 : 1 electrolyte concentration is lower than 10^{-3} mol dm^{-3}, i.e. $\kappa R > 10$),

3.5.2 The Huckel equation [7]

Soon after the publication by Debye and Huckel of the theory of the behaviour of strong electrolytes, Huckel [7] re-examined the electrophoresis problem and obtained a significantly different result from the Smoluchowski equation.

$$u = \frac{2}{3}\frac{\varepsilon_r \varepsilon_0 \zeta}{\eta} \tag{3.19}$$

The above equation applies for small particles (< 100 nm) and thick double layers (low electrolyte concentration), i.e. for the case $\kappa R < 1$.

Equation (3.19) can be simply derived by balancing the electric force on the particle, QE_z, with the frictional force given by Stokes' law $(6\pi\eta R v_E)$, i.e.,

$$QE_z = 6\pi\eta R v_E, \tag{3.20}$$

$$u_E = \frac{v_E}{E_z} = \frac{Q}{6\pi\eta R}. \tag{3.21}$$

The electric charge Q is given by the following equation,

$$Q = 4\pi\varepsilon\varepsilon_0(1 + \kappa R)\zeta. \tag{3.22}$$

Combining equations (3.21) and (3.22) one obtains,

$$u_E = \frac{2\varepsilon\varepsilon_0\zeta}{3\eta}(1 + \kappa R). \tag{3.23}$$

When $\kappa R \ll 1$, i.e. small particles with relatively thick double layers, equation (3.23) reduces to equation (3.19).

A more rigorous derivation of equation (3.19) was given by Overbeek and Bijsterbosch [8]. The action of the electric field on the double layer, causing the liquid to move in accordance with equation (3.10), is called electrophoretic retardation because it causes a reduction in the velocity of the migrating particle. Smoluchowski's treatment [6] assumes that this is the dominant force and that the particle's motion is equal and opposite to the liquid's motion. Huckel [7], on the other hand, also made proper allowance for the electrophoretic retardation in his analysis. However, as mentioned above, equation (3.19) is only valid for small values of κR when electrophoretic retardation is relatively unimportant and the main retarding force is the frictional resistance of the medium. The electrophoretic retardation at small κR remains important in the description of electrolyte conduction. In this case one must consider

the movement of ions of both positive and negative sign and the calculation of the interaction effects for a large number of ions. In electrophoresis one considers only the particle that is regarded as isolated in an infinite medium. For large particles with thin double layers, essentially all of the electrophoretic retardation is communicated directly to the particle.

3.5.3 Henry's treatment [9]

Henry [9] accounted for the discrepancy between Smoluchowski's and Huckel's treatment by considering the electric field in the neighbourhood of the particle. Huckel disregarded the deformation of the electric field by the particle, whereas Smoluchowski assumed the field to be uniform and everywhere parallel to the particle's surface. As shown in Fig. 3.9, these two assumptions are justified in the extreme cases of $\kappa R \ll 1$ and $\kappa R \gg 1$ respectively.

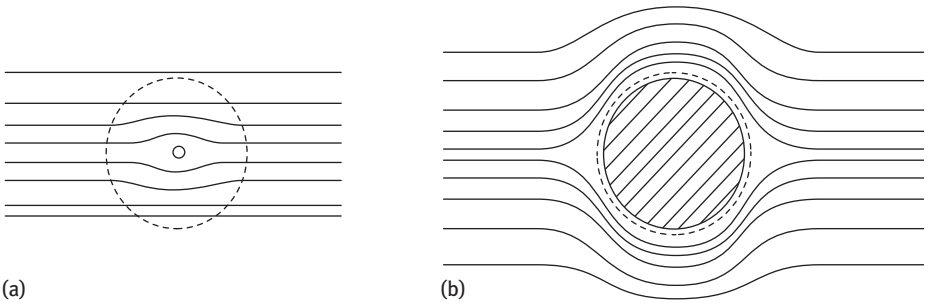

Fig. 3.9: Effect of a nonconducting particle on the applied field. (a) $\kappa R \ll 1$; (b) $\kappa R \gg 1$. The broken line is at a distance $(1/\kappa)$ from the particle's surface.

Henry [9] showed that when the external field is superimposed on the local field around the particle, the following expression for the mobility is used,

$$u = \frac{2}{3}\frac{\varepsilon_r \varepsilon_0 \zeta}{\eta} f(\kappa R). \tag{3.24}$$

The function $f(\kappa R)$ depends also on the particle's shape. Values of $f(\kappa R)$ at increasing values of κR are given in Tab. 3.2.

Tab. 3.2: Henry's correction factor $f(\kappa R)$.

κR	0	1	2	3	4	5	10	25	100	∞
$f(\kappa R)$	1.0	1.027	1.066	1.101	1.133	1.160	1.239	1.370	1.460	1.500

Henry's calculations are based on the assumption that the external field can be superimposed on the field due to the particle and hence it can only be applied for low potentials ($\zeta < 25\,\text{mV}$). It also does not take into account the distortion of the field induced by the movement of the particle (relaxation effect).

Wiersema, Loeb and Overbeek [10] introduced two corrections for Henry's treatment, namely the relaxation and retardation (movement of the liquid with the double layer ions) effects.

(i) Distortion of the field induced by the movement of the particles (distortion of the double layer symmetry and its reformation). This is referred to as the relaxation effect.
(ii) Movement of the liquid with the double layer ions, which results in reduction of the mobility of the integrating particles. This is referred to as the retardation effect.

By considering these two effects Loeb, Wiersema and Overbeek [9] derived exact expressions for the relationship between mobility and zeta potential for all κR values and any value of ζ-potential. Numerical tabulation of the relation between mobility and zeta potential has been given by Ottewill and Shaw [11]. Such tables are useful for the conversion of u to ζ at all practical values of κR.

3.6 Measurement of electrophoretic mobility and zeta potential

3.6.1 Ultramicroscopic technique (microelectrophoresis)

This is the most commonly used method since it allows direct observation of the particles using an ultramicroscope (suitable for particles that are larger than 100 nm). Microelectrophoresis has many advantages since the particles can be measured in their normal environment. It is preferable to dilute the suspension with the supernatant liquid which can be produced by centrifugation. Basically, a dilute suspension is placed in a cell (that can be circular or rectangular) consisting of a thin walled ($\approx 100\,\mu\text{m}$) glass tube that is attached to two larger bore tubes with sockets for placing the electrodes. The cell is immersed in a thermostat bath (accurate to $\pm 0.1\,^{\circ}\text{C}$) that contains an attachment for illumination and a microscope objective for observing the particles. It is also possible to use a video camera for directly observing the particles. A schematic representation of an electrophoresis apparatus is shown in Fig. 3.10 [13].

Since the glass walls are charged (usually negative at practical pH measurements), the solution in the cell will in general experience electro-osmotic flow. Thus, the observed motion of the particle when the field is applied, v_{p}, is the sum of its true velocity, v_{E}, and the total liquid velocity, v_{l}. The latter varies with the distance r from

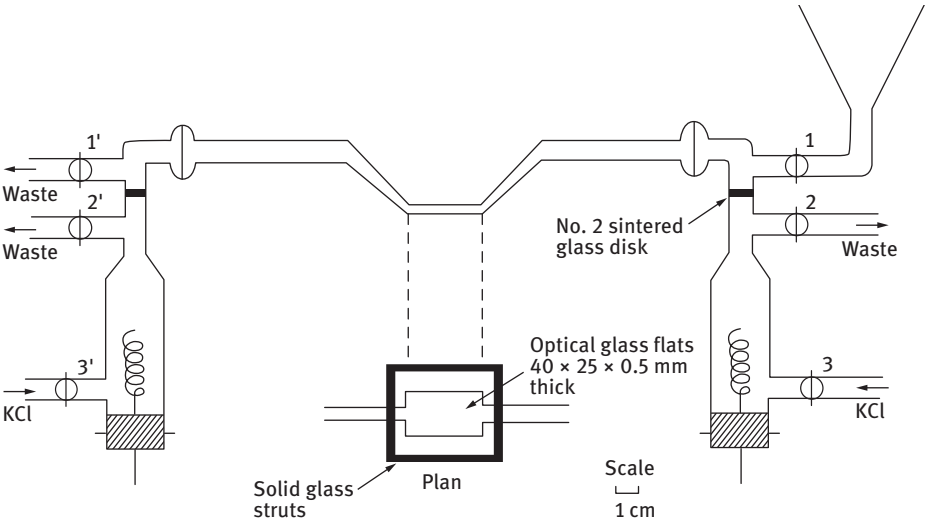

Fig. 3.10: Schematic representation of an electrophoresis apparatus.

the axis in accordance with Poiseulle's equation,

$$v_1 = p\frac{(a^2 - r^2)}{4\eta\ell}, \tag{3.25}$$

where p is the back pressure, a is the tube radius and ℓ is its length.

Thus, only where the electro-osmotic flow is zero, i.e. the so-called stationary level, can the electrophoretic mobility of the particles be measured. To establish the position of the stationary level, let us consider the situation in a microelectrophoresis cell of circular cross section as schematically represented in Fig. 3.11.

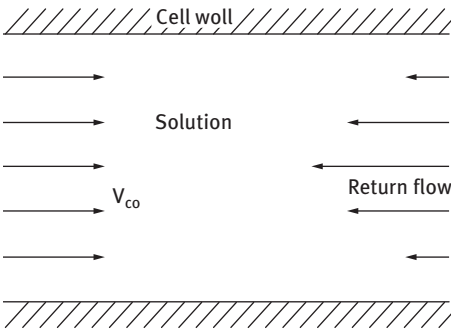

Fig. 3.11: Flow conditions within a closed cylindrical electrophoretic cell with electric field applied.

The electro-osmotic effects give rise to a solution velocity v_{eo} uniform across the cell cross section, towards the electrode of the same sign as the charge on the cell wall. If the cell is closed, a reverse flow will be set up and there will be no net transport of liquid. This is also the case if the cell is not closed, once the necessary hydrostatic pressure is built up. The reverse flow follows Poiseulle's law, where the condition of no net liquid transport is set by the following equation,

$$\int_{r=0}^{r=a} 2\pi v r \, dr = 0, \tag{3.26}$$

$$v = v_{eo} - C(a^2 - r^2), \tag{3.27}$$

where C is a constant which from equations (3.25) and (3.26) is given by,

$$C = \frac{2v_{eo}}{a^2}, \tag{3.28}$$

$$v = v_{eo}\left[\left(\frac{2r^2}{a^2}\right) - 1\right] \tag{3.29}$$

At the cell wall, $r = a$ and $v = v_{eo}$ as expected. At the centre, $r = 0$ and $v = -v_{eo}$, i.e. the velocity of the liquid flow is equal in magnitude but opposite in direction to that at the wall. The condition for zero liquid velocity is given by the condition,

$$\frac{2r^2}{a^2} = 1, \tag{3.30}$$

or,

$$r = \left(\frac{1}{2}\right)^{1/2} a = 0.707a. \tag{3.31}$$

Thus, the stationary level is located at a distance of 0.707 of the radius from the centre of the tube or 0.146 of the internal diameter from the wall. By focusing the microscope objective at the top and bottom of the walls of the tube, one can easily locate the position of the stationary levels. The average particle velocity is measured at the top and bottom stationary levels by averaging at least 20 measurements in each direction (the eye piece of the microscope is fitted with a graticule).

For large particles (> 1 μm and high density) sedimentation may occur during the measurement. In this case one can use a rectangular cell and observe the particles horizontally from the side of the glass cell. This is illustrated in Fig. 3.12.

The position of the stationary levels within the rectangular cell is more difficult to assign and it depends on the ratio of the two axes a and b in Fig. 3.12. When $a/b = \infty$, $v(x = 0) = 0$ when $y/b = 0.5774$ so that the stationary levels are at 0.211 of the cell thickness $2b$ from both the front and back walls. The position of the stationary levels for other values of a/b are given in Tab. 3.3.

Several commercial instruments for measuring electrophoretic mobility are available (e.g. Rank Brothers, Bottisham, Cambridge, England and Pen Kem in USA).

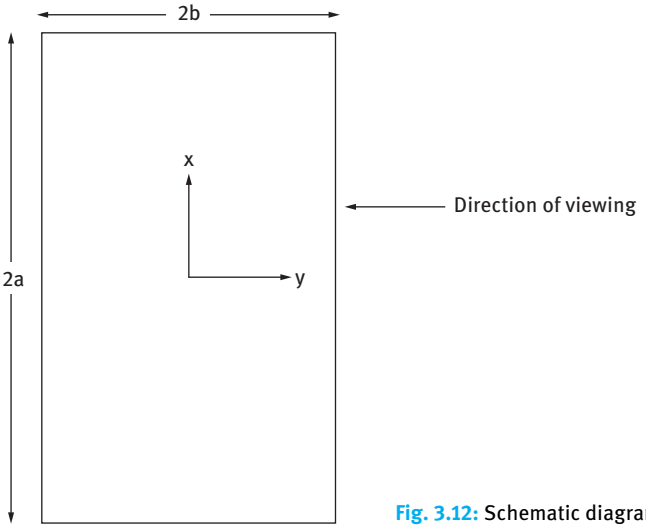

Fig. 3.12: Schematic diagram of the rectangular cell.

Tab. 3.3: Position of stationary levels in rectangular cells.

a/b	$(b-y)/2b$
∞	0.211
50	0.208
20	0.202
10	0.196

3.6.2 Laser velocimetry technique

This method is suitable for small particles that undergo Brownian motion [12]. The scattered light by small particles will show intensity fluctuation as a result of the Brownian diffusion (Doppler shift). When a light beam passes through a colloidal dispersion, an oscillating dipole movement is induced in the particles, thereby radiating the light. Due to the random position of the particles, the intensity of scattered light, at any instant, appears as random diffraction ("speckle" pattern). As the particles undergo Brownian motion, the random configuration of the pattern will fluctuate, such that the time taken for an intensity maximum to become a minimum (the coherence time), corresponds approximately to the time required for a particle to move one wavelength λ. Using a photomultiplier of active area about the diffraction maximum (i.e. one coherent area) this intensity fluctuation can be measured. The analogue output is digitized (using a digital correlator) that measures the photocount (or intensity) correlation function of scattered light. The intensity fluctuation is schematically illustrated in Fig. 3.13.

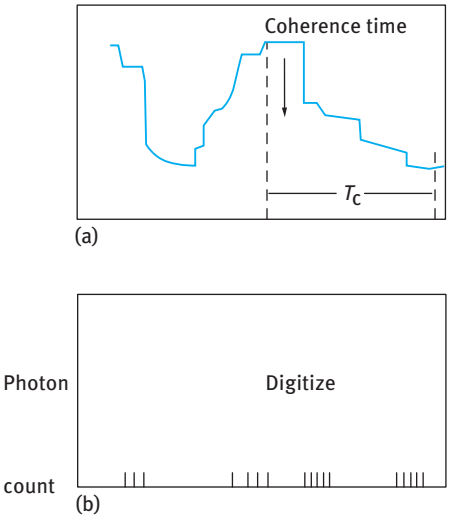

Fig. 3.13: Schematic representation of intensity fluctuation of scattered light.

The photocount correlation function $G^{(2)}(\tau)$ is given by,

$$g^{(2)} = B[1 + \gamma^2 g^{(1)}(\tau)]^2, \tag{3.32}$$

where τ is the correlation delay time.

The correlator compares $g^{(2)}(\tau)$ for many values of τ. B is the background value to which $g^{(2)}(\tau)$ decays at long delay times. $g^{(1)}(\tau)$ is the normalized correlation function of the scattered electric field and γ is a constant (≈ 1).

For monodispersed non-interacting particles,

$$g^{(1)}(\tau) = \exp(-\Gamma\gamma). \tag{3.33}$$

Γ is the decay rate or inverse coherence time, that is related to the translational diffusion coefficient D,

$$\Gamma = DK^2 \tag{3.34}$$

where K is the scattering vector,

$$K = \left(\frac{4\pi n}{\lambda_0}\right)\sin\left(\frac{\theta}{2}\right). \tag{3.35}$$

The particle radius R can be calculated from D using the Stokes–Einstein equation,

$$D = \frac{kT}{6\pi\eta_0 R}, \tag{3.36}$$

where η_0 is the viscosity of the medium.

If an electric field is placed at right angles to the incident light and in the plane defined by the incident and observation beam, the line broadening is unaffected but the centre frequency of the scattered light is shifted to an extent determined by the

electrophoretic mobility. The shift is very small compared to the incident frequency (≈ 100 Hz for an incident frequency of $\approx 6 \times 10^{14}$ Hz) but with a laser source it can be detected by heterodyning (i.e. mixing) the scattered light with the incident beam and detecting the output of the difference frequency. A homodyne method may be applied, in which case a modulator to generate an apparent Doppler shift at the modulated frequency is used. To increase the sensitivity of the laser Doppler method, the electric fields are much higher than those used in conventional electrophoresis. The Joule heating is minimized by pulsing of the electric field in opposite directions. The Brownian motion of the particles also contributes to the Doppler shift and an approximate correction can be made by subtracting the peak width obtained in the absence of an electric field from the electrophoretic spectrum. An He-Ne laser is used as the light source and the output of the laser is split into two coherent beams which are cross-focused in the cell to illuminate the sample. The light scattered by the particle, together with the reference beam is detected by a photomultiplier. The output is amplified and analysed to transform the signals to a frequency distribution spectrum. At the intersection of the beams, interferences of known spacing are formed.

A schematic diagram of a laser-Doppler electrophoresis apparatus [13] is shown in Fig. 3.14.

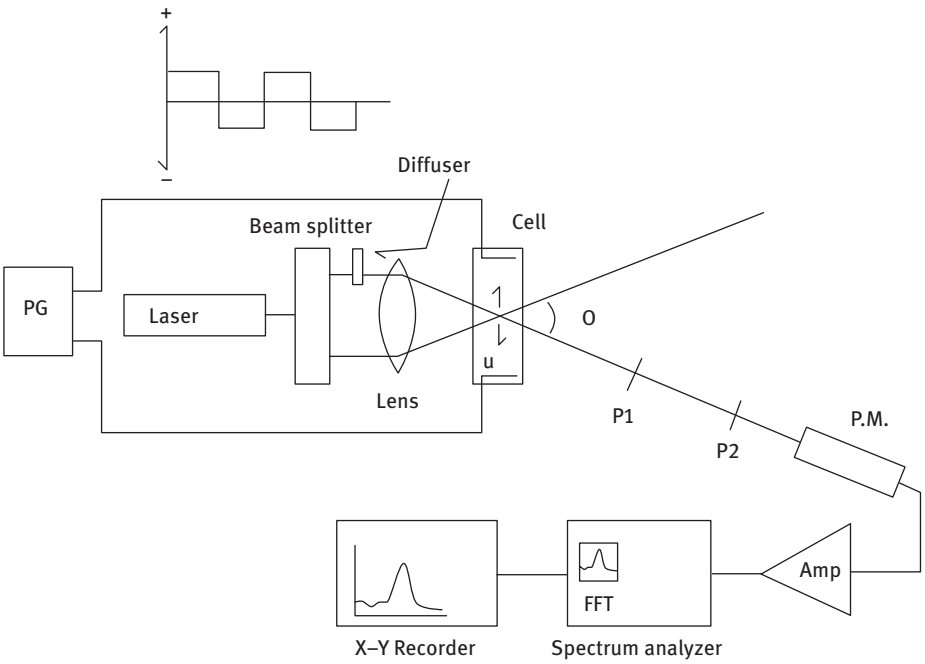

Fig. 3.14: Schematic diagram of a laser-Doppler electrophoresis apparatus: P_1, P_2 – pinholes (200 and 100 µm radii); PM – photomultiplier; FFT – spectrum analyser; PG – pulse generator.

The magnitude of the Doppler shift Δv is used to calculate the electrophoretic mobility u using the following expression,

$$\Delta V = \left(\frac{2n}{\lambda_0}\right)\sin\left(\frac{\theta}{2}\right)uE, \tag{3.37}$$

where n is the refractive index of the medium, λ_0 is the incident wavelength in vacuum, θ is the scattering angle and E is the field strength.

Several commercial instruments are available for measuring electrophoretic light scattering:

(i) The Coulter DELSA 440SX (Coulter corporation, USA) is a multi-angle laser Doppler system employing heterodyning and autocorrelation signal processing. Measurements are made at four scattering angles (8, 17, 25 and 34°) and the temperature of the cell is controlled by a Peltier device. The instrument reports the electrophoretic mobility, zeta potential, conductivity and particle size distribution.

(ii) Malvern (Malvern Instruments, UK) ZetaSizer which is a laser Doppler system using crossed beam optical configuration and homodyne detection with photon correlation signal processing. The zeta potential is measured using laser Doppler velocimetry and the particle size is measured using photon correlation spectroscopy (PCS). The ZetaSizer uses PCS to measure both movement of the particles in an electric field for zeta potential determination and random diffusion of particles at different measuring angles for size measurement on the same sample. The manufacturer claims that zeta potential for particles in the range 50 nm to 30 µm can be measured. A Peltier device is used for temperature control.

3.6.3 Electroacoustic methods

The mobility of a particle in an alternating field is termed dynamic mobility, to distinguish it from the electrophoretic mobility in a static electric field described above [13]. The principle of the technique is based on the creation of an electric potential by a sound wave transmitted through an electrolyte solution, as described by Debye [14]. The potential, termed the ionic vibration potential (IVP), arises from the difference in the frictional forces and the inertia of hydrated ions subjected to ultrasound waves. The effect of the ultrasonic compression is different for ions of different masses and the displacement amplitudes are different for anions and cations. Hence the sound waves create periodically changing electric charge densities. This original theory of Debye was extended to include electrophoretic, relaxation and pressure gradient forces [15, 16].

A much stronger effect can be observed in colloidal dispersions. The sound waves transmitted by the suspension of charged particles generate an electric field because the relative motion of the two phases is different. The displacement of a charged particle from its environment by the ultrasound waves generates an alternating potential,

termed colloidal vibration potential (CVP). The IVP and CVP are both called ultrasound vibration potential (UVP).

The converse effect, namely the generation of sound waves by an alternating electric field [18] in a colloidal dispersion can be measured and is termed the electrokinetic sonic amplitude (ESA). The theory for the ESA effect has been developed by O'Brian and co-workers [19–23]. The dynamic mobility can be determined by measuring either UVP or ESA, although in general the ESA is the preferred method. Several commercial instruments are available for measuring dynamic mobility:

(i) the ESA-8000 system from Matec Applied Sciences that can measure both CVP and ESA signals;
(ii) the Pen Kem System 7000 Acoustophoretic titrator that measures the CVP, conductivity, pH, temperature, pressure amplitude and sound velocity.

In the ESA system (from Matec) and the AcoustoSizer (from Colloidal Dynamics) the dispersion is subjected to a high frequency alternating field and the ESA signal is measured. The ESA-8000 operates at constant frequency of ≈ 1 MHz and the dynamic mobility and zeta potential (but not particle size) are measured. The AcoustoSizer operates at various frequencies of the applied electric field and can measure the particle mobility, zeta potential and particle size.

The frequency synthesizer feeds a continuous sinusoidal voltage into a grated amplifier that creates a pulse of sinusoidal voltage across the electrodes in the dispersion. The pulse generates sound waves which appear to emanate from the electrodes. The oscillation, the back-and-forth movement of the particle caused by an electric field, is the product of the particle charge times the applied field strength. When the direction of the field is alternating, particles in the suspension between the electrodes are driven away towards the electrodes. The magnitude and phase angle of the ESA signal created is measured with a piezoelectric transducer mounted on a solid nonconductive (glass) rod attached to the electrode as illustrated in Fig. 3.15. The purpose of this nonconductive acoustic delay line is to separate the transducer from the high-frequency electric field in the cell. Three pulses of the voltage signal are recorded as schematically shown in Fig. 3.16. The first pulse of the signal, shown on the left, is generated when the voltage pulse is applied to the sample and is unrelated to the ESA effect. This first pulse of the signal is received before the sound has sufficient time to pass down the glass rod and is electronic crosstalk deleted during data processing. The second and third pulses are ESA signals. The second pulse is detected by the nearest electrode. This pulse is used for data processing to determine the particle size and zeta potential. The third pulse originates from the other electrode and is deleted.

In addition to the electrodes, the sample cell of the ESA instruments also houses sensors for pH, conductivity and temperature measurements. It is also equipped with a stirrer and the system is linked to a digital titrator for dynamic mobility and zeta potential measurements as a function of pH.

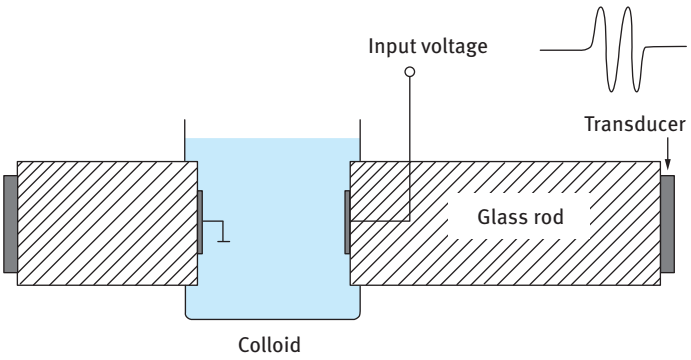

Fig. 3.15: Schematic representation of the AcoustoSizer cell.

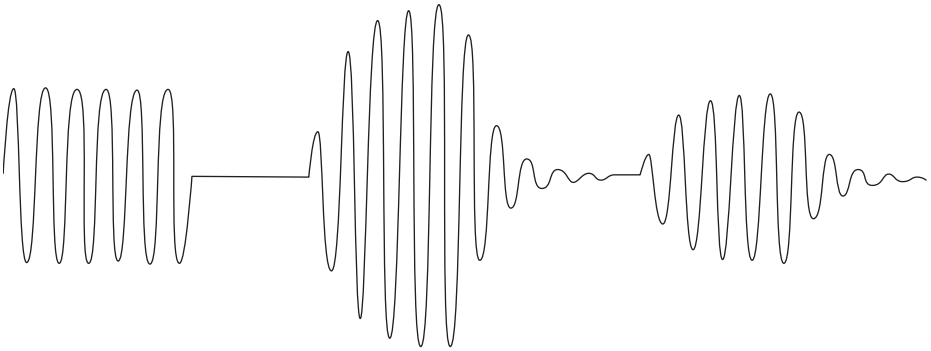

Fig. 3.16: Signals from the right hand transducer.

To convert the ESA signal to dynamic mobility one needs to know the density of the disperse phase and dispersion medium, the volume fraction of the particles and the velocity of sound in the solvent. As shown before, to convert mobility to zeta potential one needs to know the viscosity of the dispersion medium and its relative permittivity. Because of the inertia effects in dynamic mobility measurements, the weight average particle size has to be known.

For dilute suspensions with a volume fraction $\phi = 0.02$, the dynamic mobility u_d can be calculated from the electrokinetic sonic amplitude $A_{ESA}(\omega)$ using the following expression [18, 19],

$$A_{ESA}(\omega) = Q(\omega)\phi(\Delta\rho/\rho)(u_d), \tag{3.38}$$

where ω is the angular frequency of the applied field, $\Delta\rho$ is the density difference between the particle (with density ρ) and the medium. $Q(\omega)$ is an instrument-related coefficient independent of the system being measured.

For a dilute dispersion of spherical particles with $\phi < 0.1$, a thin double layer ($\kappa R > 50$) and narrow particle size distribution (with standard deviation < 20 % of the

mean size), u_d can be related to the zeta potential ζ by the equation [18],

$$u_d = \frac{2\varepsilon\varsigma}{3\eta} G\left(\frac{\omega R^2}{\nu}\right)[1 + f(\lambda, \omega)], \tag{3.39}$$

where ε is the permittivity of the liquid (that is equal to $\varepsilon_r\varepsilon_0$, defined before), R is the particle radius, η is the viscosity of the medium, λ is the double layer conductance and ν is the kinematic viscosity (= η/ρ). G is a factor that represents particle inertia, which reduces the magnitude of u_d and increases the phase lag in a monotonic fashion as the frequency increases. This inertia factor can be used to calculate the particle size from electroacoustic data. The factor $[1 + f(\lambda, \omega)]$ is proportional to the tangential component of the electric field and dependent on the particle permittivity and a surface conductance parameter λ. For most suspensions with large κR, the effect of surface conductance is insignificant and the particle permittivity/liquid permittivity $\varepsilon_p/\varepsilon$ is small. In most cases where the ionic strength is at least 10^{-3} mol dm^{-3} and a zeta potential < 75 mV, the factor $[1 + f(\lambda, \omega)]$ assumes the value 0.5. In this case the dynamic mobility is given by the simple expression,

$$u_d = \frac{\varepsilon\varsigma}{\eta} G(\alpha). \tag{3.40}$$

Equation (3.40) is identical to the Smoluchowski equation (3.17), except for the inertia factor $G(\alpha)$.

The equation for converting the ESA amplitude, A_{ESA}, to dynamic mobility is given by,

$$u_d = \frac{A_{ESA}}{\phi v_s \Delta\rho} G(\alpha)^{-1}. \tag{3.41}$$

The zeta potential ζ is given by,

$$\varsigma = \frac{u_d \eta}{\varepsilon} G(\alpha)^{-1} = \frac{A_{ESA}}{\phi v_s \Delta\rho} G(\alpha)^{-1}. \tag{3.42}$$

For a polydisperse system $\langle u_d \rangle$ is given by,

$$\langle u_d(\omega) \rangle = \int_0^\infty u(\omega, R) p(R)\, dR, \tag{3.43}$$

where $u(\omega, R)$ is the average dynamic mobility of particles with radius R at a frequency ω, and $pR\,dR$ is the mass fraction of particles with radii in the range $R \pm dR/2$.

The ESA measurements can also be applied for determining the particle size in a suspension from particle mobilities. The electric force acting upon a particle is opposed by the hydrodynamic friction and inertia of the particles. At low frequencies of alternating electric field, the inertial force is insignificant and the particle moves in the alternating electric field with the same velocity as it would have moved in a constant field. The particle mobility at low frequencies can be measured to calculate the zeta

potential. At high frequencies, the inertia of the particle increases causing the velocity of the particle to decrease and the movement of the particle to lag behind the field. This is illustrated in Fig. 3.17 which shows the variation of applied field and particle velocity with time. Since inertia depends on particle mass, both of these effects depend on the particle mass and consequently on its size. Hence both zeta potential and particle size can be determined from the ESA signal, if the frequency of the alternating field is sufficiently high. This is the method that is provided by the AcoustoSizer from Colloidal Dynamics.

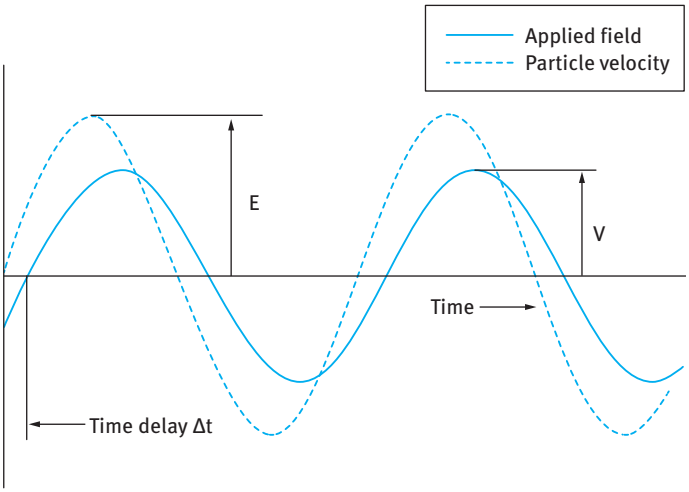

Fig. 3.17: Variation of applied field and particle velocity with time at high frequency.

Several variables affect the ESA measurements and these are listed below:

(i) Particle concentration range: Very dilute suspensions generate a weak signal and are not suitable for ESA measurements. The magnitude of the ESA signal is proportional to the average particle mobility, the volume fraction of the particles ϕ and the density difference between the particles and the medium $\Delta\rho$. To obtain a signal that is at least one order of magnitude higher than the background electrical noise (≈ 0.002 mPa M/V) the concentration and/or the density difference have to be sufficiently large. If the density difference between the particles and medium is small, e.g. polystyrene latex with $\Delta\rho \approx 0.05$, then a sufficiently high concentration ($\phi > 0.02$) is needed to obtain a reasonably strong ESA signal. The accuracy of the ESA measurement is also not good at high ϕ values. This is due to the nonlinearity of the ESA amplitude-ϕ relationship at high ϕ values. Such deviation becomes appreciable at $\phi > 0.1$. However, reasonable values of zeta potential can be obtained from ESA measurements up to $\phi = 0.2$. Above this concentration, the measurements are not sufficiently accurate and the results obtained can only be used for qualitative assessment.

(ii) Electrolyte effects: Ions in the dispersion generate electroacoustic (IVP) potential and the ESP signal is therefore a composite of the signals created by the particles and ions. However, the ionic contribution is relatively small, unless the particle concentration is low, their zeta potential is low and the ionic concentration is high. The ESA system is therefore not suitable for dynamic mobility and zeta potential measurements in systems with electrolyte concentration higher than 0.3 mol dm^{-3} KCl.

(iii) Temperature: Since the viscosity of the dispersion decreases by ≈ 2 % per °C and its conductivity increases by about the same amount, it is important that temperature is accurately controlled using a Peltier device. Temperature control should also be maintained during sample preparation, for example when the suspension is sonicated. To avoid overheating, the sample should be cooled in an ice bath at regular intervals during sonication.

(iv) Calibration and accuracy: The electroacoustic probe should be calibrated using a standard reference dispersion such as polystyrene latex or colloidal silica (Ludox). The common sources of error are unsuitable particle concentration (too low or too high), irregular particle shape, polydispersity, electrolyte signals, temperature variations, sedimentation, coagulation and entrained air bubbles. The latter in particular can cause erroneous ESA signal fluctuations resulting from weakening of the sound by the air bubbles. In many cases the zeta potential results obtained using the ESA method do not agree with those obtained using other methods such as microelectrophoresis or laser velocimetry. However, the difference seldom exceeds 20 % and this makes the ESA method more convenient for measurement of many industrial methods. The main advantages are the speed of measurement and that the dispersion does not need to be diluted, which could change the state of the suspension.

References

[1] Hunter RJ. Zeta potential in colloid science. London: Academic Press; 1981.
[2] Gouy G. J Phys. 1910;9:457; Ann Phys. 1917;7:129.
[3] Chapman DL. Phil Mag. 1913;25:475.
[4] Stern O. Z Electrochem. 1924;30:508.
[5] Grahame DC. Chem Rev. 1947;41;441.
[6] von Smoluchowski M. Handbuch der Electricitat und des Magnetismus, Vol. II. Leipzig: Barth; 1914.
[7] Huckel E. Phys Z. 1924;25:204.
[8] Overbeek JTG, Bijsterbosch BH. In: Righetti PG, van Oss CJ, Vanderhoff JW, editors. Electrokinetic separation methods. Elsevier/North Holland Biomedical Press; 1979.
[9] Henry DC. Proc Royal Soc London. 1948;A133:106.
[10] Wiersema PH, Loeb AL, Overbeek JTG. J Colloid Interface Sci. 1967;22:78.
[11] Ottewill RH, Shaw JN. J Electroanal Interfacial Electrochem. 1972;37:133.

[12] Pusey PN. In: Green JHS, Dietz R, editors. Industrial polymers: Characterisation by molecular weights. London: Transcripta Books; 1973.
[13] Kissa E. Dispersions: Characterization, testing and measurement. New York: Marcel Dekker; 1999.
[14] Debye P. J Chem Phys. 1933;1:13.
[15] Bugosh J, Yeager E, Hovarka F. J Chem Phys. 1947;15:542.
[16] Yeager E, Bugosh J, Hovarka F, McCarthy J. J Chem Phys. 1949;17:411.
[17] Dukhin AS, Goetz PJ. Colloids and Surfaces. 1998;144:49.
[18] Oja T, Petersen GL, Cannon DC. US Patent 4,497,208 (1985).
[19] O'Brian RW. J Fluid Mech. 1998;190:71.
[20] O'Brian RW. J Fluid Mech. 1990;212:81.
[21] O'Brian RW, Garaside P, Hunter RJ. Langmuir. 1994;10:931.
[22] O'Brian RW, Cannon DW, Rowlands WN. J Colloid Interface Sci. 1995;173:406.
[23] Rowlands WN, O'Brian RW. J Colloid Interface Sci. 1995;175:190.

4 Double layer repulsion

4.1 Introduction

The origin of electrostatic interactions is due to the double layer overlap that occurs when the surface-to-surface distance becomes smaller than twice the double layer thickness. When two particles or droplets, each containing an electrical double layer with extension or thickness $(1/\kappa)$ approach to a surface-to-surface separation distance h that is smaller than $(2/\kappa)$ the double layers cannot completely develop and the potential $\psi_{1/2}$ at the mid-plane between the particles or droplets is no longer zero, thus resulting in strong repulsion. As discussed in Chapter 2, the double layer extension depends on electrolyte concentration and valency of indifferent electrolytes. This clearly shows the strong dependence of double layer repulsion on the concentration of indifferent electrolytes. As discussed in Chapter 2, an increase in electrolyte concentration causes a reduction in the diffuse double layer potential, ψ_{diffuse}, and compression of the double layer, i.e. reduction of the Debye length κ^{-1}. Both of these effects affect the colloid stability of lyophobic colloids as will be discussed in Chapter 6.

In this chapter, I will start with a general description of the electrostatic repulsion in terms of the double layer property, double layer potential, particle size and electrolyte concentration and valency. Both cases of constant potential and constant charge that is maintained on particle approach are described. This is followed by a section on the interaction between similar and dissimilar double layers for flat plates. Calculation of the double layer interaction using the Gibbs approach is then described. The modification of the theory of interaction between flat plates for the case of spherical particles is then described. The effect of increasing electrolyte concentration and valency as well as the Stern potential is then described. Finally, the effect of increasing particle number concentration of double layer repulsion is described.

4.2 General expression for electrostatic repulsion

A general expression can be written to describe the electrostatic repulsion, G_{elec}, in terms of the double layer property $f(\text{DL})$ determined by the relative permittivity, particle size, the double layer potential, ψ_{diffuse}, and an exponential function determined by the Debye length and separation distance h [1],

$$G_{\text{elec}} = f(\text{DL})\psi_{\text{diffuse}}^2 \exp(-\kappa h). \tag{4.1a}$$

$(1/\kappa)$ is the Debye length that is referred to as the "thickness of the double layer" and is given by the following equation,

$$\left(\frac{1}{\kappa}\right) = \left(\frac{\varepsilon_r \varepsilon_0 kT}{2n_0 Z_i^2 e^2}\right)^{1/2}, \tag{4.1b}$$

https://doi.org/10.1515/9783110540895-005

where ε_r is the relative permittivity, ε_0 is the permittivity of free space, k is the Boltzmann constant, T is the absolute temperature, n_0 is the electrolyte concentration, Z_i is the valency of the ion and e is the electronic charge.

For two particles of different, but not too high, diffuse double layer potential, at large κh,

$$G_{\text{elec}} = f(\text{DL})\psi_1^d\psi_2^d \exp(-\kappa h). \tag{4.2}$$

In the original theory developed by Deryaguin–Landau [2], Verwey–Overbeek [3] (referred to as DLVO theory), the assumption was made that on the approach of surfaces the surface potentials remain constant and equal to that at infinite separation of the surfaces. This requires adjustment of the surface charge by surface charge regulation. In this case the isolated double layers form spontaneously by adsorption and/or desorption of potential determining ions. This is referred to as the "constant potential" case. However, with many surfaces the charge is fixed, e.g. in clay particles, and on surface approach the surface potential has to be adjusted to keep the surface charge constant. This situation is referred to as the "constant charge" case.

A schematic representation of the constant charge and constant potential cases was given by Lyklema [1] in Fig. 4.1.

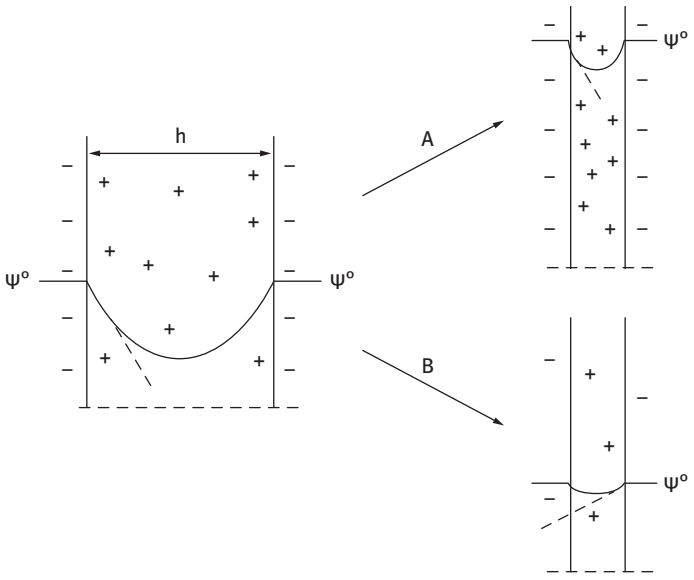

Fig. 4.1: Schematic representation of constant charge (A) and constant potential cases [1].

4.3 Interaction between similar and dissimilar flat plates

This is illustrated in Fig. 4.2 for two flat plates whereby the surface separation becomes less than twice the double layer extension [4]. The individual double layers can no longer develop unrestrictedly, since the limited space does not allow complete potential decay. The potential $\psi_{H/2}$ half way between the plates is no longer zero (as would be the case for isolated particles at $x \to \infty$). The potential distribution at an interparticle distance H is schematically depicted by the full line in Fig. 4.2. The Stern potential ψ_d is considered to be independent of the particle distance. The dashed curves show the potential as a function of distance x to the Helmholtz plane, had the particles been at infinite distance.

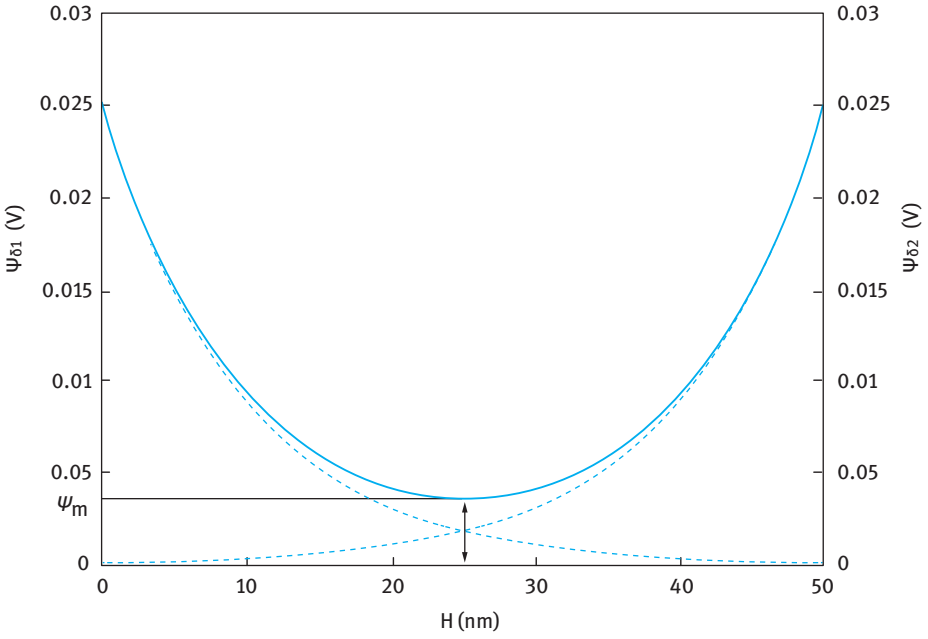

Fig. 4.2: Potential profile between two planer surfaces at 25 mV, in 10^{-3} mol dm^{-3} NaCl.

A simple model to obtain G_{elec} is to calculate the ion concentration between the surfaces in order to obtain the osmotic pressure difference between the surfaces and the bulk electrolyte, i.e. the excess osmotic pressure at the mid-plane position between the surfaces separated by a distance h. At $h/2$, $d\psi_x/dx = 0$ and $\psi_x = \psi_m$.

The difference in ionic concentration at the mid-plane and the bulk electrolyte gives the osmotic pressure $\Pi(H)$,

$$\Pi(H) = kT(n_+ + n_- - 2n_0) \tag{4.3}$$

Using the Boltzmann distribution,

$$n_i = n_{i0} \exp\left[\frac{Z_i e\psi(x)}{kT}\right], \tag{4.4}$$

where Z_i is the ion valency, e is the electronic charge, k is the Boltzmann constant and T is the absolute temperature, equation (4.2) becomes,

$$\Pi(H) = 2n_0 kT\left[\cosh\left(\frac{Ze\psi_m}{kT}\right) - 1\right]. \tag{4.5}$$

For small potentials equation (4.5) reduces to,

$$\Pi(H) \approx \frac{\kappa^2 \varepsilon_r \varepsilon_0}{2}\psi_m, \tag{4.6}$$

where ε_r is the relative permittivity of the medium, ε_0 is the permittivity of free space. The mid-plane potential ψ_m is equal to twice the potential at the mid-plane,

$$\psi_m = 2\psi_{(H/2)}. \tag{4.7}$$

Equation (4.6) becomes,

$$\Pi(H) \approx \frac{\kappa^2 \varepsilon_r \varepsilon_0}{2}\left[2\psi_d \exp\left(-\frac{\kappa H}{2}\right)\right]^2 = 2\kappa^2 \varepsilon_r \varepsilon_0 \psi_d^2 \exp(-\kappa H). \tag{4.8}$$

The electrostatic repulsion is then given by,

$$G_{elec} = -\int_{\infty}^{H} \Pi(H)\, dH. \tag{4.9}$$

Using the boundary conditions: $\Pi(H) \to 0$ as $H \to \infty$,

$$G_{elec} = 2\kappa \varepsilon_r \varepsilon_0 \psi_d^2 \exp(-\kappa H). \tag{4.10}$$

Replacing the Stern potential ψ_d with the zeta potential ζ,

$$G_{elec} \approx 2\kappa \varepsilon_r \varepsilon_0 \varsigma^2 \exp(-\kappa H). \tag{4.11}$$

For higher potentials, the Debye–Huckel approximation cannot be justified, but for weak overlap, i.e. $\kappa H > 1$, the local potentials, estimated from the isolated surfaces, can still be simply added and this results in the following expression for the double layer repulsion,

$$G_{elec} = \frac{64 n_0 kT}{\kappa}\tanh^2\left(\frac{Ze\psi_d}{4kT}\right)\exp(-\kappa H). \tag{4.12}$$

For two flat plates with different Stern potentials ψ_{d1} and ψ_{d2}, one obtains he following expression in the Debye–Huckel limit [5],

$$G_{elec} = \frac{\varepsilon_r \varepsilon_0 \kappa}{2}\left[(\psi_{d1}^2 + \psi_{d2}^2)\{1 - \coth(\kappa H) + 2\psi_{d1}\psi_{d2}\,\mathrm{cosech}(\kappa H)\}\right] \tag{4.13}$$

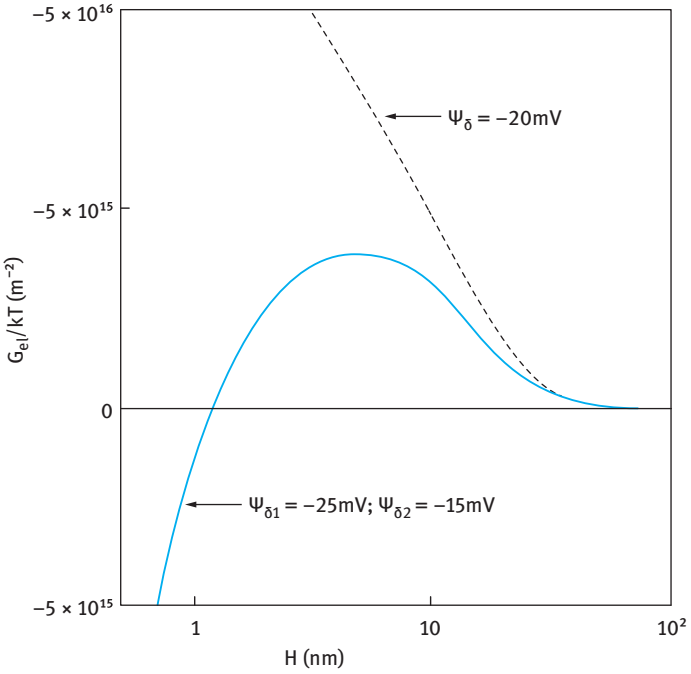

Fig. 4.3: G_{elec} versus H for two flat plates with equal Stern potential (dashed line) and two different Stern potentials (solid line).

For comparison, Fig. 4.3 shows the G_{elec}–H curve for flat plates with equal Stern potential of –20 mV and that for two flat plates with different Stern potentials of –25 and –15 mV. The curve for the flat plates at equal Stern potential shows the expected result of the exponential decay of G_{elec} with H. In contrast, the curve for two flat plates with different Stern potential shows a maximum in the interaction energy at $\kappa H = 0.5$, but with a further decrease in H beyond the maximum, G_{elec} begins to decrease and at close separations, the interaction becomes attractive. This result is very important and it illustrates the possibility of heterocoagulation of some materials with similar sign charge when the Stern potentials are different.

4.4 Calculation of electrostatic interaction using the Gibbs energy concept

Deryaguin, Landau [2], Verwey and Overbeek [3] calculated the electrostatic interaction by computing the Gibbs energy G of the system at any distance h by an isothermal reversible charging process [1]. For one flat isolated diffuse double layer, the free energy change $\Delta G_a^{\sigma d}$ is given by,

$$\Delta G_{\mathrm{a}}^{\sigma\mathrm{d}} = \frac{8cRT}{\kappa}\left[\cosh\frac{Zy^{\mathrm{d}}}{2} - 1\right]. \tag{4.14}$$

For a Gouy–Stern double layer,

$$\Delta G_{\mathrm{a}}^{\sigma} = -\frac{(\sigma^0)^2}{2C_1^i} - \frac{(\sigma^{\mathrm{d}})^2}{2C_2^i} - \frac{8cRT}{\kappa}\left[\cosh\left(\frac{Zy^{\mathrm{d}}}{2} - 1\right)\right]. \tag{4.15}$$

In the above equations, Δ refers to the difference with respect to the reference state, i.e. the uncharged surface; the subscript 'a' means G is counted per unit area. The quantities σ^0 and σ^{d} are the surface and diffuse charge densities (note that $\sigma^0 + \sigma^{\mathrm{d}} = 0$, because of electroneutrality). C_1^i and C_2^i are the inner and outer Helmholtz layer differential capacities. y is the dimensionless potential ($y^{\mathrm{d}} = F\psi^{\mathrm{d}}/RT$) and Z is the valency of the symmetrical electrolyte.

If one computes the Gibbs energy for two interacting double layers, then the Gibbs free energy of electric repulsion per unit area is obtained by subtraction of twice equation (4.14) or (4.15). Upon interaction, variation of these $\Delta G_{\mathrm{a}}^{\sigma}$'s as a function of h has to be considered [1]. The result is simply denoted as $G_{\mathrm{a,elec}}$, realizing that for the two interacting double layers the reference state is identical. It should be noted that both $\Delta G_{\mathrm{a}}^{\sigma}$ and $\Delta G_{\mathrm{a}}^{\sigma\mathrm{d}}$ are negative since the double layers are formed spontaneously. The Gibbs energy of two double layers in interaction is also negative, but less so than for two isolated double layers. Consequently $G_{\mathrm{a,elec}} > 0$.

The change in the Gibbs energy per unit area of the interface when the distance between the plates is reduced from ∞ to h is given by,

$$G_{\mathrm{a,elec}} = 2[\Delta G_{\mathrm{a}}^{\sigma}(h) - \Delta G_{\mathrm{a}}^{\sigma}(\infty)] = 2[G_{\mathrm{a}}^{\sigma}(h) - G_{\mathrm{a}}^{\sigma}(\infty)]. \tag{4.16}$$

The Δ is dropped because both terms refer to the same reference state. G_{a}^{σ} is related to the surface excess Γ_I (amount of adsorption in moles per unit area) and the chemical potential μ_I by the Gibbs equation,

$$G_{\mathrm{a}}^{\sigma} = -\sum \mu_i \Gamma_i. \tag{4.17}$$

The negative sign in equation (4.17) indicates that the adsorbate form spontaneously. As an example let us consider an oxide dispersed in an aqueous solution containing HNO_3, KNO_3 and an adsorbate organic substance A. Then, for two identical double layers [1],

$$G_{\mathrm{a}}^{\sigma} = -2(\mu_{\mathrm{HNO_3}}\Gamma_{\mathrm{HNO_3}} + \mu_{\mathrm{KNO_3}}\Gamma_{\mathrm{KNO_3}} + \mu_{\mathrm{A}}\Gamma_{\mathrm{A}}). \tag{4.18}$$

The variation of G_{a}^{σ} with distance h is given by,

$$-\left(\frac{\partial G_{\mathrm{a}}^{\sigma}}{\partial h}\right) = 2\left[\mu_{\mathrm{HNO_3}}\left(\frac{\partial \Gamma_{\mathrm{HNO_3}}}{\partial h}\right) + \mu_{\mathrm{s}}\left(\frac{\partial \Gamma_{\mathrm{s}}}{\partial h}\right) + \mu_{\mathrm{A}}\left(\frac{\partial \Gamma_{\mathrm{A}}}{\partial h}\right)\right]. \tag{4.19}$$

The subscript 's' refers to salt (KNO_3).

$\Gamma_{\mathrm{HNO_3}} = \sigma_0/F$; upon reduction of h, $\Gamma_{\mathrm{HNO_3}}$ goes down, so that the term is repulsive. On the other hand, $\Gamma_{\mathrm{s}} < 0$ (negative adsorption or depletion) and this negative term

becomes less negative on overlap, $\partial\Gamma_s/\partial h > 0$. In other words, overlap in combination with negative adsorption tends to attraction. This is the basis of depletion flocculation. The last term in equation (4.19) is also repulsive if overlap of adsorbates leads to desorption [1].

The above analysis demonstrates that there is no difference between the first and third term of equation (4.19); in both cases work is done against the binding energy of HNO_3 and A. However, with charged interfaces the first term does not come on its own; it is accompanied by a second attractive term of an electrical nature [1]. However, the repulsive term always exceeds the attractive one.

4.5 Charge and potential distribution

A schematic representation of the potential distribution is given in Fig. 4.4. Because of the overlap, $y(x)$ between the two surfaces (full line) is increased above the value it would have had for one single double layer (dashed line) [1].

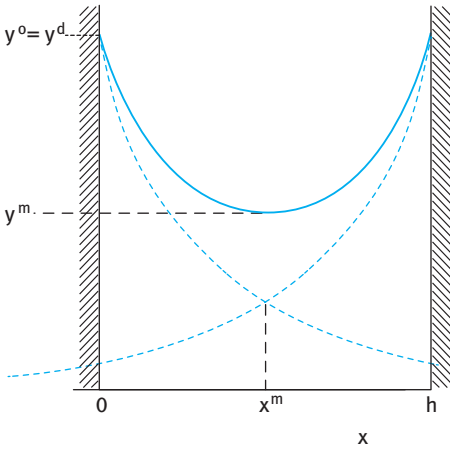

Fig. 4.4: Schematic representation of the dimensionless potential between two identical parallel flat double layers. The special variable x is counted from the left-hand side plate; $x^m = h/2$ is the mid-point value.

As the potentials at the surface ($y^d = y^0$) are assumed to remain fixed, the slopes (dy/dx) near the two surfaces decrease. These slopes give the reduction of the surface charge; adjacent to the surface,

$$\left(\frac{dy}{dx}\right)_{x\to 0} = -\frac{F\sigma^0}{RT\varepsilon\varepsilon_0}; \tag{4.20}$$

and for the right-hand side double layer,

$$\left(\frac{dy}{dx}\right)_{x\to h} = \frac{F\sigma^0}{RT\varepsilon\varepsilon_0}. \tag{4.21}$$

For homo-interaction, the minimum potential y^{m} is given by,

$$y^{\mathrm{m}} = \frac{F\psi^{\mathrm{m}}}{RT}. \tag{4.22}$$

For hetero-interaction, the symmetry is lost and the minimum is shifted towards the surface with the lower potential or there is no minimum at all. At the minimum, the field strength is zero, which means that the total charges, including those on the surface, between $x = 0$ and $x = x^{\mathrm{m}}$, and between $x = x^{\mathrm{m}}$ and $x = h$ are zero. However, the potential at the minimum is not zero; an outer force is needed to maintain its increased value. When double layer overlap is not strong, y^{m} is sometimes equal to the sum of the individual potentials. This is the linear superposition approximation that applies only around x^{m}.

To find the distribution, one must integrate the Poisson–Boltzmann equation for the range between $x = 0$ and $x = h$,

$$\frac{\mathrm{d}^2(Zy)}{\mathrm{d}x^2} = \kappa^2 \sinh(Zy). \tag{4.23}$$

The result of the integration is,

$$\left(\frac{\mathrm{d}y}{\mathrm{d}x}\right)^2 = \frac{2\kappa^2}{Z^2}[\cosh(Zy) + \mathrm{const}]. \tag{4.24}$$

The integration constant can be found from the boundary conditions: $(\mathrm{d}y/\mathrm{d}x) = 0$ for $y = y^{\mathrm{m}}$,

$$\frac{\mathrm{d}y}{\mathrm{d}x} = \mp\frac{\kappa}{Z}\left(2[\cosh(Zy) - \cosh(Zy^{\mathrm{m}})]\right)^{1/2}. \tag{4.25}$$

For $0 \le x \le x^{\mathrm{m}}$, one needs the minus sign since y is a decreasing function of x. For the right half $x^{\mathrm{m}} \le x \le h$, the plus sign is needed. To find y^{m} a second integration is needed resulting in

$$\cosh\left(\frac{\kappa h}{2}\right) = \frac{y^{\mathrm{d}}}{y^{\mathrm{m}}}; \tag{4.26}$$

or

$$y^{\mathrm{m}} = \frac{y^{\mathrm{d}}}{\cosh(\kappa h/2)} = y^{\mathrm{d}}\,\mathrm{sech}(\kappa h/2), \tag{4.27}$$

which is an analytical expression for y^{m} as a function of separation distance h.

For low potential approximation,

$$\kappa h = \frac{2\exp(-y^{\mathrm{m}})}{2}\left[F\left(\exp -y^{m/2}, \frac{\pi}{2}\right)\right] - \left[F\left(\exp -y^{m/2}, \arcsin\exp -(y^{\mathrm{d}} - y^{m/2})\right)\right], \tag{4.28}$$

in which

$$F(\kappa, \phi) - \int_0^{\phi} \frac{\mathrm{d}\chi}{(1 - \kappa^2 \sin^2\chi)} \tag{4.29}$$

is an elliptic integral for which tabulations are available [3].

Fig. 4.5 gives the results of the variation of midway potential with separation distance. For conversion of the abscissa axis into real distance, h is multiplied by κ. For 1 : 1 electrolyte, κ^{-1} is equal to 96.1, 9.61 and 0.96 nm for 10^{-5}, 10^{-3} and 10^{-1} mol dm^{-3} respectively. For 2 : 2 electrolytes the corresponding values are half as much.

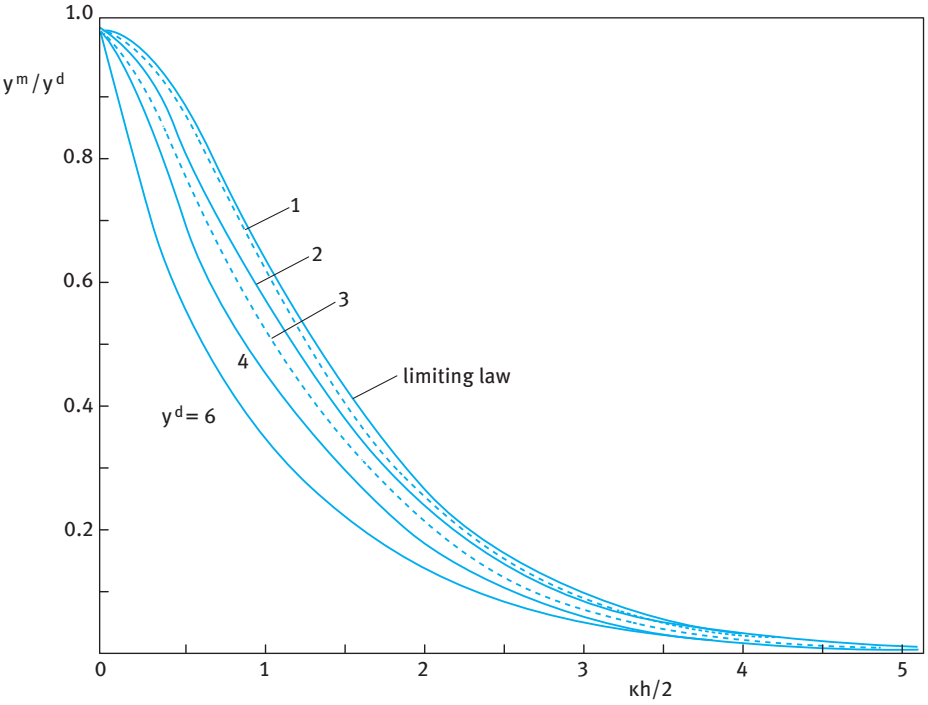

Fig. 4.5: Midway potential as a function of separation for two interacting flat double layers.

The limiting law overestimates y^m at given h, but remains a good approximation if y^d is not too high and if the overlap is not too strong. One must realize that every unit of y corresponds to 25.6 mV of potential at room temperature. Diffuse double layer potentials are rarely above 150 mV. And under conditions close to coagulation they are much lower. In addition, at high salt concentration, κ increases but y^d decreases. At low κh (strong overlap) equation (4.26) is inadequate, indicating the limited applicability of the pure diffuse double theory. One must take into account the specific adsorption of counterions and the ion size effect. These effects are considered in the Stern theory of double layers (see Chapter 2).

4.6 Interaction between spherical particles

The most common procedure to obtain the interaction between spherical particles is to use the Deryaguin approximation [6]. The interaction energy is considered to be built up of contributions of parallel rings and to approximate the total interaction as the integral over that set of infinitesimal parallel rings. A schematic illustration of the Deryaguin approximation is shown in Fig. 4.6 [1].

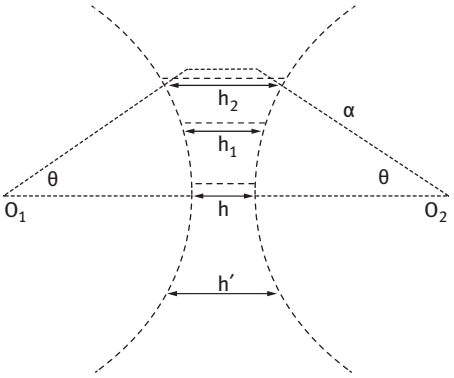

Fig. 4.6: Illustration of the Deryaguin approximation [6].

The above approximation is rigorous if there is no lateral interaction between the rings. For electrostatic interaction, this means that the field lines should run parallel to the O_1O_2 axis. This is exact for $h' = h$, but the condition becomes increasingly poorer in the direction $h' \to h_1 \to h_2$ as indicated by the dashed lines in Fig. 4.3. The Deryaguin approximation [6] is expected to work well for low κh and large κa (where a is the particle radius).

For two spheres with radii a_1 and a_2, $G_{\text{elec}}(h)$ is given by the following expression,

$$G_{\text{elec}}(h) = 2\pi \frac{a_1 a_2}{a_1 + a_2} \int_h^\infty G_{\text{a,elec}}(h')\,\mathrm{d}h'; \tag{4.30}$$

for two identical spheres, equation (4.30) becomes,

$$G_{\text{elec}}(h) = \pi a \int_h^\infty G_{\text{a,elec}}(h')\,\mathrm{d}h'; \tag{4.31}$$

and for a sphere-plate interaction,

$$G_{\text{elec}}(h) = 2\pi a \int_h^\infty G_{\text{a,elec}}(h')\,\mathrm{d}h'. \tag{4.32}$$

Numerous attempts have been made to obtain numerical results for a variety of systems and conditions, as for example described by Stankovich and Carnie [7]. An elaboration of the numerical results was given by Honig and Mul [8] who expressed $G_{\text{elec}}(h)$ by,

$$G_{\text{elec}}(h) = \frac{64\pi cRT}{\kappa^2} S(h). \tag{4.33}$$

They tabulated $S(h)$ at constant potential and constant charge for various values of $y^{\text{d}}(\infty)$, the dimensionless potential ($F\psi^{\text{d}}/RT$). For an aqueous solution at 25 °C,

$$\frac{Z^2 G_{\text{elec}}(h)}{a} = 4.751 \times 10^{11} S(h). \tag{4.34}$$

Fig. 4.7 shows the electrical contribution of the homo-interaction Gibbs energy between two spheres for different $y^{\text{d}}(\infty)$, using the Deryaguin approximation [6], at constant potential and constant charge [1]. The results predicts that the repulsion at constant charge is stronger than that at constant potential, but the difference is not large and sometimes virtually absent, namely at large κh and at high y^{d}. The curve at $y^{\text{d}} = 10$ shows no difference between $G^{(\psi)}$ and $G^{(\sigma)}$, but in this case the double layer potential

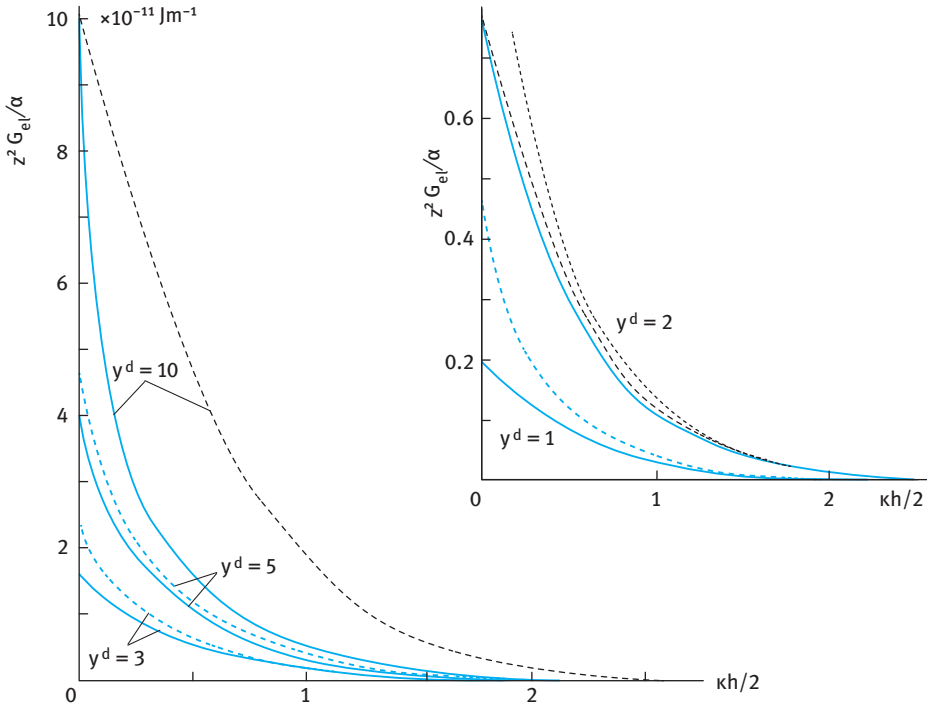

Fig. 4.7: Electric contribution to the homo-interaction Gibbs energy between two spheres for different $y^{\text{d}}(\infty)$, using the Deryaguin approximation: solid lines, constant potential; dashed lines, constant charge.

is about 250 mV which is rarely observable, except in very dilute electrolyte solutions, e.g. 10^{-4} mol dm^{-3} 1 : 1 electrolyte where $\kappa \approx 30\,\text{nm}^{-1}$. The results of the calculations clearly show that in all experiments where $\kappa h \geq 1$, the difference between interaction at constant charge and constant potential is insignificant.

The function $S(h)$ in equations (4.33) and (4.34) differs between interaction at constant potential and constant charge, but independent of the particle radius a. This means that both $G^{(\psi)}$ and $G^{(\sigma)}$ are proportional to the radius.

Several analytical expressions which are semi-quantitative are available and these are useful for practical calculation of the repulsive interaction.

For identical spheres at $\kappa a < 5$, i.e. the diffuse layer is of similar magnitude as the particle radius,

$$G^{\psi}_{\text{elec}} = 2\pi\varepsilon_r\varepsilon_0 a\psi_d^2 \exp(-\kappa h). \tag{4.35}$$

Equation (4.35) is derived using the Debye–Huckel approximation for the potential around each sphere and simply summing the two, i.e. weak overlap. As is the case for flat plates, $G^{\psi}_{\text{elec}} = G^{\sigma}_{\text{elec}}$. Equation (4.35) is best for weak interaction so that at $\kappa a > 2$ it is satisfactory over a wide range of κa. As $\kappa a \leq 1$, it is useful at close distance of approach [9].

For identical spheres at $\kappa a > 10$, i.e. the double layer is thin compared to particle radius, the result at low potential, for the constant potential case,

$$G^{\psi}_{\text{elec}} = 2\pi\varepsilon_r\varepsilon_0 a\psi_d^2 \ln[1 + \exp(-\kappa h)]. \tag{4.36}$$

h is the closest distance between the particles, i.e. $h = r - 2a$, where r is the centre–centre distance between the particles.

The constant charge expression is,

$$G^{\sigma}_{\text{elec}} = -2\pi\varepsilon_r\varepsilon_0 a\psi_d^2 \ln[1 + \exp(-\kappa h)]. \tag{4.37}$$

Equation (4.37) works well for all separations and is acceptable down to $\kappa a > 2$ if at close approach such that $\kappa h < 2$ [11].

The constant charge case, equation (4.37), should be used with caution, especially at close approach as a large overestimate can be obtained for the repulsive potential.

For two spheres with radii a_1 and a_2 at $\kappa a > 10$, Hogg et al. [10] derived the following expression for the repulsion at constant potential,

$$\psi^{\psi}_{\text{elec}} = \frac{\pi\varepsilon_r\varepsilon_0 a_1 a_2}{a_1 + a_2}(\psi_{d1}^2 + \psi_{d2}^2)\left\{\frac{2\psi_{d1}\psi_{d2}}{\psi_{d1}^2 + \psi_{d2}^2}\ln\left[\frac{1 + \exp(-\kappa h}{1 - \exp(-\kappa h)}\right] + \ln[1 - \exp(-2\kappa h)]\right\} \tag{4.38}$$

For a sphere and a flat plate, the repulsive interaction at $\kappa a < 5$ and weak overlap is twice that estimated for two similar spheres given by equation (4.35),

$$G^{\psi}_{\text{elec}} = 4\pi\varepsilon_r\varepsilon_0 a\psi_d^2 \exp(-\kappa h). \tag{4.39}$$

For close approach and large κa,

$$G_{\text{elec}}^{\psi} = 4\pi\varepsilon_r\varepsilon_0 a\psi_d^2 \ln[1 + \exp(-\kappa h)]. \tag{4.40}$$

4.7 Effect of increasing electrolyte concentration, valency of counterions and Stern potential

Increasing the electrolyte concentration results in compression of the double layer and this causes a reduction in double layer repulsion [3]. This is illustrated in Fig. 4.8 which shows the repulsive energy versus $H/2$ for two flat plates at a Stern potential of 154 mV and three values of κ for 1 : 1 electrolyte. In general, increasing the electrolyte concentration results in a decrease in the electrostatic repulsion.

The effect of valency of counterions is shown in Fig. 4.9 which compares the results for $Z = 1$ with those for $Z = 3$. As expected, increasing Z results in a decrease in the electrostatic repulsion.

The effect of increasing the Stern potential is illustrated in Fig. 4.10 which shows the values for three dimensionless y_d. An increase in the Stern potential at a given electrolyte concentration results in an increase in the electrostatic repulsion.

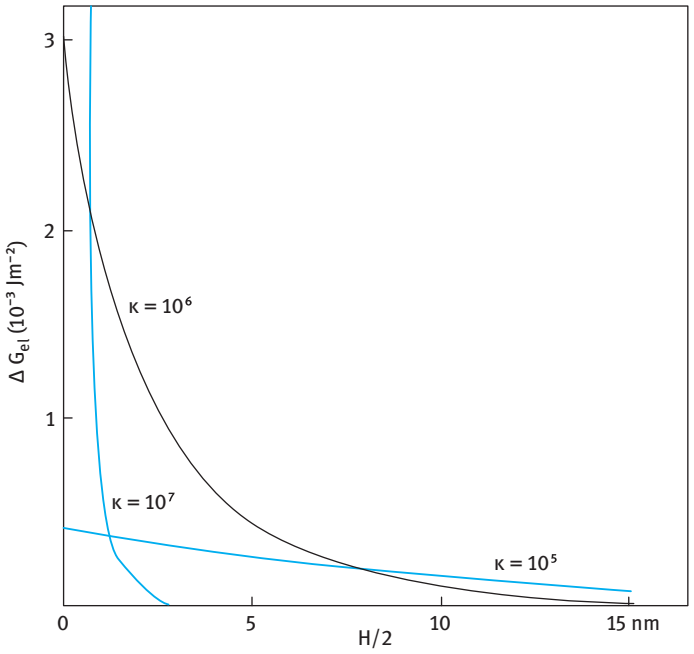

Fig. 4.8: Increase in the electrical free energy of two flat plates as a function of decreasing mutual distance for three values of the reciprocal Debye length: $\psi_d = 154$ mV; 1 : 1 electrolyte.

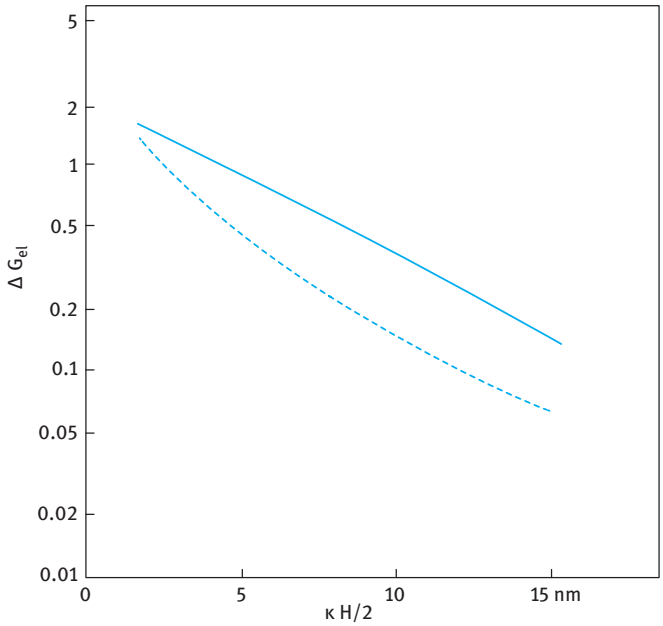

Fig. 4.9: Effect of counterion valency on the increase in free energy as a function of $\kappa H/2$ for two flat plates. Full line $y_d = 2$, $Z = 1$; dashed line $y_d = 6$, $Z = 3$. The units on the y-axis are only relative.

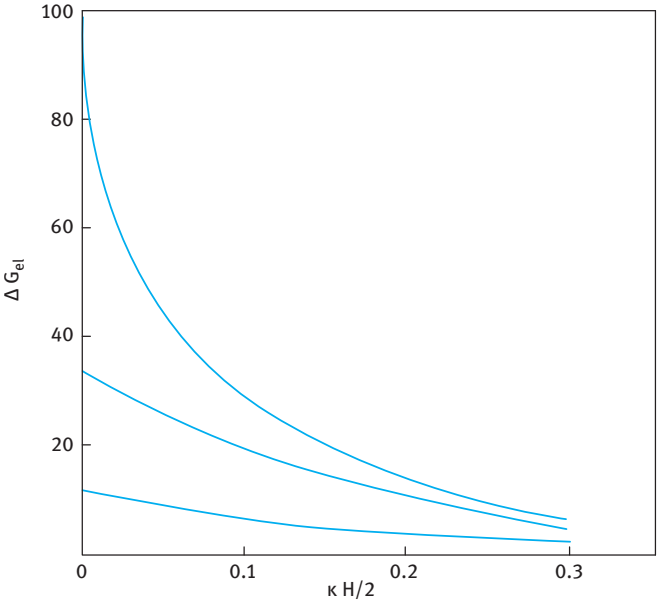

Fig. 4.10: Increase in electrical free energy of two flat plates as a function $\kappa H/2$. From top to bottom the lines correspond to dimensionless potential y_d of 8, 6 and 4, respectively. The units on the y-axis are only relative.

4.8 Effect of particle concentration

In all the above treatments the interaction is considered for isolated particles, where the time-average separation of the particles is much larger than the range of the diffuse layer. However, with most practical dispersions such a condition is seldom satisfied since in this case the separation of the particles become similar in magnitude to the range of the diffuse layer [4]. The background electrolyte now contains other particles with their counterions. Each charged particle is a "macro-ion", but the number is very much smaller than the number of corresponding counterions. Thus, the particle's contribution can be ignored without introducing a large error. However, when the volume occupied by the particles become significant, i.e. at high volume fraction, the ionic concentration in the liquid becomes larger since the particle volume is excluded to the ions. Russel et al. [11] gave a convenient expression for κ by considering the volume fraction of the particles ϕ,

$$\kappa = \left(\frac{e^2}{\varepsilon_r \varepsilon_0 kT} \frac{2Z^2 n_0 - \frac{3\sigma_0 Z\phi}{ae}}{1-\phi} \right). \tag{4.41}$$

The $(1-\phi)$ term in the denominator corrects the ion concentration for the volume occupied by the particles, σ_0 is the surface charge density which can be calculated from the Stern or zeta potential. Fig. 4.11 shows the variation of Debye length with

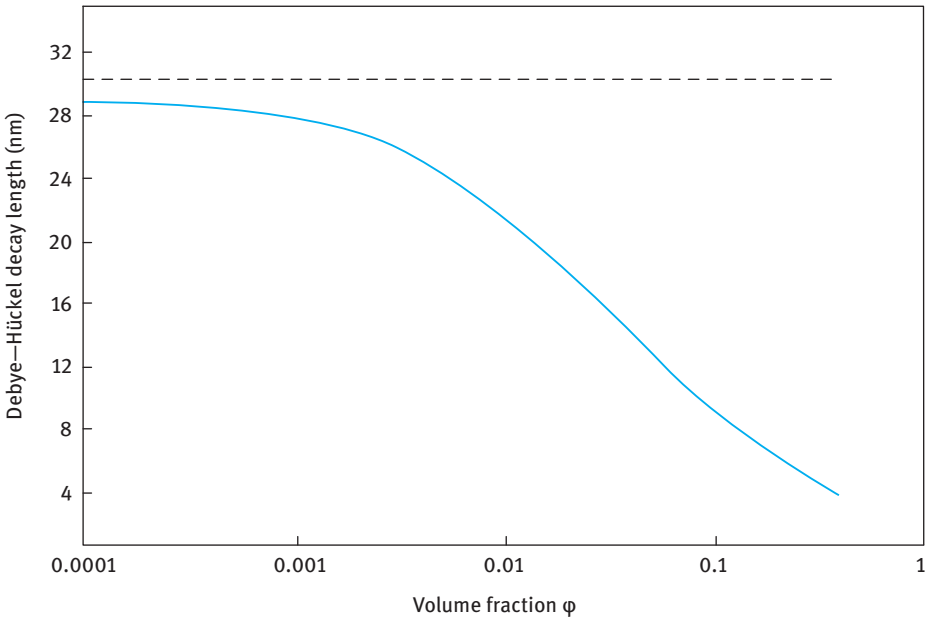

Fig. 4.11: Debye length as a function of particle volume fraction in 10^{-4} mol dm^{-3} NaCl: $a = 200$ nm; $\sigma_0 = -10\,\mu$C cm^{-2}. The dashed line represents the limiting value for zero volume fraction.

particle volume fraction in 10^{-4} mol dm^{-3} NaCl for particles of radius $a = 200$ nm and charge density σ_0 of -10 μC cm^{-2}.

It is clear from Fig. 4.11 that the Debye length decreases gradually with increasing particle volume fraction and at $\phi > 0.01$ it shows a more rapid decrease reaching about 4 nm when $\phi \approx 0.3$. This reduction in Debye length is the consequence of the increase in ion concentration produced by the counterions of the high number concentration of the particles. This reduction in Debye length is reflected in the reduction of electrostatic repulsion as illustrated in Fig. 4.12. It can be clearly seen that by increasing the particle volume fraction the electrostatic repulsion decreases due to the reduction in the Debye length (compression of the electrical double layer). This explains why in many practical dispersions prepared at high volume fraction ($\phi > 0.3$) electrostatic repulsion is insufficient for the long-term colloid stability of the dispersion.

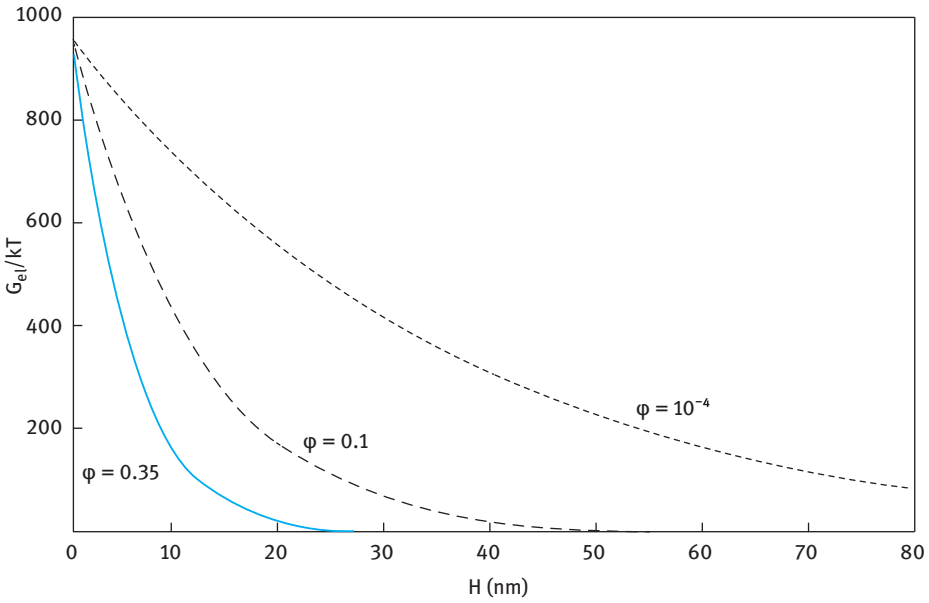

Fig. 4.12: Electrostatic repulsion for three particle volume fractions in 10^{-3} mol dm^{-3} NaCl: $a = 200$ nm; $\psi_d = -80$ mV; $\sigma_d = -10$ μC cm^{-2}.

References

[1] Lyklema J. Fundamentals of interface and colloid science. Vol. IV. London: Academic Press, Amsterdam: Elsevier; 2005.
[2] Deryaguin BV, Landau L. Acta Physicochem USSR. 1941;14:633.
[3] Verwey EJW, Overbeek JTG. Theory of stability of lyophobic colloids. Amsterdam: Elsevier; 1948.

[4] Goodwin JW. Colloids and interfaces with surfactants and polymers. London: John Wiley and Sons; 2009.
[5] Hunter RJ. Fundamentals of colloid science. Oxford: Oxford University Press; 1987.
[6] Deryaguin BV. Kolloid Z. 1934;69:155.
[7] Stankovich J, Carnie SL. Langmuir. 1996;12:1453.
[8] Honig EP, Mul PM. J Colloid Interface Sci. 1971;36:258.
[9] Glendinning AR, Russel WB. J Colloid Interface Sci. 1983;93:93.
[10] Hogg R, Healy TW, Fursteneau DW. Trans Faraday Soc. 1966;62:1683.
[11] Russel WB, Saville DA, Schowalter WR. Colloidal dispersions. Cambridge: Cambridge University Press; 1989.

5 Van der Waals attraction

5.1 Introduction

Van der Waals attraction between colloidal particles is universal and it occurs with all disperse systems. As is well known, in a one component system individual atoms or molecules always attract each other at short distances, owing to the van der Waals forces, which as will be shown below can be of three different kinds, namely dipole-dipole, dipole-induced dipole and London dispersion interaction. Since colloidal particles are essentially assemblies of molecules, the individual contributions have to be compounded. In this process, only the London interactions have to be considered, since large assemblies have neither a permanent dipole moment nor a net polarization. The assumption is made that the interaction energies between all molecules in one particle with all those in the other are simply additive.

In this chapter, I will start with a general expression for the interaction energy in terms of the work required to separate the particles. This is followed by a section on the intermolecular attraction between atoms or molecules. Two general approaches to van der Waals attraction between macroscopic bodies are discussed. The first approach, referred to as the microscopic approach, is based on a simple additively principle of all intermolecular attractions. The second approach, referred to as the macroscopic approach, is based on the principle that the electromagnetic fluctuations in two particles become correlated when they approach each other, causing a decrease in the free energy of the system. A section is devoted to the direct measurement of van der Waals forces, using the surface force apparatus.

5.2 General expression for the interaction between two particles

The interaction between two particles can in general be considered in terms of the potential energy or the work required to separate them from a centre-to-centre distance r to some large distance apart [1]. This potential energy is termed the pair potential $u(r)$ that is given by the following expression,

$$u(r) = -\int_{r}^{\infty} f(r)\,\mathrm{d}r, \tag{5.1}$$

where $f(r)$ is the force at distance r,

$$\frac{\mathrm{d}u(r)}{\mathrm{d}r} = -f(r). \tag{5.2}$$

https://doi.org/10.1515/9783110540895-006

The particles can be thought of as interacting via "colloidal springs" and the spring constant (or modulus) is the rate of change of the force with distance,

$$\frac{d^2u(r)}{dr^2} = y(r). \tag{5.3}$$

The interaction energy includes both enthalpic and entropic contributions of all components in the system, namely particles, solvent, ions, surfactants, polymers, etc. This means that the interaction energy between any two particles should take into consideration all other components, i.e. the potential of mean force. A detailed account of both intermolecular forces and interaction between the particles was given in the text by Israelachvili [2] to which the reader should refer for more detail.

Two main contributions to the interaction between the particles can be identified, namely the interparticle force that brings them together (to be referred to as van der Waals attraction) and the force that acts to separate them (to be referred to as the repulsive force or energy). It is the interplay between these forces that determines the final state of the dispersion. In this chapter, I will describe the intermolecular attraction or van der Waals forces. The repulsive forces arising from the presence of double layers was described in Chapter 4.

5.3 Intermolecular attraction between atoms or molecules

Before describing the van der Waals attraction between particles or droplets in a dispersion, one must first consider the intermolecular attraction between atoms or molecules. These interactions account for the non-ideality of gases and deviation from the ideal gas equation ($PV = nRT$, where P is the pressure, V is the volume, n is the number of moles, R is the gas constant and T is the absolute temperature). This non-ideality was described by van der Waals using a semi-empirical equation of state,

$$\left(P + \frac{an^2}{V}\right)(V - nb) = nRT, \tag{5.4}$$

where a accounts for the attraction between the molecules (now called van der Waals attraction), b is the intrinsic volume of the molecules and n is the number of molecules per unit volume.

Three main contributions to the intermolecular interaction can be considered and these are summarized below.

5.3.1 Dipole-dipole interaction (Keesom–van der Waals interaction)

This interaction arises from the presence of permanent dipoles [3], e.g. with HCl gas that has a strong dipole due to polarization of the covalent bond. The dipoles tend to

align giving the following expression for the interaction energy $u(r)_K$ at an intermolecular distance r,

$$u(r)_K = -\frac{\beta_{11K}}{r^6}, \tag{5.5}$$

where β_{11K} is a constant that depends on the particular type of the molecule. For two identical molecules with dipole moment μ, $\beta_{11K} \propto \mu^4$. Equation (5.5) shows that the Keesom interaction is short range in nature being proportional to $1/r^6$. Due to marked dipole alignment, the rotational motion of the molecules is restricted and this results in a "long time" interaction that occurs at low frequency.

5.3.2 Dipole-induced dipole interaction (Debye–van der Waals interaction)

This occurs between a polar and nonpolar molecule [4]. The dipole on the polar molecule polarizes the electron clouds of the nonpolar molecule. The molecular motion is still occurring and we could think here of frequencies associated with the interaction as those in the microwave region. The interaction free energy can be described by a similar expression to that used in the dipole-dipole interaction,

$$u(r) = -\frac{\beta_{11D}}{r^6}, \tag{5.6}$$

where β_{11D} is a constant that consists of two terms for two different molecules,

$$\beta_{11D} \propto (\alpha_1\mu_1^2 + \alpha_2\mu_2^2). \tag{5.7}$$

5.3.3 London–van der Waals interaction (dispersion interaction)

The London dispersion force is the most important, since it occurs for polar and nonpolar molecules. It arises from fluctuations in the electron density distribution [5]. It is due to the movement of the electron cloud around the atomic nucleus resulting in a dipole that fluctuates. When two atoms come into close proximity, the temporary dipoles become aligned, i.e. the fluctuations become coupled and this is a preferred (or lower) energy state. The range of interaction is similar to that of Keesom and Debye, but the timescale is now that of the electronic transition, near the visible-ultraviolet part of the electromagnetic spectrum. The London–van der Waals interaction energy is given by,

$$u(r) = -\frac{\beta_{11L}}{r^6}. \tag{5.8}$$

The London dispersion constant β_{11L} for two identical atoms is proportional to the ionization energy of the outer electrons, $h\nu_1$, and the polarizability α, where h is the Planck constant and ν is the frequency of radiation in Hz (= $\omega/2\pi$, where ω is the frequency in rad s^{-1}),

$$\beta_{11L} \propto h\nu_1\alpha^2. \tag{5.9}$$

For two different atoms,

$$\beta_{12L} \propto h\frac{\nu_{11}\nu_{12}}{\nu_{11}+\nu_{12}}\alpha_1\alpha_2. \tag{5.10}$$

The London–van der Waals intermolecular interaction is mostly much larger than the Keesom–van der Waals or Debye–van der Waals contributions. Water is exceptional since in this case the dispersion contribution is only one-quarter of the total interaction.

5.4 General approach for van der Waals attraction

As shown above, all three interactions are based on the attraction between dipoles and have the same distance separation. Therefore, it is possible to describe the attraction in a general way. The London constant in equations (5.9) and (5.10) depends on the ionization potential of the outer electrons which is in the region of the visible-ultraviolet part of the electromagnetic spectrum. Other electronic transitions also take place so that contributions at other frequencies can also occur. For a general approach one must consider the full range of frequencies, ranging from those of a few Hertz up to the ultraviolet region at $\approx 10^{16}$ Hz.

The above description considered the case of interaction of atoms or molecules in the absence of any intervening medium. The relative permittivity of the medium is an important factor. The relative permittivity $\varepsilon(\nu)$ as a function of frequency describes the dielectric behaviour at low frequencies and the refractive index $n(\nu)$ is a viable measure of the dielectric behaviour at the higher end of the spectrum. A general description of the interaction $u(r)$ was given by McLachlan [6] as a summation over the range of interaction frequencies for molecules 1 and 2 interacting in a medium 3,

$$u(r) = -\left\{\frac{3kT\alpha_1(0)\alpha_2(0)}{[4\pi\varepsilon_3(0)\varepsilon(0)]^2 r^6} + \frac{6kT}{(4\pi\varepsilon_0)^2 r^6}\sum_{n=1}^{\infty}\frac{\alpha_1(\mathrm{i}\nu)\alpha_2(\mathrm{i}\nu)}{\varepsilon_3^2(\mathrm{i}\nu)}\right\}, \tag{5.11}$$

where k is the Boltzmann constant, T is the absolute temperature and i indicates the imaginary component of the frequency. The summation is carried over all frequencies so that all interactions are captured. The first term on the right-hand side of equation (5.11) is the "zero" frequency term, whereas the second term gives the contributions for all other frequencies, with the steps in terms of kT,

$$n = \frac{h\nu_n/2\pi}{kT}. \tag{5.12}$$

This second term uses the frequency dependency of the polarizability at complex frequencies iν, with i indicating the dissipative component of the complex frequency, since we are looking at the interaction of oscillating electromagnetic field with the molecules.

5.5 Hydrogen bonding

Hydrogen bonding may be considered as a special type of Debye interaction, in so far as one of the molecules (or groups) is polar and the other is apolar. However, there are many differences so that it is more appropriate to consider them as a special case. The distinguishing feature is the involvement of a hydrogen atom in the bond. In some molecules, the very electropositive hydrogen atom acts as a concentrated site of excess positive charge. This is particularly the case for asymmetric configurations in which the proton under consideration is involved. Examples of groups in molecules possessing such a proton are –OH (in water, alcohols, carboxylic acids), -NH (in primary and secondary amines), HF and HCl. A very strong interaction ensues if such a proton comes into contact with a strongly electronegative group in another molecule, notably in an oxygen (in water, alcohols, ketones, esters, ethers, carboxylic acids), a nitrogen (in amines, pyridine), fluorine or chlorine atom. Water is a particularly strongly associated liquid because each water molecule has two hydrogen atoms, capable of binding with oxygen atoms of two other water molecules. Hydrogen bonding is a weak chemical bonding and its quantitative analysis requires quantum mechanics. Some distinguishing features can be identified:

(i) The bond is directional and the combination H...O–X, where X is the remainder of the molecule, is in principle linear;
(ii) two hydrogen bonded electronegative atoms can approach each other more closely than the sum of their crystal radii;
(iii) the bond enthalpy is in the range of 10–40 kJ mol^{-1}, which is lower than that of a chemical bond (> 150 kJ mol^{-1}) but higher than the three types of van der Waals forces ($\approx$ 1 kJ mol^{-1} at $r \approx r_m$).
(iv) Ordinary van der Waals forces can compete with thermal energy only at low T and/or when the molecules are large.

Covalent bonds break only at very high T. Hydrogen bonds take an intermediate position. It is especially in water that their presence is significant; the high boiling point of water, notwithstanding the lower molecular mass, is attributed to hydrogen bonding. This explains why hydrogen bonding plays important roles in interfacial phenomena.

5.6 Hydrophobic (bonding) interaction

Hydrophobic bonding describes the strong attraction between hydrophobic molecules or hydrophobic parts of the molecules in water. It is due to the tendency of water molecules to associate by hydrogen bonding near the hydrophobic molecules. For example, if a nonpolar molecule such as He or hydrocarbon is dissolved in water a cavity has to be formed, requiring considerable energy expenditure because many hydrogen bonds have to be broken. The van der Waals energy that is gained by inserting the apolar

molecules into the cavity is of the Debye or London type, but by no means enough to compensate for the loss in cavity formation. Thus, the total Gibbs energy of dissolution would be high and positive. The water tetrahedrons that are in contact with the apolar molecule tend to reorient so as to form as many hydrogen bonds with neighbouring molecules as possible. In this way, the loss of energy is to a large extent compensated, but now at the expense of a loss of entropy, due to the reduction of the degrees of freedom of the adjacent water molecules. The formation of a "cage" of water molecules with a stronger structure is referred to as the "hydrophobic effect". The ordered water structure is sometimes described as "icebergs". For gaseous hydrocarbons in water at room temperature the entropy term is dominant; the enthalpy is small and can be positive or negative. At higher temperatures, structure formation around the apolar molecules plays a less important role (due to increased randomization of water molecules), i.e. the entropic contribution becomes smaller. Hydrophobic bonding is the direct consequence of the "hydrophobic effect". Hydrophobic bonding plays an important role in interfacial phenomena, adsorption of surfactants from aqueous solutions, micelle formation and other association processes.

5.7 Van der Waals attraction of macroscopic bodies

There are generally two approaches for describing the van der Waals attraction between macroscopic bodies such as colloidal particles, emulsion droplets, etc. The first approach considers the London–van der Waals attraction to be the sum of the forces acting between isolated molecules. This approach, referred to as the microscopic approach, was suggested by de Boer and Hamaker [7, 8]. The second approach, developed by Lifshitz et al. [9], is based on the correlation between electric fluctuations of two macroscopic bodies. This is referred to as the macroscopic approach.

5.7.1 The microscopic approach for van der Waals attraction

This approach starts with the finding that the Gibbs energy of interaction can be given by the product of a material constant, $A_{ij(k)}$, and a function of geometry and distance h, $f(a, h)$ [10]. $A_{ij(k)}$, referred to as the Hamaker constant, refers to the interaction between two particles or macrobodies i and j across a medium k,

$$G_{\mathrm{VDW}}(h) = -A_{ij(k)} f(a, h). \tag{5.13}$$

For two identical particles in an aqueous medium, $A_{ij(k)}$ becomes $A_{11(\mathrm{w})}$. The dimensions of the distance function, $f(a, h)$, depend on the geometry of the system. For semi-finite plates $f(a, h) = f(h)$ is proportional to h^{-2} and $G_{\mathrm{VDW}}(h)$ is in J m^{-2}. For two spheres $f(a, h)$ is dimensionless and $G_{\mathrm{VDW}}(h)$ is in J.

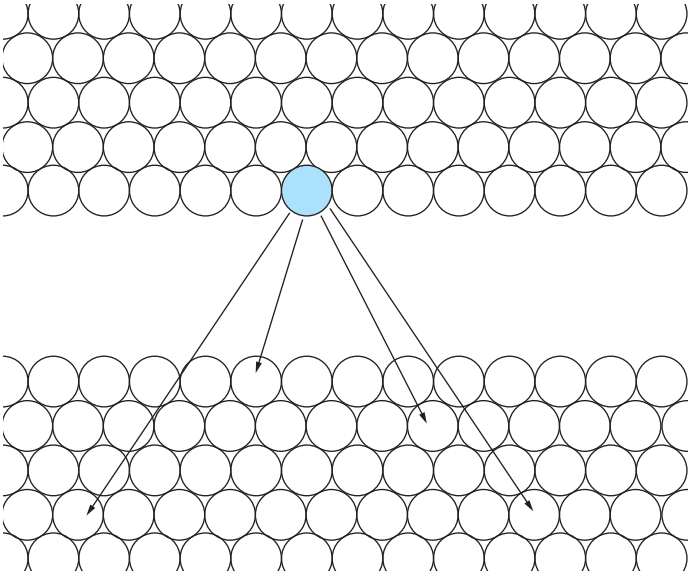

Fig. 5.1: Schematic representation of atomic dipolar interactions between two slabs of material.

Consider two slabs of interacting materials as schematically represented in Fig. 5.1.

The starting point is to consider the interaction between a single molecule and a slab of material and then extend that to two slabs interacting [1]. In the microscopic approach due to Hamaker [8], the energies are assumed to additive. In this case one can simply use equation (5.8) and add all interactions between the reference molecule in the upper slab (shown by a dark circle in Fig. 5.1) and all other molecules in the material of the lower slab. The interaction energy is given by the sum for each molecule in the lower slab. One then adds this up for all molecules in the upper slab. The interaction is then given by the sum for all molecules in the upper slab multiplied by the sum for each molecule in the lower slab.

To calculate the intermolecular distance r one can simply use the number density of molecules in the slab, $\rho_N (= N/V)$, and integrate over the volumes. This "semi-continuum" approach is the basis of the additively assumption and it would only become a problem at very close approach. The interaction energy then follows from equation (5.13),

$$G_{VDW}(h) = -\pi^2 \beta_{11L} \rho_N^2 f(a, h). \tag{5.14}$$

Equation (5.14) gives a general expression for the van der Waals attraction in terms of the material constant (that is given by the electronic polarizability, the ionization potential and the square of the product of the density and molar mass) and the shape factor and separation distance between the two bodies.

For two infinitely thick slabs, the energy of unit area of one slab interacting with the whole of the other slab is given by,

$$G_{\mathrm{VDW}}(h) = -\frac{\pi\beta_{11\mathrm{L}}\rho_{\mathrm{N}}^2}{12h^2}, \tag{5.15}$$

where $G_{\mathrm{VDW}}(h)$ represents the dispersion energy of two slabs of the same material a distance h apart and it is the energy per unit area of the surface. The numerator represents the material property whereas the denominator arises from the geometry. It is common in colloid science to express the material property as a single constant, referred to as the Hamaker constant that is simply given by,

$$A_{11} = \pi^2\beta_{11\mathrm{L}}\rho_{\mathrm{N}}^2. \tag{5.16}$$

Equation (5.15) can then be written as,

$$G_{\mathrm{VDW}}(h) = -\frac{A_{11}}{12\pi h^2}. \tag{5.17}$$

If one has a slab of material 1 interacting with material 2,

$$G_{\mathrm{VDW}}(h) = -\frac{A_{12}}{12\pi h^2}, \tag{5.18}$$

and,

$$A_{12} = \pi^2\beta_{12\mathrm{L}}\rho_{\mathrm{N1}}\rho_{\mathrm{N2}}. \tag{5.19}$$

If the "semi-infinite" slabs are replaced by plates with thickness t, equation (5.17) has to be modified,

$$G_{\mathrm{VDW}}(h) = -\frac{A_{11}}{12\pi}\left(\frac{1}{h^2} + \frac{1}{(h+2t)^2} - \frac{2}{(h+t)^2}\right) \tag{5.20}$$

Hamaker constants can be computed from equation (5.19) if the molecular properties of the materials under consideration are known. Alternatively, they can be derived from the macroscopic theory as will be discussed below. Direct measurement of van der Waals attraction can also be used to obtain the Hamaker constant (see below). Their magnitude is in the order of 10^{-20}–10^{-19} J ($\approx$ 5–50 kT) at room temperature. As we will see later, the Hamaker constants for interaction across a medium are much lower.

For curved interfaces (as is the case with spherical particles) the expression for the van der Waals attraction is more complex. However, a useful method to derive such an expression is to use the Deryaguin approximation [9], where the curved surface is replaced by a stepped one as illustrated in Fig. 5.2. The total interaction between the macroscopic bodies is considered to be built up of contributions of parallel rings where each pair contributes an amount $G_{\mathrm{A}}(x)\,\mathrm{d}A$, where $G_{\mathrm{A}}(x)$ is given by equation (5.18). From the energy per ring, the total interaction energy is obtained by integration over y (as indicated in Fig. 5.2) after replacing $\mathrm{d}A$ by $2\pi y\,\mathrm{d}y$. As the approximation is limited to short distances, the contributions of layers with large y are negligible, so that for

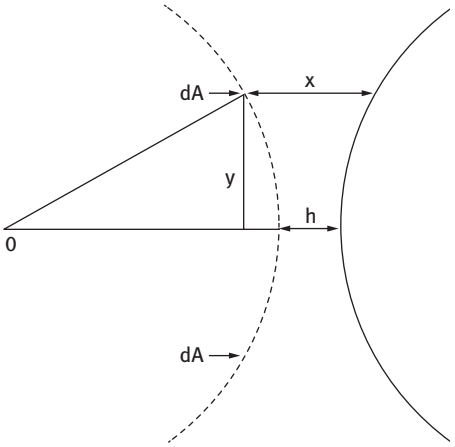

Fig. 5.2: Schematic representation of Deryaguin's approximation [9].

convenience the integration may be carried out from $y = 0$ to $y = \infty$. After relating y to x, the Deryaguin formula for two spheres of radii R_1 and R_2 becomes,

$$G_A = -\frac{2\pi R_1 R_2}{R_1 + R_2} \int_h^\infty G_A(x)\,dx. \tag{5.21}$$

Substituting equation (5.18) into (5.21) and carrying out the integration gives,

$$G_{VDW}(h) = -\frac{A_{12} R_1 R_2}{6h(R_1 + R_2)}. \tag{5.22}$$

For two spheres of equal radius,

$$G_{VDW}(h) = -\frac{A_{11} R}{12h}. \tag{5.23}$$

Equations (5.22) and (5.23) apply only for the case $h < R_1, R_2$ and $h < R$ respectively. For the general case of a wide range of h, expressions can be derived both for particles with different radii and of equal radii as schematically shown in Fig. 5.3.

For two spheres with different radii R_1 and R_2,

$$G_{VDW}(h) = -\frac{A}{12}\left[\frac{y}{x^2 + xy + x} + \frac{y}{x^2 + xy + x + y} = 2\ln\left\{\frac{x^2 + xy + y}{x^2 + xy + x + y}\right\}\right], \tag{5.24}$$

where $x = h/2R_1$ and $y = R_2/R_1$.

For two spheres with equal radii,

$$G_{VDW}(h) = -\frac{A_{11}}{6}\left[\frac{2R^2}{r^2 - 4R^2} + \frac{2R^2}{r^2} + \ln\frac{r^2 - 4R^2}{r^2}.\right] \tag{5.25}$$

Substituting $s = r/R$,

$$G_{VDW}(h) = -\frac{A_{11}}{6}\left(\frac{2}{s^2 - 4} + \frac{2}{s^2} + \ln\frac{s^2 - 4}{s^2}\right). \tag{5.26}$$

For very short distances ($h \ll R$), equation (5.26) may be approximated by equation (5.23).

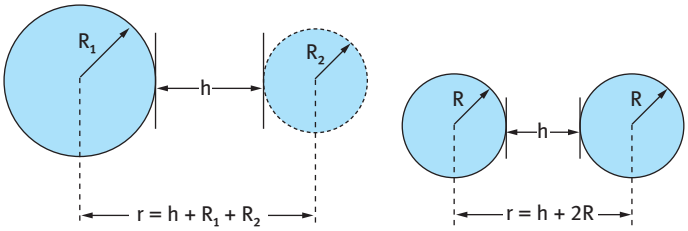

(a) Two Unequal Spheres (b) Two Equal Spheres

Fig. 5.3: Schematic representation of the interaction between spheres of different radii (a) and with the same radius (b).

For sphere-plate interaction (as is the case for particle-surface deposition and adhesion), $R_1 = R$ and $R_2 \to \infty$,

$$G_{\mathrm{VDW}}(h) = -\frac{A_{12}}{6}\left[\frac{R}{h} + \frac{R}{h+2R}\ln\frac{h}{h+2R}\right], \tag{5.27}$$

which for very small distance,

$$G_{\mathrm{VDW}}(h) = -\frac{A_{12}R}{6h}. \tag{5.28}$$

Equation (5.28) shows that the interaction of a sphere with a thick plate has a geometric factor that is twice that of two similar sized spheres.

5.7.2 Medium effect on van der Waals attraction

When the particles are dispersed in a liquid medium, the van der Waals attraction has to be modified to take into account the medium effect. When two particles are brought from infinite distance to h in a medium, an equivalent amount of medium has to be transported the other way round. Hamaker forces in a medium are excess forces.

Consider two identical spheres 1 at a large distance apart in a medium 2 as is illustrated in Fig. 5.4 (a). In this case the attractive energy is zero. Fig. 5.4 (b) gives the same situation with arrows indicating the exchange of 1 against 2. Fig. 5.4 (c) shows the complete exchange which now shows the attraction between the two particles 1 and 1 and equivalent volumes of the medium 2 and 2.

The effective Hamaker constant for two identical particles 1 and 1 in a medium 2 is given by,

$$A_{11(2)} = A_{11} + A_{22} - 2A_{12} = (A_{11}^{1/2} - A_{22}^{1/2})^2. \tag{5.29}$$

Equation (5.29) shows that two particles of the same material attract each other unless their Hamaker constants exactly matches each other. Equation (5.23) now becomes,

$$G_{\mathrm{VDW}}(h) = -\frac{A_{11(2)}R}{12h}, \tag{5.30}$$

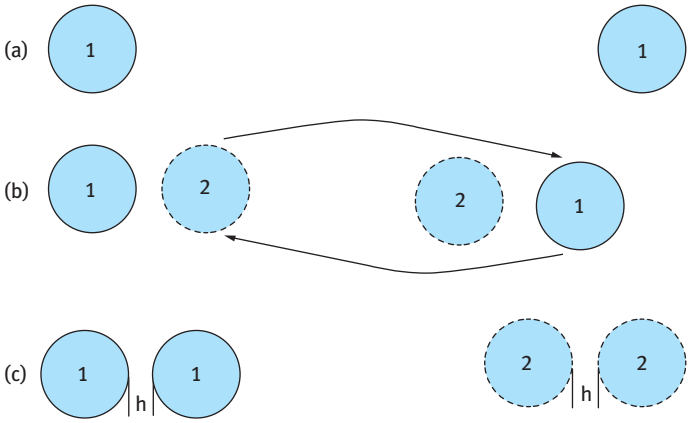

Fig. 5.4: Schematic representation of interaction of two particles in a medium.

where $A_{11(2)}$ is the effective Hamaker constant of two identical particles with Hamaker constant A_{11} in a medium with Hamaker constant A_{22}.

In most cases the Hamaker constant of the particles is higher than that of the medium. Examples of Hamaker constant for some materials in vacuum are given in Tab. 5.1. The Hamaker constant for some liquids is given in Tab. 5.2. Tab. 5.3 gives values of the effective Hamaker constant for some particles in some liquids. Generally speaking, the effect of the liquid medium is to reduce the Hamaker constant of the particles below its value in vacuum (air).

Tab. 5.1: Hamaker constant in vacuum A_{11} for some materials.

Material	$A_{11} \times 10^{20}$ **(J)**
Fused quartz (SiO_2)	6.5
Al_2O_3	15.6
Silver	50.0
Copper	40.0
Poly(methylmethacrylate)	7.1
Poly(vinylchloride)	7.8

Tab. 5.2: Hamaker constant of some liquids.

Liquid	$A_{22} \times 10^{20}$ **(J)**
Water	3.7
Ethanol	4.2
Decane	4.8
Hexadecane	5.2
Cyclohexane	5.2

Tab. 5.3: Effective Hamaker constant $A_{11(2)}$ of some particles in water.

System	$A_{11(2)} \times 10^{20}$ (J)
Fused quartz/water	0.83
Al_2O_3/water	5.32
Copper/water	30.00
Poly(methylmethacrylate)/water	1.05
Poly(vinylchloride)/water	1.03
Poly(tetrafluoroethylene)/water	0.33

G_A decreases with increasing h as schematically shown in Fig. 5.5, which illustrates G_A increasing very sharply with h at small h values. A capture distance can be defined at which all the particles become strongly attracted to each other (coagulation). At very short distances, the Born repulsion appears.

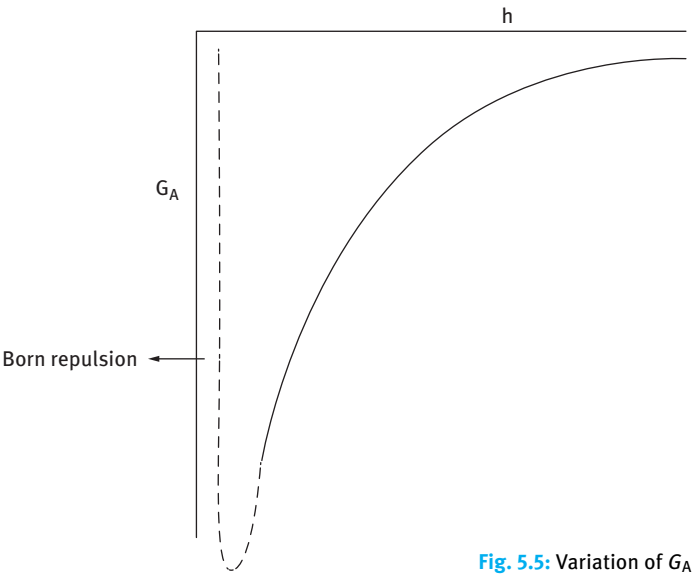

Fig. 5.5: Variation of G_A with h.

5.7.3 Macroscopic approach (Lifshitz theory of dispersion forces)

One of the problems with the microscopic approach of Hamaker [8] is the situation when one is dealing with particles in a medium such as an electrolyte solution. In this case the interaction of permanent dipoles is screened by the ionic environment and the low frequency interaction falls off more rapidly than would be the case in a vacuum. This problem can be solved by using the generalized macroscopic theory of Lifshitz [10, 11] that is described in detail by Mahanty and Ninham [12]. It is based

on the principle that the spontaneous electromagnetic fluctuations in two particles become correlated when they approach each other, causing a decrease in the free energy of the system. This theory treats the interacting bodies as continuous and ascribes the interactions to fluctuating electromagnetic fields arising from spontaneous electric and magnetic polarizations within the various media. One important result is that the interactions are described completely in terms of the complex dielectric constants of the media.

Consider two slabs of material, 1 and 2, interacting across a medium 3. Each one of these materials can be considered as a dielectric with static dielectric constants of $\varepsilon_1(0)$, $\varepsilon_2(0)$ and $\varepsilon_3(0)$, respectively. The interaction energy is given by the product of the material constant (the Hamaker constant) and a geometrical factor as described by equation (5.13). The Hamaker constant for two slabs of material 1 and 2 across medium 3 is given by,

$$A_{132} = \pi^2 \beta_{132\mathrm{L}} \rho_{\mathrm{N}1} \rho_{\mathrm{N}2}. \tag{5.31}$$

The London dispersion term, $\beta_{123\mathrm{L}}$, is given by the second term of the right-hand side of equation (5.11), which includes the polarizabilities of the molecules making up materials 1, 2 and 3. The bulk polarizability of slab 1 in medium 3 and the measurable macroscopic dielectric properties are given by,

$$\rho_{\mathrm{N}1} \alpha_1(\mathrm{i}\nu) = 2\varepsilon_0 \varepsilon_3(\mathrm{i}\nu) \frac{\varepsilon_1(\mathrm{i}\nu) - \varepsilon_3(\mathrm{i}\nu)}{\varepsilon_1(\mathrm{i}\nu) + \varepsilon_3(\mathrm{i}\nu)}. \tag{5.32}$$

Similarly the bulk polarizability of slab 2 in medium 3 is given by,

$$\rho_{\mathrm{N}2} \alpha_2(\mathrm{i}\nu) = 2\varepsilon_0 \varepsilon_3(\mathrm{i}\nu) \frac{\varepsilon_2(\mathrm{i}\nu) - \varepsilon_3(\mathrm{i}\nu)}{\varepsilon_2(\mathrm{i}\nu) + \varepsilon_3(\mathrm{i}\nu)}. \tag{5.33}$$

The frequency-dependent Hamaker function is then [2],

$$\begin{aligned} A_{132} \approx & \left[\frac{\varepsilon_1(0) - \varepsilon_3(0)}{\varepsilon_1(0) + \varepsilon_3(0)}\right]\left[\frac{\varepsilon_2(0) - \varepsilon_3(0)}{\varepsilon_2(0) + \varepsilon_3(0)}\right] \\ & + \frac{3h}{4\pi} \int_{\nu_1}^{\infty} \left[\frac{\varepsilon_1(\mathrm{i}\nu) - \varepsilon_3(\mathrm{i}\nu)}{\varepsilon_1(\mathrm{i}\nu) + \varepsilon_3(\mathrm{i}\nu)}\right]\left[\frac{\varepsilon_2(\mathrm{i}\nu) - \varepsilon_3(\mathrm{i}\nu)}{\varepsilon_2(\mathrm{i}\nu) + \varepsilon_3(\mathrm{i}\nu)}\right] \mathrm{d}\nu. \end{aligned} \tag{5.34}$$

Equation (5.34) shows that to obtain the Hamaker constant one must know the dielectric properties over the whole spectrum range. Calculation of the Hamaker constant requires extensive measurements from dielectric spectroscopy. Such information is only available for a very few systems. For example, Parsegian and Weiss [13] made such calculations for model polystyrene latex and they compared the results with those obtained by using the simple Hamaker equation. Good agreement was obtained between the data although the Hamaker calculations overestimated the interaction at long distances of separation (> 30 nm). As we will see below, this is due to the so called "retardation effect" which is included in the Lifshitz theory.

5.8 Retardation effect

The London–van der Waals forces exhibit the phenomenon of retardation. Due to the time required for electromagnetic waves to cover the distance between the plates, the h^{-2} dependence of $G_{\mathrm{VDW}}(h)$ given by equation (5.17) gradually changes to h^{-3}. Consider for example two surfaces separated by a distance of 30 nm. The propagation time from one surface to another and back would be $\approx 10^{-16}$ s. The frequency of radiation where the strongest interaction occurs is usually in the near UV region and so the propagation time represents the time taken for a significant part of the oscillation to occur. In other words, the oscillations are no longer exactly in phase (i.e. the dipoles are no longer completely aligned) and the attraction is weakened. Thus, one can conclude that the attraction at close separation between the particles using the Hamaker equation is a good approximation, but at separations > 30 nm the values calculated overestimate the interaction.

The retardation effect was first described by Casimir and Polder [14] who showed that for two identical atoms $u(r)$ decreases more rapidly with distance at large r when compared with that at small r. For very large distances,

$$u(r) = -\frac{\beta'_{11}}{r^7}. \tag{5.35}$$

For intermediate distances, there is a gradual transition from the r^{-6} to r^{-7} power law.

5.9 Direct measurement of van der Waals attraction between macroscopic bodies

Measurement of van der Waals attraction requires very smooth and clean surfaces that can be manipulated meticulously since one has to make measurements at separation distances from about 1000 nm down to contact. The best surfaces that satisfy these criteria are those of cleaved mica which can be produced molecularly smooth. These measurements were initiated by Tabor and collaborators [15, 16] and later elaborated by Israelachvili and Adams [17] who built the well-known surface force apparatus using crossed cylindrical mica surfaces both in vacuum and immersed in a variety of electrolyte solutions. As an illustration, Fig. 5.6 shows the results in vacuum at room temperature [16] and a comparison was made with the theoretical calculations based on theory with different Hamaker constants and also considering the retarded constant B.

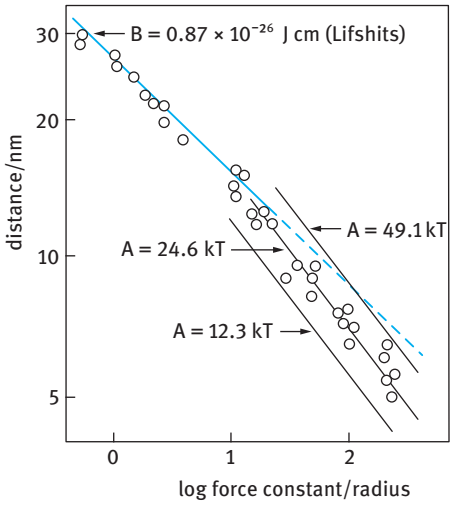

Fig. 5.6: Direct measurement of van der Waals forces between two cylindrical mica surfaces in vacuum at room temperature [16].

References

[1] Goodwin JW. Colloids and interfaces with surfactants and polymers. London: John Wiley and Sons; 2009.
[2] Israelachvili JN. Intermolecular and surface forces. London: Academic Press; 1992.
[3] Keesom WH. Proc Koninkl Nederland Wetenschap. 1915;18:636; 1920;23:939; Phsik Z. 1921;22:129; 643.
[4] Debye P. Physik Z. 1921;21:178; 1920;22:302.
[5] London F. Z Physik. 1930;63:245; Trans Faraday Soc. 1937;33:8.
[6] McLachlan AD. Proc Royal Soc London Ser A. 1963;202:224.
[7] de Boer JH. Trans Faraday Soc. 1936;32:10.
[8] Hamaker HC. Physica. 1937;4:1058.
[9] Deryaguin BV. Kolloid Z. 1934;69:155.
[10] Lifshitz EM. Soviet Physics JETP. 1956;2:73.
[11] Lyklema J. Fundamentals of interface and colloid science. Vol. IV, Chapter 3. London: Academic Press; 2005.
[12] Manhanty J, Ninham BW. Dispersion forces. London: Academic Press; 1976.
[13] Parsegian VA, Weiss GH. J Colloid Interface Sci. 1981;81:285.
[14] Casimir HBG, Polder D. Phys Rev. 1948;73:360.
[15] Tabor D, Winterton RHS. Nature. 1968;219:1120.
[16] Tabor D. J Colloid Interface Sci. 1969;31:364.
[17] Israelachvili JN, Adams GE. J Chem Soc Faraday Trans. 1978;174:975.

6 Theory of colloid stability

6.1 Introduction

The term "stability" usually refers to absence of separation of the dispersion over a period of time. However, one can distinguish between two types of instabilities. The first refers to the situation where the particles do not aggregate over this period of time. This may be referred to as "colloid stability". The second refers to the situation where the particles or droplets show a tendency to sediment or cream under gravity over a period of storage. In this case the particles or droplets may show no aggregation and the gravity force (given by the product of the particle or droplet mass, the acceleration due to gravity g and the height of the container L) exceeds the Brownian motion (kT, where k is the Boltzmann constant and T is the absolute temperature). This may be referred to as "physical or mechanical instability".

In this chapter I will consider the case of colloid stability/instability by combining the double layer repulsion described in Chapter 4 with van der Waals attraction described in Chapter 5. The total potential energy curve is a superposition of the two separate potential energies as a function of the separation distance between plates or particles. This forms the basis of the theory of lyophobic colloids formulated independently by Deryaguin and Landau [1] and Verwey and Overbeek [2] which is referred to as the DLVO theory. In this theory one can arrive at a quantitative theory for the interaction of colloid particles for all colloidal systems in which the particles are sufficiently large in comparison to the double layer extension, and accordingly an encounter of two particles may be approximated by a system of two large parallel plates [2]. As a first approximation, one may consider the particles to be represented by cubes (or another regular form) and this interaction can be represented by two plates for which the plate thickness is considerable in comparison to the thickness of the double layer. In Chapters 4 and 5, I developed expressions for the surface-to-surface distance of the two components, namely the electrostatic repulsion and van der Waals attraction. As we will see below the linear combination of the two components forms the basis of the DLVO theory.

The process of flocculation of colloidal dispersions will be described in Chapter 7. For the sake of completion, the process of "mechanical stability" (creaming of emulsions and sedimentation of suspensions) and its prevention will also be described in Chapter 7.

https://doi.org/10.1515/9783110540895-007

6.2 Examples of potential energy curves and stability of charge stabilized systems as described by the DLVO theory for flat plates

In Chapter 4, I have shown that the repulsive potential G_{elec} decreases with increasing distance according to a more or less exponential decay according to the following equation for the case $\kappa H > 1$ (where κ is the reciprocal of the Debye length and H is the separation distance between the plates),

$$G_{\text{elec}} = \frac{64 n_0 kT}{\kappa} \tanh^2\left(\frac{Ze\psi_{\text{d}}}{4kT}\right) \exp(-\kappa H), \tag{6.1}$$

where n_0 is the electrolyte concentration, k is the Boltzmann constant, T is the absolute temperature, Z is the valency of the ion, e is the electronic charge and ψ_{d} is the Stern potential.

The repulsive potential-distance curve starts with a finite value of G_{elec} for zero distance (the free energy of the double layer potential); the curve approaches a purely exponential one for moderate and large plate distances.

The attractive energy for two flat plates (material 1) immersed in a medium (material 2) is given by,

$$G_{\text{VDW}}(h) = -\frac{A_{12}}{12\pi h^2}, \tag{6.2}$$

where,

$$A_{12} = \pi^2 \beta_{12\text{L}} \rho_{\text{N1}} \rho_{\text{N2}}. \tag{6.3}$$

$\beta_{12\text{L}}$ is the London dispersion constant, ρ_{N1} and ρ_{N2} are the number densities of molecules in the slabs and the medium respectively.

Equation (6.2) shows that the attractive energy between flat plates decreases quadratically with increasing distance. This shows that the absolute value of $|G_{\text{A}}|$ will always be larger than G_{elec} for two cases, namely for very large and for very small plate distances. It is well known that an exponentially decreasing function goes to zero more rapidly than a function decreasing with a negative power. Accordingly, for large separation distances the attractive energy according to equation (6.2) will always surpass the repulsive energy according to equation (6.1). For small separation distances, G_{A} approaches the value of $-\infty$, so that at such small distances $G_{\text{A}} \gg G_{\text{elec}}$.

In the intermediate distance of separation between the plates, i.e. at h comparable to the double layer thickness $(1/\kappa)$ or $(\kappa h \approx 1)$, there are two possibilities:

(i) Curves for which G_{elec} is sufficiently large in comparison to G_{A}; the total interaction energy G_{T} represented by equation (6.4),

$$G_{\text{T}} = G_{\text{elec}} + G_{\text{A}} \tag{6.4}$$

may reach positive values over a certain region of distances. In other words, the total energy–distance curve will show a maximum beyond the horizontal axis. As with

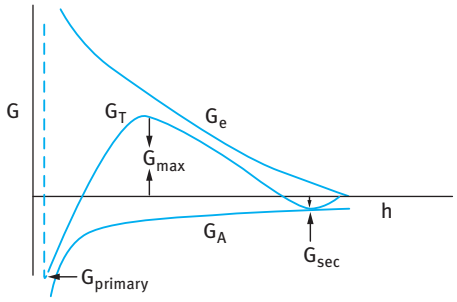

Fig. 6.1: Schematic representation of the variation of G_{elec}, G_A and G_T with h for systems with an energy maximum (barrier) according to the DLVO theory [1, 2].

increasing distance, G_T again reaches negative values and finally approaches the abscissa asymptotically; again these curves also show a weak minimum at large separation distances. This is schematically illustrated in Fig. 6.1.

The G_T–h curve shown in Fig. 6.1 can explain the characteristics of colloidal dispersions; three main aspects can be considered. Firstly, the potential energy barrier must be surmounted before the particles or droplets make lasting contact in the primary minimum. Provided the energy barrier is considerably larger than the thermal energy of the particles (that is equal to kT, where k is the Boltzmann constant and T is the absolute temperature) few particles will make contact and the system is considered to be colloidally stable. A value of 25 kT for the energy barrier is considered to be sufficient for the maintenance of colloid stability. Secondly, if the secondary minimum is of depth $\gg kT$ then the particles or droplets would flocculate with a liquid film between them in the cluster. This type of flocculation is described as "weak" and "reversible". In other words, the particles or droplets in the cluster can become disaggregated by gentle shaking or mixing. Thirdly, since both repulsive and attractive energies are directly proportional to the particle or droplet radius, the secondary minimum should become increasingly significant with increasing particle or droplet size. The effect will also increase with increasing electrolyte concentration.

(ii) Curves for which $G_{elec} + G_A$ is always zero or negative. As the minimum for long distances is very shallow, these curves will show at most a very low energy barrier; generally, however, the total potential energy will decrease continuously with decreasing plate distance.

A general description of the transition from the above two cases can be illustrated by considering the effect of increasing electrolyte concentration on the energy distance curves for spherical particles of radius 100 nm in aqueous medium (Fig. 6.2). The energy–distance curves are shown for four 1 : 1 electrolyte concentrations: 10^{-1}, 10^{-3}, 10^{-5}, 10^{-7} mol dm^{-3}, corresponding to $(1/\kappa)$ of 1, 10, 100 and 1000 nm. It can be seen from Fig. 6.2 that for $(1/\kappa)$ values of 10, 100 and 1000 nm, there is an energy barrier than can prevent flocculation in the primary minimum. This barrier increases with increasing $(1/\kappa)$. However, when $(1/\kappa)$ decreases to 1 nm, i.e. at 1 : 1 electrolyte concentration of 10^{-1} mol dm^{-3}, this energy barrier disappears and the G_T becomes negative at all separation distances. This corresponds to strong flocculation, usually referred to as coagulation.

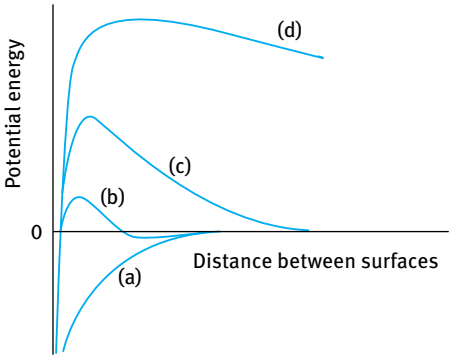

Fig. 6.2: Energy–distance curves at various electrolyte concentrations: (a) 10^{-1} mol dm^{-3}; $(1/\kappa) = 1$ nm; (b) 10^{-3} mol dm^{-3}; $(1/\kappa) = 10$ nm; (c) 10^{-5} mol dm^{-3}; $(1/\kappa) = 100$ nm; (d) 10^{-7} mol dm^{-3}; $(1/\kappa) = 1000$ nm

Another illustration of the energy–distance curves is given in Fig. 6.3 which shows the calculations of energy–distance curves for titanium dioxide (rutile) dispersions [3] with a radius of 100 nm and zeta potential of –45 mV at 10^{-3} and 10^{-2} mol dm^{-3} NaCl. These calculations are for isolated particles, i.e. very dilute dispersion [3]. The results clearly illustrate the effect of increasing NaCl concentrations which results in compression of the electric double layer and hence the reduction of the electrostatic repulsion. In 10^{-3} mol dm^{-3} NaCl, the primary maximum is about 70 kT which ensures the long-term colloid stability of the dispersion. The secondary minimum in this case is about 3 kT and this may cause weak flocculation. The calculations in 10^{-2} mol dm^{-3} NaCl show a reduced energy maximum (about 15 kT) and a deeper secondary minimum of the order of 10 kT. The energy maximum prevents aggregation in the primary minimum but the deep secondary minimum will definitely cause weak and reversible flocculation as discussed above.

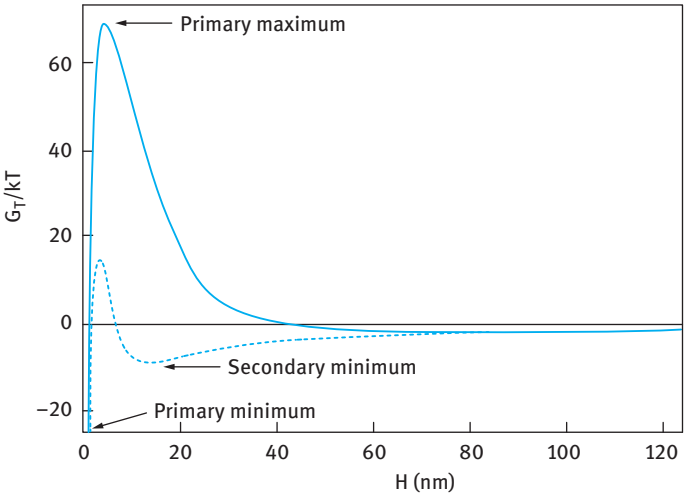

Fig. 6.3: Energy–distance curves for 100 nm TiO_2 dispersions with a zeta potential of –45 mV at 10^{-3} and 10^{-2} mol dm^{-3} NaCl [3].

The primary minimum indicates that the aggregated (coagulated) state is the lowest energy condition and this is where one expects the particles to reside [3]. The primary maximum opposes the close approach of particles or droplets and it may be considered as an activation energy that must be exceeded for aggregation to occur. The motion of the particles is governed by the thermal energy and one can describe the energy distribution by the Boltzmann equation. This predicts a kinetic stability as the rate of aggregation is proportional to $\exp(-G_{max}/kT)$. When $G_{max} \gg kT$, as is the case for TiO_2 dispersions in 10^{-3} mol dm^{-3} NaCl, the particles will be in a colloidally stable state. Since $(G_{min})_{sec} > kT$ one would expect that many of the particles will be in close proximity for much of the time (weak attraction). However, since the net attractive energy is only slightly larger than the thermal energy, any aggregation in the secondary minimum is reversible. As mentioned above, $(G_{min})_{sec}$ reaches $10\,kT$ in 10^{-2} mol dm^{-3} NaCl which is significantly larger than the thermal energy and in this case the particles will remain in close proximity for much longer time when compared with the dispersion in 10^{-3} mol dm^{-3} NaCl. The flocculation rate in the secondary minimum at such higher NaCl concentrations will be higher, but this flocculation is still reversible.

The contributions to G_T, namely double layer repulsion and van der Waals attraction, have been discussed in detail in Chapters 4 and 5. If there is strong attraction so that $-G_A \gg kT$, there will be strong aggregation or coagulation of the particles when these come into close contact. For emulsions, this coagulation is usually a precursor for coalescence, where two or more droplets join together. If there is a net repulsive interaction between particles or droplets such that $G_{max} \gg kT$, the particles or droplets will not aggregate and the system is considered to be colloidally stable. There are other situations where the particles are attracted at long distances but do not come into close contact. This occurs because of the presence of $(G_{min})_{sec}$ that has an attractive energy $> kT$. This type of aggregation is sometimes referred to as "flocculation" to distinguish it from the aggregation that occurs at $(G_{min})_{primary}$ that can reach attractive energy $> 100\,kT$. Flocculation in the secondary minimum is reversible and the flocs may be redispersed with moderate shearing forces. In contrast, coagulation is usually irreversible and to break the aggregates a high shearing force is required, e.g. using a bead mill.

6.3 Energy–distance curves for spherical particles according to DLVO theory [1, 2]

Colloidal particles are certainly not infinitely large plates and, therefore, one must consider the interaction between two spherical particles with radius a. This will give a picture of reality, irrespective of the shape of the particles, when they are far apart. In addition, in the theory of spherical particles, the influence of the size of the particles can be evaluated. The border effects caused by the curvature of the particles can

be taken into account. Deryaguin [4] showed that it is possible to calculate the interaction of spherical particles by simple integration, when the interaction of infinitely large flat surfaces is known. Deryaguin [4] used this method to investigate the stability of colloids. Deryaguin's method [4] is more satisfactory with thin double layers and large particles ($\kappa a \gg 1$), as will be discussed below. In the case of small particles with an extended double layer ($\kappa a < 1$), the application of linear approximation may be allowed and gives reliable results, even for relatively high potentials.

6.3.1 Large particles with thin double layers ($\kappa a \gg 1$)

Consider two spheres with radius a, with a distance between their centres (O_1 and O_2) equal to R, as represented in Fig. 6.4.

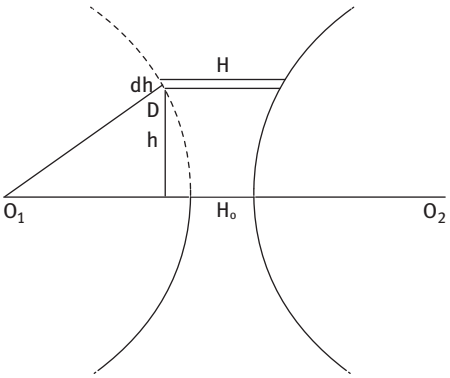

Fig. 6.4: Illustration of the build-up of the repulsion between two spheres out of the repulsion between quasi-parallel layers [2].

The smallest distance between the surfaces is denoted as H_0,

$$H_0 = R - 2a. \tag{6.5}$$

The extension of the double layer is of the order of $(1/\kappa)$ and for large particles with thin double layer $\kappa a \gg 1$. Let us denote $\kappa a = \tau$ and $R/a = s$. The repulsive energy between two spheres is considered to be formed by the contributions of infinitesimal parallel rings, each pair of rings contributing to the potential energy by an amount equal to,

$$2\pi h \cdot 2(f_h - f_\infty)\,\mathrm{d}h, \tag{6.6}$$

$2f_h$ being the free energy per m^2 of two parallel plates at a distance H, h being the distance of the ring considered from the axis of symmetry as illustrated in Fig. 6.4. This implies the supposition that the interaction is not influenced by the adjacent elements having either a larger or a smaller distance from each other. In other words, it is supposed that the lines of force remain parallel to the axis of symmetry O_1 and O_2. In reality the lines of force will be curved outwards, the more so the greater the distance

from the line O_1O_2. As the lines of force insert perpendicular to the surface of the spheres, their curvature will be negligible as long as the angle O_1O_2D is small.

The total repulsive energy is obtained by integrating equation (6.6) over the whole surface of the spheres. Since we started with the assumption that the range of the repulsion is much smaller than the dimensions of the spheres, the contribution of layers far from the axis are unimportant, and it is immaterial what upper limit of integration one takes. The value ∞ is chosen since it gives the most simple expression. This same assumption ensures that the layers giving important contributions shall be practically parallel, the curvature of the surface beginning to be felt only where the contribution to the repulsive energy is negligible.

Based on the above assumptions, the repulsive energy G_{elec} is given by,

$$G_{\text{elec}} = \int_0^\infty 2\pi h \cdot 2(f_h - f_\infty)\,\mathrm{d}h. \tag{6.7}$$

Since,

$$\left(\frac{H - H_0}{2}\right) = a - (a^2 - h^2)^{1/2}. \tag{6.8}$$

Then,

$$2h\,\mathrm{d}h = a \cdot \mathrm{d}H\left(1 - \frac{h^2}{a^2}\right)^{1/2} \tag{6.9}$$

and it may be approximated to $a\,\mathrm{d}H$ for small values of h.

Thus, the repulsive energy is now given by,

$$G_{\text{elec}} = 2\pi a \int_{H_0}^\infty (f_H - f_\infty)\,\mathrm{d}H \tag{6.10}$$

for small potentials $(f_H - f_\infty)$ it is given by the following expression,

$$2(f_H - f_\infty) = \frac{2nkT}{\kappa} z^2\left(1 - \tanh\frac{\kappa H}{2}\right) = \frac{\varepsilon\kappa\psi_0^2}{4\pi}\left(1 - \tanh\frac{\kappa H}{2}\right), \tag{6.11}$$

where z is the dimensionless potential that is given by $(Ze\psi_0/kT)$.

Equation (6.10) may be integrated giving,

$$G_{\text{elec}} = \frac{\varepsilon a\psi_0^2}{2}\int_{H_0}^\infty \left(1 - \tanh\frac{\kappa H}{2}\right)\mathrm{d}\left(\frac{\kappa H}{2}\right) = \frac{\varepsilon a\psi_0^2}{2}\ln(1 + \exp -\kappa H_0), \tag{6.12}$$

or,

$$\frac{G_{\text{elec}}}{\varepsilon a\psi_0^2} = \frac{\ln(1 - \exp -\kappa H_0)}{2}. \tag{6.13}$$

Since $H_0 = R - 2a$, κH_0 may be replaced by $\kappa R - 2\kappa a = \tau(s - 2)$, so that,

$$\frac{G_{\text{elec}}}{\varepsilon a\psi_0^2} = \frac{1}{2}\ln[1 + \exp -\tau(s - 2)]. \tag{6.14}$$

In order to find the minimum value of $\tau(=\kappa a)$ for which equation (6.14) may be applied with some accuracy, two approximations are introduced, both of which tend to make the value of G_{elec} too high. Firstly, the upper limit of integration is put equal to $H = \infty$, whereas the highest value having any physical sense should be $H = 2a + H_0$. This gives an error in the final expression for the repulsive energy equal to,

$$2\pi a \int_{2a+H_0}^{\infty} (f_H - f_\infty)\,\mathrm{d}H = \frac{\varepsilon a \psi_0^2}{2} \int_{2a+H_0}^{\infty} \left(1 - \tanh\frac{\kappa H}{2}\right) \mathrm{d}\frac{\kappa H}{2}$$
$$= \frac{\varepsilon a \psi_0^2}{2} \ln[1 + \exp -\kappa(H_0 + 2a)]$$
$$= \frac{\varepsilon a \psi_0^2}{2} \ln(1 + \exp -\tau s). \tag{6.15}$$

It is easy to verify that this error remains under one percent, when $(\tau s - 5) > \tau(s - 2)$, which means that expression (6.14) should not be used if $\tau < 25$.

In the second place, the surfaces of the spheres are not parallel to each other. This would certainly cause the reduction to be smaller than it would have been if the surfaces are exactly parallel. For rings, the repulsive energy will be between $4\pi h(f_H - f_\infty)\,\mathrm{d}h$ as a minimum and $2\pi a(f_H - f_\infty)\,\mathrm{d}H$ as a maximum value. As a maximum value using $4\pi h\,\mathrm{d}h$ instead of $2\pi a\,\mathrm{d}H$, the error for $\tau = 10$ is about 5 %; $\tau = 5$ is about 10 % and for $\tau = 2$ it is about 30 %. Probably the actual errors are much smaller.

To apply the complete Gouy–Chapman equations instead of the linear approximation, one has to replace the value of $(f_H - f_\infty)$ given by equation (6.11) with the more exact value of $f(u, z)$ where u is equal to $(Ze\psi_\mathrm{d}/kT)$ and z is equal to $(Ze\psi_0/kT)$,

$$f(u, z) = \frac{Z^2}{\kappa} 2(f_H - f_\infty). \tag{6.16}$$

$f(u, z)$ is computed as a function of $(\kappa H/2)$. A graphic integration leads to,

$$G(\kappa H_0) = 2\pi \int_{H_0}^{\infty} f(u, z)\,\mathrm{d}\frac{\kappa H}{2}. \tag{6.17}$$

The function G as found by this integration for a number of values of reduced potential $z(= Ze\psi_0/kT)$ is represented in Fig. 6.5 together with the approximate values according to equation (6.14).

It can be seen from Fig. 6.5 that for $z = 2$, the difference between the exact and approximate expressions is very small, but for $z = 3$ and higher values it becomes more and more important. The exact curves are always lower than the approximate ones. They are flatter at large distances and steeper at small distances.

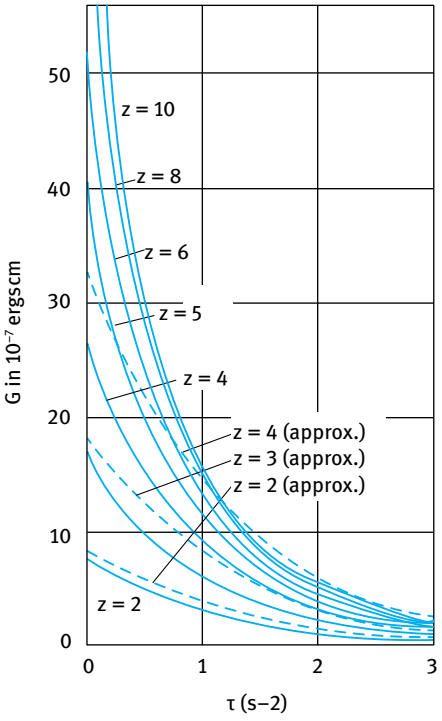

Fig. 6.5: Repulsive potential between two spherical particles using the exact expression (6.17) and approximate expression (6.14) for high potentials.

6.3.2 Small particles and extended double layers (κa is small)

The method that could be used for calculating the interaction for the case of large κa (described above) cannot be applied for small κa. In the latter case, one calculates the electric field in the double layer around the particles, and after that the free energy of the double layers that is given by the following expression [2],

$$F = -\int_{\text{surface}} \mathrm{d}S \int_0^{\psi_0} q' \,\mathrm{d}\psi_0', \tag{6.18}$$

in which q' is the specific charge of a surface element $\mathrm{d}S'$ and ψ_0'. The integration has to be carried out over the whole interface of the system.

The problem is simplified by introducing the approximation of small potentials, whereby q' is directly proportional to ψ_0' and the first integration leads to the simple result,

$$\int_0^{\psi_0} q' \,\mathrm{d}\psi_0' = \frac{1}{2} q_0 \psi_0. \tag{6.19}$$

Since the potential of the surface is considered constant, the second integration is equally simple and the whole integral (6.18) transforms to,

$$F = -\int \mathrm{d}S \int q'\psi_0' = -\frac{1}{2}Q\psi_0, \tag{6.20}$$

where Q represents the total charge of the interface.

Considering two particles which approach each other from an infinite distance to a distance h where the interaction is sensible, the potential energy of interaction G_{elec}, which is equal to the change in the free energy, is given by,

$$G_{\mathrm{elec}} = \Delta F = Q_\infty\psi_0 - Q_1\psi_0 = \psi_0(Q_\infty - Q_1), \tag{6.21}$$

where Q_∞ and Q_1 are the charges of one particle when the particles are at infinitely large distance and at a distance h, respectively. The factor 1/2 of equation (6.20) is cancelled since one is considering two identical particles.

Equation (6.21) gives the fundamental expression where one finds the relation between the charge Q and the potential ψ_0.

Assuming that the potential of the surface remains constant, the potential energy of interaction at the approaching of the particles is given by,

$$G_{\mathrm{elec}} = \psi_0(Q_\infty - Q_R). \tag{6.22}$$

Using the relationship between charge and potential, the energy of interaction is given by,

$$G_{\mathrm{elec}} = \psi_0^2\varepsilon a\frac{\exp -\tau(s-2)}{s}\beta, \tag{6.23}$$

where ε is the permittivity, a is the particle radius, $\tau = \kappa a$, $s = R/a$ (with R being the centre-to-centre separation between the particles) and β is given by,

$$\beta = \frac{1+\alpha}{1 + \frac{\exp -\tau(s-2)}{2s\tau}(1+\exp -2\tau)(1+\alpha)}, \tag{6.24}$$

where α is the integration constant for the charge Q,

$$Q = A\varepsilon(1+\tau)\exp -\tau\{1-\delta(1+\alpha)\}, \tag{6.25}$$

where A is a constant.

$$\delta = \frac{\exp -\tau(s-2)}{2s\tau}\left(\frac{\tau-1}{\tau+1} + \exp -2\tau\right) \tag{6.26}$$

$$\alpha = \lambda_1\left(1+\frac{1}{s\tau}\right) + \lambda_2\left(1+\frac{3}{s\tau}+\frac{3}{(s\tau)^2}\right) \tag{6.27}$$

Equation (6.23) shows that the potential energy of interaction is directly proportional to the square of the surface potential, the radius of the particle and the two ratios τ (ratio of the particle radius to the thickness of the double layer) and s (ratio of separation distance to particle radius).

As an illustration Fig. 6.6 shows the potential energy of repulsion between two spherical particles (at constant surface potential) as a function of $\tau(s-2)$ at various values of τ. The quantity $\tau(s-2)$ gives the distance between the surfaces of two particles expressed in the thickness $(1/\kappa)$ of the double layer as unity. The repulsion is only important when the particles are closer together than a few times the thickness of the double layer. At immediate contact ($s = 2$), the potential energy is practically independent of the value of κa. This is a striking contrast to the case of flat plates, where the limiting potential energy is found to be inversely proportional to the thickness of the double layer. It can also be seen from Fig. 6.6 that V_R (or G_{elec}) is always positive and diminishes monotonously with growing s.

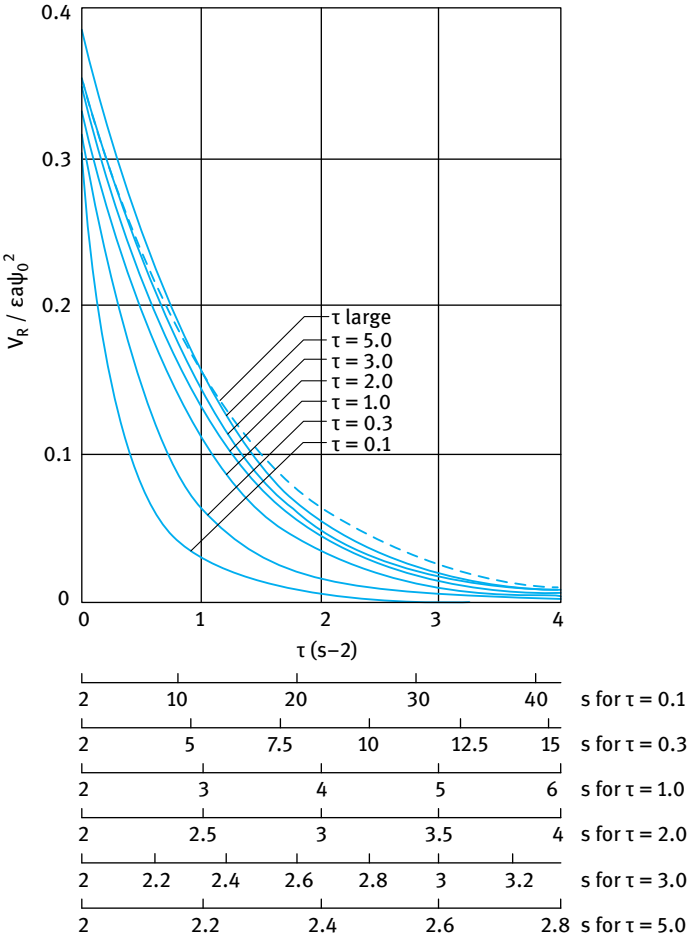

Fig. 6.6: Potential energy of repulsion between two spherical particles (at constant potential) $\tau = \kappa a$; $s = R/a$, as a function of $\tau(s-2) = \kappa(R-2a)$.

Since β is always between 0.60 and 1.0, one may neglect its influence on repulsion. This leads to the simple approximate expression for G_{elec},

$$G_{\text{elec}} = \varepsilon a \psi_0^2 \frac{\exp -\tau(s-2)}{s}. \tag{6.28}$$

6.3.3 Total energy of interaction

Similar to the case of flat plates, the total energy of interaction is the sum of double layer repulsion and van der Waals attraction. The latter is given by the following expression (see Chapter 5),

$$G_{\text{A}} = -\frac{A}{6}\left(\frac{2}{s^2-4} + \frac{2}{s^2} + \ln\frac{s^2-4}{s^2}\right), \tag{6.29}$$

where A is the Hamaker constant.

When the particles are very close to each other and putting $s = 2 + H/a$, in which H is the shortest distance between the spheres, and assuming that $H \ll a$, G_{A} may be approximated by,

$$G_{\text{A}} = -\frac{Aa}{12H} = -\frac{A}{12}\frac{1}{s-2}. \tag{6.30}$$

Thus, the free energy of attraction decays very slowly, namely reciprocally with distance, and ever slower than it does in the case of flat plates, where it goes reciprocally with the square of the distance. At larger separations of the two spheres, the decay is of course faster.

As an illustration Fig. 6.7 shows the total potential energy of interaction as a function of s for various κ values (i.e. electrolyte concentrations) [2]. The potential energy curves have the same characteristics as those found for flat plates, although there are differences in detail. All energy curves show a negative value (attraction) at large separations, because the van der Waals energy has a smaller slope ($\approx 1/s^6$) to the repulsive energy $\{\approx \exp(-\tau s)\}$. At very small distances the van der Waals energy is again most important, the energy reaching large negative values. At intermediate distances, i.e. when $\tau(s-2)$ is of the order of unity, there may be a maximum energy if the conditions of ψ_0, κ and A are well chosen. In Fig. 6.7 the radius of the particles, the Hamaker constant and the surface potential are all kept constant ($a = 100\,\text{nm}$, $A = 10^{-19}$ J and $\psi_0 = 25.6\,\text{mV}$).

In Fig. 6.8 κ is kept constant ($10^8\,\text{m}^{-1}$) whereas the surface potential ψ_0 is varied [2]. In both Fig. 6.7 and 6.8 the ordinate is expressed in ergs and also in multiples of kT (4.1×10^{-14} ergs) units. It can be seen from Fig. 6.7 and 6.8 that the maximum is always situated at about $\tau(s-2) \approx 1$, shifting to somewhat smaller distances when the maximum is high and to somewhat larger distances when τ is small.

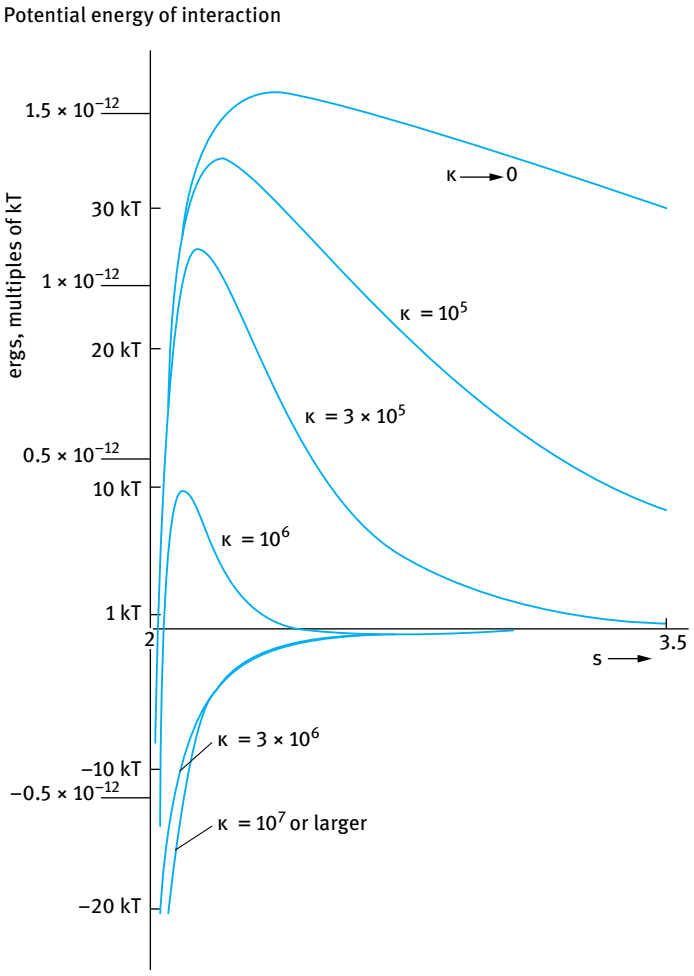

Fig. 6.7: Influence of electrolyte concentration (κ) on the total potential energy of interaction [2].

6.4 Influence of particle number concentration

The formulation of the DLVO theory is based on the interaction between colloidal particles in dilute dispersions. In other words, the particles are considered to be separated by large distances such that only binary collisions are considered. For more concentrated colloidal dispersions one must consider the effect of multibody collisions and theories that consider such complex systems are still lacking. It is perhaps useful to define the concentration range above which a dispersion may be considered concentrated. The particle number concentration and volume fraction, ϕ, above which a dispersion may be considered concentrated is best defined in terms of the balance between the particle translational motion and interparticle interaction. At one extreme,

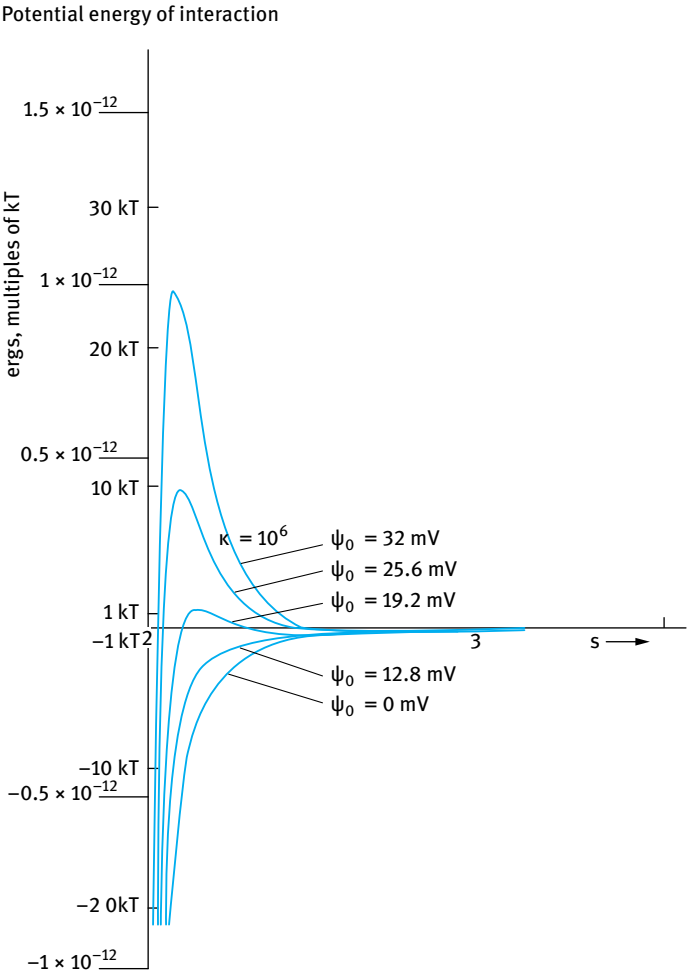

Fig. 6.8: Influence of surface potential (ψ_0) on the total potential energy of interaction [2].

a suspension may be considered dilute if the thermal motion (Brownian diffusion) of the particles predominates over the imposed interparticle interaction [5, 6]. In this case, the particle translational motion is large and only occasional contacts occur between the particles, i.e. the particles do not "see" each other until collision occurs, giving a random arrangement of particles. In this case, the particle interactions can be represented by two-body collisions. In such "dilute" systems, gravity effects may be neglected and if the particle size range is within the colloid range (1 nm–1 µm) no settling occurs. The properties of the dispersion are time independent and, therefore, any time-average quantity such as viscosity or scattering may be extrapolated to infinite dilution.

As the particle number concentration is increased in a suspension, the volume of space occupied by the particles increases relative to the total volume. Thus, a proportion of the space is excluded in terms of its occupancy by a single particle. Moreover, the particle-particle interaction increases and the forces of interaction between the particles play a dominant role is determining the properties of the system. With a further increase in particle number concentration, the interactive contact between the particles increases until a situation is reached where the interaction produces a specific order between the particles, and a highly developed structure is reached. With solid-in-liquid dispersions, such a highly ordered structure, which is close to the maximum packing fraction ($\phi = 0.74$ for hexagonally closed packed array of Môn disperse particles), is referred to as "solid" suspension. In such a system, any particle in the system interacts with many neighbours and the vibration amplitude is small relative to particle size; the properties of the system are essentially time independent [5, 6].

In between the random arrangement of particles in "dilute" suspensions and the highly ordered structure of "solid" suspensions, one may easily define "concentrated" suspensions. In this case, the particle interactions occur by many body collisions and the translational motion of the particles is restricted. However, this reduced translational motion is not as great as with "solid" suspensions, i.e. the vibrational motion of the particles is large compared with particle size. A time-dependent system arises in which there will be spatial and temporal correlation.

To understand the property of any dispersion, one must consider the arrangement of the particles in the system: random arrangement with free diffusion; dilute or "vapour-like"; loosely ordered with restricted diffusion; concentrated or "liquid-like"; highly-ordered; solid or "crystal-like".

The microstructure of the dispersion may be investigated using small angle X-ray or neutron scattering. Once the microstructure of the system is understood, it is possible to know how the interparticle interaction influences the macrostructure of the system such as its osmotic pressure and rheology.

A convenient method to describe the structure of the suspension is to use the radial distribution function $g(r)$. Consider a system containing N_p particles in a volume V, then the average macroscopic density, ρ_0, is expressed by [7, 8],

$$\rho_0 = \frac{N_p}{V}. \tag{6.31}$$

If the container is examined more closely on a microscopic scale, one can obtain the distribution of particles around any reference particle, as is illustrated in Fig. 6.9. In the immediate vicinity of the central particle, there is a space in which the particle density is zero. With an increasing distance r from the centre of the chosen particle, and circumscribing a ring of thickness dr, we see it contains more particles. As r becomes very large, the number of particles within such an annulus will tend to ρ_0. A function must therefore be defined to describe the distribution of particles relative to the central reference particle. This is defined as $\rho(r)$ which varies with r and which describes the

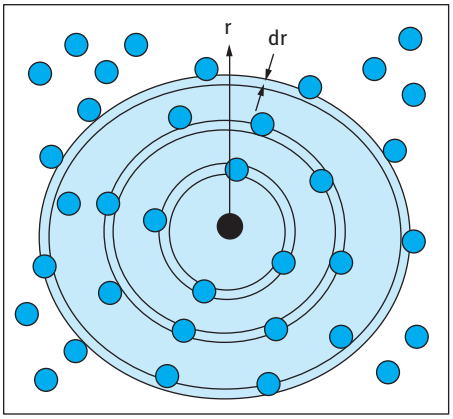

Fig. 6.9: Microscopic view (schematic) of the distribution of particles around a central one.

distribution of particles. This density function will have two limiting values: $\rho(r) \to 0$ as $r \to 2R$ (where R is the particle radius); $\rho(r) \to \rho_0$ as $r \to \infty$.

The pair distribution function, $g(r)$ can be defined as,

$$g(r) = \frac{\rho(r)}{\rho_0}. \tag{6.32}$$

It leads to the radial distribution function $4\pi r^2 \rho(r)$. $g(r)$ has the properties $g(r) \to 0$ as $r \to 2R$ and $g(r) \to 1$ as $r \to \infty$.

$g(r)$ is directly related to the potential $\phi(r)$ of mean force acting between the particles,

$$g(r) = \exp -\left(\frac{\phi(r)}{kT}\right), \tag{6.33}$$

$$\phi(r) = V(r) + \psi(r), \tag{6.34}$$

where $V(r)$ is the simple pair potential and $\psi(r)$ is a perturbation term that takes into account the effect of many body interactions.

For very dilute systems, with particles undergoing Brownian motion, the distribution will be random and only occasional contacts will occur between the particles, i.e. there will be only pairwise interaction ($\psi(r) = 0$). In this case $g(r)$ increases rapidly from the value of zero at $r = 2R$ to its maximum value of unity beyond the first shell (Fig. 6.10 (a)). With such dilute systems ("vapour-like"), no structure develops.

For "solid" suspensions, $g(r)$ shows distinct, sharp peaks similar to those observed with atomic and molecular crystals (Fig. 6.10 (c)). For "concentrated" dispersions ("liquid-like"), $g(r)$ shows the form represented in Fig. 6.10 (b). This consists of a pronounced first peak followed by a number of oscillatory peaks damping to unity beyond four or five particle diameters. As one proceeds outwards from the first shell, the peaks become broader.

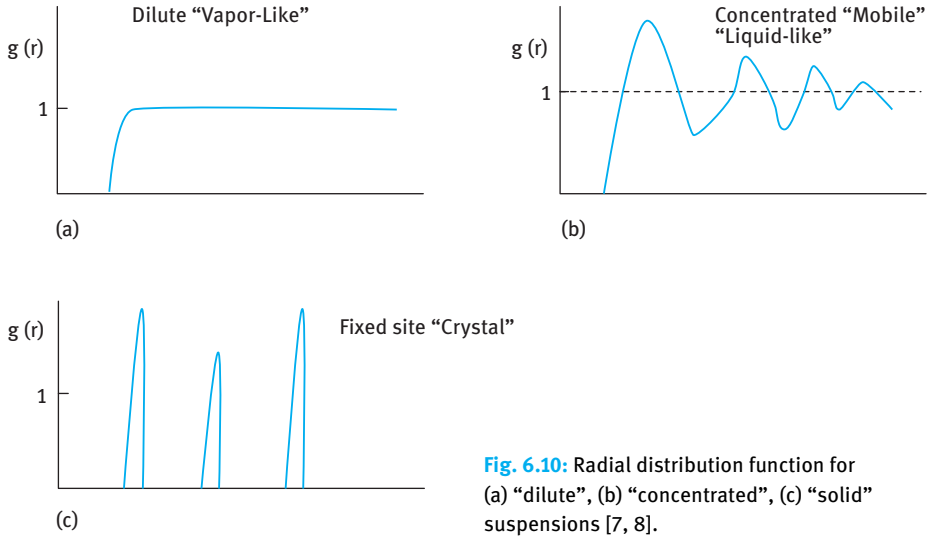

Fig. 6.10: Radial distribution function for (a) "dilute", (b) "concentrated", (c) "solid" suspensions [7, 8].

The dependency of $g(r)$ on r for colloidal dispersions can be determined by scattering techniques [7, 8]. As an illustration Fig. 6.11 (a) shows the results for polystyrene latex dispersions (particle radius 19 nm) in 10^{-4} mol dm^{-3} at volume fractions of 0.01, 0.04 and 0.13, whereas Fig. 6.11 (b) shows the effect of electrolyte concentration (NaCl at 10^{-5}, 10^{-3} and 5×10^{-3} mol dm^{-3}) at a constant volume fraction of 0.04, on the radial distribution function.

The results in Fig. 6.11 (a) show that the $g(r)$–r curve for the most dilute latex ($\phi = 0.01$) resembles that shown in Fig. 6.10 for "dilute" systems. At $\phi = 0.04$ the initial part of the curve becomes much steeper as the particles are close packed together, and a clear maximum occurs followed by an oscillatory curve resembling the curve in Fig. 6.10 for "concentrated" dispersions. At $\phi = 0.13$, the amplitude of the first maximum has increased, indicating more structure; the particles move even closer and are interacting more strongly.

The effect of changing the electrolyte concentration is illustrated in Fig. 6.11 (b), which clearly shows that the average distance between the particles is larger the lower the electrolyte concentration. The decrease in the amplitude of the first peak with increasing electrolyte concentration indicates a weakening of the structure.

It is possible, in principle, to relate the microscopic properties of the concentrated dispersion, described above, to its macroscopic properties, such its osmotic pressure and the high frequency shear modulus (rigidity modulus). The osmotic pressure is described by [7, 8],

$$\pi = N_p kT - \frac{2\pi N_p^2}{3} \int_0^\infty g(r) r^3 \frac{d\phi(r)}{dr} dr; \tag{6.35}$$

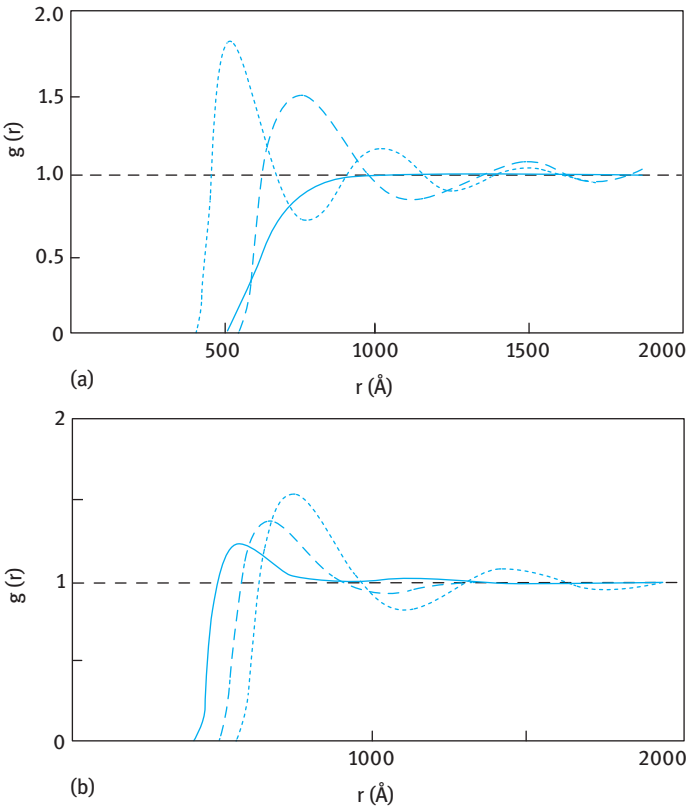

Fig. 6.11: (a) $g(r)$ versus r for PS latex in 10^{-4} mol dm^{-3} NaCl: — $\phi = 0.01$, --- $\phi = 0.04$, ··· $\phi = 0.13$. (b) PS latex, $\phi = 0.04$, ··· $C_{NaCl} = 10^{-5}$, --- $C_{NaCl} = 10^{-3}$, $C_{NaCl} = 5 \times 10^{-3}$ mol dm^{-3} [7, 8].

and the high frequency shear modulus is given by,

$$G_\infty = N_p kT + \frac{2\pi N_p^2}{15} \int_0^\infty g(r) \frac{d}{dr}\left(r^4 \frac{d\phi(r)}{dr}\right) dr. \tag{6.36}$$

As an illustration Fig. 6.12 shows the variation of the experimental values of G_∞ with ϕ for polystyrene latex in 10^{-4} mol dm^{-3} NaCl. The theoretical calculations based on equation (6.36) are shown (solid line) in the same figure. The agreement between experimental values of G_∞ is not particularly good and the trends obtained must be regarded as approximate [7, 8].

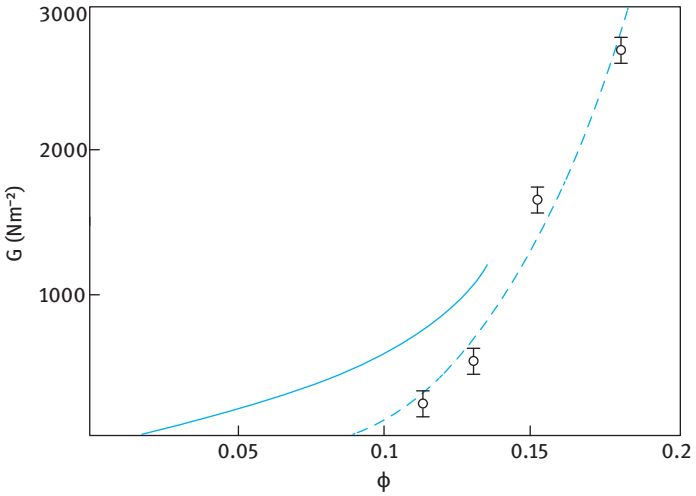

Fig. 6.12: Shear modus G versus ϕ for polystyrene latex dispersions in 10^{-4} mol dm^{-3} NaCl: ○ experimental points; — calculated based on equation (6.36).

References

[1] Deryaguin BV, Landau L. Acta Physicochem USSR. 1941;14:633.
[2] Verwey EJW, Overbeek JTG. Theory of stability of lyophobic colloids. Amsterdam: Elsevier; 1948.
[3] Goodwin JW. Colloids and interfaces with surfactants and polymers. London: John Wiley and Sons; 2009.
[4] Deryaguin BV. Kolloid Z. 1934;69:155; Acta Physicochem USSR. 1939;10:333.
[5] Ottewill RH. In: Tadros T, editor. Solid/liquid dispersions. London; Academic Press; 1987. Chapter 9.
[6] Tadros T. Dispersion of powders in liquids and stabilization of suspensions. Weinheim: Wiley-VCH; 2012.
[7] Ottewill RH. In: Goodwin LW, editor. Colloidal dispersions. London: Royal Society of Chemistry; 1982.
[8] Ottewill RH. Phil Trans R Soc London A. 1985;310:67.

7 Flocculation of colloidal dispersions

7.1 Mechanism of aggregation

The DLVO theory [1, 2] predicts the process of aggregation on addition of electrolytes with different valency. Addition of electrolyte reduces the range of the repulsive component (due to compression of the electrical double layer) and this results in reduction of the energy maximum, G_{max}. This is illustrated in Fig. 7.1 which shows the effect of addition of 1 : 1 electrolyte on the energy–distance curves.

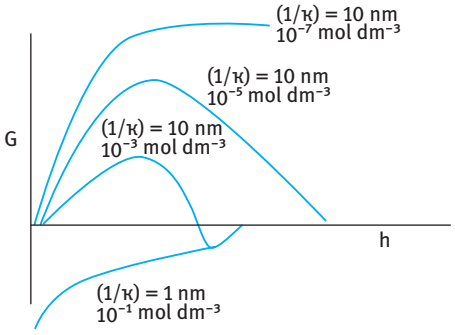

Fig. 7.1: Variation of G with h at various electrolyte concentrations.

At very low electrolyte concentration of 10^{-7} mol dm^{-3} (corresponding to a double layer thickness of 1000 nm), the energy maximum is very high (much higher than 100 kT) and that prevents any close approach of the particles. In this case the particles remain dispersed for a very long period of time (some years). By increasing the electrolyte concentration to 10^{-5} mol dm^{-3} (corresponding to a double layer thickness of 100 nm), the energy maximum is still high (> 100 kT) and this prevents any aggregation of the particles. On increasing the electrolyte concentration to 10^{-3} mol dm^{-3} (corresponding to a double layer thickness of 10 nm), the energy maximum is reduced but still high enough (> 25 kT) to prevent aggregation. However, when the electrolyte concentration is increased to 10^{-1} mol dm^{-3} (corresponding to a double layer thickness of 1 nm), the energy maximum disappears and the energy–distance curve becomes attractive at all separation distances. In this case, the dispersion shows rapid coagulation and the particles in the aggregates are strongly bound to each other.

Another factor that affects electrostatic repulsion is the magnitude of the surface or zeta potential. As discussed in Chapter 4, G_{elec} is proportional to the square of the surface or zeta potential. As an illustration Fig. 7.2 shows calculations of the energy–distance curves for polystyrene latex particles of 500 nm radius at various NaCl concentrations and zeta potential [3].

https://doi.org/10.1515/9783110540895-008

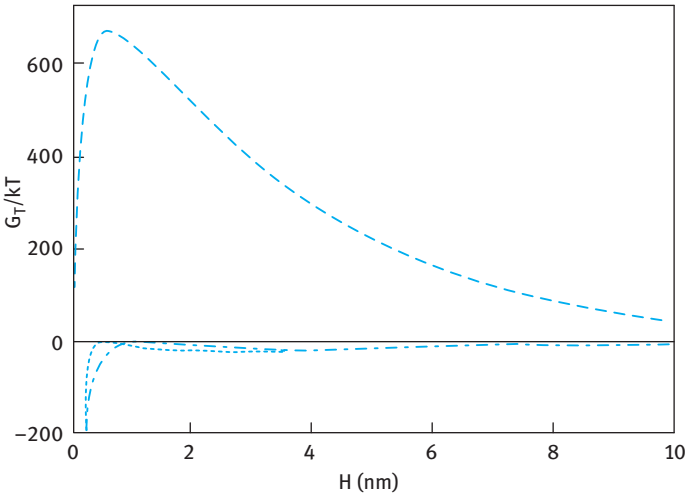

Fig. 7.2: Energy–distance curves for 500 nm radius polystyrene latex particles: (—), 10^{-2} mol dm^{-3} NaCl, ζ-potential = −50 mV; (·····), 10^{-2} mol dm^{-3} NaCl, ζ-potential = −20 mV; (···), 4×10^{-1} mol dm^{-3} NaCl, ζ-potential = −30 mV.

It can be seen that a high energy maximum is obtained at 10^{-2} mol dm^{-3} NaCl and ζ-potential of −50 mV. When the ζ-potential is reduced to −20 mV while keeping the NaCl concentration the same, the maximum disappears. Also, at higher NaCl concentration of 4×10^{-1} mol dm^{-3} the maximum disappears even when the ζ-potential is increased to −30 mV.

Since approximate formulae are available for G_{elec} and G_A, quantitative expressions for $G_T(h)$ can also be formulated. These can be used to derive expressions for the coagulation concentration, which is that concentration that causes every encounter between two colloidal particles to lead to destabilization. Verwey and Overbeek [2] introduced the following criteria for transition between stability and instability,

$$G_T(= G_{elec} + G_A) = 0, \tag{7.1}$$

$$\frac{dG_T}{dh} = 0, \tag{7.2}$$

$$\frac{dG_{elec}}{dh} = -\frac{dG_A}{dh}. \tag{7.3}$$

Using the equations for G_{elec} and G_A, the critical coagulation concentration, CCC, could be calculated as will be shown below. The theory predicts that the CCC is directly proportional to the surface potential ψ_0 and inversely proportional to the Hamaker constant A and the electrolyte valency Z. As will be shown below, the CCC is inversely proportional to Z^6 at high surface potential and inversely proportional to Z^2 at low surface potential.

7.2 Kinetics of flocculation of dispersions

7.2.1 Diffusion limited aggregation (fast flocculation kinetics)

Fast flocculation kinetics represents the case where no energy barrier exists and hence the process becomes diffusion controlled. This process was treated by Smoluchowki [4], who modelled the system as that of diffusing spherical particles which stick on collision but the pair potential is zero up to this contact [5, 6]. If r is the centre-to-centre distance between a reference spherical particle with radius R and an approaching particle with the same radius R (for a monodisperse dispersion) then contact occurs when $r = 2R$. As both particles are diffusing, the net diffusion coefficient is equal to $2D\,\mathrm{m^2\,s^{-1}}$ [2]. The net velocity of the incoming particle is therefore $2D/R\,\mathrm{m\,s^{-1}}$. The surface area of the "collision sphere" is $4\pi(2R)^2$. The flux resulting from Brownian diffusion J_B through the collision sphere, if there are initially no particles per unit volume, is

$$J_B = n_0 \frac{2D}{R} 4\pi(2R)^2. \tag{7.4}$$

Since the above process is occurring with each particle, the collision frequency due to Brownian diffusion is,

$$c_B = \frac{n_0 J_B}{2}. \tag{7.5}$$

The factor of 2 is introduced to prevent double counting. The diffusion coefficient is given by the Stokes–Einstein equation,

$$D = \frac{kT}{6\pi\eta_0 R}, \tag{7.6}$$

where η_0 is the viscosity of the medium.

Combining equations (7.4)–(7.6),

$$c_B = n_0^2 \frac{8kT}{3\eta_0}. \tag{7.7}$$

As each collision results in coagulation, the initial coagulation rate is given by,

$$-\frac{\mathrm{d}n_0}{\mathrm{d}t} = n_0^2 \frac{8kT}{3\eta_0}. \tag{7.8}$$

The half-life $t_{1/2}$ for the rapid coagulation rate is determined for this second-order rate equation as,

$$t_{1/2} = \frac{3\eta_0}{4kTn_0}. \tag{7.9}$$

A simple analysis of fast flocculation kinetics is to consider the process to be represented by second-order kinetics and the process is simply diffusion controlled. The number of particles n at any time t may be related to the initial number (at $t = 0$) n_0 by the following expression,

$$n = \frac{n_0}{1 + k_0 n_0 t}, \tag{7.10}$$

where k_0 is the rate constant for fast flocculation that is related to the diffusion coefficient of the particles D, i.e.,

$$k = 8\pi DR. \tag{7.11}$$

D is given by the Stokes–Einstein equation (7.6)

Combining equations (7.6) and (7.11),

$$k = \frac{4}{3}\frac{kT}{\eta} = 5.5 \times 10^{-18}\ \mathrm{m^3\ s^{-1}} \text{ for water at } 25\,^{\circ}\mathrm{C}. \tag{7.12}$$

Equation (7.12) shows that the rate constant for flocculation is directly proportional to the temperature and inversely proportional to the viscosity of the medium. It should also be mentioned that the viscosity of the medium decreases with increasing temperature, which means that the overall effect of an increase in temperature will be an increase in the rate constant.

The half-life $t_{1/2}$ ($n = (1/2)n_0$) can be calculated at various n_0 or volume fraction ϕ as given in Tab. 7.1.

Tab. 7.1: Half-life of suspension flocculation.

R (μm)	ϕ			
	10^{-5}	10^{-2}	10^{-1}	5×10^{-1}
0.1	765 s	76 ms	7.6 ms	1.5 ms
1.0	21 h	76 s	7.6 s	1.5 s
10.0	4 month	21 h	2 h	25 min

7.2.2 Potential limited aggregation (slow flocculation kinetics)

Slow flocculation kinetics was treated by Fuchs [7] who considered the effect of the presence of an energy barrier. In this case, the pair potential slows the approach of two particles. At any distance, the fraction of particles with thermal energy in excess of the potential at that distance is given by the Boltzmann factor: $\exp(-GT/kT)$. The flux through successive spherical shells as the particles approach is slowed from the simple collision case and only a fraction of the particles that encounter one another approach close enough to stick. The fraction of encounters that stick is $1/W$, where W is known as the stability ratio.

$$W = \frac{k_0}{k}. \tag{7.13}$$

W can be expressed as the ratio of the two fluxes,

$$W = 2R\int_{2R}^{\infty} \exp\left(\frac{G_T}{kT}\right)\frac{\mathrm{d}r}{r^2}. \tag{7.14}$$

Reerink and Overbeek [8] pointed out that the maximum in the pair potential, G_{max}, is the dominant factor in restricting the approach of particles and they showed a useful approximation to the integral of equation (7.14),

$$W \approx \frac{1}{2\kappa R} \exp\left(\frac{G_{max}}{kT}\right). \tag{7.15}$$

Since G_{max} is determined by the salt concentration C and valency, one can derive an expression relating W to C and Z [8],

$$\log W = -2.06 \times 10^9 \left(\frac{R\gamma^2}{Z^2}\right) \log C, \tag{7.16}$$

where γ is a function that is determined by the surface potential ψ_0,

$$\gamma = \left[\frac{\exp(Ze\psi_0/kT) - 1}{\exp(Ze\psi_0/kT) + 1}\right]. \tag{7.17}$$

Plots of log W versus log C are shown in Fig. 7.3. The condition log $W = 0$ ($W = 1$) is the onset of fast flocculation. The electrolyte concentration at this point defines the critical flocculation concentration CCC. Above the CCC, $W < 1$ (due to the contribution of van der Waals attraction which accelerates the rate above the Smoluchowski value). Below the CCC, $W > 1$ and it increases with decreasing electrolyte concentration. The above figure also shows that the CCC decreases with increasing valency. At low surface potentials, CCC $\propto 1/Z^2$. This referred to as the Schultze–Hardy rule.

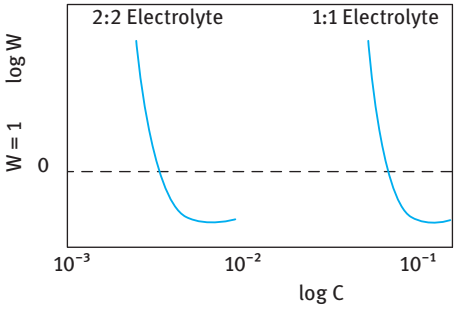

Fig. 7.3: log W–log C curves.

7.2.3 Weak (reversible) flocculation

Another mechanism of flocculation is that involving the secondary minimum (G_{min}) which is few kT units. In this case flocculation is weak and reversible and hence one must consider both the rate of flocculation (forward rate k_f) and deflocculation (backward rate k_b). In this case the rate or decrease of particle number with time is given

by the expression,

$$-\frac{dn}{dt} = -k_f n^2 + k_b n. \tag{7.18}$$

The backward reaction (break-up of weak flocs) reduces the overall rate of flocculation.

7.2.4 Orthokinetic flocculation

This process of flocculation occurs under shearing conditions and is referred to as orthokinetic (to distinguish it from the diffusion controlled perikinetic process). The simplest analysis is for laminar flow, since for turbulent flow with chaotic vortices (as is the case in a high-speed mixer) the particles are subjected to a wide and unpredictable range of hydrodynamic forces. For laminar flow, the particle will move at the velocity of the liquid at the plane coincident with the centre of the particle, v_p. In this case the total collision frequency due to flow, c_f, is given by the following expression,

$$c_f = \frac{16}{3} n_p^2 R^3 \left(\frac{dv}{dx}\right). \tag{7.19}$$

As the particles approach in the shear field, the hydrodynamic interactions cause the colliding pair to rotate and with the combination of the slowing approach due to liquid drainage (lubrication stress) and Brownian motion, not all collisions will lead to aggregation. Equation (7.19) must be reduced by a factor α (the collision frequency) to account for this,

$$c_f = \alpha \frac{16}{3} n_p^2 R^3 \left(\frac{dv}{dx}\right). \tag{7.20}$$

The collision frequency α is of the order 1 and a typical value would be $\alpha \approx 0.8$.

(dv/dx) is the shear rate so that equation (7.20) can be written as,

$$c_f = \alpha \frac{16}{3} n_p^2 R^3 \dot{\gamma}. \tag{7.21}$$

And the rate of orthokinetic flocculation is given by,

$$-\frac{dn}{dt} = \alpha \frac{16}{3} n_p^2 R^3 \dot{\gamma}. \tag{7.22}$$

A comparison can be made between the collision frequency or rate of orthokinetic and perikinetic flocculation by comparing equations (7.22) and (7.7),

$$\frac{c_f}{c_B} = \frac{2\alpha\eta_0 R^3 \dot{\gamma}}{kT}. \tag{7.23}$$

If the particles are dispersed in water at a temperature of 25 °C, the ratio in equation (7.23) becomes,

$$\frac{c_f}{c_B} \approx 4 \times 10^{17} R^3 \dot{\gamma}. \tag{7.24}$$

When a liquid is stirred in a beaker using a rod the velocity gradient r shear rate is in the range 1–10 s^{-1}, with a mechanical stirrer it is about 100 s^{-1} and at the tip of a turbine in a large reactor it can reach values as high as 1000–10 000 s^{-1}. This means that the particle radius R must be less than 1 µm if even slow mixing can be disregarded. This shows how the effect of shear can increase the rate of aggregation.

It should be mentioned that the above analysis is for the case where there is no energy barrier, i.e. the Smoluchowski case [4]. In the presence of an energy barrier, i.e. potential limited aggregation, one must consider the contribution due to the hydrodynamic forces acting on the colliding pair [6]. Fig. 7.4 shows the forces acting on a collision doublet in simple shear [3]. The figure shows the trajectory with the points at which maximum compression and tension occur, i.e. at an angle $\theta = 45°$ to the shear plane. The particles have the same radius R and the reference particle is at $z = 0$.

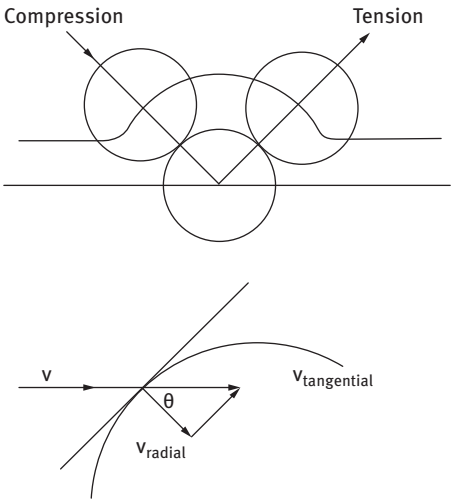

Fig. 7.4: Schematic representation of the geometry of a colliding pair of particles with maximum compression and tension at $\theta = 45°$ to the shear plane.

The velocity of the streamline coincident with the centre of colliding particle, v, at the orientation giving the maximum force is,

$$v = \dot{\gamma} 2R \sin(45). \tag{7.25}$$

The radial component of the Stokes drag force on the particle is given by,

$$F_h = 6\pi\eta_0 R v_{\text{radial}} = 6\pi\eta_0 R \cos(45). \tag{7.26}$$

F_h can be written as,

$$F_h = \pm\dot{\gamma} 6\pi\eta_0 2R^2 \sin(45)\cos(45), \tag{7.27a}$$

$$F_h = \pm\dot{\gamma} 6\pi\eta_0 2R^2, \tag{7.27b}$$

where the sign '±' indicates compression (+) or tension (–). The trajectory would be altered by the colloidal forces on approach, i.e. whether there is net repulsion or attraction. Equation (7.27b) can be used to indicate where the stability or instability boundaries are for a particular dispersion. This requires calculation of the interparticle force at the maximum and minimum points on the force-distance curve. Some calculations were made by Goodwin [3] for polystyrene latex particles with a radius of 500 nm in the presence of 50 mM 1 : 1 electrolyte and a zeta potential of –40 mV. F_T is given by,

$$F_T = 2\pi\varepsilon_r\varepsilon_0\kappa R\psi_d\frac{\exp(-\kappa H)}{1+\exp(-\kappa H)} - \frac{A_{11}R}{12H^2}. \tag{7.28}$$

The value of κR is 368 and therefore the interparticle forces change in the region very close to the particle surface. This indicates that hydrodynamics control the trajectories until the particles are very close to each other. The force-distance curve is shown in Fig. 7.5, where ζ is assumed to be equal to ψ_d.

Fig. 7.5 shows a force maximum F_{max} of 3.96×10^{-10} N and a force minimum F_{min} of -3.8×10^{-11} N. The stability boundaries are calculated as a function of shear rate as illustrated in Fig. 7.6. This clearly shows the change in the aggregation state at different values of ζ-potential [3].

Several features can be identified from the stability map shown in Fig. 7.6. At ζ-potentials less than –20 mV, the dispersion is coagulated at all shear rates. With a small increase in the ζ-potential above –20 mV, the dispersion shows weak flocculation (secondary minimum aggregation) at low shear rates, but at high shear rates

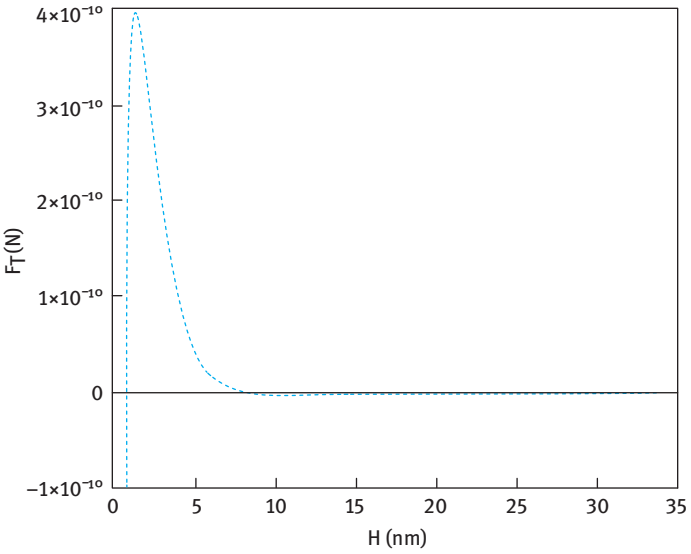

Fig. 7.5: Force-distance curve for 500 nm polystyrene particles at 50 mM 1 : 1 electrolyte and ζ-potential of –40 mV [3].

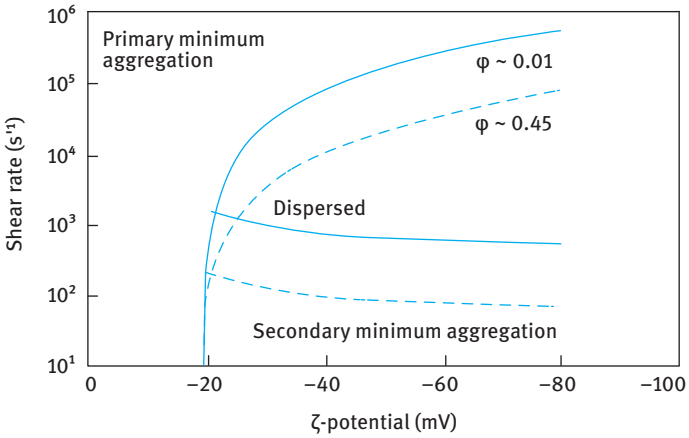

Fig. 7.6: Stability map for polystyrene latex dispersions ($R = 500$ nm and 1 : 1 electrolyte concentration of 50 mM) as a function of ζ-potential and shear rate.

of the order of $10^5\ s^{-1}$, the hydrodynamic forces are sufficient to cause the dispersion to form doublets which are coagulated. This shear induced coagulation is referred to as orthokinetic flocculation as discussed above. It is interesting to note that the shear forces on this particle size, ionic strength and diffuse potential combination will only break down the doublets flocculated in the secondary minimum when the shear rates exceed $10^3\ s^{-1}$. Although such high shear rates are readily attainable in a viscometer, they would require a high stirrer speed when using a paddle stirrer. Clearly such shear rates are easily achieved in pumps and large reactors with turbine mixers. Such shear rates can also be achieved when using rotor-stator mixers (such as Ultra-Turrax and Silverson mixers). Equations (7.27a) and (7.27b) show that the shear forces increase as the square of the particle radius and so the stability boundaries drop rapidly with increasing particle size as the colloidal forces change more slowly with radius than the hydrodynamic forces. Thus particles with a radius of 3–4 μm are much more sensitive to shear-induced aggregation than particles with an order of magnitude lower in radius (0.3–0.4 μm).

The effect of increasing the volume fraction of the dispersion ϕ, as is the case with most practical systems, has a big impact on the shear-induced aggregation as clearly illustrated in Fig. 7.6 which shows the stability map as ϕ is increased from 0.01 to 0.45. When dealing with concentrated dispersions one must consider the "multibody" hydrodynamic forces. Using a mean field approximation, Krieger and Dougherty [9, 10] related the viscosity of the suspension η with that of the medium η_0 by the following semi-empirical equation,

$$\eta = \eta_0 \left(1 - \frac{\phi}{\phi_p}\right)^{-[\eta]\phi_p}, \tag{7.29}$$

where ϕ_p is the maximum packing fraction that is ≈ 0.605 (for random packing) and $[\eta]$ is the intrinsic viscosity that is equal to 2.5 for hard spheres. Equation (7.29) becomes,

$$\eta = \eta_0\left(1 - \frac{\phi}{0.605}\right)^{-1.513}. \tag{7.30}$$

The stability boundaries for $\phi = 0.45$ are shown in Fig. 7.6 (dashed line) and this clearly shows the drop resulting from the increase in the viscous forces at high volume fraction as predicted by equation (7.30). The boundaries drop in proportion to the viscous forces as expected, so it is easier to break up flocculated pairs with an applied shear field. This means that a larger fraction of the stable area that is occupied by the particles that can be considered "dispersed" occurs at lower shear rates when compared with the case of dilute dispersions. The range of stability under shear at moderate ζ-potentials is reduced with increasing the solid volume fraction.

7.2.5 Aggregate structure

When dealing with aggregated systems, the floc structure plays an important role in applications. For example, the rheological properties change dramatically so that handling can become very difficult. A good example is the case of "dewatering" of suspensions by filtration. Filtration may start as an easy separation process once the system is aggregated, but the final "dewatering" is limited so subsequent drying can be a slow and expensive process. In this case, a weakly aggregated structure would be a preferable situation so that collapse of the filter cake to high solids density can be achieved. In the case of ceramic pastes, the rheology of the weakly aggregated open structures is excellent for shape formation with minimum elastic recovery after yield has occurred at moderate to high stress. However, this open structure results in considerable shrinkage on drying and firing.

The mode of aggregation that occurs in the absence (diffusion-limited aggregation) of a barrier can result in the formation of an open-dendritic or fractal-type of structure. In this case, the particles collide and stick as they diffuse. Computer models generate this type of open branched structure and some careful experiments have confirmed these models [6]. As these aggregates grow by accretion of "stick" particles, they grow into each other and span the available space [3]. This point is referred to as the "percolation threshold". At higher concentrations, denser structures result and these are more difficult to define by a single parameter such as the "fractal dimension". These structures are modified in practice by addition of coagulants and application of shear during mixing. The shear forces on these large and fragile structures compact them to relatively high densities [11]. In some cases, systems of monodisperse particles can be compacted by shearing the coagulating system to random packing densities $\phi \approx 0.64$. These strongly aggregated systems are "metastable" structures. The lowest energy configuration would be a very dense unit with the maximum number and/or

area of contacts. However, the fractal structure of a dilute, strongly aggregated system would be very long lived in the absence of external forces since $(G_{\min})_{\text{primary}} \gg kT$ and densification purely by diffusive motion would be imperceptibly slow.

The structures obtained depend on the processing and strength of the attractive interaction. The latter can be controlled by addition of materials to the surface prior to coagulation, e.g. by adding nonionic surfactants or polymers which provide a steric barrier thus limiting the aggregation to weak flocculation [12].

References

[1] Deryaguin BV, Landau L. Acta Physicochem USSR. 1941;14:633.
[2] Verwey EJW, Overbeek JTG. Theory of stability of lyophobic colloids. Amsterdam: Elsevier; 1948.
[3] Goodwin JW. Colloids and interfaces with surfactants and polymers. London: John Wiley and Sons; 2009.
[4] von Smoluchowski M. Physik Z. 1916;17:557, 585.
[5] Hunter RJ. Foundations of colloid science. Oxford: Oxford University Press; 1987.
[6] Russel WB, Saville DA, Schowalter WR. Colloidal dispersions. Cambridge: Cambridge University Press; 1989.
[7] Fuchs N. Z Physik. 1936;89:736.
[8] Reerink H, Overbeek JTG. Discussion Faraday Soc. 1954;18:74.
[9] Krieger IM, Dougherty TJ. Trans Soc Rheol. 1959;3:137.
[10] Krieger IM, Advances Colloid and Interface Sci. 1972;3:111.
[11] Goodwin JW, Mercer-Chalmers J. Flow induced aggregation of colloidal dispersions. In: Ottewill RH, Rennie AR, editors. Modern aspects of colloidal dispersions. Dordrecht: Kluwer; 1998. p. 61–75.
[12] Napper DH. Polymeric stabilisation of colloidal dispersions. London: Academic Press; 1983.

8 Association colloids

8.1 Introduction

As mentioned in Chapter 1, surfactants form association structures (self-assembly units) forming micelles with different shapes that have dimensions in the colloid range. Before describing the driving force for micelle formation, it is essential to give a description of the general classification of surfactant systems. This is followed by a section on the physical chemistry of surfactant solutions and the thermodynamics of the association process. By considering the free energy of micelle formation it is possible to demonstrate the spontaneous process of micelle formation. The various association structures that are produced are then described. In order to understand the driving force for micelle formation, one must consider the enthalpy and entropy of micellization. As will be shown, the driving force for micelle formation is determined by the large and positive entropy that is determined by the reduction of contact between hydrocarbon chains and the water molecules (the so-called hydrophobic effect). As a result, the water molecules around the hydrocarbon chains associate by hydrogen bonding forming "icebergs". On association of the surfactant molecules, these "icebergs" melt, resulting in an increase of the entropy of the system.

8.2 General classification of surfactants

A simple classification of surfactants based on the nature of the hydrophilic group is commonly used. Four main classes may be distinguished, namely anionic, cationic, amphoteric and nonionic [1, 2]. A useful technical reference is McCutcheon [3], which is produced annually to update the list of available surfactants. A text by van Os et al. [4] listing the physicochemical properties of selected anionic, cationic and nonionic surfactants has been published by Elsevier. Another useful text is the Handbook of Surfactants by Porter [5]. It should be mentioned also that a fifth class of surfactants, usually referred to as polymeric surfactants, has been used for many years for preparation of emulsions and suspensions and their stabilization.

8.2.1 Anionic surfactants

These are the most widely used class of surfactants in industrial applications [5–7]. This is due to their relatively low cost of manufacture and they are practically used in every type of detergent. For optimum detergency, the hydrophobic chain is a linear alkyl group with a chain length in the region of 12–16 C atoms and the polar head group should be at the end of the chain. Linear chains are preferred since they are

https://doi.org/10.1515/9783110540895-009

more effective and more degradable than the branched chains. The most commonly used hydrophilic groups are carboxylates, sulphates, sulphonates and phosphates. A general formula may be ascribed to anionic surfactants as follows:

- Carboxylates: $C_nH_{2n+1}COO^-X^+$
- Sulphates: $C_nH_{2n+1}OSO_3^-X^+$
- Sulphonates: $C_nH_{2n+1}SO_3^-X^+$
- Phosphates: $C_nH_{2n+1}OPO(OH)O^-X^+$
  with n being the range 8–16 atoms and the counterion X^+ is usually Na^+.

Several other anionic surfactants are commercially available such as sulphosuccinates, isethionates (esters of isothionic acid with the general formula $RCOOCH_2–CH_2–SO_3Na$) and taurates (derivatives of methyl taurine with the general formula $RCON(R')CH_2–CH_2–SO_3Na$), sarchosinates (with the general formula RCON(R′)COO Na) and these are sometimes used for special applications. Below a brief description of the above anionic classes is given with some of their applications.

8.2.1.1 Carboxylates

These are perhaps the earliest known surfactants, since they constitute the earliest soaps, e.g. sodium or potassium stearate, $C_{17}H_{35}COONa$, sodium myristate, $C_{14}H_{29}COO$ Na. The alkyl group may contain unsaturated portions, e.g. sodium oleate, which contains one double bond in the C_{17} alkyl chain. Most commercial soaps will be a mixture of fatty acids obtained from tallow, coconut oil, palm oil, etc. They are simply prepared by saponification of the triglycerides of oils and fats. The main attraction of these simple soaps is their low cost, their ready biodegradability and low toxicity. Their main disadvantage is their ready precipitation in water containing bivalent ions such as Ca^{2+} and Mg^{2+}. To avoid their precipitation in hard water, the carboxylates are modified by introducing some hydrophilic chains, e.g. ethoxy carboxylates with the general structure $RO(CH_2CH_2O)_nCH_2COO^-$, ester carboxylates containing hydroxyl or multi-COOH groups, sarcosinates which contain an amide group with the general structure $RCON(R')COO^-$. The addition of the ethoxylated groups results in increased water solubility and enhanced chemical stability (no hydrolysis). The modified ether carboxylates are also more compatible with electrolytes. They are also compatible with other nonionic, amphoteric and sometimes even cationic surfactants. The ester carboxylates are very soluble in water, but they suffer from the problem of hydrolysis. The sarcosinates are not very soluble in acid or neutral solutions but they are quite soluble in alkaline media. They are compatible with other anionics, nonionics and cationics. The phosphate esters have very interesting properties being intermediate between ethoxylated nonionics and sulphated derivatives. They have good compatibility with inorganic builders and they can be good emulsifiers. A specific salt of a fatty acid is lithium 12-hydroxystearic acid that forms the major constituent of greases.

8.2.1.2 Sulphates

These are the largest and most important class of synthetic surfactants, which are produced by reaction of an alcohol with sulphuric acid, i.e. they are esters of sulphuric acid. In practice, sulphuric acid is seldom used and chlorosulphonic or sulphur dioxide/air mixtures are the most common methods of sulphating the alcohol. However, due to their chemical instability (hydrolysing to the alcohol, particularly in acid solutions), they are now overtaken by the sulphonates which are chemically stable. The properties of sulphate surfactants depend on the nature of the alkyl chain and the sulphate group. The alkali metal salts show good solubility in water, but they tend to be affected by the presence of electrolytes. The most common sulphate surfactant is sodium dodecyl sulphate (abbreviated as SDS and sometimes referred to as sodium lauryl sulphate) which is extensively used both for fundamental studies as well as in many applications in industry. At room temperature ($\approx 25\,°C$) this surfactant is quite soluble and 30 % aqueous solutions are fairly fluid (low viscosity). However, below 25 °C, the surfactant may separate out as a soft paste as the temperature falls below its Krafft point (the temperature above which the surfactant shows a rapid increase in solubility with a further increase in temperature). The latter depends on the distribution of chain lengths in the alkyl chain: the wider the distribution the lower the Krafft temperature. Thus, by controlling this distribution one may achieve a Krafft temperature of $\approx 10\,°C$. As the surfactant concentration is increased to 30–40 % (depending on the distribution of chain length in the alkyl group), the viscosity of the solution increases very rapidly and may produce a gel but then falls at about 60–70 % to give a pourable liquid, after which it increases again to a gel. The concentration at which the minimum occurs varies according to the alcohol sulphate used, and also the presence of impurities such as unsaturated alcohol. The viscosity of the aqueous solutions can be reduced by addition of short chain alcohols and glycols. The critical micelle concentration (cmc) of SDS (the concentration above which the properties of the solution show abrupt changes) is $8 \times 10^{-3}\,\text{mol}\,\text{dm}^{-3}$ (0.24 %). The alkyl sulphates give good foaming properties with an optimum at C_{12}–C_{14}. As with the carboxylates, the sulphate surfactants are also chemically modified to change their properties. The most common modification is to introduce some ethylene oxide units in the chain, usually referred to as alcohol ether sulphates. These are made by sulphation of ethoxylated alcohols. For example, sodium dodecyl 3-mole ether sulphate, which is essentially dodecyl alcohol reacted with 3 mol EO, then sulphated and neutralized by NaOH. The presence of PEO confers improved solubility when compared with the straight alcohol sulphates. In addition, the surfactant becomes more compatible with electrolytes in aqueous solution. The ether sulphates are also more chemically stable than the alcohol sulphates. The cmc of the ether sulphates is also lower than the corresponding surfactant without the EO units. The viscosity behaviour of aqueous solutions is similar to alcohol sulphates, giving gels in the range 30–60 %. The ether sulphates show a pronounced salt effect, with a significant increase in the

viscosity of a dilute solution on addition of electrolytes such as NaCl. The ether sulphates are commonly used in hand dishwashing and in shampoos in combination with amphoteric surfactants.

8.2.1.3 Sulphonates

With sulphonates, the sulphur atom is directly attached to the carbon atom of the alkyl group and this gives the molecule stability against hydrolysis, when compared with the sulphates (whereby the sulphur atom is indirectly linked to the carbon of the hydrophobe via an oxygen atom). The alkyl aryl sulphonates are the most common type of these surfactants (for example sodium alkyl benzene sulphonate) and these are usually prepared by reaction of sulphuric acid with alkyl aryl hydrocarbons, e.g. dodecyl benzene. A special class of sulphonate surfactants are the naphthalene and alkyl naphthalene sulphonates, which are commonly used as dispersants. As with the sulphates, some chemical modification is used by introducing ethylene oxide units, e.g. sodium nonylphenol 2-mole ethoxylate ethane sulphonate $C_9H_{19}C_6H_4(OCH_2CH_2)_2SO_3^-Na^+$. The paraffin sulphonates are produced by sulpho-oxidation of normal linear paraffins with sulphur dioxide and oxygen and catalyzed with ultraviolet or gamma radiation. The resulting alkane sulphonic acid is neutralized with NaOH. These surfactants have excellent water solubility and biodegradability. They are also compatible with many aqueous ions. The linear alkyl benzene sulphonates (LABS) are manufactured from alkyl benzene and the alkyl chain length can vary from C_8 to C_{15} and their properties are mainly influenced by the average molecular weight and the spread of carbon number of the alkyl side chain. The cmc of sodium dodecyl benzene sulphonate is 5×10^{-3} mol dm^{-3} (0.18 %). The main disadvantage of LABS is their effect on the skin and hence they cannot be used in personal care formulations.

Another class of sulphonates is the α-olefin sulphonates which are prepared by reacting linear α-olefin with sulphur trioxide, typically yielding a mixture of alkene sulphonates (60–70 %), 3- and 4-hydroxyalkane sulphonates (≈ 30 %) and some disulphonates and other species. The two main α-olefin fractions used as starting material are C_{12}–C_{16} and C_{16}–C_{18}. Fatty acid and ester sulphonates are produced by sulphonation of unsaturated fatty acids or esters. A good example is sulphonated oleic acid,

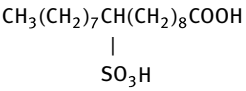

A special class of sulphonates are sulphosuccinates which are esters of sulphosuccinic acid,

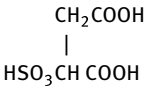

Both mono- and diesters are produced. A widely used diester in many formulations is sodium di(2-ethylhexyl)sulphosuccinate (that is sold commercially under the trade name Aerosol OT). The cmc of the diesters is very low, in the region of 0.06 % for C_6–C_8 sodium salts and they give a minimum surface tension of 26 mN m^{-1} for the C_8 diester. Thus these molecules are excellent wetting agents. The diesters are soluble both in water and in many organic solvents. They are particularly useful for preparation of water-in-oil (W/O) microemulsions.

8.2.1.4 Isethionates

These are esters of isethionic acid $HOCH_2CH_2SO_3H$. They are prepared by reaction of acid chloride (of the fatty acid) with sodium isethionate. The sodium salts of $C_{12–14}$ are soluble at high temperature (70 °C) but they have very low solubility (0.01 %) at 25 °C. They are compatible with aqueous ions and hence they can reduce the formation of scum in hard water. They are stable at pH 6–8 but they undergo hydrolysis outside this range. They also have good foaming properties.

8.2.1.5 Taurates

These are derivatives of methyl taurine $CH_2–NH–CH_2–CH_2–SO_3$. This is made by reaction of sodium isethionate with methyl amine. The taurates are prepared by reaction of fatty acid chloride with methyl taurine. Unlike the isethionates, the taurates are not sensitive to low pH. They have good foaming properties and they are good wetting agents.

8.2.1.6 Phosphate containing anionic surfactants

Both alkyl phosphates and alkyl ether phosphates are made by treating the fatty alcohol or alcohol ethoxylates with a phosphorylating agent, usually phosphorous pentoxide, P_4O_{10}. The reaction yields a mixture of mono- and diesters of phosphoric acid. The ratio of the two esters is determined by the ratio of the reactants and the amount of water present in the reaction mixture. The physicochemical properties of the alkyl phosphate surfactants depend on the ratio of the esters. They have properties intermediate between ethoxylated nonionics (see below) and the sulphated derivatives.

They have good compatibility with inorganic builders and good emulsifying properties. Phosphate surfactants are used in the metal working industry due to their anticorrosive properties.

8.2.2 Cationic surfactants

The most common cationic surfactants are the quaternary ammonium compounds [8, 9] with the general formula $R'R''R'''R''''N^+X^-$, where X^- is usually a chloride ion and R represents alkyl groups. These quaternaries are made by reacting an appropriate tertiary amine with an organic halide or organic sulphate. A common class of cationics is the alkyl trimethyl ammonium chloride, where R contains 8–18 C atoms, e.g. dodecyl trimethyl ammonium chloride, $C_{12}H_{25}(CH_3)_3NCl$. Another widely used cationic surfactant class is that containing two long chain alkyl groups, i.e. dialkyl dimethyl ammonium chloride, with the alkyl groups having a chain length of 8–18 C atoms. These dialkyl surfactants are less soluble in water than the monoalkyl quaternary compounds, but they are commonly used in detergents as fabric softeners. A widely used cationic surfactant is alkyl dimethyl benzyl ammonium chloride (sometimes referred to as benzalkonium chloride and widely used as bactericide), having the structure,

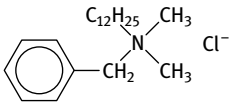

Imidazolines can also form quaternaries, the most common product being the ditallow derivative quaternized with dimethyl sulphate,

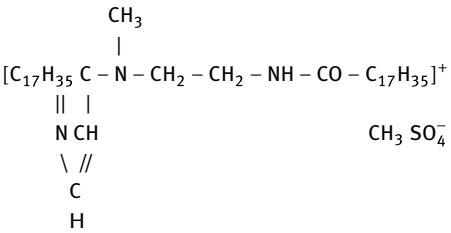

Cationic surfactants can also be modified by incorporating polyethylene oxide chains, e.g. dodecyl methyl polyethylene oxide ammonium chloride having the structure,

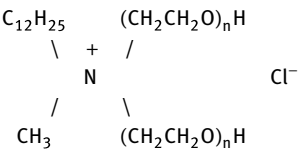

Cationic surfactants are generally water soluble when there is only one long alkyl group. When there are two or more long chain hydrophobes, the product becomes dispersible in water and soluble in organic solvents. They are generally compatible with most inorganic ions and hard water, but they are incompatible with metasilicates and highly condensed phosphates. They are also incompatible with protein-like materials. Cationics are generally stable to pH changes, both acid and alkaline. They are incompatible with most anionic surfactants, but they are compatible with nonionics. These cationic surfactants are insoluble in hydrocarbon oils. In contrast, cationics with two or more long alkyl chains are soluble in hydrocarbon solvents, but they become only dispersible in water (sometimes forming bilayer vesicle-type structures). They are generally chemically stable and can tolerate electrolytes. The cmc of cationic surfactants is close to that of anionics with the same alkyl chain length. For example, the cmc of benzalkonium chloride is 0.17 %. The prime use of cationic surfactants is their tendency to adsorb at negatively charged surfaces, e.g. anticorrosive agents for steel, flotation collectors for mineral ores, dispersants for inorganic pigments, antistatic agents for plastics, antistatic agents and fabric softeners, hair conditioners, anticaking agent for fertilizers and as bactericides.

8.2.3 Amphoteric (zwitterionic) surfactants

These are surfactants containing both cationic and anionic groups [10]. The most common amphoterics are the N-alkyl betaines which are derivatives of trimethyl glycine $(CH_3)_3NCH_2COOH$ (that was described as betaine). An example of betaine surfactant is lauryl amido propyl dimethyl betaine $C_{12}H_{25}CON(CH_3)_2CH_2COOH$. These alkyl betaines are sometimes described as alkyl dimethyl glycinates. The main characteristic of amphoteric surfactants is their dependence on the pH of the solution in which they are dissolved. In acid pH solutions, the molecule acquires a positive charge and it behaves like a cationic, whereas in alkaline pH solutions they become negatively charged and behave like an anionic. A specific pH can be defined at which both ionic groups show equal ionization (the isoelectric point of the molecule). This can be described by the following scheme,

$$\underset{\text{acid pH} < 3}{N^+ \ldots COOH} \leftrightarrow \underset{\text{isoelectric}}{N^+ \ldots COO^-} \leftrightarrow \underset{\text{pH} > 6 \text{ alkaline}}{NH \ldots COO^-}$$

Amphoteric surfactants are sometimes referred to as zwitterionic molecules. They are soluble in water, but the solubility shows a minimum at the isoelectric point. Amphoterics show excellent compatibility with other surfactants, forming mixed micelles. They are chemically stable both in acids and alkalis. The surface activity of amphoterics varies widely and it depends on the distance between the charged groups, and they show a maximum in surface activity at the isoelectric point.

Another class of amphoterics are the N-alkyl amino propionates having the structure R–$NHCH_2CH_2COOH$. The NH group is reactive and can react with another acid molecule (e.g. acrylic) to form an amino dipropionate R–$N(CH_2CH_2COOH)_2$. Alkyl imidazoline-based product can also be produced by reacting alkyl imidazoline with a chloro acid. However, the imidazoline ring breaks down during the formation of the amphoteric.

The change in charge with pH of amphoteric surfactants affects their properties, such as wetting, detergency, foaming, etc. At the isoelectric point (IEP), the properties of amphoterics resemble those of nonionics very closely. Below and above the IEP, the properties shift towards those of cationic and anionic surfactants respectively. Zwitterionic surfactants have excellent dermatological properties. They also exhibit low eye irritation and they are frequently used in shampoos and other personal care products (cosmetics). Due to their mild characteristics, i.e. low eye and skin irritation, amphoterics are widely used in shampoos. They also provide antistatic properties to hair, good conditioning and foam booster.

8.2.4 Nonionic surfactants

The most common nonionic surfactants are those based on ethylene oxide, referred to as ethoxylated surfactants [11–13]. Several classes can be distinguished: alcohol ethoxylates, alkyl phenol ethoxylates, fatty acid ethoxylates, monoalkaolamide ethoxylates, sorbitan ester ethoxylates, fatty amine ethoxylates and ethylene oxide-propylene oxide copolymers (sometimes referred to as polymeric surfactants). Another important class of nonionics are the multihydroxy products such as glycol esters, glycerol (and polyglycerol) esters, glucosides (and polyglucosides) and sucrose esters. Amine oxides and sulphinyl surfactants represent nonionics with a small head group.

8.2.4.1 Alcohol ethoxylates

These are generally produced by ethoxylation of a fatty chain alcohol such as dodecanol. Several generic names are given to this class of surfactants such as ethoxylated fatty alcohols, alkyl polyoxyethylene glycol, monoalkyl polyethylene oxide glycol ethers, etc. A typical example is dodecyl hexaoxyethylene glycol monoether with the chemical formula $C_{12}H_{25}(OCH_2CH_2O)_6OH$ (sometimes abbreviated as $C_{12}E_6$). In practice, the starting alcohol will have a distribution of alkyl chain lengths and the resulting ethoxylate will have a distribution of ethylene oxide (EO) chain lengths. Thus the numbers listed in the literature refer to average numbers.

The cmc of nonionic surfactants is about two orders of magnitude lower than the corresponding anionics with the same alkyl chain length. At a given alkyl chain length, the cmc decreases with decreasing number of EO units. The solubility of the al-

cohol ethoxylates depends both on the alkyl chain length and the number of ethylene oxide units in the molecule. Molecules with an average alkyl chain length of 12 C atoms and containing more than 5 EO units are usually soluble in water at room temperature. However, as the temperature of the solution is gradually raised, the solution becomes cloudy (as a result of dehydration of the PEO chain and the change in the conformation of the PEO chain) and the temperature at which this occurs is referred to as the cloud point (CP) of the surfactant. At a given alkyl chain length, the CP increases with increasing EO chain of the molecule. The CP changes with changing concentration of the surfactant solution and the trade literature usually quotes the CP of a 1% solution. The CP is also affected by the presence of electrolyte in the aqueous solution. Most electrolytes lower the CP of a nonionic surfactant solution. Nonionics tend to have maximum surface activity near to the cloud point. The CP of most nonionics increases markedly on the addition of small quantities of anionic surfactants. The surface tension of alcohol ethoxylate solutions decreases with as its concentration increase, until it reaches its cmc, after which it remains constant with any further increase in its concentration. The minimum surface tension reached at and above the cmc decreases with decreasing number of EO units of the chain (at a given alkyl chain). The viscosity of a nonionic surfactant solution increases gradually with increasing its concentration, but at a critical concentration (which depends on the alkyl and EO chain length) the viscosity shows a rapid increase and ultimately a gel-like structure appears. This results from the formation of liquid crystalline structure of the hexagonal type. In many cases, the viscosity reaches a maximum after which it shows a decrease due to the formation of other structures (e.g. lamellar phases) (see below).

8.2.4.2 Alkyl phenol ethoxylates

These are prepared by reaction of ethylene oxide with the appropriate alkyl phenol. The most common surfactants of this type are those based on nonylphenol. These surfactants are cheap to produce, but they suffer from the problem of biodegradability and potential toxicity (the by-product of degradation is nonylphenol which has considerable toxicity for fish and mammals). In spite of these problems, nonylphenol ethoxylates are still used in many industrial applications, due to their advantageous properties, such as their solubility both in aqueous and nonaqueous media, their good emulsification and dispersion properties, etc.

8.2.4.3 Fatty acid ethoxylates

These are produced by reaction of ethylene oxide with a fatty acid or a polyglycol and they have the general formula $RCOO–(CH_2CH_2O)_nH$. When a polyglycol is used, a mixture of mono- and diester ($RCOO–(CH_2CH_2O)_n–OCOR$) is produced. These surfactants are generally soluble in water provided there are enough EO units and the alkyl chain length of the acid is not too long. The mono-esters are much more soluble in water

than the diesters. In the latter case, a longer EO chain is required to render the molecule soluble. The surfactants are compatible with aqueous ions, provided there is not much unreacted acid. However, these surfactants undergo hydrolysis in highly alkaline solutions.

8.2.4.4 Sorbitan esters and their ethoxylated derivatives (Spans and Tweens)

The fatty acid esters of sorbitan (generally referred to as Spans, an Atlas commercial trade name) and their ethoxylated derivatives (generally referred to as Tweens) are perhaps one of the most commonly used nonionics. They were first commercialized by Atlas in the USA, which has since been purchased by ICI. The sorbitan esters are produced by reaction of sorbitol with a fatty acid at a high temperature (> 200 °C). The sorbitol dehydrates to 1,4-sorbitan and then esterification takes place. If one mole of fatty acid is reacted with one mole of sorbitol, one obtains a mono-ester (some diester is also produced as a by-product). Thus, sorbitan mono-ester has the following general formula,

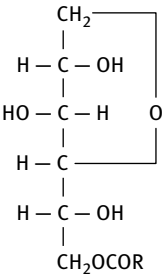

The free OH groups in the molecule can be esterified, producing di- and triesters. Several products are available depending on the nature of the alkyl group of the acid and whether the product is a mono-, di- or triester. Some examples are given below,

- Sorbitan monolaurate – Span 20
- Sorbitan monopalmitate – Span 40
- Sorbitan monostearate – Span 60
- Sorbitan mono-oleate – Span 80
- Sorbitan tristearate – Span 65
- Sorbitan trioleate – Span 85

The ethoxylated derivatives of Spans (Tweens) are produced by reaction of ethylene oxide on any hydroxyl group remaining on the sorbitan ester group. Alternatively, the sorbitol is first ethoxylated and then esterified. However, the final product has different surfactant properties to the Tweens. Examples of Tween surfactants are given below,

- Polyoxyethylene (20) sorbitan monolaurate – Tween 20
- Polyoxyethylene (20) sorbitan monopalmitate – Tween 40

- Polyoxyethylene (20) sorbitan monostearate – Tween 60
- Polyoxyethylene (20) sorbitan mono-oleate – Tween 80
- Polyoxyethylene (20) sorbitan tristearate – Tween 65
- Polyoxyethylene (20) sorbitan tri-oleate – Tween 85

The sorbitan esters are insoluble in water, but soluble in most organic solvents (low HLB number surfactants). The ethoxylated products are generally soluble in water and they have relatively high HLB numbers. One of the main advantages of the sorbitan esters and their ethoxylated derivatives is their approval as food additives. They are also widely used in cosmetics and some pharmaceutical preparations.

8.2.4.5 Ethoxylated fats and oils

A number of natural fats and oils have been ethoxylated, e.g. lanolin (wool fat) and castor oil ethoxylates. These products are useful for applications in pharmaceutical products, e.g. as solubilizers.

8.2.4.6 Amine ethoxylates

These are prepared by addition of ethylene oxide to primary or secondary fatty amines. With primary amines both hydrogen atoms on the amine group react with ethylene oxide and therefore the resulting surfactant has the structure,

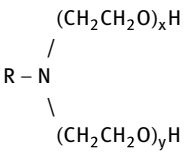

The above surfactants acquire a cationic character if the EO units are small in number and if the pH is low. However, at high EO levels and neutral pH they behave very similarly to nonionics. At low EO content, the surfactants are not soluble in water, but become soluble in an acid solution. At high pH, the amine ethoxylates are water soluble provided the alkyl chain length of the compound is not long (usually a C_{12} chain is adequate for reasonable solubility at sufficient EO content.

8.2.4.7 Amine oxides

These are prepared by oxidizing a tertiary nitrogen group with aqueous hydrogen peroxide at temperatures in the region 60–80 °C. Several examples can be quoted: N-alkyl amidopropyl-dimethyl amine oxide, N-alkyl bis(2-hydroxyethyl) amine oxide and N-alkyl dimethyl amine oxide. They have the general formula,

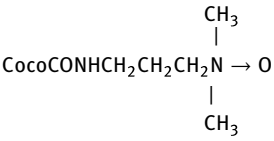

Alkyl amidopropyl-dimethyl amine oxide

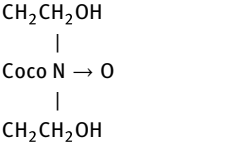

Coco bis (2-hydroxyethyl) amine oxide

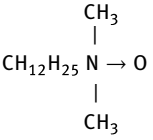

Lauryl dimethyl amine oxide

In acid solutions, the amino group is protonated and acts as a cationic surfactant. In neutral or alkaline solution the amine oxides are essentially nonionic in character. Alkyl dimethyl amine oxides are water soluble up to C_{16} alkyl chain. Above pH 9, amine oxides are compatible with most anionics. At pH 6.5 and below some anionics tend to interact and form precipitates. In combination with anionics, amine oxides can be foam boosters (e.g. in shampoos).

8.2.4.8 Surfactants derived from mono- and polysaccharides

Several surfactants have been synthesized starting from mono- or oligo-saccharides by reaction with the multifunctional hydroxyl groups: alkyl glucosides, alkyl polyglucosides [14], sugar fatty acid esters and sucrose esters [15], etc. The technical problem is one of joining a hydrophobic group to the multihydroxyl structure. Several surfactants have been made, e.g. esterification of sucrose with fatty acids or fatty glycerides to produce sucrose esters having the following structure,

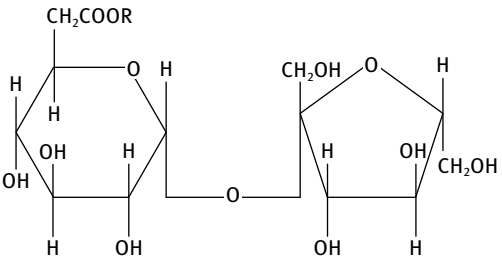

The most interesting sugar surfactants are the alkyl polyglucosides (APG) which are synthesized using a two stage transacetalization process [15]. In the first stage, the carbohydrate reacts with a short chain alcohol, e.g. butanol or propylene glycol. In the second stage, the short chain alkyl glucoside is transacetalized with a relatively long chain alcohol ($C_{12–14}$–OH) to form the required alkyl polyglucoside. This process is applied if oligo- and polyglucoses (e.g. starch, syrups with a low dextrose equivalent, DE) are used. In a simplified transacetalization process, syrups with high glucose content (DE > 96 %) or solid glucose types can react with short chain alcohols under normal pressure. The scheme for alkyl polyglucoside synthesis is shown below. Commercial alkyl polyglucosides (APG) are complex mixtures of species varying in the degree of polymerization (DP, usually in the range 1.1–3) and in the length of the alkyl chain. When the latter is shorter than C_{14} the product is water soluble. The cmc values of APGs are comparable to nonionic surfactants and they decrease with increasing alkyl chain length.

APG surfactants have good solubility in water and they have high cloud points (> 100 °C). They are stable in neutral and alkaline solutions but are unstable in strong acid solutions. APG surfactants can tolerate high electrolyte concentrations and they are compatible with most types of surfactants. They are used in personal care products for cleansing formulations as well as for skin care and hair products. They are also used in hard-surface cleaners and laundry detergents. Several applications in agrochemical formulations can be mentioned, such as wetting agents and penetrating agents for the active ingredient.

8.3 Aggregation of surfactants, self-assembly structures, liquid crystalline phases

The physical properties of surface active agent solutions differ from those of non-amphipathic molecule solutions (such as sugars) in one major aspect, namely the abrupt changes in their properties above a critical concentration [16]. This is illustrated in Fig. 8.1 which shows plots of several physical properties (osmotic pressure, surface tension, turbidity, solubilization, magnetic resonance, equivalent conductivity and self-diffusion) as a function of concentration for an anionic surfactant. At low concentrations, most properties are similar to those of a simple electrolyte. One notable exception is the surface tension, which decreases rapidly with increasing surfactant concentration. However, all the properties (interfacial and bulk) show an abrupt change at a particular concentration, which is consistent with the fact that at and above this concentration, surface active molecules or ions associate to form larger units. These associated units are called micelles (self-assembled structures) and the first formed aggregates are generally approximately spherical in shape. A schematic representation of a spherical micelle is given in Fig. 8.2 [17].

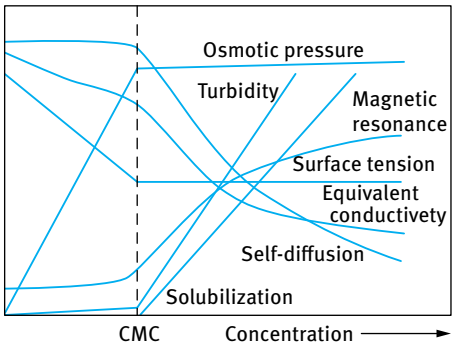

Fig. 8.1: Variation of solution properties with surfactant concentration.

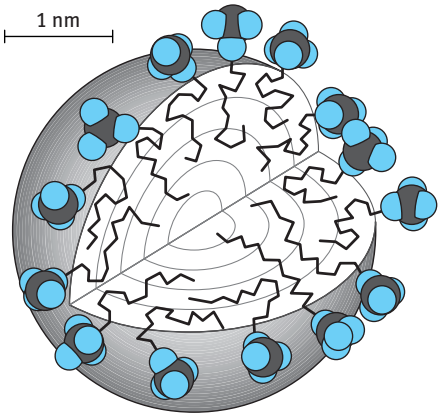

Fig. 8.2: Illustration of a spherical micelle for dodecyl sulphate [17].

The concentration at which this association phenomenon occurs is known as the critical micelle concentration (cmc). Each surfactant molecules has a characteristic cmc value at a given temperature and electrolyte concentration. The most common technique for measuring the cmc is surface tension, γ, which shows a break at the cmc, after which γ remains virtually constant with any further increase in concentration. However, other techniques such as self-diffusion measurements, NMR and fluorescence spectroscopy can be applied. A compilation of cmc values has been given in 1971 by Mukerjee and Mysels [18], which is clearly not an up-to-date text, but is an extremely valuable reference. As an illustration, the cmc values of a number of surface active agents are given in Tab. 8.1, to show some of the general trends [18]. Within any class of surface active agent, the cmc decreases with increasing chain length of the hydrophobic portion (alkyl group). As a general rule, the cmc decreases by a factor of 2 for ionics (without added salt) and by a factor of 3 for nonionics on adding one methylene group to the alkyl chain. With nonionic surfactants, increasing the length of the hydrophilic group (polyethylene oxide) causes an increase in cmc.

In general, nonionic surfactants have lower cmc values than their corresponding ionic surfactants of the same alkyl chain length. Incorporation of a phenyl group in

Tab. 8.1: Critical micelle concentration of surfactant classes.

Surface active agent	cmc (mol dm^{-3})
(A) *Anionic*	
Sodium octyl-l-sulphate	1.30×10^{-1}
Sodium decyl-l-sulphate	3.32×10^{-2}
Sodium dodecyl-l-sulphate	8.39×10^{-3}
Sodium tetradecyl-l-sulphate	2.05×10^{-3}
(B) *Cationic*	
Octyl trimethyl ammonium bromide	1.30×10^{-1}
Decetryl trimethyl ammonium bromide	6.46×10^{-2}
Dodecyl trimethyl ammonium bromide	1.56×10^{-2}
Hexactecyltrimethyl ammonium bromide	9.20×10^{-4}
(C) *Nonionic*	
Octyl hexaoxyethylene glycol monoether C_8E_6	9.80×10^{-3}
Decyl hexaoxyethylene glycol monoether $C_{10}E_6$	9.00×10^{-4}
Decyl nonaoxyethylene glycol monoether $C_{10}E_9$	1.30×10^{-3}
Dodecyl hexaoxyethylene glycol monoether $C_{12}E_6$	8.70×10^{-5}
Octylphenyl hexaoxyethylene glycol monoetherC_8E_6	2.05×10^{-4}

the alkyl group increases its hydrophobicity to a much smaller extent than increasing its chain length with the same number of carbon atoms. The valency of the counterion in ionic surfactants has a significant effect on the cmc. For example, increasing the valency of the counterion from 1 to 2 causes a reduction of the cmc by roughly a factor of 4.

The cmc is, to a first approximation, independent of temperature. This is illustrated in Fig. 8.3 which shows the variation of cmc of SDS with temperature. The cmc varies in a non-monotonic way by ca. 10–20 % over a wide temperature range. The shallow minimum around 25 °C can be compared with a similar minimum in the solu-

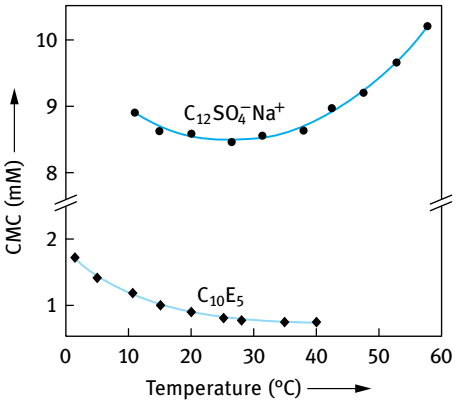

Fig. 8.3: Temperature dependence of the cmc of SDS and $C_{10}E_5$ [19].

bility of hydrocarbon in water [19]. However, nonionic surfactants of the ethoxylate type show a monotonic decrease [19] of cmc with increasing temperature as illustrated in Fig. 8.3 for $C_{10}E_5$. The effect of addition of cosolutes, e.g. electrolytes and non-electrolytes, on the cmc can be very striking. For example, addition of 1 : 1 electrolyte to a solution of anionic surfactant gives a dramatic lowering of the cmc, which may amount to one order of magnitude. The effect is moderate for short chain surfactants, but is much larger for long chain ones. At high electrolyte concentrations, the reduction in cmc with an increase in the number of carbon atoms in the alkyl chain is much stronger than without added electrolyte. This rate of decrease at high electrolyte concentrations is comparable to that of nonionics. The effect of added electrolyte also depends on the valency of the added counterions. In contrast, for nonionics, addition of electrolytes causes only small variation in the cmc.

Non-electrolytes such as alcohols can also cause a decrease in the cmc [20]. The alcohols are less polar than water and are distributed between the bulk solution and the micelles. The more preference they have for the micelles, the more they stabilize them. A longer alkyl chain leads to a less favourable location in water and more favourable location in the micelles.

The presence of micelles can account for many of the unusual properties of solutions of surface active agents. For example, it can account for the near constant surface tension value, above the cmc (see Fig. 8.1). It also accounts for the reduction in molar conductance of the surface active agent solution above the cmc, which is consistent with the reduction in mobility of the micelles as a result of counterion association. The presence of micelles also accounts for the rapid increase in light scattering or turbidity above the cmc. The presence of micelles was originally suggested by McBain [21] who suggested that below the cmc most of the surfactant molecules are unassociated, whereas in the isotropic solutions immediately above the cmc, micelles and surfactant ions (molecules) are though to co-exist, the concentration of the latter changing very slightly as more surfactant is dissolved. However, the self-association of an amphiphile occurs in a stepwise manner with one monomer added to the aggregate at a time. For a long chain amphiphile, the association is strongly cooperative up to a certain micelle size where counteracting factors became increasingly important. Typically the micelles have a closely spherical shape in a rather wide concentration range above the cmc. Originally, it was suggested by Adam [22] and Hartley [23] that micelles are spherical in shape and have the following properties:

(i) the association unit is spherical with a radius approximately equal to the length of the hydrocarbon chain;
(ii) the micelle contains about 50–100 monomeric units; aggregation number generally increases with increasing alkyl chain length;
(iii) with ionic surfactants, most counterions are bound to the micelle surface, thus significantly reducing the mobility from the value to be expected from a micelle with non-counterion bonding;

(iv) micellization occurs over a narrow concentration range as a result of the high association number of surfactant micelles;
(v) the interior of the surfactant micelle has essentially the properties of a liquid hydrocarbon.

This is confirmed by the high mobility of the alkyl chains and the ability of the micelles to solubilize many water insoluble organic molecules, e.g. dyes and agrochemicals. To a first approximation, micelles can, over a wide concentration range above the cmc, be viewed as microscopic liquid hydrocarbon droplets covered with polar head groups, which interact strongly with water molecules. It appears that the radius of the micelle core constituted of the alkyl chains is close to the extended length of the alkyl chain, i.e. in the range 1.5030 nm. As we will see later, the driving force for micelle formation is the elimination of the contact between the alkyl chains and water. The larger a spherical micelle, then the more efficient this is, since the volume-to-area ratio increases. It should be noted that the surfactant molecules in the micelles are not all extended. Only one molecule needs to be extended to satisfy the criterion that the radius of the micelle core is close to the extended length of the alkyl chain. The majority of surfactant molecules are in a disordered state. In other words, the interior of the micelle is close to that of the corresponding alkane in a neat liquid oil. This explains the large solubilization capacity of the micelle towards a broad range of nonpolar and weakly polar substances. At the surface of the micelle, associated counterions (in the region of 50–80 % of the surfactant ions) are present. However, simple inorganic counterions are very loosely associated with the micelle. The counterions are very mobile (see below) and there is no specific complex formed with a definite counterion-head group distance. In other words, the counterions are associated by long-range electrostatic interactions.

A useful concept for characterizing micelle geometry is the critical packing parameter, CPP. The aggregation number N is the ratio between the micellar core volume, V_{mic}, and the volume of one chain, v,

$$N = \frac{V_{\mathrm{mic}}}{v} = \frac{(4/3)\pi R_{\mathrm{mic}}^3}{v}, \tag{8.1}$$

where R_{mic} is the radius of the micelle.

The aggregation number, N, is also equal to the ratio of the area of a micelle, A_{mic}, to the cross-sectional area, a, of one surfactant molecule,

$$N = \frac{A_{\mathrm{mic}}}{a} = \frac{4\pi R_{\mathrm{mic}}^2}{a}. \tag{8.2}$$

Combining equations (8.1) and (8.2),

$$\frac{v}{R_{\mathrm{mic}} a} = \frac{1}{3}. \tag{8.3}$$

Since R_{mic} cannot exceed the extended length of a surfactant alkyl chain, l_{max},

$$l_{\mathrm{max}} = 1.5 + 1.265 n_{\mathrm{c}} \tag{8.4}$$

This means that for a spherical micelle,

$$\frac{v}{l_{\max} a} \leq \frac{1}{3}. \tag{8.5}$$

The ratio $v/(l_{\max} a)$ is denoted as the critical packing parameter (CPP).

Although, the spherical micelle model accounts for many of the physical properties of solutions of surfactants, a number of phenomena remain unexplained, without considering other shapes. For example, McBain [24] suggested the presence of two types of micelles, spherical and lamellar, in order to account for the drop in molar conductance of surfactant solutions. The lamellar micelles are neutral and hence they account for the reduction in the conductance. Later, Harkins et al. [25] used McBain's model of lamellar micelles to interpret his X-ray results in soap solutions. Moreover, many modern techniques such as light scattering and neutron scattering indicate that in many systems the micelles are not spherical. For example, Debye and Anacker [26] proposed a cylindrical micelle to explain the light scattering results on hexadecyltrimethyl ammonium bromide in water. Evidence for disc-shaped micelles has also been obtained under certain conditions. A schematic representation of the spherical, lamellar and rod-shaped micelles, suggested by McBain, Hartley and Debye, is given in Fig. 8.4. Many ionic surfactants show dramatic temperature-dependent solubility as illustrated in Fig. 8.5. The solubility first increases gradually with rising temperature, and then, above a certain temperature, there is a sudden increase of solubility with a further increase of temperature. The cmc increases gradually with increasing temperature. At a particular temperature, the solubility becomes equal to the cmc, i.e. the solubility curve intersects the cmc, and this temperature is referred to as the Krafft temperature. At this temperature an equilibrium exists between solid hydrated surfactant, micelles and monomers (i.e. the Krafft temperature is a "triple point"). Surfactants with ionic head groups and long straight alkyl chains have high Krafft temperatures. The Krafft temperature increases with increasing alkyl chain of the

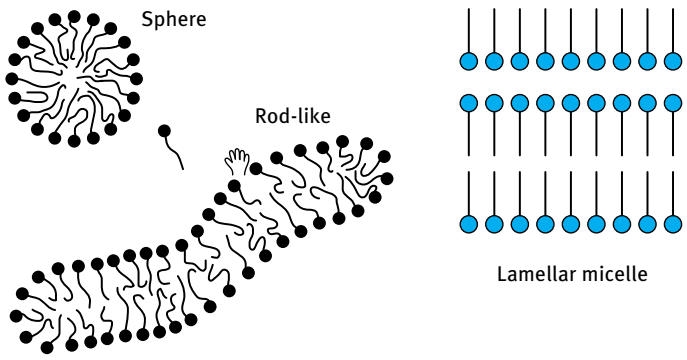

Fig. 8.4: Shape of micelles.

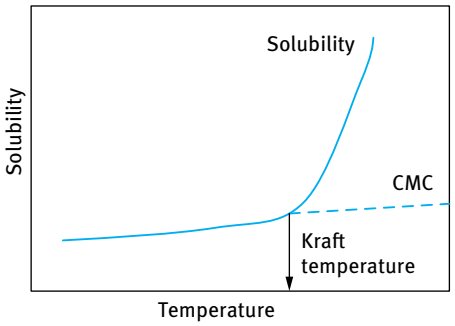

Fig. 8.5: Variation of solubility and critical micelle concentration (cmc) with temperature.

surfactant molecule. It can be reduced by introducing branching in the alkyl chain. The Krafft temperature is also reduced by using alkyl chains with a wide distribution of chain lengths. Addition of electrolytes causes an increase in the Krafft temperature.

With nonionic surfactants of the ethoxylate type, an increase in temperature for a solution at a given concentration causes dehydration of the PEO chains and at a critical temperature the solution become cloudy. This is illustrated in Fig. 8.6 which shows the phase diagram of $C_{12}E_6$. Below the cloud point (CP) curve one can identify different liquid crystalline phases Hexagonal–Cubic–Lamellar which are schematically shown in Fig. 8.7.

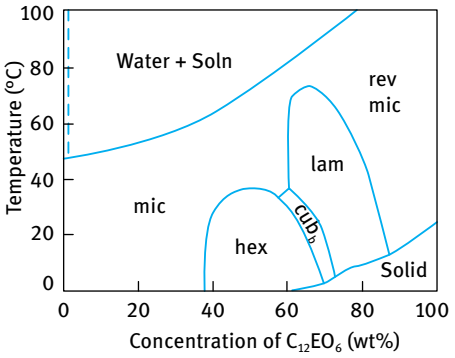

Fig. 8.6: Phase diagram of $C_{12}E_6$.

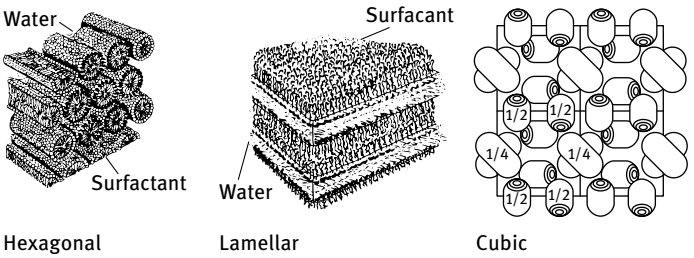

Fig. 8.7: Schematic picture of liquid crystalline phases.

8.4 Thermodynamics of micellization

The process of micellization is one of the most important characteristics of surfactant solution and hence it is essential to understand its mechanism (the driving force for micelle formation). This requires analysis of the dynamics of the process (i.e. the kinetic aspects) as well as the equilibrium aspects whereby the laws of thermodynamics may be applied to obtain the free energy, enthalpy and entropy of micellization.

8.4.1 Kinetic aspects

Micellization is a dynamic phenomenon in which n monomeric surfactant molecules associate to form a micelle S_n, i.e.,

$$nS \Leftrightarrow S_n. \tag{8.6}$$

Hartley [23] envisaged a dynamic equilibrium whereby surface active agent molecules are constantly leaving the micelles whilst other molecules from solution enter the micelles. The same applies to the counterions with ionic surfactants, which can exchange between the micelle surface and bulk solution. Experimental investigations using fast kinetic methods such as stop flow, temperature and pressure jumps, and ultrasonic relaxation measurements have shown that there are two relaxation processes for micellar equilibrium [27–33] characterized by relaxation times τ_1 and τ_2. The first relaxation time, τ_1, is of the order of 10^{-7} s (10^{-8} to 10^{-3} s) and represents the lifetime of a surface active molecule in a micelle, i.e. it represents the association and dissociation rate for a single molecule entering and leaving the micelle, which may be represented by the equation,

$$S + S_{n-1} \underset{K^-}{\overset{K^+}{\rightleftarrows}} S_n, \tag{8.7}$$

where K^+ and K^- represent the association and dissociation rate respectively for a single molecule entering or leaving the micelle.

The slower relaxation time τ_2 corresponds to a relatively slow process, namely the micellization dissolution process represented by equation (8.6). The value of τ_2 is of the order of milliseconds (10^{-3}–1 s) and hence can be conveniently measured by stopped flow methods. The fast relaxation time τ_1 can be measured using various techniques depending on its range. For example, τ_1 values in the range of 10^{-8}–10^{-7} s are accessible to ultrasonic absorption methods, whereas τ_1 in the range of 10^{-5}–10^{-3} s can be measured by pressure jump methods. The value of τ_1 depends on surfactant concentration, chain length and temperature. τ_1 increases with increasing chain length of surfactants, i.e. the residence time increases with increasing chain length.

The above discussion emphasizes the dynamic nature of micelles and it is important to realize that these molecules are in continuous motion and that there is a constant interchange between micelles and solution. The dynamic nature also applies

to the counterions which exchange rapidly with lifetimes in the range 10^{-9}–10^{-8} s. Furthermore, the counterions appear to be laterally mobile and not to be associated with (single) specific groups on the micelle surfaces.

8.5 Equilibrium aspects: thermodynamics of micellization

Various approaches have been employed in tackling the problem of micelle formation. The simplest approach treats micelles as a single phase, and this is referred to as the phase separation model. In this model, micelle formation is considered as a phase separation phenomenon and the cmc is then the saturation concentration of the amphiphile in the monomeric state whereas the micelles constitute the separated pseudophase. Above the cmc, a phase equilibrium exists with a constant activity of the surfactant in the micellar phase. The Krafft point is viewed as the temperature at which solid hydrated surfactant, micelles and a solution saturated with undissociated surfactant molecules are in equilibrium at a given pressure.

Consider an anionic surfactant, in which n surfactant anions, S^-, and n counterions M^+ associate to form a micelle, i.e.,

$$n\,S^- + n\,M^+ \Leftrightarrow S_n. \tag{8.8}$$

The micelle is simply a charged aggregate of surfactant ions plus an equivalent number of counterions in the surrounding atmosphere and is treated as a separate phase. The chemical potential of the surfactant in the micellar state is assumed to be constant, at any given temperature, and this may be adopted as the standard chemical potential, μ_m^0, by analogy to a pure liquid or a pure solid. Considering the equilibrium between micelles and monomer, then,

$$\mu_m^0 = \mu_1^0 + RT \ln a, \tag{8.9}$$

where μ_1 is the standard chemical potential of the surfactant monomer and a_1 is its activity which is equal to $f_1\,x_1$, where f_1 is the activity coefficient and x_1 the mole fraction. Therefore, the standard free energy of micellization per mol of monomer, ΔG_m^0, is given by,

$$\Delta G_m^0 = \mu_m^0 - \mu_1^0 = RT \ln a_1 \approx RT \ln x_1, \tag{8.10}$$

where f_1 is taken as unity (a reasonable value in very dilute solution). The cmc may be identified with x_1 so that

$$\Delta G_m^0 = RT \ln[\text{cmc}]. \tag{8.11}$$

In equation (8.10), the cmc is expressed as a mole fraction, which is equal to $C/(55.5 + C)$, where C is the concentration of surfactant in mol dm^{-3}, i.e.,

$$\Delta G_m^0 = RT \ln C - RT \ln(55.5 + C). \tag{8.12}$$

It should be stated that ΔG^0 should be calculated using the cmc expressed as a mole fraction as indicated by equation (8.12). However, most cmc quoted in the literature are given in mol dm^{-3} and, in many cases of ΔG^0 values have been quoted, when the cmc was simply expressed in mol dm^{-3}. Strictly speaking, this is incorrect, since ΔG^0 should be based on x_1 rather than on C. The value of ΔG^0, when the cmc is expressed in mol dm^{-3} is substantially different from the ΔG^0 value when the cmc is expressed in mole fraction. For example, dodecyl hexaoxyethylene glycol, the quoted cmc value is 8.7×10^{-5} mol dm^{-3} at 25 °C. Therefore,

$$\Delta G^0 = RT \ln \frac{8.7 \times 10^{-5}}{55.5 + 8.7 \times 10^{-5}} = -33.1 \text{ kJ mol}^{-1}, \tag{8.13}$$

when the mole fraction scale is used. On the other hand,

$$\Delta G^0 = RT \ln 8.7 \times 10^{-5} = -23.2 \text{ kJ mol}^{-1}, \tag{8.14}$$

when the molarity scale is used.

The phase separation model has been questioned for two main reasons. Firstly, according to this model a clear discontinuity in the physical property of a surfactant solution, such as surface tension, turbidity, etc. should be observed at the cmc. This is not always found experimentally and the cmc is not a sharp break point. Secondly, if two phases actually exist at the cmc, then equating the chemical potential of the surfactant molecule in the two phases would imply that the activity of the surfactant in the aqueous phase would be constant above the cmc. If this was the case, the surface tension of a surfactant solution should remain constant above the cmc. However, careful measurements have shown that the surface tension of a surfactant solution decreases slowly above the cmc, particularly when using purified surfactants.

A convenient solution for relating ΔG_m to [cmc] was given for ionic surfactants by the following expression,

$$\Delta G_m^0 = \{2 - (p/n)\} RT \ln[\text{cmc}], \tag{8.15}$$

where p is the number of free (unassociated) surfactant ions and n is the total number of surfactant molecules in the micelle. For many ionic surfactants, the degree of dissociation $(p/n) \approx 0.2$ so that,

$$\Delta G_m^0 = 1.8RT \ln[\text{cmc}]. \tag{8.16}$$

Comparison with equation (8.11) clearly shows that for similar ΔG_m, the [cmc] is about two orders of magnitude higher for ionic surfactants when compared with nonionic surfactant of the same alkyl chain length (see Tab. 8.1).

In the presence of excess added electrolyte, with mole fraction x, the free energy of micellization is given by the expression,

$$\Delta G_m^0 = RT \ln[\text{cmc}] + \{1 - (p/n)\} \ln x. \tag{8.17}$$

Equation (8.17) shows that as x increases, the [cmc] decreases.

It is clear from equation (8.15) that as $p \to 0$, i.e. when most charges are associated with counterions,

$$\Delta G_{\mathrm{m}}^{0} = 2RT \ln[\mathrm{cmc}], \tag{8.18}$$

whereas when $p \approx n$, i.e. the counterions are bound to micelles,

$$\Delta G_{\mathrm{m}}^{0} = RT \ln[\mathrm{cmc}], \tag{8.19}$$

which is the same equation for nonionic surfactants.

8.6 Enthalpy and entropy of micellization

The enthalpy of micellization can be calculated from the variation of cmc with temperature. This follows from,

$$-\Delta H^{0} = RT^{2} \frac{\mathrm{d} \ln[\mathrm{cmc}]}{\mathrm{d}T}. \tag{8.20}$$

The entropy of micellization can then be calculated from the relationship between ΔG^{0} and ΔH^{0}, i.e.,

$$\Delta G^{0} = \Delta H^{0} - T\Delta S^{0}. \tag{8.21}$$

Therefore ΔH^{0} may be calculated from the surface tension–log C plots at various temperatures. Unfortunately, the errors in locating the cmc (which in many cases is not a sharp point) leads to a large error in the value of ΔH^{0}. A more accurate and direct method of obtaining ΔH^{0} is microcalorimetry. As an illustration, the thermodynamic parameters, ΔG^{0}, ΔH^{0} and $T\Delta S^{0}$ for octylhexaoxyethylene glycol monoether (C_8E_6) are given in Tab. 8.2.

Tab. 8.2: Thermodynamic quantities for micellization of octylhexaoxyethylene glycol monoether.

Temp. (°C)	ΔG^{0} (kJ mol^{-1})	ΔH^{0} (kJ mol^{-1})	ΔH^{0} (kJ mol l^{-1})	$T\Delta S^{0}$ (kJ mol^{-1})
		(from cmc)	(from calorimetry)	
25	−21.3 ± 2.1	8.0 ± 4.2	20.1 ± 0.8	41.8 ± 1.0
40	−23.4 ± 2.1		14.6 ± 0.8	38.0 ± 1.0

It can be seen from Tab. 8.2 that ΔG^{0} is large and negative. However, ΔH^{0} is positive, indicating that the process is endothermic. In addition, $T\Delta S^{0}$ is large and positive which implies that in the micellization process there is a net increase in entropy. This positive enthalpy and entropy points to a different driving force for micellization from that encountered in many aggregation processes.

The influence of alkyl chain length of the surfactant on the free energy, enthalpy and entropy of micellization was demonstrated by Rosen [34] who listed these parameters as a function of alkyl chain length for sulphoxide surfactants. The results

Tab. 8.3: Change of thermodynamic parameters of micellization of alkyl sulphoxide with increasing chain length of the alkyl group.

Surfactant	ΔG (kJ mol^{-1})	ΔH^0 (kJ mol^{-1})	$T\Delta S^0$ (kJ mol^{-1})
$C_6H_{13}S(CH_3)O$	−12.0	10.6	22.6
$C_7H_{15}S(CH_3)O$	−15.9	9.2	25.1
$C_8H_{17}S(CH_3)O$	−18.8	7.8	26.4
$C_9H_{19}S(CH_3)O$	−22.0	7.1	29.1
$C_{10}H_{21}S(CH_3)O$	−25.5	5.4	30.9
$C_{11}H_{23}S(CH_3)O$	−28.7	3.0	31.7

are given in Tab. 8.3 and it can be seen that the standard free energy of micellization becomes increasingly negative as the chain length increases. This is to be expected since the cmc decreases with increasing alkyl chain length. However, ΔH^0 becomes less positive and $T\Delta S$ becomes more positive with increasing chain length of the surfactant. Thus, the large negative free energy of micellization is made up of a small positive enthalpy (which decreases slightly with increasing chain length of the surfactant) and a large positive entropy term $T\Delta S^0$, which becomes more positive as the chain is lengthened. As we will see in the next section, these results can be accounted for in terms of the hydrophobic effect which will be described in some detail.

8.7 Driving force for micelle formation

Until recently, the formation of micelles was regarded primarily as an interfacial energy process, analogous to the process of coalescence of oil droplets in an aqueous medium. If this was the case, micelle formation would be a highly exothermic process, as the interfacial free energy has a large enthalpy component. As mentioned above, experimental results have clearly shown that micelle formation involves only a small enthalpy change and is often endothermic. The negative free energy of micellization is the result of a large positive entropy. This led to the conclusion that micelle formation must be predominantly entropy driven process. Two main sources of entropy have been suggested. The first is related to the so-called "hydrophobic effect". This effect was first established from a consideration of the free energy enthalpy and entropy of transfer of hydrocarbon from water to a liquid hydrocarbon. Some results are listed in Tab. 8.4. This table also lists the heat capacity change ΔC_p on transfer from water to a hydrocarbon, as well as $C_p^{0,gas}$, i.e. the heat capacity in the gas phase. It can be seen from Tab. 8.4 that the principal contribution to the value of ΔG^0 is the large positive value of ΔS^0, which increases with increasing hydrocarbon chain length, whereas ΔH^0 is positive, or small and negative.

To account for this large positive entropy of transfer several authors [35–37] suggest that the water molecules around a hydrocarbon chain are ordered, forming "clus-

Tab. 8.4: Thermodynamic parameters for transfer of hydrocarbons from water to liquid hydrocarbon at 25 °C.

Hydrocarbon	ΔG^0 (kJ mol^{-1})	ΔH^0 (kJ mol^{-1})	ΔS^0 (kJ mol^{-1} K^{-1})	ΔC_p^0 (kJ mol^{-1} K^{-1})	$C_p^{0,gas}$ (kJ mol^{-1} K^{-1})
C_2H_6	−16.4	10.5	88.2	—	—
C_3H_8	−20.4	7.1	92.4	—	—
C_4H_{10}	−24.8	3.4	96.6	−273	−143
C_5H_{12}	−28.8	2.1	105.0	−403	−172
C_6H_{14}	−32.5	0	109.2	−441	−197
C_6H_6	−19.3	−2.1	58.8	−227	−134
$C_6H_5CH_3$	−22.7	−1.7	71.4	−265	−155
$C_6H_5C_2H_5$	−26.0	−2.0	79.8	−319	−185
$C_6H_5C_3H_8$	−29.0	−2.3	88.2	−395	—

ters" or "icebergs". On transfer of an alkane from water to a liquid hydrocarbon, these clusters are broken, thus releasing water molecules which now have a higher entropy. This accounts for the large entropy of transfer of an alkane from water to a hydrocarbon medium. This effect is also reflected in the much higher heat capacity change on transfer, ΔC_p^0, when compared with the heat capacity in the gas phase, C_p^0. This effect is also operative on transfer of surfactant monomer to a micelle, during the micellization process. The surfactant monomers will also contain "structured" water around their hydrocarbon chain. On transfer of such monomers to a micelle, these water molecules are released and they have a higher entropy.

The second source of entropy increase on micellization may arise from the increase in flexibility of the hydrocarbon chains on their transfer from an aqueous to a hydrocarbon medium [35]. The orientations and bendings of an organic chain are likely to be more restricted in an aqueous phase compared to an organic phase. It should be mentioned that with ionic and zwitterionic surfactants, an additional entropy contribution, associated with the ionic head groups, must be considered. Upon partial neutralization of the ionic charge by the counterions when aggregation occurs, water molecules are released. This will be associated with an entropy increase which should be added to the entropy increase resulting from the hydrophobic effect mentioned above. However, the relative contribution of the two effects is difficult to assess in a quantitative manner.

8.8 Micellization in surfactant mixtures (mixed micelles)

In most industrial applications, more than one surfactant molecule is used in the formulation. It is, therefore, necessary to predict the type of possible interactions and whether this leads to some synergistic effects. Two general cases may be considered: surfactant molecules with no net interaction (with similar head groups) and systems

with net interaction [16]. The first case is that when mixing two surfactants with the same head group but with different chain lengths. In analogy with the hydrophilic-lipophilic balance (HLB) for surfactant mixtures, one can also assume the cmc of a surfactant mixture (with no net interaction) to be an average of the two cmcs of the single components [16],

$$\mathrm{cmc} = x_1 \mathrm{cmc}_1 + x_2 \mathrm{cmc}_2, \tag{8.22}$$

where x_1 and x_2 are the mole fractions of the respective surfactants in the system. However, the mole fractions should not be those in the whole system, but those inside the micelle. This means that equation (8.22) should be modified,

$$\mathrm{cmc} = x_1^{\mathrm{m}} \mathrm{cmc}_1 + x_2^{\mathrm{m}} \mathrm{cmc}_2. \tag{8.23}$$

The superscript 'm' indicates that the values are inside the micelle. If x_1 and x_2 are the solution composition, then,

$$\frac{1}{\mathrm{cmc}} = \frac{x_1}{\mathrm{cmc}_1} + \frac{x_2}{\mathrm{cmc}_2}. \tag{8.24}$$

The molar composition of the mixed micelle is given by,

$$x_1^{\mathrm{m}} = \frac{x_1 \mathrm{cmc}_2}{x_1 \mathrm{cmc}_2 + x_2 \mathrm{cmc}_1}. \tag{8.25}$$

Fig. 8.8 shows the calculated cmc and the micelle composition as a function of solution composition using equations (8.24) and (8.25) for three cases where $\mathrm{cmc}_2/\mathrm{cmc}_1 = 1$, 0.1 and 0.01. As can be seen, the cmc and micellar composition change dramatically with solution composition when the cmcs of the two surfactants vary considerably, i.e. when the ratio of cmcs is far from 1. This fact is used when preparing microemulsions where the addition of medium chain alcohol (like pentanol or hexanol) changes the properties considerably. If component 2 is much more surface active, i.e. $\mathrm{cmc}_2/\mathrm{cmc}_1 \ll 1$, and it is present in low concentrations (x_2 is of the order of 0.01), then from equation (8.25), $x_1^{\mathrm{m}} \approx x_2^{\mathrm{m}} \approx 0.5$, i.e. at the cmc of the systems the micelles are up to 50 % composed of component 2. This illustrates the role of contaminants in surface activity, e.g. dodecyl alcohol in sodium dodecyl sulphate (SDS).

Fig. 8.9 shows the cmc as a function of molar composition of the solution and in the micelles for a mixture of SDS and nonylphenol with 10 mol ethylene oxide (NP–E_{10}). If the molar composition of the micelles is used as the x-axis, the cmc is more or less the arithmetic mean of the cmcs of the two surfactants. If, on the other hand, the molar composition in the solution is used as the x-axis (which at the cmc is equal to the total molar concentration), then the cmc of the mixture shows a dramatic decrease at low fractions of NP–E_{10}. This decrease is due to the preferential absorption of NP–E_{10} in the micelle. This higher absorption is due to the higher hydrophobicity of the NP–E_{10} surfactant when compared with SDS.

With many industrial formulations, surfactants of different kinds are mixed together, for example anionics and nonionics. The nonionic surfactant molecules shield

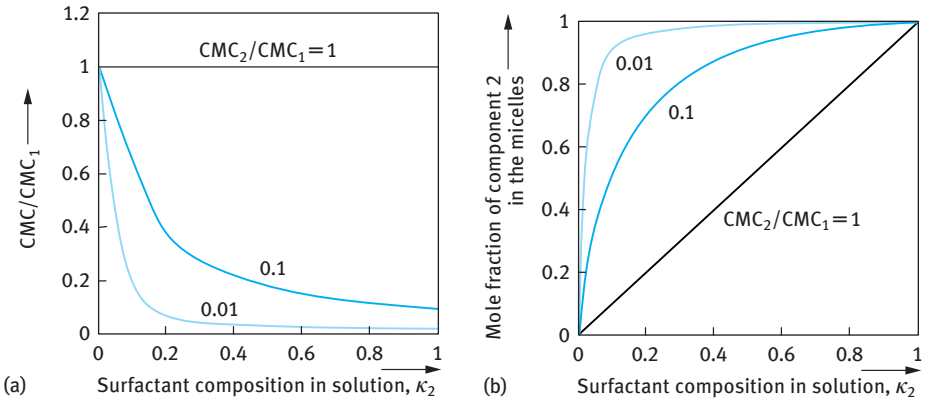

Fig. 8.8: Calculated cmc (a) and micellar composition (b) as a function of solution composition for three ratios of cmcs.

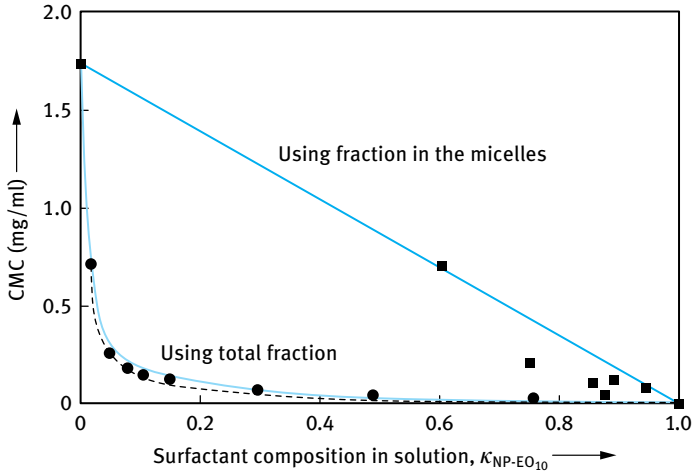

Fig. 8.9: cmc as a function of surfactant composition, x_1, or micellar surfactant composition, x_1^m for the system SDS + NP–E_{10}.

the repulsion between the negative head groups in the micelle and hence there will be a net interaction between the two types of molecules. Another example is the case when anionic and cationic surfactants are mixed, whereby very strong interaction will take place between the oppositely charged surfactant molecules. To account for this interaction, equation (8.25) has to be modified by introducing activity coefficients of the surfactants, f_1^m and f_2^m in the micelle,

$$\text{cmc} = x_1^m f_1^m \text{cmc}_1 + x_2^m f_2^m \text{cmc}_2. \tag{8.26}$$

An expression for the activity coefficients can be obtained using the regular solutions theory [16],

$$\ln f_1^{\mathrm{m}} = (x_2^{\mathrm{m}})^2 \beta, \tag{8.27}$$

$$\ln f_2^{\mathrm{m}} = (x_2^{\mathrm{m}})^2 \beta, \tag{8.28}$$

where β is an interaction parameter between the surfactant molecules in the micelle. A positive β value means that there is a net repulsion between the surfactant molecules in the micelle, whereas a negative β value means a net attraction.

The cmc of the surfactant mixture and the composition x_1 are given by the following equations,

$$\frac{1}{\mathrm{cmc}} = \frac{x_1}{f_1^{\mathrm{m}} \mathrm{cmc}_1} + \frac{x_2}{f_2^{\mathrm{m}} \mathrm{cmc}_2} \tag{8.29}$$

$$x_1^{\mathrm{m}} = \frac{x_1 f_2^{\mathrm{m}} \mathrm{cmc}_2}{x_1 f_2^{\mathrm{m}} \mathrm{cmc}_2 + x_2 f_2^{\mathrm{m}} \mathrm{cmc}_1}. \tag{8.30}$$

Fig. 8.10 shows the effect of increasing the β parameter on the cmc and micellar composition for two surfactants with a cmc ratio of 0.1.

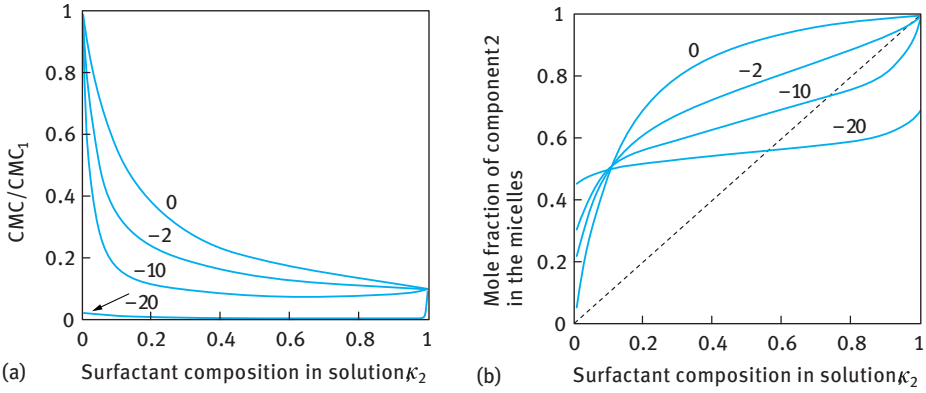

Fig. 8.10: cmc (a) and micellar composition (b) for various values of β for a system with a cmc ratio $\mathrm{cmc}_2/\mathrm{cmc}_1 = 0.1$.

Fig. 8.10 shows that as β becomes more negative, the cmc of the mixture decreases. β values in the region of –2 are typical for anionic/nonionic mixtures, whereas values in the region of –10 to –20 are typical of anionic/cationic mixtures. With increasing the negative value of β, the mixed micelles tend towards a mixing ratio of 50 : 50, which reflects the mutual electrostatic attraction between the surfactant molecules. The predicted cmc and micellar composition depends both on the ratio of the cmcs as well as the value of β. When the cmcs of the single surfactants are similar, the predicted

value of the cmc is very sensitive to small variation in β. On the other hand, when the ratio of the cmcs is large, the predicted value of the mixed cmc and the micellar composition are insensitive to variation of the β parameter. For mixtures of nonionic and ionic surfactants, the β decreases with increasing electrolyte concentration. This is due to the screening of the electrostatic repulsion on the addition of electrolyte. With some surfactant mixtures, the β decreases with increasing temperature, i.e. the net attraction decreases with increasing temperature.

8.9 Surfactant self-assembly

Surfactant micelles and bilayers are the building blocks of most self-assembly structures. One can divide the phase structures into two main groups [16]:

(i) those that are built of limited or discrete self-assemblies, which may be characterized roughly as spherical, prolate or cylindrical;
(ii) infinite or unlimited self-assemblies whereby the aggregates are connected over macroscopic distances in one, two or three dimensions.

The hexagonal phase (see below) is an example of one-dimensional continuity, the lamellar phase of two-dimensional continuity, whereas the bicontinuous cubic phase and the sponge phase (see later) are examples of three-dimensional continuity. These two types are schematically illustrated in Fig. 8.11.

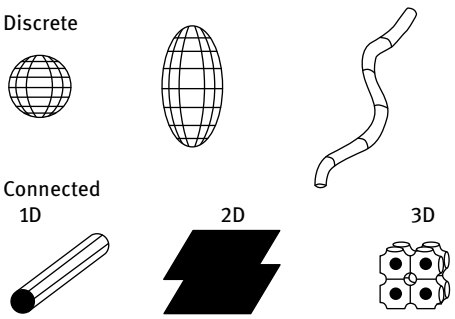

Fig. 8.11: Schematic representation of self-assembly structures.

8.10 Structure of liquid crystalline phases

The above mentioned unlimited self-assembly structures in 1D, 2D or 3D are referred to as liquid crystalline structures. These behave as fluids and are usually highly viscous. At the same time, X-ray studies of these phases yield a small number of relatively sharp lines which resemble those produced by crystals [16]. Since they are fluids then they

are less ordered than crystals, but because of the X-ray lines and their high viscosity it is also apparent that they are more ordered than ordinary liquids. Thus, the term liquid crystalline phase is very appropriate for describing these self-assembled structures. Below a brief description of the various liquid crystalline structures that can be produced with surfactants is given and Tab. 8.5 shows the most commonly used notation to describe these systems.

Tab. 8.5: Notation of the most common liquid crystalline structures.

Phase structure	Abbreviation	Notation
Micellar	mic	L_1, S
Reversed micellar	rev mic	L_2, S
Hexagonal	hex	H_1, E, M_1, middle
Reversed hexagonal	rev hex	H_2, F, M_2
Cubic (normal micellar)	cub_m	I_1, S_{1c}
Cubic (reversed micelle)	cub_m	I_2
Cubic (normal bicontinuous)	cub_b	I_1, V_1
Cubic (reversed bicontinuous)	cub_b	I_2, V_2
Lamellar	lam	L_α, D, G, neat
Gel	gel	L_β
Sponge phase (reversed)	spo	L_3 (normal), L_4

8.10.1 Hexagonal phase

This phase is built up of (infinitely) long cylindrical micelles arranged in a hexagonal pattern, with each micelle being surrounded by six other micelles, as schematically shown in Fig. 8.7. The radius of the circular cross section (which may be somewhat deformed) is again close to the surfactant molecule length [1].

8.10.2 Micellar cubic phase

This phase is built up of regular packing of small micelles, which have similar properties to small micelles in the solution phase. However, the micelles are short prolates (axial ratio 1 : 2) rather than spheres since this allows a better packing. The micellar cubic phase is highly viscous. A schematic representation of the micellar cubic phase [1] is shown in Fig. 8.7.

8.10.3 Lamellar phase

This phase is built of layers of surfactant molecules alternating with water layers. The thickness of the bilayers is somewhat lower than twice the surfactant molecule length.

The thickness of the water layer can vary over wide ranges, depending on the nature of the surfactant. The surfactant bilayer can range from being stiff and planar to being very flexible and undulating. A schematic representation of the lamellar phase [16] is shown in Fig. 8.7.

8.10.4 Bicontinuous cubic phases

These phases can have a number of different structures, where the surfactant molecules form aggregates that penetrate space, forming a porous connected structure in three dimensions. They can be considered as structures formed by connecting rod-like micelles (branched micelles), or bilayer structures [16] as illustrated in Fig. 8.12.

Fig. 8.12: Bicontinuous structure with the surfactant molecules aggregated into connected films characterized by two curvatures of opposite sign [9].

8.10.5 Reversed structures

Except for the lamellar phase, which is symmetrical around the middle of the bilayer, the different structures have a reversed counterpart in which the polar and nonpolar parts have changed roles. For example, a hexagonal phase is built up of hexagonally packed water cylinders surrounded by the polar head groups of the surfactant molecules and a continuum of the hydrophobic parts. Similarly, reversed (micellar-type) cubic phases and reversed micelles consist of globular water cores surrounded by surfactant molecules. The radii of the water cores are typically in the range 2–10 nm.

8.11 Experimental studies of the phase behaviour of surfactants

One of the earliest (and qualitative) techniques for identifying the different phases is the use of polarizing microscopy. This is based on the scattering of normal and polarized light which differs for isotropic (such as the cubic phase) and anisotropic (such as the hexagonal and lamellar phases) structures. Isotropic phases are clear and transparent, while anisotropic liquid crystalline phases scatter light and appear more or

less cloudy. Using polarized light and viewing the samples through cross polarizers give a black picture for isotropic phases, whereas anisotropic ones give bright images. The patterns in a polarization microscope are distinctly different for different anisotropic phases and can therefore be used to identify the phases, e.g. to distinguish between hexagonal and lamellar phases [38]. A typical optical micrograph for the hexagonal and lamellar phases (obtained using polarizing microscopy) is shown in Fig. 8.13. The hexagonal phase shows a "fan-like" appearance, whereas the lamellar phase shows "oily streaks" and "Maltese crosses".

(a) (b)

Fig. 8.13: Texture of the hexagonal (a) and lamellar phase (b) obtained using polarizing microscopy.

Another qualitative method is to measure the viscosity as a function of surfactant concentration. The cubic phase is very viscous and often quite stiff and it appears as a clear "gel". The hexagonal phase is less viscous than the cubic phase and the lamellar phase is much less viscous than the cubic phase. However, viscosity measurements do not allow an unambiguous determination of the phases in the sample.

Most qualitative techniques for identification of the various liquid crystalline phases are based on diffraction studies, either light, X-ray or neutron. The liquid crystalline structures have a repetitive arrangement of aggregates and observation of a diffraction pattern can give evidence of long-range order and it can distinguish between alternative structures.

Another very useful technique to identify the different phases is NMR spectroscopy. One observes the quadrupole splittings in deuterium NMR [39]. This is illustrated in Fig. 8.14. For isotropic phases such as micelles, cubic and sponge phases one observes a narrow singlet (Fig. 8.14 (a)). For a single isotropic phase such as hexagonal or lamellar structures, a doublet is obtained (Fig. 8.14 (b)).

The magnitude of the "splitting" depends on the type of liquid crystalline phase, which is twice as much for the lamellar phase when compared with the hexagonal phase. For one isotropic and one anisotropic phase, one obtains one singlet and one

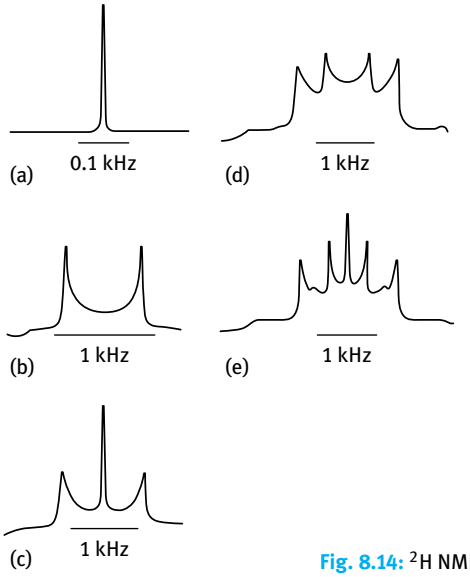

Fig. 8.14: ^{2}H NMR spectra of surfactants in heavy water (D_2O).

doublet (Fig. 8.14 (c)). For two anisotropic phases (lamellar and hexagonal) one observes two doublets (Fig. 8.14 (d)). In a three-phase region with two anisotropic phases and one isotropic phase, one observes two doublets and one singlet (Fig. 8.14 (e)).
The distinction between normal and reversed phases can be easily carried out using conductivity measurements. For normal phases which are "water rich", the conductivity is high. In contrast, for reversed phases that are "water poor", the conductivity is much lower (by several orders of magnitude).

References

[1] Tadros T. Applied surfactants. Weinheim: Wiley-VCH; 2005.
[2] Holmberg K, Jonsson B, Kronberg B, Lindman B. Surfactants and polymers in aqueous solution. 2nd edition. USA: John Wiley & Sons; 2003.
[3] McCutcheon. Detergents and Emulsifiers. New Jersey: Allied Publishing Co. Published annually.
[4] van Os NM, Haak JR, Rupert LAM. Physico-chemical properties of selected anionic, cationic and nonionic surfactants. Amsterdam: Elsevier Publishing Co.; 1993.
[5] Porter MR. Handbook of surfactants. Blackie, USA: Chapman and Hall; 1994.
[6] Linfield WM (editor). Anionic surfactants. New York: Marcel Dekker; 1967.
[7] Lucassen-Reynders EH. Anionic surfactants – Physical chemistry of surfactant action. New York: Marcel Dekker; 1981.
[8] Jungermana E. Cationic surfactants. New York: Marcel Dekker; 1970.
[9] Rubingh N, Holland PM (editors). Cationic surfactants – Physical chemistry. New York: Marcel Dekker; 1991.
[10] Buestein BR, Hiliton CL. Amphoteric surfactants. New York: Marcel Dekker; 1982.
[11] Schick MJ, editor. Nonionic surfactants. New York: Marcel Dekker; 1966.

[12] Schick MJ, editor. Nonionic surfactants: Physical chemistry. New York: Marcel Dekker; 1987.
[13] Schonfeldt N. Surface active ethylene oxide adducts. USA: Pergamon Press; 1970.
[14] von Rybinsky W, Hill K. In: Holberg K, editor. Novel surfactants. New York: Marcel Dekker; 2003. Chapter 2.
[15] Drummond CJ, Fong C, Krodkiewska I, Boyd BJ, Baker IJA. In: Holberg K, editor. Novel surfactants. New York: Marcel Dekker; 2003. Chapter 3.
[16] Lindman B. In: Tadros TF, editor. Surfactants. London: Academic Press; 1984.
[17] Israelachvili JN. Intermolecular and surface forces, with special applications to colloidal and biological systems. London: Academic Press; 1985. p. 251.
[18] Mukerjee P, Mysels KJ. Critical micelle concentrations of aqueous surfactant systems. Washington DC: National Bureau of Standards Publication; 1971.
[19] Elworthy PH, Florence AT, Macfarlane CB. Solubilization by surface active agents. London: Chapman and Hall; 1968.
[20] Shinoda K, Nagakawa T, Tamamushi BI, Isemura T. Colloidal surfactants, some physicochemical properties. London: Academic Press; 1963.
[21] McBain JW. Trans Faraday Soc. 1913;9:99.
[22] Adam NK. J Phys Chem. 1925;29:87.
[23] Hartley GS. Aqueous solutions of paraffin chain salts. Paris: Hermann and Cie; 1936.
[24] McBain JW. Colloid science. Boston: Heath; 1950.
[25] Harkins WD, Mattoon WD, Corrin ML. J Amer Chem Soc. 1946;68:220; J Colloid Sci. 1946;1:105.
[26] Debye P, Anaker EW. J Phys Colloid Chem. 1951;55:644.
[27] Anainsson EAG, Wall SN. J Phys Chem. 1974;78:1024; 1975;79:857.
[28] Anainsson EAG, Wall SN, Almagren M, Hoffmann H, Ulbricht W, Zana R, Lang J, Tondre C. J Phys Chem. 1976;80:905.
[29] Rassing J, Sams PJ, Wyn-Jones E. J Chem Soc, Faraday II. 1974;70:1247.
[30] Jaycock MJ, Ottewill RH. Fourth Int. Congress Surface Activity. 1964;2:545.
[31] Okub T, Kitano H, Ishiwatari T, Isem N. Proc Royal Soc. 1979;A36:81.
[32] Phillips JN. Trans Faraday Soc. 1955;51:561.
[33] Kahlweit M, Teubner M. Adv Colloid Interface Sci. 1980;13:1.
[34] Rosen ML. Surfactants and interfacial phenomena. New York: Wiley-Interscience; 1978.
[35] Tanford C. The hydrophobic effect. 2nd edition. New York: Wiley; 1980.
[36] Stainsby G, Alexander AE. Trans Faraday Soc. 1950;46:587.
[37] Arnow RH, Witten L. J Phys Chem. 1960;64:1643.
[38] Rosevaar FB. J Soc Cosmet Chem. 1968;19:581.
[39] Khan A, Fontell K, Lindblom G, Lindman B. J Phys Chem. 1982;86:4266

9 Adsorption of surfactants at the liquid/liquid interface

9.1 Introduction

When two immiscible phases α and β come into contact, an interfacial region develops. The interfacial region is not a layer that is one molecule thick; it is a region with thickness δ with properties different from the two bulk phases α and β. In bringing phases α and β into contact, the interfacial regions of these phases undergo some changes, resulting in a concomitant change in the internal energy. If we were to move a probe from the interior of α to that of β, one would at some distance from the interface start to observe deviations in composition, in density, in structure; the closer to phase β the larger the deviations until eventually the probe arrives in the homogeneous phase β. The thickness of the transition layer will depend on the nature of the interfaces and on other factors. Gibbs [1] considered the two phases α and β to have uniform thermodynamic properties up to the interfacial region. He assumed a mathematical plane Z^σ in the interfacial region in order to define the surface or interfacial tension γ. A schematic representation of the interfacial region and the Gibbs mathematical plane is given in Fig. 9.1.

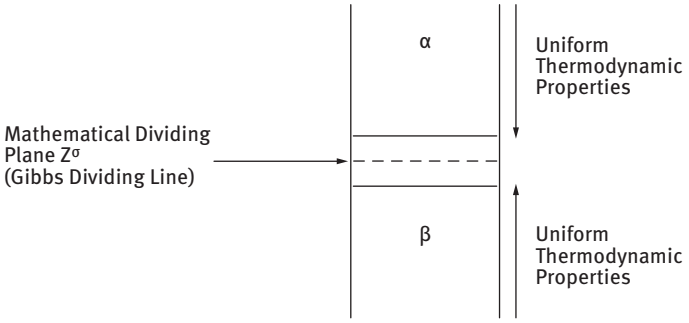

Fig. 9.1: The Gibbs dividing line.

Using the Gibbs model, it is possible to obtain a definition of the surface or interfacial tension γ. The surface free energy $\mathrm{d}G^\sigma$ is made of three components: an entropy term, $S^\sigma\,\mathrm{d}T$; an interfacial energy term, $A\,\mathrm{d}\gamma$; a composition term $\sum n_i\,\mathrm{d}\mu_i$ (n_i is the number of moles of component i with chemical potential μ_i).

The Gibbs–Deuhem equation is,

$$\mathrm{d}G^\sigma = -S^\sigma \mathrm{d}T + A\,\mathrm{d}\gamma + \sum n_i\,\mathrm{d}\mu_i. \tag{9.1}$$

https://doi.org/10.1515/9783110540895-010

At constant temperature and composition,

$$dG^{\sigma} = A\,d\gamma,$$
$$\gamma = \left(\frac{\partial G^{\sigma}}{\partial A}\right)_{T,n_i}. \tag{9.2}$$

For a stable interface γ is positive, i.e. if the interfacial area increases G^{σ} increases. Note that γ is energy per unit area (mJ m^{-2}) which is dimensionally equivalent to force per unit length (mN m^{-1}), the unit usually used to define surface or interfacial tension. It is obvious from equation (9.2) that for a stable interface γ should be positive. In other words, the free energy should increase if the area of the interface increases, otherwise the interface will become convoluted, increasing the interfacial area, until the two "immiscible" phases dissolve in each other (for the L/L case).

It is clear from equation (9.2) that surface or interfacial tension, i.e. the force per unit length tangentially to the surface measured in units of mN m^{-1}, is dimensionally equivalent to an energy per unit area measured in mJ m^{-2}. For this reason, it has been stated that the excess surface free energy is identical to the surface tension, but this is true only for a single component system, i.e. a pure liquid (where the total adsorption is zero).

For a curved interface, one should consider the effect of the radius of curvature. Fortunately, γ for a curved interface is estimated to be very close to that of a planer surface, unless the droplets are very small (< 10 nm).

Curved interfaces produce some other important physical phenomena which affect emulsion properties, e.g. the Laplace pressure Δp which is determined by the radii of curvature of the droplets,

$$\Delta p = \gamma\left(\frac{1}{r_1} + \frac{1}{r_2}\right), \tag{9.3}$$

where r_1 and r_2 are the two principal radii of curvature.

For a perfectly spherical droplet $r_1 = r_2 = r$ and,

$$\Delta p = \frac{2\gamma}{r}. \tag{9.4}$$

For a hydrocarbon droplet with radius 100 nm, and $\gamma = 50$ mN m^{-1}, $\Delta p \approx 10^6$ Pa ($\approx$ 10 atm.)

9.2 Surfactant adsorption

Knowledge of the amount of surfactant adsorbed Γ (moles per unit area), sometimes referred to as surface excess, is crucial in understanding the role of surfactants in emulsion formation and stability. From Γ one can calculate the area per surfactant molecule or ion and this provides information on the orientation of surfactant molecules at the liquid/liquid (L/L) interface. This molecular orientation is crucial in understanding emulsion stability. As we will see below, Γ can be obtained from the variation

of interfacial tension with surfactant concentration and application of the second law of thermodynamics.

There are generally two approaches for treating surfactant adsorption at the L/L interface. The first approach, adopted by Gibbs, treats adsorption as an equilibrium phenomenon whereby the second law of thermodynamics may be applied using surface quantities. The second approach, referred to as the equation of state approach, treats the surfactant film as a two-dimensional layer with a surface pressure π that may be related the surface excess Γ (amount of surfactant adsorbed per unit area). Below, these two approaches are summarized.

9.2.1 The Gibbs adsorption isotherm

Gibbs [2] derived a thermodynamic relationship between the surface or interfacial tension γ and the surface excess Γ (adsorption per unit area). The starting point of this equation is the Gibbs–Deuhem equation given above (equation (9.1)). At equilibrium (where the rate of adsorption is equal to the rate of desorption), $\mathrm{d}G^{\sigma} = 0$. At constant temperature, but in the presence of adsorption,

$$\begin{aligned} \mathrm{d}G^{\sigma} &= -S^{\sigma}\,\mathrm{d}T + A\,\mathrm{d}\gamma + \sum n_i\,\mathrm{d}\mu_i, \\ \mathrm{d}\gamma &= -\sum \frac{n_i^{\sigma}}{A}\,\mathrm{d}\mu_i = -\sum \Gamma_i\,\mathrm{d}\mu_i, \end{aligned} \tag{9.5}$$

where $\Gamma_i = n_i^{\sigma}/A$ is the number of moles of component i and adsorbed per unit area.

Equation (9.5) is the general form for the Gibbs adsorption isotherm. The simplest case of this isotherm is a system of two components in which the solute (2) is the surface active component, i.e. it is adsorbed at the surface of the solvent (1). For such a case, equation (9.5) may be written as,

$$-\mathrm{d}\gamma = \Gamma_1^{\sigma}\,\mathrm{d}\mu_1 + \Gamma_2^{\sigma}\,\mathrm{d}\mu_2, \tag{9.6}$$

and if the Gibbs dividing surface is used, $\Gamma_1 = 0$ and,

$$-\mathrm{d}\gamma = \Gamma_{1,2}^{\sigma}\,\mathrm{d}\mu_2, \tag{9.7}$$

where $\Gamma_{2,1}^{\sigma}$ is the relative adsorption of (2) with respect to (1). Since,

$$\mu_2 = \mu_2^0 + RT\ln a_2^{\mathrm{L}}, \tag{9.8}$$

or,

$$\mathrm{d}\mu_2 = RT\mathrm{d}\ln a_2^{\mathrm{L}}, \tag{9.9}$$

then,

$$-\mathrm{d}\gamma = \Gamma_{2,1}^{\sigma}RT\mathrm{d}\ln a_2^{\mathrm{L}}, \tag{9.10}$$

or

$$\Gamma^{\sigma}_{2,1} = -\frac{1}{RT}\left(\frac{\mathrm{d}\gamma}{\mathrm{d}\ln a^{\mathrm{L}}_{2}}\right), \tag{9.11}$$

where a^{L}_{2} is the activity of the surfactant in bulk solution that is equal to $C_2 f_2$ or $x_2 f_2$, where C_2 is the concentration of the surfactant in mol dm^{-3} and x_2 is its mole fraction.

Equation (9.11) allows one to obtain the surface excess (abbreviated as Γ_2) from the variation of surface or interfacial tension with surfactant concentration. Note that $a_2 \approx C_2$ since in dilute solutions $f_2 \approx 1$. This approximation is valid since most surfactants have low cmc (usually less than 10^{-3} mol dm^{-3}) and adsorption is complete at or just below the cmc.

The surface excess Γ_2 can be calculated from the linear portion of the γ–log C_2 curves before the cmc. Such γ–log C curves are illustrated in Fig. 9.2 for the air/water and O/W interfaces; $[C_{\mathrm{SAA}}]$ denotes the concentration of surface active agent in bulk solution. It can be seen that for the A/W interface, γ decreases from the value for water (72 mN m^{-1} at 20 °C) reaching about 25–30 mN m^{-1} near the cmc. This is clearly schematic since the actual values depend on the surfactant nature. For the O/W case, γ decreases from a value of about 50 mN m^{-1} (for a pure hydrocarbon-water interface) to ≈ 1–5 mN m^{-1} near the cmc (again depending on the nature of the surfactant).

As mentioned above, Γ_2 can be calculated from the slope of the linear position of the curves shown in Fig. 9.2 just before the cmc is reached. From Γ_2, the area per surfactant ion or molecule can be calculated since,

$$\text{Area/molecule} = \frac{1}{\Gamma_2 N_{\mathrm{av}}}, \tag{9.12}$$

where N_{av} is the Avogadro constant.

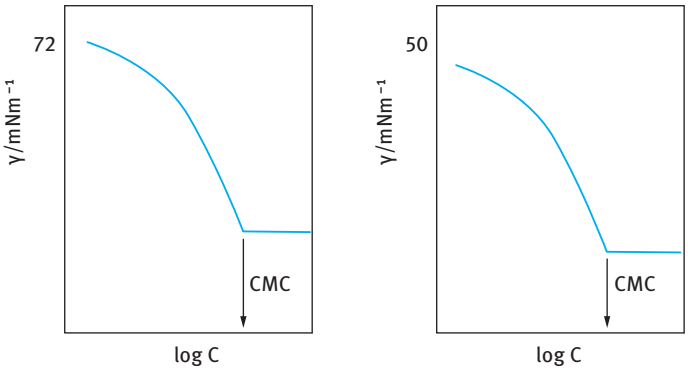

Fig. 9.2: Variation of surface and interfacial tension with log$[C_{\mathrm{SAA}}]$ at the air/water and oil/water interface.

Determining the area per surfactant molecule is very useful since it gives information on surfactant orientation at the interface. For example, for ionic surfactants such as alkyl sulphates, the area per surfactant is determined by the area occupied by the alkyl chain and head group if these molecules lie flat at the interface. In this case the area per molecule increases with increasing alkyl chain length. For vertical orientation, the area per surfactant ion is determined by that occupied by the charged head group, which at low electrolyte concentration will be in the region of 0.40 nm^2. Such an area is larger than the geometrical area occupied by a sulphate group, as a result of the lateral repulsion between the head groups. On addition of electrolytes, this lateral repulsion is reduced and the area/surfactant ion for vertical orientation will be lower than 0.4 nm^2 (reaching in some cases 0.2 nm^2).

Another important point can be made from the γ–log C curves. At concentration just before the breakpoint, one has the condition of constant slope, which indicates that saturation adsorption has been reached.

$$\left(\frac{\partial \gamma}{\partial \ln a_2}\right)_{p,T} = \text{const.} \tag{9.13}$$

Just above the breakpoint,

$$\left(\frac{\partial \gamma}{\partial \ln a_2}\right)_{p,T} = 0, \tag{9.14}$$

indicating the constancy of γ with log C above the cmc. Integration of equation (9.12) gives,

$$\gamma = \text{const}\, x \ln a_2. \tag{9.15}$$

Since γ is constant in this region, then a_2 must remain constant. This means that addition of surfactant molecules, above the cmc, must result in association to form units (micellar) with low activity.

As mentioned before, the hydrophilic head group may be unionized, e.g. alcohols or poly(ethylene oxide) alkane or alkyl phenol compounds, weakly ionized such as carboxylic acids or strongly ionized such as sulphates, sulphonates and quaternary ammonium salts. The adsorption of these different surfactants at the air/water and oil/water interface depends on the nature of the head group. With nonionic surfactants, repulsion between the head groups is small and these surfactants are usually strongly adsorbed at the surface of water from very dilute solutions. Nonionic surfactants have much lower cmc values when compared with ionic surfactants with the same alkyl chain length. Typically, the cmc is in the region of 10^{-5}–10^{-4} mol dm^{-3}. Such nonionic surfactants form closely packed adsorbed layers at concentrations lower than their cmc values. The activity coefficient of such surfactants is close to unity and is only slightly affected by addition of moderate amounts of electrolytes (or change in the pH of the solution). Thus, nonionic surfactant adsorption is the simplest case since the solutions can be represented by a two component system and the adsorption can be accurately calculated using equation (9.9).

With ionic surfactants, on the other hand, the adsorption process is relatively more complicated since one has to consider the repulsion between the head groups and the effect of presence of any indifferent electrolyte. Moreover, the Gibbs adsorption equation has to be solved taking into account the surfactant ions, the counterions and any indifferent electrolyte ions present. For a strong surfactant electrolyte such as an Na^+R^-

$$\Gamma_2 = \frac{1}{2RT}\frac{\partial \gamma}{\partial \ln a_{\pm}}. \tag{9.16}$$

The factor of 2 in equation (9.16) arises because both surfactant ion and counterion must be adsorbed to maintain neutrally, and $d\gamma/d \ln a_{\pm}$ is twice as large as for an unionized surfactant.

If a nonadsorbed electrolyte, such as NaCl, is present in large excess, then any increase in concentration of Na^+R^- produces a negligible increase in Na^+ ion concentration and therefore $d\mu_{Na}$ becomes negligible. Moreover, $d\mu_{Cl}$ is also negligible, so that the Gibbs adsorption equation reduces to,

$$\Gamma_2 = -\frac{1}{RT}\left(\frac{\partial \gamma}{\partial \ln C_{NaR}}\right), \tag{9.17}$$

i.e. it becomes identical to that for a nonionic surfactant.

The above discussion clearly illustrates that for calculation of Γ_2 from the γ–log C curve one has to consider the nature of the surfactant and the composition of the medium. For nonionic surfactants, the Gibbs adsorption equation (9.9) can be directly used. For ionic surfactants, in the absence of electrolytes, the right-hand side of equation (9.9) should be divided by 2 to account for surfactant dissociation. This factor disappears in the presence of a high concentration of an indifferent electrolyte.

9.2.2 Equation of state approach

In this approach, one relates the surface pressure π with the surface excess Γ_2. The surface pressure is defined by the equation [3–5],

$$\pi = \gamma_0 - \gamma, \tag{9.18}$$

where γ_0 is the surface or interfacial tension before adsorption and γ that after adsorption.

For an ideal surface film, behaving as a two-dimensional gas the surface pressure π is related to the surface excess Γ_2 by the equation,

$$\pi A = n_2 RT, \tag{9.19}$$

or

$$\pi = (n_2/A)RT = \Gamma_2 RT. \tag{9.20}$$

Differentiating equation (9.20) at constant temperature,

$$d\pi = RT\, d\Gamma_2. \tag{9.21}$$

Using the Gibbs equation,

$$d\pi = -d\gamma = \Gamma_2 RT\, d\ln a_2 \approx \Gamma_2 RT\, d\ln C_2. \tag{9.22}$$

Combining equations (9.21) and (9.22)

$$d\ln \Gamma_2 = d\ln C_2, \tag{9.23}$$

or

$$\Gamma_2 = KC_2^{\alpha}. \tag{9.24}$$

Equation (9.24) is referred to as the Henry law isotherm which predicts a linear relationship between Γ_2 and C_2.

It is clear that equations (9.17) and (9.21) are based on an idealized model in which the lateral interaction between the molecules has not been considered. Moreover, in this model the molecules are considered to be dimensionless. This model can only be applied at very low surface coverage where the surfactant molecules are so far apart that lateral interaction may be neglected. Moreover, under these conditions the total area occupied by the surfactant molecules is relatively small compared to the total interfacial area.

At significant surface coverage, the above equations have to be modified to take into account both lateral interaction between the molecules as well as the area occupied by them. Lateral interaction may reduce π if there is attraction between the chains (e.g. with most nonionic surfactants) or it may increase π as a result of repulsion between the head groups in the case of ionic surfactants.

Various equations of state have been proposed, taking into account the above two effects, in order to fit the π–A data. The two-dimensional van der Waals equation of state is probably the most convenient for fitting these adsorption isotherms, i.e.,

$$\left(\pi + \frac{(n_2)^2 \alpha}{A_2}\right)(A - n_2 A_2^0) = n_2 RT, \tag{9.25}$$

where A_2^0 is the excluded area or co-area of type 2 molecule in the interface and α is a parameter which allows for lateral interaction.

Equation (9.25) leads to the following theoretical adsorption isotherm, using the Gibbs equation,

$$C_2^{\alpha} = K_1\left(\frac{\theta}{1-\theta}\right)\exp\left(\frac{\theta}{1-\theta} - \frac{2\alpha\theta}{a_2^0 RT}\right), \tag{9.26}$$

where θ is the surface coverage ($\theta = \Gamma_2/\ \Gamma_{2,\max}$), K_1 is a constant that is related to the free energy of adsorption of surfactant molecules at the interface ($K_1 \propto \exp(-\Delta G_{\text{ads}}/kT)$) and a_2^0 is the area/molecule.

For a charged surfactant layer, equation (9.23) has to be modified to take into account the electrical contribution from the ionic head groups, i.e.,

$$C_2^{\alpha} = K_1\left(\frac{\theta}{1-\theta}\right)\exp\left(\frac{\theta}{1-\theta}\right)\exp\left(\frac{e\psi_0}{kT}\right) \tag{9.27}$$

where Ψ_0 is the surface potential. Equation (9.27) shows how the electrical potential energy (Ψ_0/kT) of adsorbed surfactant ions affects the surface excess. Assuming that the bulk concentration remains constant, then Ψ_0 increases as θ increases. This means that $[\theta/(1-\theta)]\exp[\theta/(1-\theta)]$ increases less rapidly with C_2, i.e. adsorption is inhibited as a result of ionization.

9.2.3 The Langmuir, Szyszkowski and Frumkin equations

In addition to the Gibbs equation, three other equations have been suggested that relate the surface excess Γ_1, surface or interfacial tension, and equilibrium concentration in the liquid phase C_1. The Langmuir equation [6] relates Γ_1 to C_1 by,

$$\Gamma_1 = \frac{\Gamma_m C_1}{C_1 + a}, \tag{9.28}$$

where Γ_m is the saturation adsorption at monolayer coverage by surfactant molecules, a is a constant that is related to the free energy of adsorption ΔG^0_{ads},

$$a = 55.3\exp\left(\frac{\Delta G^0_{ads}}{RT}\right), \tag{9.29}$$

where R is the gas constant and T is the absolute temperature.

A linear form of the Gibbs equation is,

$$\frac{1}{\Gamma_1} = \frac{1}{\Gamma_m} + \frac{a}{\Gamma_m C_1}. \tag{9.30}$$

Equation (9.30) shows that a plot of $1/\Gamma_1$ versus $1/C_1$ gives a straight line from which Γ_m and a can be calculated from the intercept and slope of the line.

The Szyszkowski [7] equation gives a relationship between the surface pressure π and bulk surfactant concentration C_1; it is a form of equation of state,

$$\gamma_0 - \gamma = \pi = 2.303RT\Gamma_m \log\left(\frac{C_1}{a} + 1\right). \tag{9.31}$$

The Frumkin equation [8] is another equation of state,

$$\gamma_0 - \gamma = \pi = -2.303RT\Gamma_m \log\left(1 - \frac{\Gamma_1}{\Gamma_m}\right). \tag{9.32}$$

9.3 Effectiveness of surfactant adsorption at the liquid/liquid interface

The surface excess concentration at surface saturation, Γ_m is a useful measure of the effectiveness of the surfactant at the liquid/liquid interface [9]. This is an important factor in determining such properties of the surfactant in several processes such as emulsification and emulsion stability. In most cases, a tightly packed, coherent film obtained by vertically oriented surfactant molecules is required. The area occupied by a surfactant molecule consisting of a linear alkyl chain and one hydrophilic group, either ionic or nonionic, is larger than the cross-sectional area of an aliphatic chain (which is 0.2 nm^2) indicating that the area occupied by a surfactant molecule is determined by the area occupied by the hydrated hydrophilic chain. For example for a series of alkyl sulphates the area occupied by the surfactant molecule is in the region of 0.5 nm^2 which is the cross-sectional area of a sulphate group. As mentioned before, addition of electrolytes reduces the area occupied by the surfactant molecule due to charge screening of the sulphate group. With nonionic surfactants based on a polyethylene oxide (PEO) hydrophilic group, the amount of adsorption at saturation Γ_m decreases with increasing PEO chain length and this results in an increase in the area occupied by a single surfactant molecule.

9.4 Efficiency of adsorption of surfactant at the liquid/liquid interface

The efficiency of surfactant adsorption at the liquid/liquid interface can be determined by measuring the surfactant concentration that produces a given amount of adsorption at the interface [9]. This can also be related to the free energy change involved in the adsorption. A convenient measure of the efficiency of adsorption is the negative logarithm of surfactant concentration C in bulk solution required to produce a 20 mN m^{-1} reduction in the interfacial tension γ,

$$-\log C_{(-\Delta\gamma=20)} \equiv pC_{20} \tag{9.33}$$

Observation of various γ–log C results for various surfactants at the oil/water interface shows that when γ is reduced by 20 mN m^{-1}, the surface excess concentration Γ_1 is close to its saturation value Γ_m. This is confirmed by the use of the Frumkin equation (9.32). For many surfactant systems, Γ_m is in the range $1–4.4 \times 10^{-6}$ mol m^{-2}. Solving for Γ_1 in the Frumkin equation when $\pi = \gamma_0 - \gamma = 20$ mN m^{-1}, $\Gamma_m = 1–4.4 \times 10^{-6}$ mol m^{-2}, $\Gamma_1 = 0.84–0.99\Gamma_m$ at 25 °C, indicating that when γ is reduced by 20 mN m^{-1}, the surface concentration is 84–99 % saturated.

pC_{20} can be related to the free energy change on adsorption at infinite dilution ΔG^0 by application of the Langmuir [6] and Szyszkowski [7] equations (9.28) and (9.31). As

mentioned above for $\pi = 20\,\mathrm{mN\,m^{-1}}$, $\Gamma_1 = 0.84\text{–}0.99\Gamma_\mathrm{m}$. From the Langmuir equation $C_1 = 5.2\text{–}999 \times a$. Thus,

$$\log\left[\left(\frac{C_1}{a}\right) + 1\right] \approx \log\left(\frac{C_1}{a}\right). \tag{9.34}$$

The Szyszkowski equation becomes,

$$\pi = \gamma_0 - \gamma = -2.303RT\Gamma_\mathrm{m} \log\left(\frac{C_1}{a}\right), \tag{9.35}$$

and,

$$\log\left(\frac{1}{C_1}\right)_{\pi=20} = -\left(\log a + \frac{\gamma_0 - \gamma}{2.303RT\Gamma_\mathrm{m}}\right). \tag{9.36}$$

Since,

$$a = 55 \exp\left(\frac{\Delta G^0}{RT}\right), \tag{9.37}$$

$$\log a = 1.74 + \frac{\Delta G^0}{2.303RT}, \tag{9.38}$$

$$\log\left(\frac{1}{C_1}\right)_{\pi=20} \equiv \mathrm{p}C_{20} \equiv -\left(\frac{\Delta G^0}{2.303RT} + 1.74 + \frac{20}{2.303RT\Gamma_\mathrm{m}}\right). \tag{9.39}$$

For a straight chain surfactant molecule consisting of m $-CH_2-$ groups and one hydrophilic head group (h), ΔG^0 can be broken into the standard free energy associated with the transfer of the terminal CH_3, the $-CH_2-$ groups of the hydrocarbon chain and the hydrophilic group h from the interior of the liquid phase to the interface at $\pi = 20\,\mathrm{mN\,m^{-1}}$,

$$\Delta G^0 = m \cdot \Delta G^0(-CH_2-) + \Delta G^0(\mathrm{h}) + \mathrm{const.} \tag{9.40}$$

For a homologous series of surfactants with the same hydrophilic group h, the value of Γ_m and the area per surfactant molecule does not change much with an increase in the number of C atoms and $\Delta G^0(\mathrm{h})$ can be considered constant. In this case, $\mathrm{p}C_{20}$ can be related to the free energy change per $-CH_2-$ group by,

$$\mathrm{p}C_{20} = \left[\frac{-\Delta G^0(-CH_2-)}{2.303RT}\right]m + \mathrm{const.} \tag{9.41}$$

Equation (9.41) shows that $\mathrm{p}C_{20}$ is a linear function of the number of C atoms in the surfactant chain m. The larger the value of $\mathrm{p}C_{20}$ the more efficiently the surfactant is adsorbed at the interface and the more efficiently it reduces the interfacial tension.

The efficiency of surfactant adsorption at the liquid/liquid interface as measured by $\mathrm{p}C_{20}$ increases with an increase in the number of C atoms in the surfactant. Straight alkyl chains are generally more efficient than branched ones with the same C number. A single hydrophilic group at the end of the hydrophobic chain gives more efficient adsorption than one where the hydrophilic group is located at the centre of the chain. Nonionic and zwitterionic surfactants generally give more efficient adsorption compared to ionic ones. With ionic surfactants, increasing the ionic strength of the aqueous solution increases the efficiency of surfactant adsorption.

9.5 Adsorption from mixtures of two surfactants

Mixtures of two or more different types of surfactants often show a "synergistic" interaction [10, 11]. In other words, the interfacial properties of the mixture are more pronounced than those of the individual components themselves. These mixtures are widely used in many industrial applications such as in emulsification and emulsion stability. A study of the adsorption of the individual components in the mixture and the interaction between them allows one to understand the role played by each component. This will also enable one to make the right selection of surfactant mixtures for a specific application.

The Gibbs adsorption equation (9.8) for two surfactants in dilute solution can be written as,

$$\mathrm{d}\gamma = RT(\Gamma_1 \,\mathrm{d}\ln a_1 + \Gamma_2 RT \,\mathrm{d}\ln a_2), \tag{9.42}$$

where Γ_1 and Γ_2 are the surface excess concentrations of the two surfactants at the interface and a_1 and a_2 are their respective activities in solution. Since the solutions are dilute, a_1 and a_2 can be replaced by the molar concentrations C_1 and C_2.

Using equation (9.42),

$$\Gamma_1 = \frac{1}{RT}\left(-\frac{\partial\gamma}{\partial\ln C_1}\right)_{C_2} = \frac{1}{2.303RT}\left(-\frac{\partial\gamma}{\partial\log C_1}\right)_{C_2}, \tag{9.43}$$

$$\Gamma_2 = \frac{1}{RT}\left(-\frac{\partial\gamma}{\partial\ln C_2}\right)_{C_1} = \frac{1}{2.303RT}\left(-\frac{\partial\gamma}{\partial\log C2}\right)_{C_1}. \tag{9.44}$$

Therefore, the concentration of each surfactant at the interface can be calculated from the slope of the γ–log C plot of each surfactant, holding the solution concentration of the second surfactant constant.

For ideal mixing of two surfactants (with no net interaction), C_1 and C_2 are given by the expressions [12],

$$C_1 = C_1^0 f_1 X_1 \tag{9.45}$$

$$C_2 = C_2^0 f_2 X_2 \tag{9.46}$$

where f_1 and f_2 are the activity coefficients of surfactant 1 and 2 respectively, X_1 is the mole fraction of surfactant 1 at the interface, i.e. $X_1 = 1 - X_2$, C_1^0 is the molar concentration required to attain a given interfacial tension in a solution of pure surfactant 1, and C_2^0 is the molar concentration required to attain a given interfacial tension in a solution of pure surfactant 2.

For non-ideal mixing, i.e. when there is interaction between the surfactant molecules, the activity coefficient has to include the interaction parameter β^σ,

$$\ln f_1 = \beta^\sigma (1 - X_1)^2 \tag{9.47}$$

$$\ln f_2 = \beta^\sigma (X_1)^2 \tag{9.48}$$

Combining equations (9.45)–(9.48),

$$\frac{(X_1)^2 \ln(C_1/C_1^0 X_1)}{(1-X_1)^2 \ln[\frac{C_2}{C_2^0(1-X_1)}]} = 1. \tag{9.49}$$

The interfacial tension–total surfactant concentration (C_t) curves for two pure surfactants and their mixture at a fixed value α, the mole fraction of surfactant 1 in the total surfactant in the solution phase, (Fig. 9.3) are used to determine $C_1(= \alpha C_{12})$, C_1^0, $C_2[= (1-\alpha)C_{12}]$ and C_2^0, the molar concentration at the same surface tension. Equation (9.49) permits it to be solved iteratively for X_1 and $X_2(= 1 - X_1)$. The ratio of surfactant 1 : surfactant 2 at the interface at that particular value of α is then X_1/X_2.

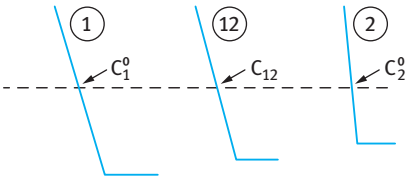

Fig. 9.3: Evaluation of X_1 and X_2; (1) pure surfactant 1; (2) pure surfactant 2; (12) mixture of 1 and 2 at a fixed value of α.

9.6 Interfacial tension measurements

These methods may be classified into two categories: those in which the properties of the meniscus is measured at equilibrium, e.g. pendent drop or sessile drop profile and Wilhelmy plate methods, and those where the measurement is made under nonequilibrium or quasi-equilibrium conditions such as the drop volume (weight) or the de Nouy ring method. The latter methods are faster, although they suffer from the disadvantage of premature rupture and expansion of the interface, causing adsorption depletion. For measurement of low interfacial tensions ($< 0.1\,\mathrm{mN\,m^{-1}}$), the spinning drop technique is applied. Below a brief description of each of these techniques is given.

9.6.1 The Wilhelmy plate method

In this method [13] a thin plate made from glass (e.g. a microscope cover slide) or platinum foil is either detached from the interface (nonequilibrium condition) or its weight is measured statically using an accurate microbalance. In the detachment method, the total force F is given by the weight of the plate W and the interfacial tension force,

$$F = W + \gamma p, \tag{9.50}$$

where p is the "contact length" of the plate with the liquid, i.e., the plate perimeter. Provided the contact angle of the liquid is zero, no correction is required for equation (9.50). Thus, the Wilhelmy plate method can be applied in the same manner as the du Nouy technique that is described below.

The static technique may be applied for following the interfacial tension as a function of time (to follow the kinetics of adsorption) until equilibrium is reached. In this case, the plate is suspended from one arm of a microbalance and allowed to penetrate the upper liquid layer (usually the oil) into the aqueous phase to ensure wetting of the plate. The whole vessel is then lowered to bring the plate into the oil phase. At this point the microbalance is adjusted to counteract the weight of the plate (i.e., its weight now becomes zero). The vessel is then raised until the plate touches the interface. The increase in weight ΔW is given by the following equation,

$$\Delta W = \gamma p \cos\theta, \tag{9.51}$$

where θ is the contact angle. If the plate is completely wetted by the lower liquid as it penetrates, $\theta = 0$ and γ may be calculated directly from ΔW. Care should always be taken that the plate is completely wetted by the aqueous solution. For that purpose, a roughened platinum or glass plate is used to ensure a zero contact angle. However, if the oil is more dense than water, a hydrophobic plate is used so that when the plate penetrates through the upper aqueous layer and touches the interface it is completely wetted by the oil phase.

9.6.2 The pendent drop method

If a drop of oil is allowed to hang from the end of a capillary that is immersed in the aqueous phase, it will adopt an equilibrium profile shown in Fig. 9.4 that is a unique function of the tube radius, the interfacial tension, its density and the gravitational field.

The interfacial tension is given by the following equation [14],

$$\gamma = \frac{\Delta\rho g d_e^2}{H}, \tag{9.52}$$

where $\Delta\rho$ is the density difference between the two phases, d_e is the equatorial diameter of the drop (see Fig. 9.4) and H is a function of d_s/d_e, where d_s is the diameter measured at a distance d from the bottom of the drop (see Fig. 9.4). The relationship between H and the experimental values of d_s/d_e has been obtained empirically using pendent drops of water. Accurate values of H have been obtained by Niederhauser and Bartell [15].

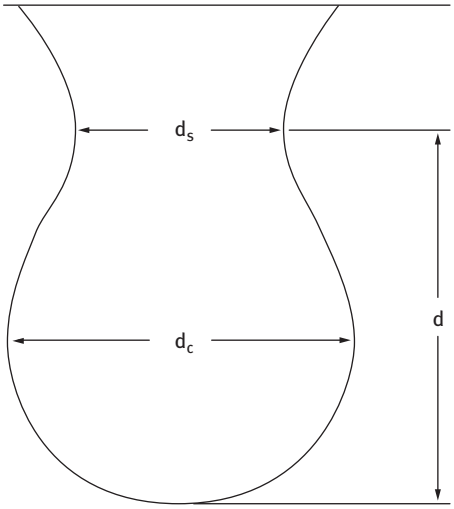

Fig. 9.4: Schematic representation of the profile of a pendent drop.

9.6.3 The du Nouy ring method

Basically one measures the force required to detach a ring or loop of wire from the liquid/liquid interface [16]. As a first approximation, the detachment force is taken to be equal to the interfacial tension γ multiplied by the perimeter of the ring, i.e.,

$$F = W + 4\pi R\gamma, \tag{9.53}$$

where W is the weight of the ring. Harkins and Jordan [17] introduced a correction factor f (that is a function of meniscus volume V and radius r of the wire) for more accurate calculation of γ from F, i.e.,

$$f = \frac{\gamma}{\gamma_{\text{ideal}}} = f\left(\frac{R^3}{V}, \frac{R}{r}\right). \tag{9.54}$$

Values of the correction factor f were tabulated by Harkins and Jordan [17]. Some theoretical account of f was given by Freud and Freud [18].

When using the du Nuoy method for measurement of γ one must be sure that the ring is kept horizontal during the measurement. Moreover, the ring should be free from any contaminant and this is usually achieved by using a platinum ring that is flamed before use.

9.6.4 The drop volume (weight) method

Here one determines the volume V (or weight W) of a drop of liquid (immersed in the second, less dense liquid) which becomes detached from a vertically mounted capillary tip having a circular cross section of radius r. The ideal drop weight W_{ideal} is given

by the expression,

$$W_{\text{ideal}} = 2\pi r\gamma. \tag{9.55}$$

In practice, a weight W is obtained which is less than W_{ideal} because a portion of the drop remains attached to the tube tip. Thus, equation (9.55) should include a correction factor ϕ, that is a function of the tube radius r and some linear dimension of the drop, i.e., $V^{1/3}$. Thus,

$$W = 2\pi r\gamma\phi\left(\frac{r}{V^{1/3}}\right). \tag{9.56}$$

Values of $(r/V^{1/3})$ have been tabulated by Harkins and Brown [19]. Lando and Oakley [20] used a quadratic equation to fit the correction function to $(r/V^{1/3})$. A better fit was provided by Wilkinson and Kidwell [21].

9.6.5 The spinning drop method

This method is particularly useful for the measurement of very low interfacial tensions ($< 10^{-1}$ mN m^{-1}) which are particularly important in applications such as spontaneous emulsification and the formation of microemulsions. Such low interfacial tensions may also be reached with emulsions, particularly when mixed surfactant films are used. A drop of the less dense liquid A is suspended in a tube containing the second liquid B. On rotating the whole mass (Fig. 9.5), the drop of the liquid moves to the centre. With increasing speed of revolution, the drop elongates as the centrifugal force opposes the interfacial tension force that tends to maintain the spherical shape, i.e., that having minimum surface area.

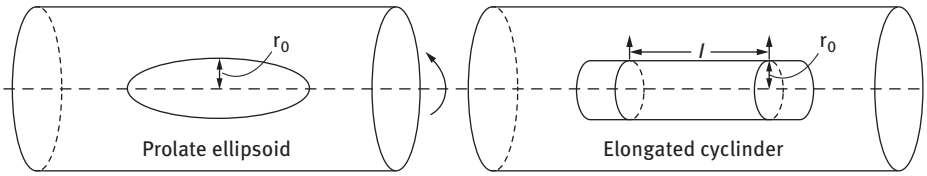

Fig. 9.5: Schematic representation of a spinning drop: (a) prolate ellipsoid; (b) elongated cylinder.

An equilibrium shape is reached at any given speed of rotation. At moderate speeds of rotation, the drop approximates to a prolate ellipsoid, whereas at very high speeds of revolution, the drop approximates to an elongated cylinder. This is schematically shown in Fig. 9.5.

When the shape of the drop approximates a cylinder (Fig. 9.5 (b)), the interfacial tension is given by the following expression [22],

$$\gamma = \frac{\omega_2 \Delta\rho r_0^4}{4}, \tag{9.57}$$

where ω is the speed of rotation, $\Delta\rho$ is the density difference between the two liquids A and B and r_0 is the radius of the elongated cylinder. Equation (9.57) is valid when the length of the elongated cylinder is much larger than r_0.

9.7 Interfacial rheology

As mentioned above, a fluid interface in equilibrium exhibits an intrinsic state of tension that is characterized by its interfacial tension γ which is given by equation (9.2). Adsorption of surfactants or polymers lowers the interfacial tension and this produces a two-dimensional surface pressure π that is given by equation (9.17).

9.7.1 Interfacial shear viscosity

The interface is considered to be a macroscopically planer, dynamic fluid interface. Thus, the interface is regarded as a two-dimensional entity independent of the surrounding three-dimensional fluid. The interface is considered to correspond to a highly viscous insoluble monolayer and the interfacial stress σ_s acting within such a monolayer is sufficiently large compared to the bulk-fluid stress acting across the interface and in this way one can define an interfacial shear viscosity η_s,

$$\sigma_s = \eta_s \dot{\gamma}, \tag{9.58}$$

where $\dot{\gamma}$ is the shear rate. η_s is given in surface Pa s (Nm^{-1} s) or surface poise (dyne cm^{-1} s). It should be mentioned that the surface viscosity of a surfactant-free interface is negligible and it can reach high values for adsorbed rigid molecules such as proteins.

9.7.2 Measurement of interfacial viscosity

Many surface viscometers utilize torsional stress measurements upon a rotating ring, disk or knife edge (shown schematically in Fig. 9.6) within or near to the liquid/liquid interface [23]. This type of viscometer is moderately sensitive; for a disk viscometer the interfacial shear viscosity can be measured in the range $\eta_s \geq 10^{-2}$ surface Pa s.

The disk is rotated within the plane of the interface with angular velocity ω. A torque is exerted upon the disk of radius R by both the surfactant film with surface viscosity η_s and the viscous liquid (with bulk viscosity η) that is given by the expression,

$$M = (8/3)R^3\eta\omega + 4\pi R^2\eta_s\omega. \tag{9.59}$$

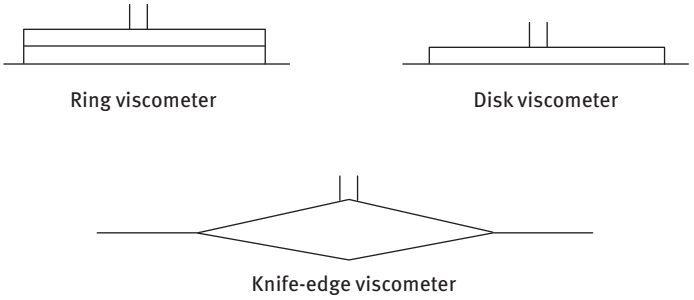

Fig. 9.6: Schematic representation of surface viscometers.

9.7.3 Interfacial dilational elasticity

The interfacial dilational (Gibbs) elasticity ε, which is an important parameter in determining emulsion stability (reduction of coalescence during formation), is given by the following equation,

$$\varepsilon = \frac{\mathrm{d}\gamma}{\mathrm{d}\ln A}, \tag{9.60}$$

where $\mathrm{d}\gamma$ is the change in interfacial tension during expansion of the interface by an amount $\mathrm{d}A$ (referred to as interfacial tension gradient resulting from non-uniform surfactant adsorption on expansion of the interface).

One of the most convenient methods for measuring ε is to use a Langmuir trough with two moving barriers for expansion and compression of the interface. Another method for measuring ε is to use the oscillating bubble technique and instruments are commercially available.

A useful method for measuring ε is the pulsed drop method [24]. Rapid expansion of a droplet at the end of a capillary from a radius r_1 to r_2 is obtained by application of pressure. The pressure drop within the droplet is measured as a function of time using a sensitive pressure transducer. From the pressure drop one can obtain the interfacial tension as a function of time. The Gibbs dilational elasticity is determined from values of the time-dependent interfacial tension. Measurement can be made as a function of frequency as is illustrated in Fig. 9.7 for stearic acid at the decane-water interface at pH = 2.5.

9.7.4 Interfacial dilational viscosity

Measurement of the dilational viscosity is more difficult than measurement of the interfacial shear viscosity. This is due to the coupling between dilational viscous and elastic components. The most convenient method for measuring dilational viscosity is the maximum bubble pressure technique that can only be applied at the air/water interface. According to this technique, the pressure drop across the bubble surface at

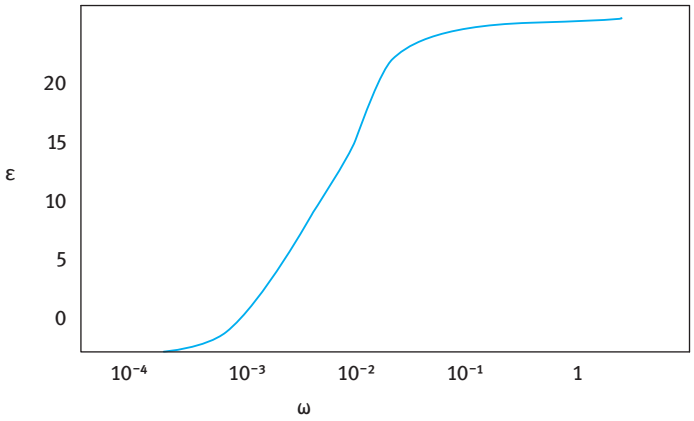

Fig. 9.7: Gibbs dilational elasticity versus frequency.

the instant when the bubble possesses a hemispherical shape (corresponding to the maximum pressure) is due to a combination of bulk viscous, surface tension and surface dilational viscosity effects and this allows one to obtain the interfacial dilational viscosity.

9.7.5 Non-Newtonian effects

Most adsorbed surfactant and polymer coils at the oil/water (O/W) interface show non-Newtonian rheological behaviour. The surface shear viscosity η_s depends on the applied shear rate, showing shear thinning at high shear rates. Some films also show Bingham plastic behaviour with a measurable yield stress.

Many adsorbed polymers and proteins show viscoelastic behaviour and one can measure viscous and elastic components using sinusoidally oscillating surface dilation. For example the complex dilational modulus ε^* obtained can be split into an "in-phase" (the elastic component ε') and "out-of-phase" (the viscous component ε'') components. Creep and stress relaxation methods can be applied to study viscoelasticity.

9.8 Correlation of emulsion stability with interfacial rheology

9.8.1 Mixed surfactant films

Prins et al. [25] found that a mixture of sodium dodecyl sulphate (SDS) and dodecyl alcohol give a more stable O/W emulsion when compared to emulsions prepared using SDS alone. This enhanced stability is due to the higher interfacial dilational elasticity ε

for the mixture when compared to that of SDS alone. Interfacial dilational viscosity did not play a major role since the emulsions are stable at high temperature whereby the interfacial viscosity becomes lower.

The above correlation is not general for all surfactant films since other factors such as thinning of the film between emulsion droplets (which depends on other factors such as repulsive forces) can also play a major role.

9.8.2 Protein films

Biswas and Haydon [26] found some correlation between the viscoelastic properties of protein (albumin or arabinic acid) films at the O/W interface and the stability of emulsion drops against coalescence. Viscoelastic measurements were carried out using creep and stress relaxation measurements (using a specially designed interfacial rheometer). A constant torque or stress σ (mN m^{-1}) was applied and the deformation γ was measured as a function of time for 30 minutes. After this period the torque was removed and γ (which changes sign) was measured as a function of time to obtain the recovery curve. The results are illustrated in Fig. 9.8.

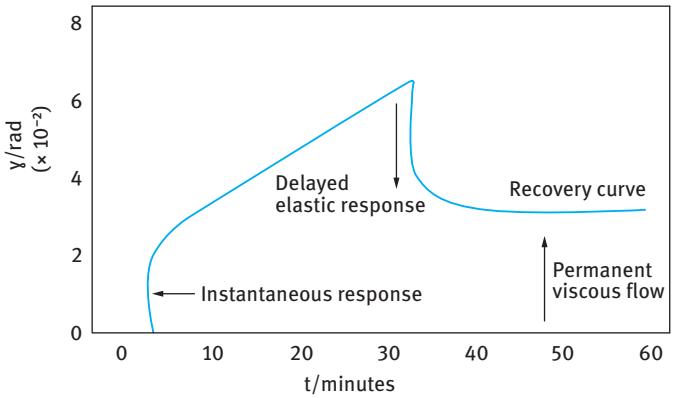

Fig. 9.8: Creep curve for protein film at the O/W interface.

From the creep curves one can obtain the instantaneous modulus G_0 (σ/γ_{int}) and the surface viscosity η_s from the slope of the straight line (which gives the shear rate) and the applied stress. G_0 and η_s are plotted versus pH as shown in Fig. 9.9. Both show an increase with increasing pH reaching a maximum at pH $\approx$ 6 (the isoelectric point of the protein) at which the protein molecules show maximum rigidity at the interface.

The stability of the emulsion was assessed by measuring the residence time t of several oil droplets at a planer O/W interface containing the adsorbed protein. Fig. 9.9 shows the variation of $t_{1/2}$ (time taken for half the number of oil droplets to coalesce

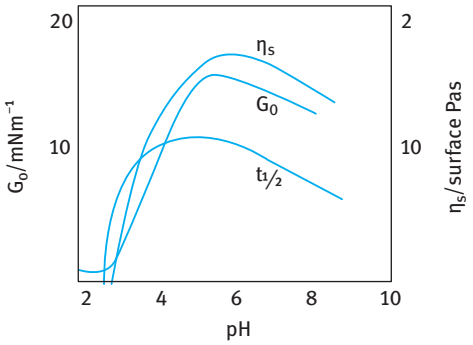

Fig. 9.9: Variation of $t_{1/2}$ and G_0 and η_s with pH.

with the oil at the O/W interface) with pH. Good correlation between $t_{1/2}$ and G_0 and η_s is obtained.

Biswas and Haydon [26] derived a relationship between coalescence time τ and surface viscosity η_s, instantaneous modulus G_0 and adsorbed film thickness h,

$$\tau = \eta_s \left[3C' \frac{h^2}{A} - \frac{1}{G_0} - \phi(t) \right], \tag{9.61}$$

where $3C'$ is a critical deformation factor, A is the Hamaker constant and $\phi(t)$ is the elastic deformation per unit stress.

Equation (9.61) shows that τ increases with increasing η_s, but most importantly it is directly proportional to h^2. These results show that viscoelasticity is necessary but not sufficient to ensure stability against coalescence. To ensure stability of an emulsion one must make sure that h is large enough and film drainage is prevented.

References

[1] Gibbs JW. Collected papers. Vol. 1. Thermodynamics. New York: Dover; 1961.
[2] Gibbs JW. Collected works. Vol. 1. New York: Longman; 1928. p. 219.
[3] Aveyard R, Briscoe BJ. Trans Faraday Soc. 1970;66:2911.
[4] Aveyard R, Briscoe BJ, Chapman J. Trans Faraday Soc. 1972;68:10.
[5] Aveyard R, Chapman J. Can J Chem. 1975;53:916.
[6] Langmuir I. J Amer Chem Soc. 1917;39:1848.
[7] Szyszkowski B. Z Phys Chem. 1908;64:385.
[8] Frumkin A. Z Phys Chem. 1925;116:466.
[9] Rosen MJ, Kunjappu JT. Surfactants and interfacial phenomena. New Jersey: John Wiley and Sons; 2012.
[10] de Lisi R, Inglese A, Milioto S, Pellento A. Langmuir. 1997;13:192.
[11] Nakano TY, Sugihara G, Nakashima T, Yu SC. Langmuir. 2002;18:8777.
[12] Rosen MJ, Hua XY. J Colloid Interface Sci. 1982;86:164.
[13] Wilhelmy L. Ann Phys. 1863;119:177.
[14] Bashforth F, Adams JC. An attempt to test the theories of capillary action. Cambridge: University Press; 1883.

[15] Nierderhauser DO, Bartell FE. Report of progress, fundamental research on occurrence of petroleum. Publication of the American Petroleum Institute. Baltimore: Lord Baltimore Press; 1950. p. 114.
[16] Du Nouy PL. J Gen Physiol. 1919;1:521.
[17] Harkins WD, Jordan HF. J Amer Chem Soc. 1930;52:1715.
[18] Freud BB, Freud HZ. J Amer Chem Soc. 1930;52:1772.
[19] Harkins WD, Brown FE. J Amer Chem Soc. 1919;41:499.
[20] Lando JL, Oakley HT. J Colloid Interface Sci. 1967;25:526.
[21] Wilkinson MC, Kidwell RL. J Colloid Interface Sci. 1971;35:114.
[22] Vonnegut B. New Sci Intrum. 1942;13:6.
[23] Criddle DW. The viscosity and viscoelasticity of interfaces. In: Eirich FR, editor. Rheology. Vol. 3. New York: Academic Press; 1960. Chapter 11.
[24] Edwards DA, Brenner H, Wasan DT. Interfacial transport processes and rheology. Boston, London: Butterworth-Heinemann; 1991.
[25] Prince A, Arcuri C, van den Tempel M. J Colloid and Interface Sci. 1967;24:811.
[26] Biswas B, Haydon DA. Proc Roy Soc. 1963;A271:296; 1963;A2:317; Kolloid Z. 1962;185,31; 1962;186,57.

10 Adsorption of surfactants at the solid/liquid interface

10.1 Introduction

Surfactants, both of the ionic and nonionic type, are used for preparation of solid/liquid dispersions (suspensions) and their subsequent colloid stability. In order to understand the role of surfactants in dispersion stabilization it is necessary to determine their adsorption and conformation at the solid surface. With ionic surfactants, the molecules impart a charge on the surface of the solid resulting in the formation of an electrical double layer. This results in electrostatic stabilization as discussed in detail in Chapter 6. With nonionic surfactants, the surfactant adsorbed layer provides stabilization by a mechanism referred to as steric repulsion. In this case the repulsion occurs as a result of two main effects, namely unfavourable mixing of the surfactant chains when these are in good solvent conditions and reduction of entropy on considerable overlap of the surfactant chains. The details of the process of steric repulsion will be discussed in Chapter 13.

Surfactants consist of a small number of units and they mostly are reversibly adsorbed, allowing one to apply thermodynamic treatments. In this case, it is possible to describe the adsorption in terms of the various interaction parameters, namely chain-surface, chain-solvent and surface-solvent. Moreover, the conformation of the surfactant molecules at the interface can be deduced from these simple interaction parameters. However, in some cases these interaction parameters may involve ill-defined forces, such as hydrophobic bonding, solvation forces and chemisorption. In addition, the adsorption of ionic surfactants involves electrostatic forces particularly with polar surfaces containing ionogenic groups. For that reason, the adsorption of ionic and nonionic surfactants will be treated separately. The surfaces (substrates) can also be hydrophobic or hydrophilic and these may be treated separately. Thus, four cases can be considered:

(i) adsorption of ionic surfactants on hydrophobic (nonpolar) surfaces;
(ii) adsorption of ionic surfactants on polar (charged) surfaces;
(iii) adsorption of nonionic surfactants on hydrophobic surfaces;
(iv) adsorption of nonionic surfactants on polar surfaces.

(i) and (iii) are governed by hydrophobic interaction between the alkyl chain and the hydrophobic surface; the charge plays a minor role. (ii) and (iv) are determined by charge and/or polar interaction.

At the solid/liquid interface one is interested in determining the following parameters:

https://doi.org/10.1515/9783110540895-011

(i) The amount of surfactant adsorbed, Γ, per unit mass or unit area of the solid adsorbent at a given temperature.
(ii) The equilibrium concentration of the surfactant C (mol dm^{-3} or mole fraction $x = C/55.51$) in the liquid phase required to produce a given value of Γ at a given temperature.
(iii) The surfactant concentration at full saturation of the adsorbent Γ_{sat}.
(iv) The orientation of the adsorbed surfactant ion or molecule that can be obtained from the area occupied by the ion or molecule at full saturation.
(v) The effect of adsorption on the properties of the adsorbent (nonpolar, polar or charged).

The general equation for calculating the amount of surfactant adsorbed onto a solid adsorbent from a binary solution containing two components (surfactant component 1 and solvent component 2) is given by [1],

$$\frac{n_0 \Delta x_1}{m} = n_1^s x_2 - n_2^s x_1. \tag{10.1}$$

n_0 is the number of moles of solution before adsorption, $\Delta x_1 = x_{1,0} - x_1$, $x_{1,0}$ is the mole fraction of component 1 before adsorption, x_1 and x_2 are the mole fractions of components 1 and 2 at adsorption equilibrium, m is the mass of adsorbent in grams, n_1^s and n_2^s are the number of components 1 and 2 adsorbed per gram of adsorbent at adsorption equilibrium.

When the liquid phase is a dilute solution of surfactant (component 1) that much more strongly adsorbed onto the solid substrate than the solvent (component 2), then $n_0 \Delta x_1 = \Delta n_1$ where Δn_1 is the change in number of moles of component 1 in solution, $n_2^s \approx 0$ and $x_2 \approx 1$. In this case equation (10.1) reduces to,

$$n_1^s = \frac{\Delta n_1}{m} = \frac{\Delta C_1 V}{m}, \tag{10.2}$$

where $\Delta C_1 = C_{1,0} - C_1$, $C_{1,0}$ is the molar concentration of component 1 before adsorption, C_1 is the molar concentration of component 1 after adsorption and V is the volume of the liquid phase in litres.

The surface concentration Γ_1 in mol m^{-2} can be calculated from a knowledge of surface area A (m^2 g^{-1}),

$$\Gamma_1 = \frac{\Delta C_1 V}{mA}. \tag{10.3}$$

The adsorption isotherm is represented by a plot of Γ_1 versus C_1. In most cases, the adsorption increases gradually with increasing C_1 and a plateau Γ_1^∞ is reached at full coverage corresponding to a surfactant monolayer. The area per surfactant molecule or ion at full saturation can be calculated,

$$a_1^s = \frac{10^{18}}{\Gamma_1^\infty N_{av}} \text{ nm}^2, \tag{10.4}$$

where N_{av} is the Avogadro number.

10.2 Adsorption of ionic surfactants on hydrophobic surfaces

The adsorption of ionic surfactants on hydrophobic surfaces such as carbon black, polymer surfaces and ceramics (silicon carbide or silicon nitride) is governed by hydrophobic interaction between the alkyl chain of the surfactant and the hydrophobic surface. In this case, electrostatic interaction will play a relatively smaller role. However, if the surfactant head group is of the same sign of charge as that on the substrate surface, electrostatic repulsion may oppose adsorption. In contrast, if the head groups are of opposite sign to the surface, adsorption may be enhanced. Since the adsorption depends on the magnitude of the hydrophobic bonding free energy, the amount of surfactant adsorbed increases directly with increasing alkyl chain length in accordance with Traube's rule.

The adsorption of ionic surfactants on hydrophobic surfaces may be represented by the Stern–Langmuir isotherm [2]. Several assumptions have been made in deriving the Stern–Langmuir equation:

(i) Only one type of ion, the surfactant ion, is specifically adsorbed; this assumption is reasonable at low coverage.
(ii) One surfactant ion replaces one solvent molecule, i.e. the ion and solvent molecules are of the same size.
(iii) The surface is considered homogeneous.
(iv) Dipole terms and self-atmosphere potentials, as well as lateral chain-chain interactions are neglected.

Consider a substrate containing N_s sites (mol m^{-2}) on which Γ mol m^{-2} of surfactant ions are adsorbed. The surface coverage θ is (Γ/N_s) and the fraction of uncovered surface is $(1-\theta)$.

The rate of adsorption is proportional to the surfactant concentration expressed in mole fraction, $(C/55.5)$, and the fraction of free surface $(1-\theta)$, i.e.

$$\text{rate of adsorption} = k_{ads}\left(\frac{C}{55.5}\right)(1-\theta), \tag{10.5}$$

where k_{ads} is the rate constant for adsorption.

The rate of desorption is proportional to the fraction of surface covered θ,

$$\text{rate of desorption} = k_{des}\theta. \tag{10.6}$$

At equilibrium, the rate of adsorption is equal to the rate of desorption and the ratio of (k_{ads}/k_{des}) is the equilibrium constant K, i.e.,

$$\frac{\theta}{(1-\theta)} = \frac{C}{55.5}K \tag{10.7}$$

The equilibrium constant K is related to the standard free energy of adsorption by,

$$-\Delta G^0_{ads} = RT\ln K \tag{10.8}$$

R is the gas constant and T is the absolute temperature. Equation (10.8) can be written in the form,

$$K = \exp\left(-\frac{\Delta G^0_{\text{ads}}}{RT}\right). \tag{10.9}$$

Combining equations (10.7) and (10.9),

$$\frac{\theta}{1-\theta} = \frac{C}{55.5}\exp\left(-\frac{\Delta G^0_{\text{ads}}}{RT}\right). \tag{10.10}$$

Equation (10.10) applies only at low surface coverage ($\theta < 0.1$) where lateral interaction between the surfactant ions can be neglected.

At high surface coverage ($\theta > 0.1$) one should take the lateral interaction between the chains into account, by introducing a constant A, e.g. using the Frumkin–Fowler–Guggenheim equation [3],

$$\frac{\theta}{(1-\theta)}\exp(A\theta) = \frac{C}{55.5}\exp\left(-\frac{\Delta G^0_{\text{ads}}}{RT}\right). \tag{10.11}$$

The value of A can be estimated from the maximum slope $(\mathrm{d}\theta/\ln C)_{\max}$ of the isotherm which occurs at $\theta = 0.5$. Furthermore, at $\theta = 0.5$ substitution of A into equation (10.11) gives the value of ΔG^0_{ads}.

The above treatment using the FFG isotherm has two limitations. Firstly, it is assumed that A is constant and independent of surface coverage. In reality, A could change in sign as well as increase in θ. At low coverages, A would reflect repulsive (electrostatic) interaction between adsorbed surfactant ions. At higher coverage, attractive chain-chain interaction becomes more important. The apparent adsorption energy becomes more favourable at high surface coverage and this could lead to the formation of "hemimicelles". Secondly, electrostatic interactions are strongly affected by the level of supporting electrolyte.

Various authors [4, 5] have used the Stern–Langmuir equation in a simple form to describe the adsorption of surfactant ions on mineral surfaces,

$$\Gamma = 2rC\exp\left(-\frac{\Delta G^0_{\text{ads}}}{RT}\right). \tag{10.12}$$

Various contributions to the adsorption free energy may be envisaged. To a first approximation, these contributions may be considered to be additive. In the first instance, ΔG_{ads} may be taken to consist of two main contributions, i.e.,

$$\Delta G_{\text{ads}} = \Delta G_{\text{elec}} + \Delta G_{\text{spec}} \tag{10.13}$$

where ΔG_{elec} accounts for any electrical interactions (coulombic as well as polar) and ΔG_{spec} is a specific adsorption term which contains all contributions to the adsorption free energy that are dependent on the "specific" (non-electrical) nature of the

system [6]. ΔG_{elec} is given by the sum of the coulombic interactions ΔG_{coul} and a dipole term, ΔG_{dip},

$$\Delta G_{elec} = \Delta G_{coul} + \Delta G_{dip}, \tag{10.14}$$

$$\Delta G_{coul} = Z_i e \psi_d, \tag{10.15}$$

where Z_i is the ion valency, e is the electronic charge and ψ_d is the Stern potential.

$$\Delta G_{dip} = \sum_j \Delta n_j \mu_j E_s. \tag{10.16}$$

Δn_j is the change in the number of adsorbed dipoles j of moment μ_j and E_s is the electrical field strength across the plane of the adsorbed species (taken as the inner Helmholtz plane). Surfactant dipoles as well as water dipoles are accounted for in equation (10.16).

If one neglects ΔG_{dip} (as in the original Stern equation), the basic interpretation of ΔG_{elec} can be simplified. Three cases may be considered:

(i) when the surfactant ions are counterions to the net charge density ($\sigma_0 + \sigma_d$), then Z_i and ψ_d are of opposite sign, so $Z_i e \psi_d < 0$ and electrical interaction promotes the adsorption process. In the absence of other specifically adsorbed ions (such that σ_d is initially zero), this situation will exist at low surface coverages ($|\sigma_d| < |\sigma_0|$, where σ_d and σ_0 are of opposite sign) for cationic surfactant/negatively charged surface and anionic surfactant/positively charged surface combinations.

(ii) If ($\sigma_0 + \sigma_d$) is of the same sign as the surfactant ion, then Z_i and ψ_d are of like sign and $Z_i e \psi_d > 0$, i.e. the electrical interactions oppose adsorption. In the absence of specific adsorption, this situation will exist for anionic surfactant/negatively charged surface and cationic surfactant/positively charged surface combinations. It will also occur at high surface coverage for the combinations cited in the first example, i.e. sufficient surfactant ions, initially as counterions, adsorb until $|\sigma_d| > |\sigma_0|$ (allowed for in terms of a ΔG_{spec} contribution). In other words, the isoelectric point (IEP) is traversed and ψ_d is reversed in sign, so $Z_i e \psi_d$ becomes positive and opposes the favourable ΔG_{spec} term.

(iii) At the IEP ΔG_{elec} becomes zero and adsorption is governed by the ΔG_{spec} term.

The above predictions were confirmed by studying the adsorption of sodium dodecyl sulphonate on alumina (which has an IEP of pH = 9) as a function of pH [1]. This is illustrated in Fig. 10.1.

At low surface coverage the adsorption of the anionic surfactant on positive alumina surface (at pH < 9) is determined by ΔG_{elec}. As expected, the surfactant adsorption decreases with increasing pH since the surface becomes less positive.

Several authors subdivided ΔG_{spec} into supposedly separate independent interactions [6, 7], e.g.,

$$\Delta G_{spec} = \Delta G_{cc} + \Delta G_{cs} + \Delta G_{hs} + \cdots, \tag{10.17}$$

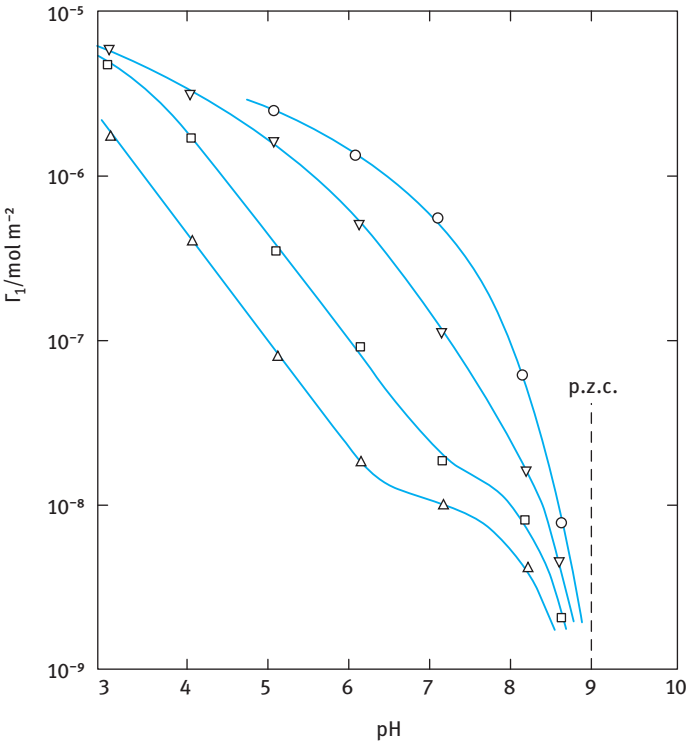

Fig. 10.1: Amount of sodium dodecyl sulphonate adsorbed on alumina as a function of pH (at 2×10^{-3} mol dm^{-3} ionic strength). Surfactant concentration in mol dm^{-3}: △, 1×10^{-5}; □, 3×10^{-5}; ▽, 1×10^{-4}; ○, 2.5×10^{-4}.

where ΔG_{cc} is a term that accounts for the cohesive chain-chain interaction between the hydrophobic moieties of the adsorbed ions, ΔG_{cs} is the term for chain/substrate interaction whereas ΔG_{hs} is a term for the head group/substrate interaction. The driving force of the hydrophobic interactions ΔG_{cc} and ΔG_{cs} is entropic in nature, arising from the destruction of the short-lived structures of water molecules organized around nonpolar moieties [8]. These interactions depend on the nature of the solid surface and any associated structured water, and whether or not this structure is disrupted by the hydrophobic chains. Several other contributions to ΔG_{spec} may be envisaged e.g. ion-dipole, ion-induced dipole or dipole-induced dipole interactions.

Since there is no rigorous theory that can predict adsorption isotherms, the most suitable method to investigate adsorption of surfactants is to determine the adsorption isotherm. Measurement of surfactant adsorption is fairly straightforward. A known mass m (g) of the particles (substrate) with known specific surface area A_s (m^2 g^{-1}) is equilibrated at constant temperature with surfactant solution with initial concentration C_1. The suspension is kept stirred for sufficient time to reach equilibrium. The

particles are then removed from the suspension by centrifugation and the equilibrium concentration C_2 is determined using a suitable analytical method. The amount of adsorption Γ (mol m^{-2}) is calculated using equation (10.3).

The adsorption isotherm is represented by plotting Γ versus C_2. A range of surfactant concentrations should be used to cover the whole adsorption process, i.e. from the initial values to the plateau values. To obtain accurate results, the solid should have a high surface area (usually > 1 m^2).

10.3 Examples of adsorption isotherms for ionic surfactants on hydrophobic surfaces

Several examples may be quoted from the literature to illustrate the adsorption of surfactant ions on solid surfaces. For a model hydrophobic surface, carbon black has been chosen [9, 10]. Fig. 10.2 shows typical results for the adsorption of sodium dodecyl sulphate (SDS) on two carbon black surfaces, namely Spheron 6 (untreated) and Graphon (graphitized) which also describes the effect of surface treatment.

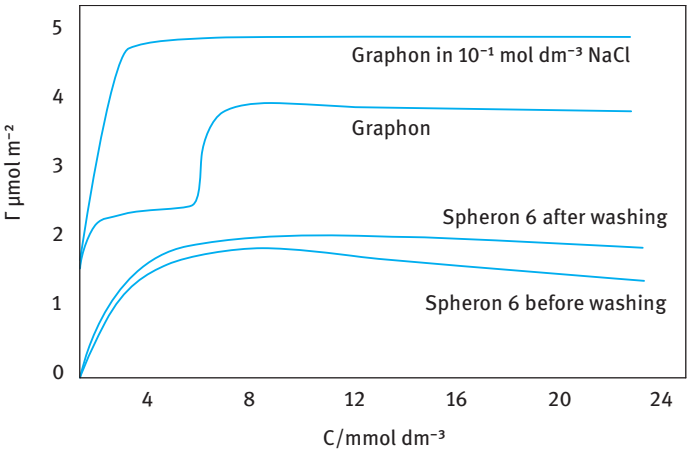

Fig. 10.2: Adsorption isotherms for sodium dodecyl sulphate on carbon substrates.

The adsorption of SDS on untreated Spheron 6 tends to show a maximum that is removed on washing. This suggests the removal of impurities from the carbon black which becomes extractable at high surfactant concentration. The plateau adsorption value is $\approx 2 \times 10^{-6}$ mol m^{-2} (≈ 2 µmol m^{-2}). This plateau value is reached at ≈ 8 mmol dm^{-3} SDS, i.e. close to the cmc of the surfactant in the bulk solution. The area per surfactant ion in this case is ≈ 0.7 nm^2. Graphitization (Graphon) removes the hydrophilic ionizable groups (e.g. –C=O or –COOH), producing a surface

that is more hydrophobic. The same occurs by heating Spheron 6 to 2700 °C. This leads to a different adsorption isotherm (Fig. 10.2) showing a step (inflection point) at a surfactant concentration in the region of $\approx 6\,\mathrm{mmol\,dm^{-3}}$. The first plateau value is $\approx 2.3\,\mu\mathrm{mol\,m^{-2}}$ whereas the second plateau value (that occurs at the cmc of the surfactant) is $\approx 4\,\mu\mathrm{mol\,m^{-2}}$. It is likely in this case that the surfactant ions adopt different orientations at the first and second plateaus. In the first plateau region, a more "flat" orientation (alkyl chains adsorbing parallel to the surface) is obtained whereas at the second plateau vertical orientation is more favourable, with the polar head groups being directed towards the solution phase. Addition of electrolyte ($10^{-1}\,\mathrm{mol\,dm^{-3}}$ NaCl) enhances the surfactant adsorption. This increase is due to the reduction of lateral repulsion between the sulphate head groups and this enhances the adsorption. The disappearance of the inflection point in the presence of NaCl is considered to be a consequence of the much steeper rise in adsorption at low surfactant concentration.

The adsorption of ionic surfactants on hydrophobic polar surfaces resembles that for carbon black [11, 12]. For example, Saleeb and Kitchener [11] found a similar limiting area for cetyltrimethyl ammonium bromide on Graphon and polystyrene ($\approx 0.4\,\mathrm{nm^2}$). As with carbon black, the area per molecule depends on the nature and amount of added electrolyte. This can be accounted for in terms of reduction of head group repulsion and/or counterion binding.

Surfactant adsorption close to the cmc may appear Langmuirian, although this does not automatically imply a simple orientation. For example, rearrangement from horizontal to vertical orientation or electrostatic interaction and counterion binding may be masked by simple adsorption isotherms. It is essential, therefore, to combine the adsorption isotherms with other techniques such as microcalorimetry and various spectroscopic methods to obtain a full picture on surfactant adsorption.

The effect of increasing the alkyl chain length on ionic surfactant adsorption was investigated by Conner and Ottewill [13] who measured the adsorption isotherms for a series of alkyltrimethylammonium ions with C_8, C_{10}, C_{12} and C_{16} on polystyrene latex. The results are shown in Fig. 10.3. For each of these isotherms the inflection at low surfactant concentration can be accounted for by reversal of the sign of ΔG_{elec} on adsorption of the cationic ions on the negative polystyrene latex particles. Initial adsorption of the cations causes charge neutralization and at a certain surfactant concentration, the isoelectric point is reached and a further increase of surfactant concentration causes charge reversal. The inflection at the higher surfactant concentration may reflect the orientation of the alkyl chain from a horizontal orientation of saturation coverage into a vertically oriented monolayer as the surfactant concentration is increased. In this way the solid-water and surfactant chain-water interactions would be minimized at high coverage. For a hydrocarbon surface, one would expect that ΔG_{cs} per CH_2 group would be of the same order of magnitude as ΔG_{cc}, that is about $1\,kT$.

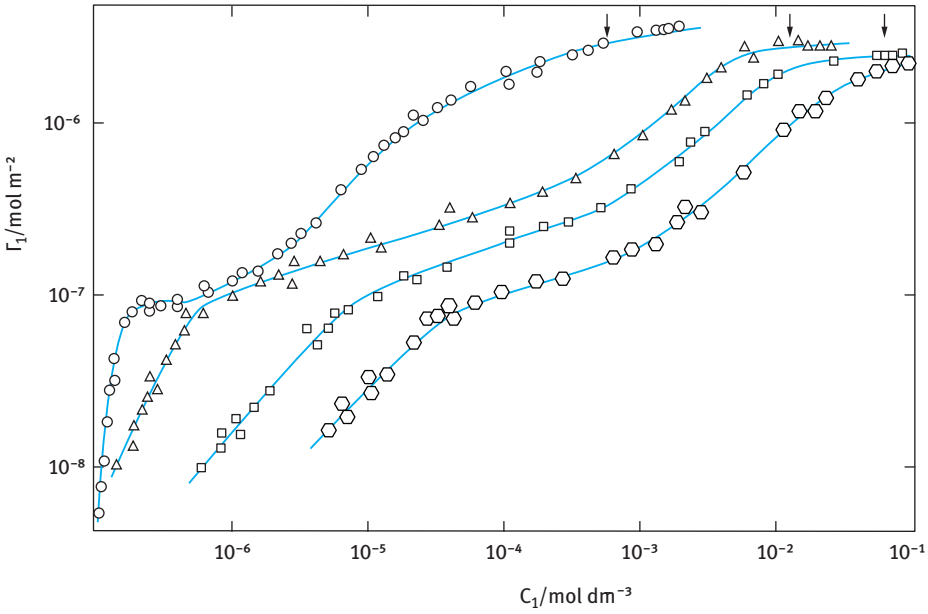

Fig. 10.3: Adsorption isotherms for alkyltrimethylammonium ions on polystyrene latex at pH = 8: ○, C_{16}; △, C_{12}; □, C_{10}.

10.4 Adsorption of ionic surfactants on polar surfaces

The adsorption of ionic surfactants on polar surfaces that contain ionizable groups may show characteristic features due to additional interaction between the head group and substrate and/or possible chain-chain interaction. This is best illustrated by the results of adsorption of sodium dodecyl sulphonate (SDSe) on alumina at pH = 7.2 obtained by Fuersetenau [14] and shown in Fig. 10.4. At the pH value, the alumina is positively charged (the isoelectric point of alumina is at pH ≈ 9) and the counterions are Cl^- from the added supporting electrolyte. In Fig. 10.4, the saturation adsorption Γ_1 is plotted versus equilibrium surfactant concentration C_1 in logarithmic scale. The figure also shows the results of zeta potential (ζ) measurements (which are a measure of the magnitude sign of charge on the surface). Both adsorption and zeta potential results show three distinct regions. The first region, which shows a gradual increase of adsorption with increasing concentration, with virtually no change in the value of the zeta potential, corresponds to an ion exchange process [14]. In other words, the surfactant ions simply exchange with the counterions (Cl^-) of the supporting electrolyte in the electrical double layer. At a critical surfactant concentration, the desorption increases dramatically with any further increase in surfactant concentration (region II). In this region, the positive zeta potential gradually decreases, reaching a zero value (charge neutralization) after which a negative value is obtained

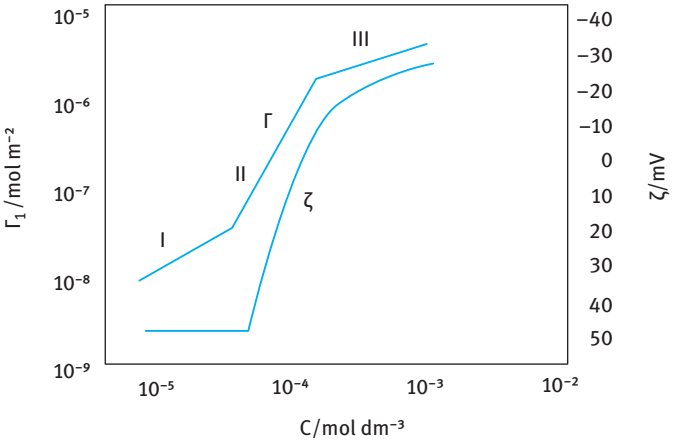

Fig. 10.4: Adsorption isotherm for sodium dodecyl sulphonate on alumina and corresponding zeta (ζ) potential.

which increases rapidly with increasing surfactant concentration. The rapid increase in region II was explained in terms of "hemimicelle formation" that was originally postulated by Gaudin and Fuerestenau [15]. In other words, at a critical surfactant concentration (to be denoted the cmc of "hemimicelle formation" or better the critical aggregation concentration CAC), the hydrophobic moieties of the adsorbed surfactant chains are "squeezed out" from the aqueous solution by forming two-dimensional aggregates on the adsorbent surface. This is analogous to the process of micellization in bulk solution. However, the CAC is lower than the cmc, indicating that the substrate promotes surfactant aggregation. At a certain surfactant concentration in the hemimicellization process, the isoelectric point is exceeded and, thereafter, adsorption is hindered by the electrostatic repulsion between the hemimicelles and hence the slope of the adsorption isotherm is reduced (region III).

10.5 Adsorption of nonionic surfactants

Several types of nonionic surfactants exist, depending on the nature of the polar (hydrophilic) group. The most common type is that based on a poly(oxyethylene) glycol group, i.e. $(CH_2CH_2O)_nOH$ (where n can vary from as little as 2 units to as high as 100 or more units) linked either to an alkyl (C_xH_{2x+1}) or alkyl phenyl ($C_xH_{2x+1}-C_6H_4-$) group. These surfactants may be abbreviated as C_xE_n or $C_x\phi E_n$ (where C refers to the number of C atoms in the alkyl chain, ϕ denotes C_6H_4 and E denotes ethylene oxide). These ethoxylated surfactants are characterized by a relatively large head group compared to the alkyl chain (when $n > 4$). However, there are nonionic surfactants with small head group such as amine oxides ($-N \rightarrow 0$) head group, phosphate oxide

($-P \rightarrow 0$) or sulphinyl-alkanol ($-SO-(CH_2)_n-OH$). Most adsorption isotherms in the literature are based on the ethoxylated type surfactants.

The adsorption isotherms of nonionic surfactants are in many cases Langmuirian, like those of most other highly surface active solutes adsorbing from dilute solutions and adsorption is generally reversible. However, several other adsorption types are produced [16] and those are illustrated in Fig. 10.5. The steps in the isotherm may be explained in terms of the various adsorbate-adsorbate, adsorbate-adsorbent and adsorbate-solvent interactions. These orientations are schematically illustrated in Fig. 10.6.

In the first stage of adsorption (denoted by I in Fig. 10.5 and 10.6), surfactant-surfactant interaction is negligible (low coverage) and adsorption occurs mainly by van der Waals interaction. On a hydrophobic surface, the interaction is dominated

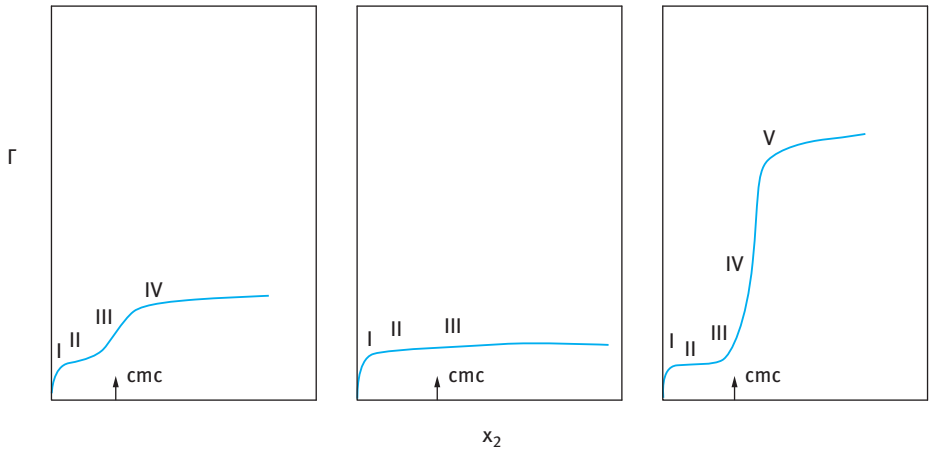

Fig. 10.5: Adsorption isotherms corresponding to the three adsorption sequences shown in Fig. 10.6.

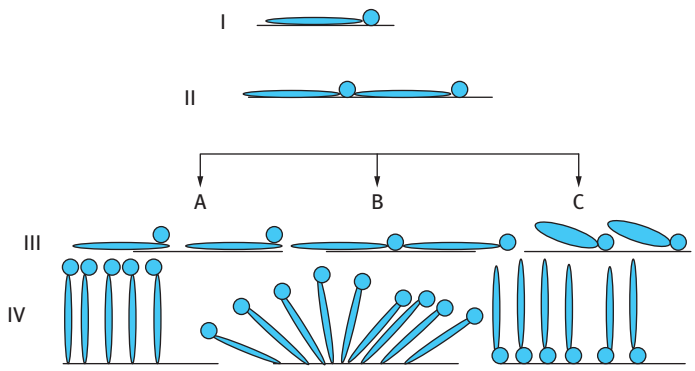

Fig. 10.6: Model for adsorption of nonionic surfactants.

by the hydrophobic portion of the surfactant molecule. This is mostly the case with pharmaceuticals and agrochemicals which have hydrophobic surfaces. Nevertheless, the polar groups of the surfactant may have some interaction with the surface, and the hydrophilic EO groups can have a slight positive adsorption even on a nonpolar adsorbent. When the interaction is due to dispersion forces the heat of adsorption is relatively small and corresponds to the heat liberated by replacing solvent molecules with surfactant. At this stage, the molecule tends to lie flat on the surface because its hydrophobic portion is positively adsorbed, as are also most types of hydrophilic head groups, especially large PEO chains. With the molecule lying parallel to the surface, the adsorption energy will increase in almost equal increments for each additional carbon atom in its alkyl chain, and the initial slope of the isotherm will increase accordingly according to Traube's rule. The same also happens with each additional EO group.

The approach to monolayer saturation with the molecules lying flat (Fig. 10.6 II) is accompanied by a gradual decrease in the slope of the adsorption isotherm as shown in Fig. 10.5. Although most of the "free" solvent molecules will have been displaced from the surface by the time the monolayer is complete, the surfactant molecules themselves will probably stay hydrated at this stage. An increase in the size of the surfactant molecule, e.g. by increasing the length of the alkyl chain or the PEO chain, will decrease the adsorption (expressed in mol m^{-2}). Increasing temperature should increase the adsorption because dehydration decreases the size of the adsorbate molecules. Increasing temperature reduces the solubility of the nonionic surfactant and this enhances its adsorption (higher surface activity).

The subsequent stages of adsorption are increasingly dominated by adsorbate-adsorbate interaction, although it is the adsorbate-adsorbent interaction that initially determines how the adsorption progresses when stage II is completed. The adsorbate-adsorbent interaction depends on the nature of the adsorbent and the HLB of the surfactant. When the hydrophilic group (e.g. PEO) is only weakly adsorbed it will be displaced from the surface by the alkyl chain of the surfactant molecule (Fig. 10.6 III A). This is particularly the case with nonpolar adsorbents such as C black or polystyrene when the surfactant has a short PEO chain (relatively low HLB number). However, if the interaction between the hydrophilic chain (PEO) and polar adsorbent such as silica or silicates is strong, the alkyl chain is displaced as is illustrated in Fig. 10.6 III C. The intermediate situation (Fig. 10.5 III B) occurs when neither type of displacement is favoured and the adsorbate molecules remain flat on the surface.

The change in the amount of adsorption in the third stage (stage III of Fig. 10.6) is unlikely to be large, but as the concentration of the surfactant in bulk solution approaches the critical micelle concentration (cmc) there will be a tendency for the alkyl chains of the adsorbed molecules to aggregate. This will cause the molecules to be vertically oriented and there will be a large increase in adsorption (stage IV). The lateral forces due to alkyl chain interactions will compress the head group, and for a PEO chain this will result in a less coiled, more extended conformation. The longer the

alkyl chain the greater will be the cohesion force and hence the smaller the surfactant cross-sectional area. This may explain the increase in saturation adsorption with increasing alkyl chain length and decreasing number of EO units in the PEO chain. With nonpolar adsorbents the adsorption energy per methylene group is almost the same as the micellization energy, so surface aggregation can occur quite easily even at concentrations below the cmc. However, with polar adsorbents, the head group may be strongly bound to the surface, and partial displacement of a large PEO chain from the surface, needed for close packing, may not be achieved until the surfactant concentration is above the cmc. When the adsorption layer is like that shown in Fig. 10.6 IV C, the surface becomes hydrophobic.

The interactions occurring in the adsorption layer during the fourth and subsequent stages of adsorption are similar to interactions in bulk solution where enthalpy changes caused by increased alkyl-alkyl interactions balance those due to head group interactions and the dehydration process. For this reason, the heat of adsorption remains constant, although adsorption increases with increasing temperature due to dehydration of the head group and its more compact nature.

The parallel between bulk micellization and the surface aggregation process has been emphasized by Klimenko [17, 18] who suggested that above the cmc the adsorbed surfactant molecules form micellar aggregates on the surface as illustrated in Fig. 10.6 V. Both hemimicelles and full micelles can be formed on the surface. This picture was supported by Klimenko [17] who found close agreement between saturation adsorption and adsorption calculated based on the assumption that the surface is covered with close-packed hemimicelles.

10.6 Theoretical treatment of surfactant adsorption

Kleminko [17, 18] developed a theoretical model for the three stages of adsorption of nonionic surfactants. In the first stage (flat orientation) a modified Langmuir adsorption equation was used,

$$c_2 K_a = \left[\frac{\Gamma_2}{\Gamma_2^* - \Gamma_2(1 - a_1/a_2')a_2'} \frac{a_1}{a_2'} \right] f_2' \,, \tag{10.18}$$

where c_2 is the equilibrium concentration of surfactant in bulk solution, Γ_2 is the surface excess concentration at c_2, Γ_2^* is the surface excess at the cmc, K_a is a constant, a_1 and a_2' are the effective cross-sectional areas of the solvent and adsorbate molecules in the surface, and f_a' is an adsorbate surface activity coefficient. The term in the square bracket is a type of surface "concentration", which is defined as the ratio of numbers of adsorbed surfactant molecules to the number of solvent molecules in the equilibrium interfacial layer. The constant K_a allows for adsorbate-adsorbent interactions and is therefore related to the energy of adsorption at infinite dilution. The adsorbate surface activity coefficient f_a' accounts for the adsorbate-adsorbate interaction and it is

assumed to have the following dependence on Γ_2 in the first stage of adsorption,

$$f_2' = \exp\left[\frac{\Gamma_2}{\Gamma_2^* - \Gamma_2} - \frac{K_2\Gamma_2}{\Gamma_2^*}\right], \tag{10.19}$$

where K_2 is an adsorbate-adsorbate interaction constant.

When all the solvent molecules have been displaced and the surface is covered with a close-packed monolayer of horizontal adsorbate molecules, the second stage begins and the EO chains are progressively displaced by alkyl chains of adsorbate molecules. This allows the surface "concentration" to increase by the following amount,

$$\frac{\Gamma_2 - \Gamma_2'}{\Gamma_2'(a_E'/a_1) - (\Gamma_2 - \Gamma_2')(a_2/a_1)}, \tag{10.20}$$

where Γ_2' is the surface excess at the beginning of the second stage, a_E' is the cross-sectional area of the EO chain lying flat on the surface, and a_2 is the area of the surface covered by each surfactant molecule. The adsorption isotherm for the second stage is given by [17–19],

$$c_2K_a = \left[\frac{\Gamma_2'}{\Gamma_2^* - \Gamma_2'(1 - a_1/a_2')a_2'}\frac{a_1}{a_2'} + \frac{\Gamma_2 - \Gamma_2'}{\Gamma_2'a_E' - (\Gamma_2 - \Gamma_2')a_2}a_1\right]f_a''. \tag{10.21}$$

The activity coefficient f_a'' is assumed to include contributions from EO chain interactions and therefore to differ from f_a' in its dependence on Γ_2. The logarithm of f_a'' is arbitrarily assumed to have linear dependence on Γ_2:

$$\ln f_a'' = \ln(f_a')_{\Gamma_2'} + [\ln(f_a'')_{\Gamma_2^*} - \ln(f_a')_{\Gamma_2'}]\Gamma_2/(\Gamma_2^* - \Gamma_2'). \tag{10.22}$$

In equation (10.22) f_a' with subscript Γ_2', the maximum value of f_a' which is reached when $\Gamma_2 = \Gamma_2'$, is obtained by substituting the value of Γ_2' into equation (10.19); f_a'' with subscript Γ_2^*, the maximum value of f_a'' which is reached when $c_2 = c^*$, the cmc, and $\Gamma_2 = \Gamma_2^*$ can be obtained by substitution into equation (10.21).

In the final adsorption stage, which starts at the cmc, Klimenko [17–19] assumes that the adsorbed surfactant associates into hemimicelles on the surface. By considering the equilibrium between molecules in the bulk solution and "free" positions in these surface micelles, he drives a simple Langmuir isotherm,

$$C_2K_a^* = \frac{\Gamma_2}{(\Gamma_2^\infty - \Gamma_2)}, \tag{10.23}$$

where Γ_2^∞ is the maximum surface excess, i.e. the surface excess when the surface is covered with close-packed hemimicelles, K_a^* is a constant that is inversely proportional to the cmc because it is assumed that the surface micelles are similar to the bulk solution micelles, and c_2 is the equilibrium concentration. Equation (10.23) does not contain an activity coefficient because it is assumed that above the cmc deviations from ideality in the surface and in bulk solution derive from a similar association effect with the result that the two activity coefficients will cancel each other out in the adsorption equation.

10.7 Examples of typical adsorption isotherms of model nonionic surfactants on hydrophobic solids

Corkill et al. [20] studied the adsorption of very pure alkyl polyoxyethylene glycol monoethers C_xE_n on Graphon (with a nitrogen BET specific surface area of 91 $m^2\,g^{-1}$). The adsorption isotherms were mostly simple Langmuirian with saturation adsorption reached near or above the cmc. The maximum adsorption increases with increasing the alkyl chain length and decreasing the EO chain length. From the saturation adsorption, the area per molecule at 25 °C was calculated and compared with the value obtained at the solution/air interface (which was obtained from the γ–log c curves and application of the Gibbs adsorption isotherm). The results are given in Tab. 10.1.

Tab. 10.1: Area per molecule at the Graphon/solution interface and air/solution interface at 25 °C.

Surfactant	Area/molecule (nm^2)	
	Graphon/solution interface	Air/solution interface
E_6	1.68	—
C_6E_6	0.93	0.94
C_8E_6	0.81	0.83
$C_{10}E_6$	0.65	0.72
$C_{12}E_6$	0.55	0.61
C_8E_9	1.09	1.02
$C_{16}E_9$	—	0.47

The similarity between the areas at the two interfaces suggests that, at saturation, molecules adsorbed on the solid are vertically oriented as in Fig. 10.6 IV. Hexaoxyethylene glycol (E_6) is also positively adsorbed on Graphon, indicating some affinity to the carbon surface.

The heat of wetting of Graphon with solutions of C_8E_6 was measured as a function of surface excess and the results showed an initial linear change in heat with surface coverage corresponding to the replacement of water at the interface by the hydrated surfactant molecules until the surface is saturated with horizontal adsorbate molecules. The plateau value for the heat of immersion is reached at a molecular area of 1.32 nm^2, which is close to the cross-sectional area of C_8E_6 lying flat. The constancy of the heat of immersion at higher concentrations is attributed to the balance between decreasing enthalpy, due to elimination of the alkyl/solution interface as the molecules become vertically oriented, and increasing enthalpy associated with the dehydration of the adsorbing molecule. The adsorption thus occurs with a net increase in entropy analogous to the process of micellization.

The adsorption of nonionic surfactants based on poly(ethylene oxide) increases with increasing temperature as illustrated in Fig. 10.7 for C_8E_6 and C_8E_3. Increasing

temperature gradually dehydrates the PEO head group and this makes the molecule less hydrophilic and more compact, thus increasing the surface activity and saturation adsorption values. The importance of the surfactant/solvent interaction is apparent on the effect of temperature on the adsorption of C_8E_3. At 4.5 °C the adsorption isotherm is a simple Langmuirian, but at 25 °C and 40 °C there is a very steep rise in adsorption at high surfactant concentrations. This is characteristic of a surface condensation effect and the steep rise occurs at concentrations below those at which surfactant phase separation occurs in bulk solution. These concentrations are shown by broken lines in Fig. 10.7.

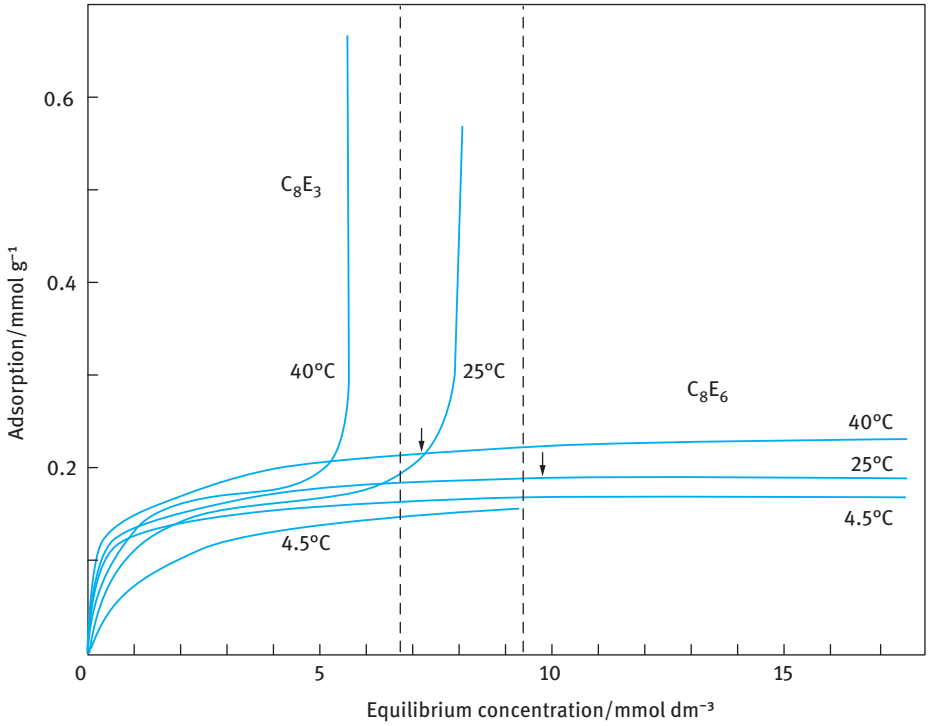

Fig. 10.7: Effect of temperature on the adsorption of C_8E_6 and C_8E_3 on Graphon.

Corkill et al. [21, 22] studied the adsorption of alkylsulphenyl alkanol surfactants, $C_xH_{2x+1}SO(CH_2)_nOH$ on Graphon. They found that the saturation adsorption, like that of the ethoxylated surfactants, increases with increasing alkyl chain length and decreasing head group size. A summary of the results obtained is given in Tab. 10.2. From the magnitude of the area occupied (A) by the surfactant at saturation and the observation that the carbon black dispersions were well stabilized, it was concluded that at saturation the surfactant molecule was vertically oriented. The minimum areas were

Tab. 10.2: Adsorption results for n-alkylsulphinyl alkanols on Graphon at 25 °C [22].

Adsorbate	A (nm^2)				$-\Delta H_2$ (kJ/mol)
	At isotherm inflection	From horizontal model	At saturation	From vertical model	
$C_4H_9SO(CH_2)_2OH$	—	0.58	≈ 0.83	0.25	—
$C_6H_{13}SO(CH_2)_2OH$	0.84	0.70	0.44	0.25	42
$C_8H_{17}SO(CH_2)_2OH$	1.08	0.83	0.25	0.25	59
$C_{10}H_{21}SO(CH_2)_2OH$	≈ 1.68	0.98	—	0.25	109
$C_8H_{17}SO(CH_2)_3OH$	1.31	0.90	0.32	0.25	84
$C_8H_{17}SO(CH_2)_4OH$	1.68	0.98	0.36	0.25	117

slightly larger than the smallest cross-sectional area of the fully extended surfactant molecule. This difference was attributed to the head group hydration.

Most of the isotherms show an inflection point at the cmc as illustrated in Fig. 10.5. This is clearly illustrated in Fig. 10.8 for the adsorption of octylsulphinyl ethanol [22]. The heat of wetting for the alkylsulphinyl alkanols changes linearly with surface coverage until adsorption reaches a value that corresponds fairly closely to the inflection point of the isotherm. Thereafter the heat of adsorption is constant except for that of decylsulphinyleethanol which continues to increase but less rapidly. This may be due to the surfactant being close to its solubility limit. The change in heat with cover-

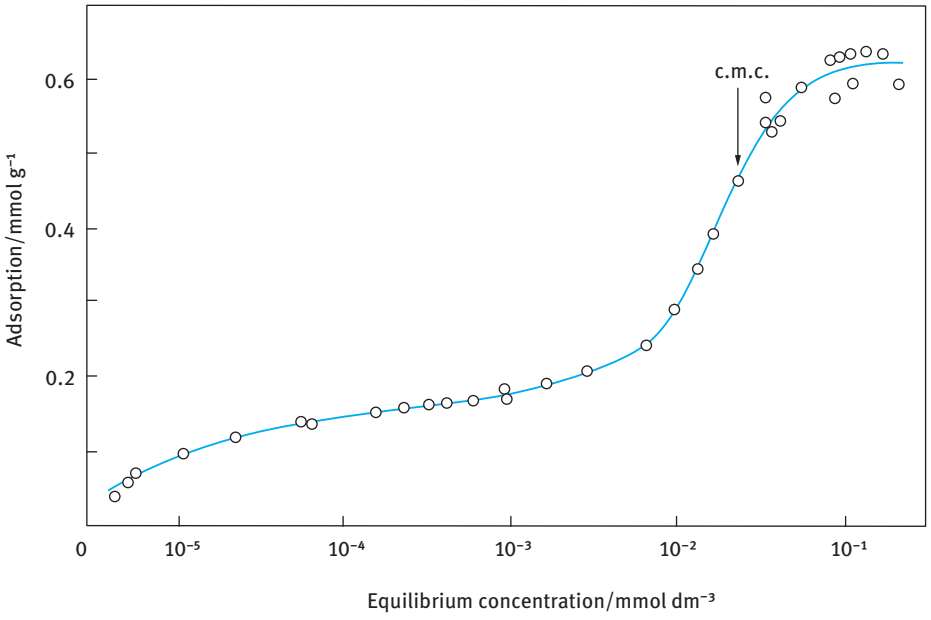

Fig. 10.8: Adsorption isotherm of octylsulphinylethanol on Graphon at 25 °C [22].

age is greater for the longer alkyl chains and larger number of head group methylene groups. The partial molar heat of adsorption of the surfactant ΔH_2 was calculated by assuming that the surface concentration of "free" solvent became zero when the heat of wetting became constant. ΔH_2 had large negative values which increased as x and n increased (Tab. 10.2). Corkill et al. [22] concluded that the alkylsulphenyl alkanol system was very similar to the ethoxylated alcohol systems.

The surfactant is initially adsorbed as a highly hydrated molecule lying parallel to the surface, and the initial enthalpy changes are associated with the displacement of the solvent molecules from the surface. When compete monolayer coverage has been achieved, adsorbate-adsorbate interactions, similar to the process of micellization in bulk solution, causes orientation changes and a large increase in adsorption occurs near the cmc. The heat of adsorption becomes constant because the negative enthalpy due to elimination of alkyl/solution interface is offset by the positive enthalpy due to de-solvation.

References

[1] Hough DB, Randall HM. In: Parfitt GD, Rochester CH, editors. Adsorption from solution at the solid/liquid interface. London: Academic Press; 1983. p. 247.
[2] Rendall HM, Smith AL, Williams LA. J Chem Soc Faraday Trans I. 1979;75:669.
[3] de Kaizer A, Lyklema J. J Colloid Interface Sci. 1980;75:171.
[4] Fuerstenau DW, Healy TW. In: Lemlich R, editor. Adsorptive bubble separation techniques. London: Academic Press; 1972. p. 91.
[5] Somasundaran P, Goddard ED. Modern Aspects Electrochem. 1979;13:207.
[6] Healy TW. J Macromol Sci Chem. 1974;118:603.
[7] Somasundaran P, Hannah HS. In: Shah DO, Schechter RS, editors. Improved oil recovery by surfactant and polymer flooding. London: Academic Press; 1979. p. 205.
[8] Clark AH, Frank F, Smani S. J Chem Soc Faraday Trans I. 1977;73:290.
[9] Greenwood FG, Parfitt GD, Picton NH, Wharton DG. Adv Chem Ser. 1968;79:135.
[10] Day RE, Greenwood FG, Parfitt GD. 4th Int. Congress of Surface Active Substances. 1967;18:1005.
[11] Saleeb FZ, Kitchener JA. J Chem Soc. 1965:911.
[12] Saleeb FZ, Kitchener JA. 4th Int. Congress of Surface Active Substances. 1967;2B:129.
[13] Conner P, Ottewill RH. J Colloid Interface Sci. 1971;37:642.
[14] Fuerestenau DW. In: Hair ML, editor. The chemistry of biosurfaces. New York: Marcel Dekker; 1971. p. 91.
[15] Gaudin AM, Fuertsenau DW. Trans AIME. 1955;202:958.
[16] Clunie JS, Ingram BT. In: Parfitt GD, Rochester CH, editors. Adsorption from solution at the solid/liquid interface. London: Academic Press; 1983. p. 105.
[17] Klimenko NA. Tryasorukova and Permilouskayan. Kolloid Zh. 1974;36:678.
[18] Klimenko NA. Kolloid Zh. 1978;40:1105.
[19] Klimenko NA. Kolloid Zh. 1979;41:781.
[20] Corkill JM, Goodman JF, Tate JR. Trans Faraday Soc. 1966;62:979.
[21] Corkill JM, Goodman JF, Tate JR. Wetting. SCI Monograph No. 2. London: Society of Chemical Industry; 1966. p. 363.
[22] Corkill JM, Goodman JF, Tate JR. Trans Faraday Soc. 1967;63:2264.

11 Polymers and polymeric surfactants and their association

11.1 Introduction

Polymers and polymeric surfactants form units in solution with dimensions in the colloid range. Homopolymers form random coils in solution that have radius of gyration in the colloid range. With block (A–B and A–B–A) and graft (BA_n or AB_n) copolymers consisting of two components A (that is soluble in the medium) and B (that is insoluble in the medium), the copolymers associate in solution forming self-assembly structures with a core of the B components and a "corona" with the A components. These association structures have dimensions in the colloid range.

In this chapter, I will start with general classification of polymers and polymeric surfactants. This is followed by a section on the solution properties of polymers and polymeric surfactants and their phase behaviour.

11.2 General classification of polymers and polymeric surfactants

11.2.1 Homopolymers

Perhaps the simplest type of a polymeric surfactant is a homopolymer [1–4], that is formed from the same repeating units, such as poly(ethylene oxide) that is also referred to as polyethylene glycol and has the following chemical structure with the repeating units of ethylene oxide,

$H–(O–CH_2–CH_2)_n–OH$

Another homopolymer that is used in many pharmaceutical formulations is poly(vinyl pyrrolidone) that is formed from repeating units of vinyl pyrrolidone,

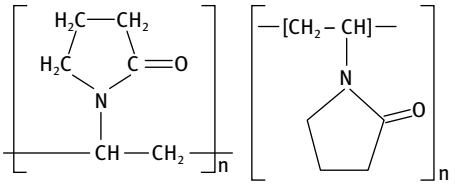

https://doi.org/10.1515/9783110540895-012

These homopolymers have little surface activity at the O/W interface, since the homopolymer segments (ethylene oxide or vinylpyrrolidone) are highly water soluble and have little affinity to the interface. However, such homopolymers may adsorb significantly at the S/L interface, e.g. on silica. Even if the adsorption energy per monomer segment to the surface is small (fraction of kT, where k is the Boltzmann constant and T is the absolute temperature), the total adsorption energy per molecule may be sufficient to overcome the unfavourable entropy loss of the molecule at the S/L interface [1–4].

11.2.2 Random copolymers

As mentioned above, homopolymers are not the most suitable emulsifiers or dispersants. A small variant is to use polymers that contain specific groups that have high affinity to the surface that are randomly attached to the polymer chain [1–4]. This is exemplified by partially hydrolysed poly(vinyl acetate) (PVAc), technically referred to as poly(vinyl alcohol) (PVA). The polymer is prepared by partial hydrolysis of PVAc, leaving some residual vinyl acetate groups. Most commercially available PVA molecules contain 4–20 mol % acetate groups. These acetate groups, which are hydrophobic, give the molecule its amphipathic character. This blocky distribution of acetate groups on the poly(vinyl alcohol) backbone provides more effective anchoring of the polymeric surfactant chain on the particles or emulsion droplets. On a hydrophobic surface such as polystyrene or a hydrocarbon oil, the polymer adsorbs with preferential attachment of the acetate groups on the surface, leaving the more hydrophilic vinyl alcohol segments dangling in the aqueous medium. These partially hydrolysed PVA molecules also exhibit surface activity at the O/W interface as indicated by the reduction of the interfacial tension with increasing polymer concentration.

11.2.3 Block and graft copolymers

The most convenient polymeric surfactants are those of the block and graft copolymer type. A block copolymer is a linear arrangement of blocks of variable monomer composition. The nomenclature for a diblock is poly-A-block–poly-B and for a triblock is poly-A-block–poly-B–poly-A. One of the most widely used triblock polymeric surfactants are the “Pluronics” or “Poloxamers” (BASF, Germany), which consists of two poly-A blocks of poly(ethylene oxide) (PEO) and one block of poly(propylene oxide) (PPO). Several chain lengths of PEO and PPO are available as indicated in the chemical structure below,

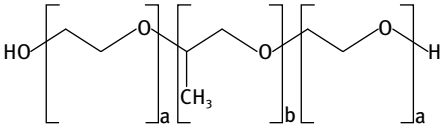

General structure
with a = 2–130 and b = 15–67

For the Pluronics the trade name is coded with a letter L (liquid), P (paste) and F (flake) that defines its physical form at room temperature. This is followed by two or three digits; the first one or two digits multiplied by 300 indicate the approximate molar mass of PPO and the last digit multiplied by 10 indicates the percentage of PEO. For example, Pluronic L61 indicates a liquid with PPO molar mass of 1800 and 10 % PEO. Pluronic F127 indicates a flake with PPO molar mass 3,600 and 70 % PEO. The Poloxamers (which are FDA approved) are commonly named with the letter P followed by three digits; the first two digits multiplied by 10 gives the approximate molar mas of PPO and the last digit multiplied by 10 gives the percentage of PEO. For example, Poloxamer P407 has a molar mass of PPO of 400 and 70 % PEO. Later, triblocks of PPO–PEO–PPO (inverse Pluronics) became available for some specific applications. These polymeric triblocks can be applied as emulsifiers or dispersants, whereby the assumption is made that the hydrophobic PPO chain resides at the hydrophobic surface, leaving the two PEO chains dangling in aqueous solution and hence providing steric repulsion. Although these triblock polymeric surfactants have been widely used in various applications in emulsions and suspensions, some doubt has arisen on how effective these can be. It is generally accepted that the PPO chain is not sufficiently hydrophobic to provide a strong "anchor" to a hydrophobic surface or to an oil droplet. Indeed, the reason for the surface activity of the PEO–PPO–PEO triblock copolymers at the O/W interface may stem from a process of "rejection" anchoring of the PPO chain since it is not soluble both in oil and water [1–4].

Several other di- and triblock copolymers have been synthesized, although these are of limited commercial availability. Typical examples are diblocks of polystyrene-block–polyvinyl alcohol, triblocks of poly(methyl methacrylate)–block poly(ethylene oxide)–block poly(methyl methacrylate), diblocks of polystyrene block–polyethylene oxide and triblocks of polyethylene oxide–block polystyrene–polyethylene oxide [1–4]. An alternative (and perhaps more efficient) polymeric surfactant is the amphipathic graft copolymer consisting of a polymeric backbone B (polystyrene or polymethyl methacrylate) and several A chains ("teeth") such as polyethylene oxide. This graft copolymer is sometimes referred to as a "comb" stabilizer. This copolymer is usually prepared by grafting a macromonomer such as methoxy polyethylene oxide methacrylate with polymethyl methacrylate. The "grafting onto" technique has also been used to synthesize polystyrene-polyethylene oxide graft copolymers.

11.2.4 Polymeric surfactants based on polysaccharides

Several surface active graft copolymers are available based on a hydrophilic backbone of polysaccharide to which several hydrophobic alkyl chains are attached. A good example is Emulsan that is produced by micro-organisms (bacteria). It consists of a backbone of hetero-polysaccharide with repeating trisaccharide carrying a negative charge. Fatty acid chains are covalently linked to the polysaccharide through ester linkages [5], as illustrated in Fig. 11.1.

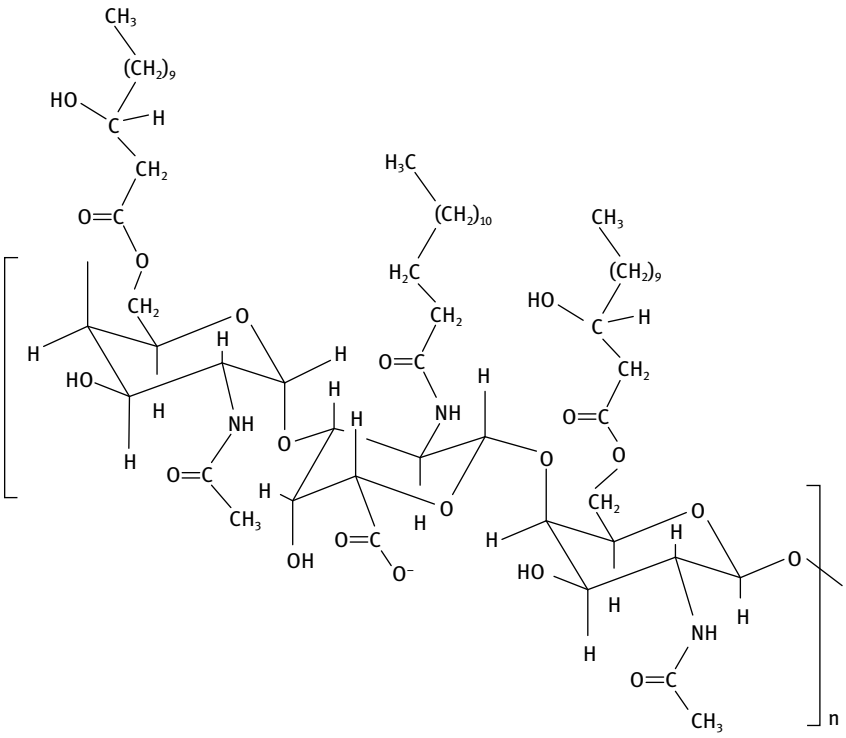

Fig. 11.1: Structure of Emulsan.

Emulsan is moderately surface active showing a small reduction of the O/W interfacial tension (for example it reduces the interfacial tension of hexane/water from 47 to around 55 mN m^{-1}). However, it has a strong tendency to adsorb at the O/W interface and can be very effective in stabilizing emulsions of specific oils in water.

Natural polysaccharides can be chemically modified into the equivalent of lipopolysaccharides by attachment of long alkyl or alkyl acryl chains [5]. For example, cellulose can be modified with ethylene oxide and alkyl chloride. The cellulose is

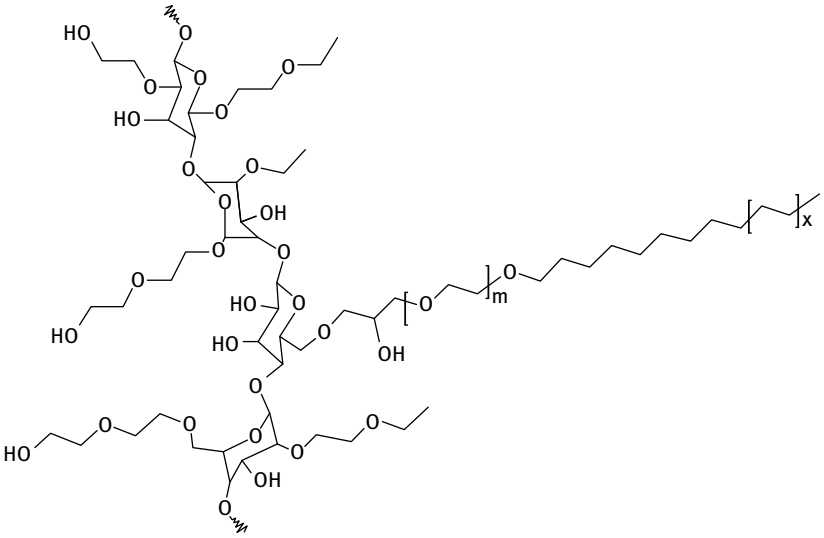

Fig. 11.2: Structure of cellulose modified with ethylene oxide and alkyl chloride.

swollen in strong alkali and the semi-soluble material is reacted with ethylene oxide and alkyl chloride resulting in the formation of a polymeric surfactant with the structure shown in Fig. 11.2. If the alkyl group is short, e.g. ethyl, the molecule is moderately surface active. If some of the ethyl groups are replaced with long chain alkyls, a polymer with higher surface activity is obtained. Such graft copolymers are commercially available and they are referred to as "associative thickeners". They are used for rheology control of many aqueous formulations, e.g. water-borne paints.

Another example of hydrophobically modified nonionic cellulose ether (HM-EHEC) is shown in Fig. 11.3. The cellulose can be modified by a relatively random substitution of hydroxyethyl and ethyl groups to give ethyl(hydroxyethyl) cellulose (EHEC). A low fraction of hydrophobic alkyl groups is inserted to give HM-EHEC.

Another sugar-based surfactant is alkyl polyglucoside which is prepared by reacting starch or glucose with butanol using acid catalyst [6]. The resulting butyl oligoglycoside intermediate is reacted with dodecanol using acid catalyst to produce dodecyl polyglucosides as illustrated in Fig. 11.4. The reaction yields a mixture in which on average more than one glucose unit is attached to an alcohol molecule. The average number of glucose units linked to an alcohol group is described as the (average) degree of polymerization (DP). Alkyl monoglycosides are the main group of components with a content of more than 50 % followed by the diglycosides and higher oligomers up to heptaglucosides. Due to the presence of molecules with DP > 1, the surfactant may be considered as polymeric. The alkyl polyglucosides show high surface activity at the air/water and oil/water interfaces. They also have low critical micelle concentrations comparable to those of nonionic surfactants.

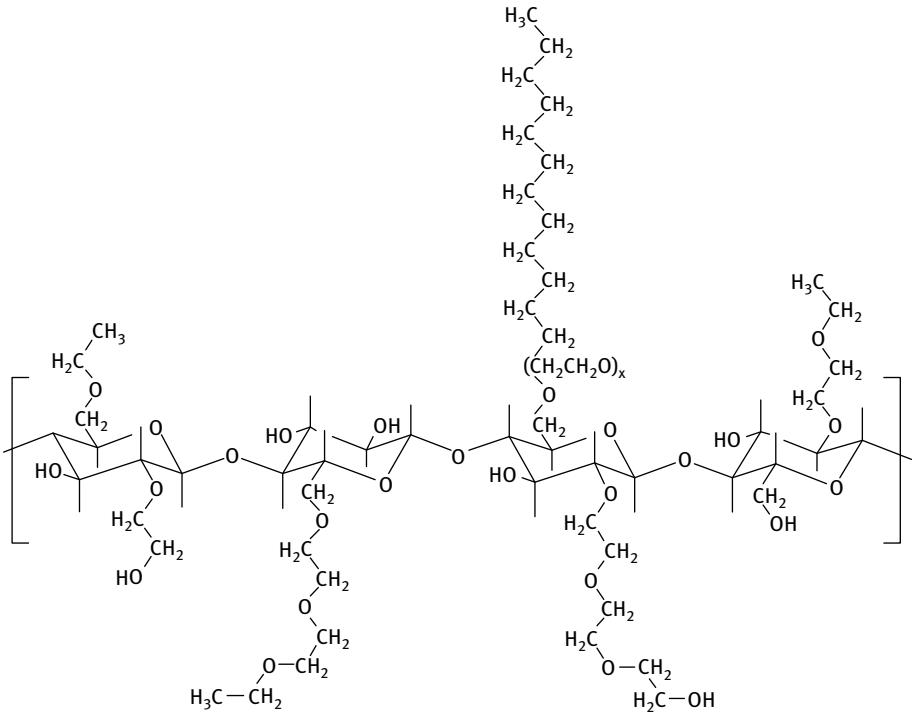

Fig. 11.3: Structure of hydrophobically modified ethylhydroxyethyl cellulose (HM-EHEC).

More recently, graft copolymers based on polysaccharides have been developed for stabilization of disperse systems. One of the most useful graft copolymers are those based on inulin that is obtained from chicory roots [7–9]. It is a linear polyfructose chain with a glucose end. When extracted from chicory roots, inulin has a wide range of chain lengths ranging from 2 to 65 fructose units. It is fractionated to obtain a molecule with narrow molecular weight distribution with a degree of polymerization > 23 and this is commercially available as INUTEC® N25. The latter molecule is used to prepare a series of graft copolymers by random grafting of alkyl chains (using alkyl isocyanate) on the inulin backbone. The first molecule of this series is INUTEC® SP1 that is obtained by random grafting of C_{12} alkyl chains. It has an average molecular weight of ≈ 5000 Daltons and its structure is given in Fig. 11.5. The molecule is schematically illustrated in Fig. 11.6 which shows the hydrophilic polyfructose chain (backbone) and the randomly attached alkyl chains.

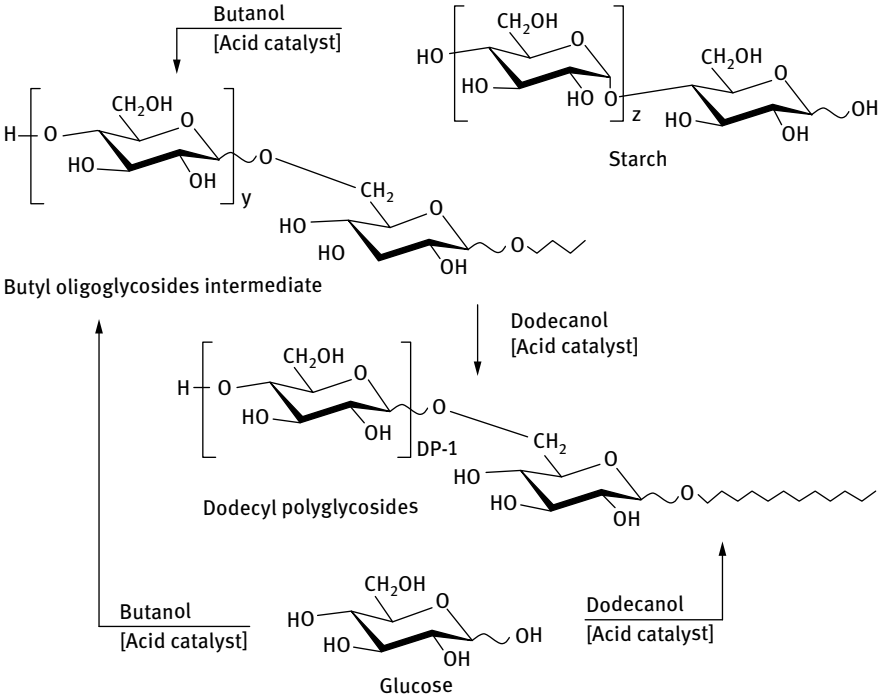

Fig. 11.4: Pathway for alkyl polyglucoside synthesis.

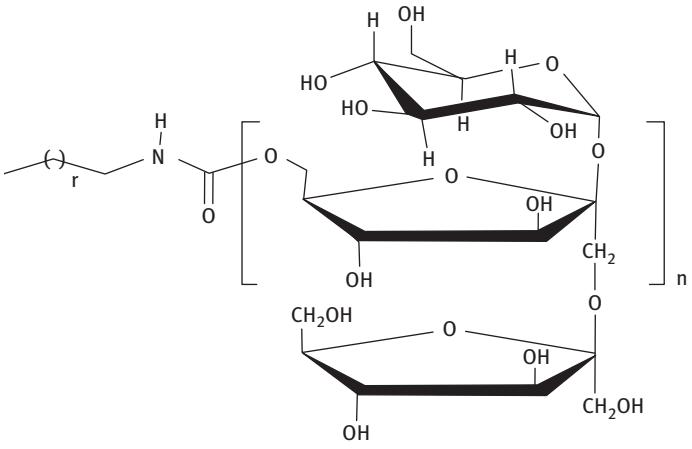

Fig. 11.5: Structure of INUTEC® SP1.

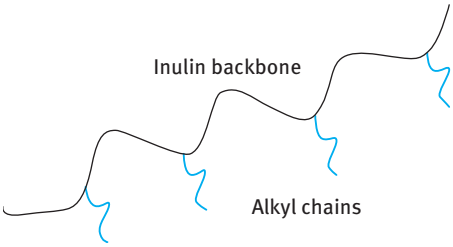

Fig. 11.6: Schematic representation of INUTEC® SP1 polymeric surfactant.

The main advantages of INUTEC® SP1 as stabilizer for disperse systems are:

(i) Strong adsorption to the particle or droplet by multipoint attachment with several alkyl chains. This ensures lack of desorption and displacement of the molecule from the interface.

(ii) Strong hydration of the linear polyfructose chains, both in water and in the presence of high electrolyte concentrations and high temperatures. This ensures effective steric stabilization [10].

11.2.5 Natural polymeric biosurfactants

Most food emulsions require the use of naturally occurring polymeric surfactants that must be approved by the Food and Drug Administration (FDA). One of the most commonly used natural polysaccharide emulsifiers is gum arabic [11] which is amphiphilic. It has a nonpolar polypeptide backbone with a number of polar polysaccharide chains attached. On adsorption to oil droplet surfaces, the polypeptide chain protrudes to the oil droplet surfaces, whereas the polysaccharide chains dangle into the water. This leads to the formation of a relatively thick hydrophilic coating around the oil droplets that prevents any aggregation and coalescence of the oil droplets.

A number of other naturally occurring amphiphilic polysaccharides that are suitable for use as emulsifiers have been identified, e.g. pectin fractions isolated from beet, citrus, apple, etc. These polymeric surfactants show surface activity at the oil/water (O/W) interface and are able to stabilize the emulsion against flocculation and coalescence. Chitosan, a cationic polysaccharide, typically isolated from crustacean shells, is also capable of emulsion formation and stability.

One of the most common naturally occurring polymeric surfactants that are commonly used in food emulsions are the proteins. They are biopolymers consisting of strings of amino acid units covalently linked by peptide bonds [11]. The type, number and position of the amino acids in the polypeptide chain determine the molar mass and functional properties of food proteins. Most proteins contain a mixture of polar and nonpolar amino acids and, therefore, the amphiphilic molecules can adsorb at the O/W interface thus stabilizing the emulsion. The relative balance of polar and nonpolar groups exposed on their surfaces governs the surface activity of proteins.

If the surface hydrophobicity is too low, the driving force for protein adsorption is not strong enough to overcome the entropy loss associated with adsorption. Conversely, if the surface hydrophobicity is too high, then the proteins tend to aggregate, become water-insoluble, and lose their surface activity. Consequently, an optimum level of surface hydrophobicity is required for a protein to be a good emulsifier. Most proteins also have a mixture of anionic, nonionic and cationic amino acids along the polypeptide chains, which determines the charge of the protein molecule under different pH conditions. At a certain pH, referred to as isoelectric point (IEP), the protein molecule has a net zero charge. When the pH > IEP, the protein molecule is negatively charged, whereas when pH < IEP the protein molecule becomes positively charged. The charged chains play a major role in electrostatic stabilization.

Proteins may adopt various conformations in aqueous solution, depending on the balance of van der Waals forces, hydrophobic interactions, electrostatic interactions, hydrogen bonds, steric effects and entropy effects [11]. The balance is determined by solution and environmental conditions such as pH, ionic strength and temperature. Consequently, the conformation of a protein at an interface may change when these conditions are altered. The two mostly common conformations of surface active proteins used as emulsifiers are globular and random coil. Globular proteins have fairly compact spheroid structures where the majority of the nonpolar groups are located within the interior, and the majority of the polar groups are present at the exterior. These globular proteins have surface activity because some of the nonpolar groups remain exposed at their surfaces, which gives the driving force for adsorption at the O/W interface. Random coils have a more flexible structure, although there may still be some regions that have local order such as helical and sheet structures. The most common random coil proteins used as emulsifiers in the food industry are casein and gelatin. The structure of the protein often changes after they adsorb at the O/W interface. For example, globular proteins may unfold after they adsorb to droplet surfaces and expose groups normally located in their interiors, such as nonpolar and sulfhydryl groups. After adsorption to the oil droplet surfaces, the protein molecule may adopt a configuration where many of the hydrophilic groups protrude into the water phase, whereas most of the hydrophobic groups protrude into the oil phase. This results in high surface activity at the O/W interface and effective stabilization of the emulsion.

11.2.6 Silicone surfactants

Silicone surfactants are graft copolymers (“comb” type) with a backbone based on polydimethylsiloxane, which is highly hydrophobic and insoluble in water [5, 12]. The side chains (“teeth”) are water soluble, charged or uncharged, and the molecule becomes surface active in aqueous solution. Poly(ethylene glycol) (EO) or poly(ethylene glycol)–poly(propylene glycol) (PEO–PPO) are by far the most common constituents of the side chains. The side chain may contain a weakly polar group such as an ester

or amine or it may be an ionic group. The general structure of the silicone surfactant is shown in Fig. 11.7 with X being an ionic or nonionic polar group such as PEO or PEO–PPO. The linkage between Si and the polyether chain may be either Si–O–C or Si–C. The Si–O–C link is made by esterification of chloropolysiloxanes with hydroxyl-functional organic compounds such as PEO–PPO copolymer. This makes the molecule unstable undergoing hydrolysis in acid or alkaline conditions. However, the Si–C linkage, where a carbon of the PEO–PPO copolymer is directly linked to the Si atom, is stable. Such a linkage is usually made by a Pt-catalysed hydrosilating addition of an Si–H function in the polysiloxane to a terminal olefinic bond in the substituted polymer [5].

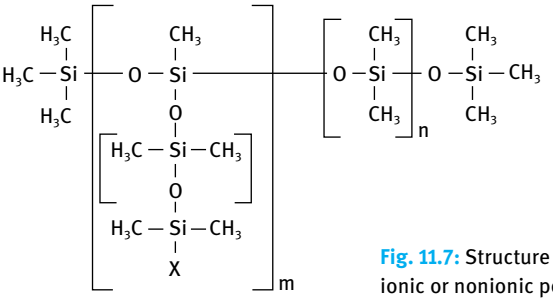

Fig. 11.7: Structure of silicone surfactants with X being an ionic or nonionic polar group such as PEO or PEO–PPO.

Silicone surfactants have unique properties when compared with hydrocarbon surfactants. They are very effective in lowering the surface tension of water to values around 20 mN m^{-1} (when compared with the value of around 30 mN m^{-1} obtained with most hydrocarbon surfactants). They also have excellent wetting on low energy surfaces such as polytetrafluroethane (PTFE). They are also powerful antifoamers.

11.2.7 Polymeric surfactants for nonaqueous dispersions

Block and graft copolymers based on poly(12-hydroxystearic acid) are used for nonaqueous systems such as water-in-oil (W/O) emulsions and nonaqueous dispersions, e.g. paints [13]. The poly(12-hydroxystearic acid) chains (the A chains of an A–B–A block copolymer or the A side chains of a graft copolymer), which are of low molecular weight (≈ 1000 Daltons), provide steric stabilization analogous to how PEO behaves in aqueous solution [5]. The B anchor chains are chosen to be highly insoluble in the nonaqueous medium and have some specific interaction with the surface of the droplet or particle. For water-in-oil (W/O) emulsions an A–B–A block copolymer of poly (12-hydroxystearic acid) (PHS) (the A chains) and poly (ethylene oxide) (PEO) (the B chain): PHS–PEO–PHS, is commercially available (Arlacel P135). The PEO chain (that is soluble in the water droplets) forms the anchor chain, whereas the PHS chains

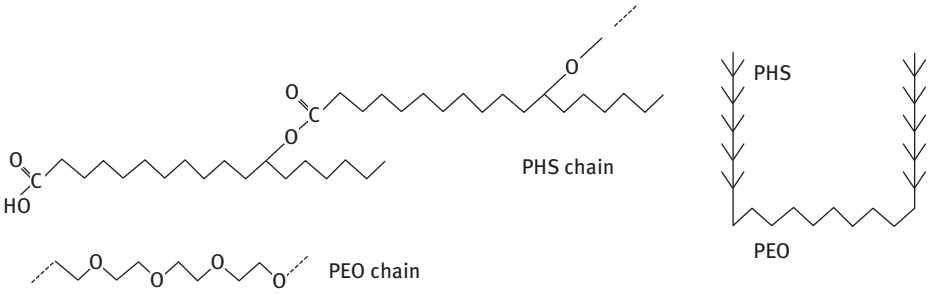

Fig. 11.8: Schematic representation of the structure of PHS–PEO–PHS block copolymer.

form the stabilizing chains. PHS is highly soluble in most hydrocarbon solvents and is strongly solvated by its molecules. The structure of the PHS–PEO–PHS block copolymer is schematically shown in Fig. 11.8.

In the nonaqueous dispersion process (referred to as NAD) the monomer, normally an acrylic, is dissolved in a nonaqueous solvent, normally an aliphatic hydrocarbon and an oil soluble initiator and a stabilizer (to protect the resulting particles from flocculation, sometimes referred to as "protective colloid") is added to the reaction mixture. The most successful stabilizers used in NAD are block and graft copolymers. These block and graft copolymers are assembled in a variety of ways to provide the molecule with an "anchor chain" and a stabilizing chain. As mentioned above, the anchor chain should be sufficiently insoluble in the medium and have a strong affinity to the polymer particles produced. In contrast, the stabilizing chain should be soluble in the medium and strongly solvated by its molecules to provide effective steric stabilization. The length of the anchor and stabilizing chains has to be carefully adjusted to ensure strong adsorption (by multipoint attachment of the anchor chain to the particle surface) and a sufficiently "thick" layer of the stabilizing chain that prevents close approach of the particles to a distance where the van der Waals attraction becomes strong. Several configurations of block and graft copolymers are possible as is illustrated in Fig. 11.9.

Typical preformed graft stabilizers based on poly(12-hydroxy stearic acid) (PHS) are simple to prepare and effective in NAD polymerization. Commercial 12-hydroxystearic acid contains 8–15 % palmitic and stearic acids which limits the molecular weight during polymerization to an average of 1500–2000. This oligomer may be converted to a "macromonomer" by reacting the carboxylic group with glycidyl methacrylate. The macromonomer is then copolymerized with an equal weight of methyl methacrylate (MMA) or similar monomer to give a "comb" graft copolymer with an average molecular weight of 10 000–20 000. The graft copolymer contains on average 5–10 PHS chains pendent from a polymeric anchor backbone of PMMA. This graft copolymer can stabilize latex particles of various monomers. The major limitation of the monomer composition is that the polymer produced should be insoluble in the medium used.

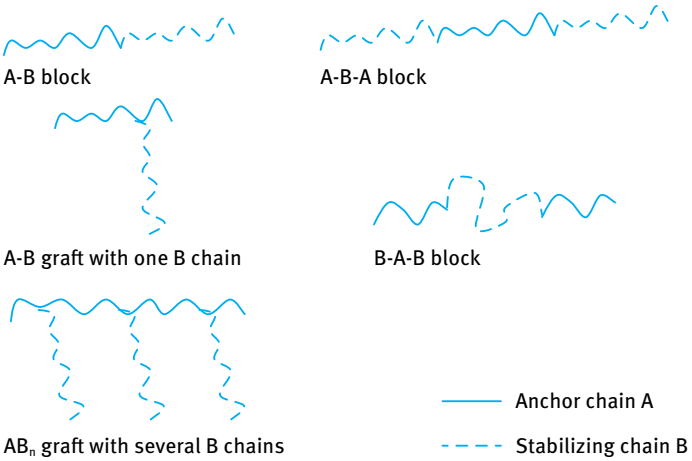

Fig. 11.9: Configurations of block and graft copolymers.

Several other examples of block and graft copolymers that are used in dispersion polymerization are given in Tab. 11.1 which also shows the continuous phase and disperse polymer that can be used with these polymers.

Tab. 11.1: Block and graft copolymers used in emulsion polymerization.

Polymeric surfactant	Continuous phase	Disperse polymer
Polystyrene-block–poly(dimethyl siloxane)	Hexane	Polystyrene
Polystyrene-block–poly(methacrylic acid)	Ethanol	Polystyrene
Polybutadiene-graft–poly(methacrylic acid)	Ethanol	Polystyrene
Poly(2-ethylhexyl acrylate)-graft–poly(vinyl acetate)	Aliphatic hydrocarbon	Poly(methyl methacrylate)
Polystyrene-block–poly(t-butylstyrene)	Aliphatic hydrocarbon	Polystyrene

11.2.8 Polymerizable surfactants

Polymerizable surfactants are amphipathic molecules containing somewhere in their structure a polymerizable group such as styrenic, acrylic or methacrylic, vinylic, maleic, crotonic or allylic [14]. These groups may be located in different places such as at the end or head of the hydrophilic sequence, the end of the hydrophobic moiety, between the two, or finally along the surfactant structure or pendent (side) groups. They are generally referred to as surfmers [14]. One of the main applications of polymerizable surfactants is for stabilization of vesicles. The second major use of polymerizable surfactants is their application as stabilizers in polymerization in dispersed media, both in emulsion and dispersion polymerization. The surfactant is covalently linked

to the surface of the particles, thus improving latex stability. A second kind of benefit is expected in the case of film-forming latexes. In a conventional emulsion, the surfactants are not firmly attached to the particles and thus are able to migrate toward the surface of the film. This may result in defects of adhesion if the film is expected to protect the surface of a substrate. In addition, during coalescence phase separation may occur. These problems are overcome when using surfactants that are covalently linked to the surface of the latex. A third kind of benefit takes place if it is intended that the latex will release material upon flocculation. If the surfactant is covalently linked to the surface of the polymer particles, a smaller amount of it will be rejected to the water phase [13].

11.3 Solution properties of polymeric surfactants

11.3.1 Polymer conformation and structure

Long flexible macromolecules have a large number of internal degrees of freedom. A typical primary structure of such molecules is a linear chain of units connected by covalent bonds referred to as the backbone. By rotation about the bonds in the backbone the molecule changes its shape resulting in a wide spectrum of conformations. The rotation is hindered by the side groups, so that some of these conformations may be rather unfavourable. In some macromolecules such as proteins sequences of preferred orientations show up as helical or folded sections.

For flexible linear polymers the energy barriers associated with rotation around the bonds are small with respect to thermal motion. Such molecules have a randomly fluctuating three-dimensional tertiary structure, referred to as a random coil, as illustrated in Fig. 11.10. The chain conformation is described as a random flight chain of N bonds of length ℓ. The fluctuating distance between the end points is r. The quantity $\langle r^2 \rangle^{1/2}$, that is referred to as the mean end-to-end distance, is a measure of the size of the chain, i.e. its mean coil diameter [15–19],

$$\langle r^2 \rangle^{1/2} = N^{1/2} \ell. \tag{11.1}$$

Another useful parameter is the radius of gyration $\langle s^2 \rangle^{1/2}$ which is a measure of the effective size of a polymer molecule (it is the root mean-square distance of the elements of the chain from its centre of gravity).

For linear polymers,

$$\langle s^2 \rangle^{1/2} = \frac{\langle r^2 \rangle^{1/2}}{6^{1/2}}. \tag{11.2}$$

In real polymers the bonds cannot assume arbitrary directions but there are fixed angles between them. In addition, rotation about bonds is not entirely free, because the potential energy shows maxima and minima as a function of rotation angle. To

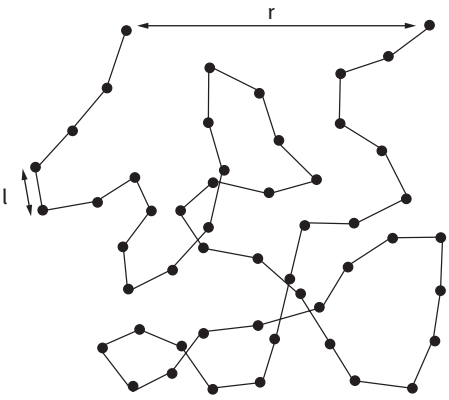

Fig. 11.10: Schematic representation of the chain conformation for a random coil.

account for these effects the above equations are modified by introducing a rigidity parameter p (stiffness "persistence") which depends on the architecture of the chain,

$$\langle r^2 \rangle^{1/2} = 6^{1/2} p^{1/2} N^{1/2} \ell, \tag{11.3}$$

$$\langle s^2 \rangle^{1/2} = p^{1/2} N^{1/2} \ell; \tag{11.4}$$

$p = 1/6$ for a (hypothetically) fully flexible chain and p increases as the chain becomes less flexible, for example when the side groups are bulky. Typical p values for real chains are in the range 0.5–4.

A useful parameter, called the characteristic ratio, was introduced by Flory [15] and is defined as,

$$C_\infty = \frac{\langle r^2 \rangle}{N \ell_b^2}; \tag{11.5}$$

ℓ_b^2 stands for the sum of the squares of the lengths of the backbone bonds of one monomer unit,

$$\ell_b^2 = \sum_i a_i^2. \tag{11.6}$$

The main consequence of the above equations is that for ideal chains the dimensions (root mean square end-to-end distance and radius of gyration) are proportional to $N^{1/2}$. This is only valid for ideal chains where the volume of the segments and solvency effects are entirely ignored. In other words, a walk may return to its origin without any hindrance. This is unrealistic for segments which occupy a volume. In good solvents where the chains swell the excluded volume becomes important. The segments cannot overlap and there is an exclusion volume that automatically leads to coil expansion. In very good solvents, where the segments repel each other the excluded volume is larger than the exclusion volume. In contrast, in a poor solvent the segments experience net attraction, the effective excluded volume is small and the ideal chain model gives a reasonable description.

In most synthetic methods for preparation of macromolecules the result is a mixture with various molar masses. Thus, one needs to characterize the molar mass distribution (that can be determined for example by gel permeation chromatography). If the molar mass is denoted by M, then the number density distribution function $p(M)$ and hence the fraction of polymer with molar mass $p(M)\,\mathrm{d}M$ in the range M to $M + \mathrm{d}M$ can be normalized by,

$$\int_0^\infty p(M)\,\mathrm{d}M = 1. \tag{11.7}$$

The number average molar mass is given by,

$$\bar{M}_\mathrm{n} = \int_0^\infty p(M)M\,\mathrm{d}M. \tag{11.8}$$

The weight average molar mass is given by,

$$\bar{M}_\mathrm{w} = \frac{\int_0^\infty p(M)M \cdot M\,\mathrm{d}M}{\int_0^\infty p(M)M\,\mathrm{d}M}. \tag{11.9}$$

The polydispersity coefficient U (which is a measure of polydispersity) is given by,

$$U = \frac{\bar{M}_\mathrm{w}}{\bar{M}_\mathrm{n}} - 1. \tag{11.10}$$

The molar mass distribution varies a great deal between different polymeric compounds. In step polymerization, where monomers react in such a way that groups which are linked together can be coupled with other groups, the molar mass distribution is broad. In chain polymerization, where reactive centres are created that react at the beginning and become shifted after the reaction to the new end of the chain, thus growing, a much narrower distribution is produced.

Large variations in the chemical structure can be obtained by a combination of different monomers. This procedure is referred to as copolymerization and produces statistical and block copolymers. In the first case, coupling is statistical and is determined by the probabilities of attachment of two monomers in a growing chain. The resulting polymer is sometimes referred as random copolymer. In the second case, the molecule is produced by coupling of long macromolecular sequences of uniform composition. Depending on the number of sequences, di-, tri- or multi-block copolymers may be prepared.

The above description refers to linear chains. However, several other structures that contain short or long chain branches are produced. These side chains can be short or long thus producing grafted chain polymers. A special type is that of star polymers where several polymer chains emanate from one common multifunctional centre.

As each macromolecule possesses a large number of internal degrees of freedom, the analysis of the properties of the individual polymer becomes an important point

of concern [15]. It is obvious that understanding single chain behaviour is a necessary prerequisite for treatment of aggregate properties. Phenomena that are dominated by intermolecular forces, such as the phase behaviour of binary polymer mixtures and the structure of polyelectrolyte solutions, are important for treatment of polymer solutions. Other important phenomena such as the viscoelasticity of most polymer solutions also deserve particular attention.

The conformational state of a single polymer chain can be considered in terms of its full steric structure. For example, a polymer chain like polyethylene possesses a great internal flexibility and is able to change its conformation totally. Basically, the number of degrees of freedom of the chain is given by three times the number of atoms and it is convenient to split them into two different groups [15, 20]. A first group concerns changes in valence angles and bond lengths, because they occur during molecular vibrations with frequencies in the infrared range. These movements are limited and do not affect the overall form of the chain. The second group of motions is of a different character, in that they have the potential to alter the form. These are the rotations about the C–C bond, which can convert the stretched chain into a coil and accomplish the transitions between all conformational states. In dealing with the conformational properties of a given polymer, only the latter group of degrees of freedom has to be considered.

The huge number of rotational isomeric states that a polymer chain may adopt becomes effective in fluid phase. Polymers in solution or the melt change between the different states and these are populated according to the law of Boltzmann statistics [5]. Because the large majority of conformations are coil-like, it is said that the polymers in fluid state represent random coils. Fig. 11.11 shows a polymer coil as it might look at limited resolution; a bent chain with a continuous appearance.

For the representation of the polymer coil, one can choose a curvilinear coordinate l from $l = 0$ to $l = l_{cr}$ at the other end and describe the varying local chain direction by unit vectors $e(l)$. The chains may be stiff, i.e. opposing strong bending, or highly flexible, thus facilitating coiling. The polymer chains possess, on length scale in the order of some nanometres, properties that are independent of the chemical structure. They may be grouped into two main classes, namely Gaussian or ideal chains (for van-

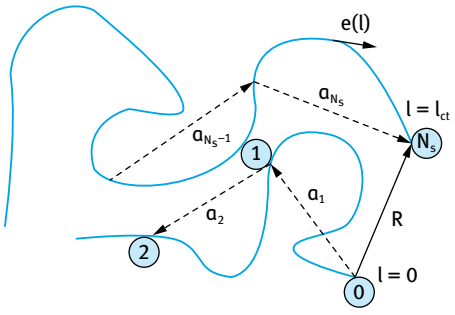

Fig. 11.11: Polymer chain in low resolution (contour length l_{cr}, local chain direction $e(l)$ together with an associated chain of N_S freely joined segments, connecting the junction points 0 to N_S) [20].

ishing excluded volume interactions) and expanded chain. This classification holds only for chains with large molar masses. Real chains with moderate molar masses often exhibit intermediate structures depending on the selected length scale. For example, chains can be expanded over their whole length but follow Gaussian statistics with parts, or chains can resemble straight rods for low molar masses and turn into ideal coils for high molar masses.

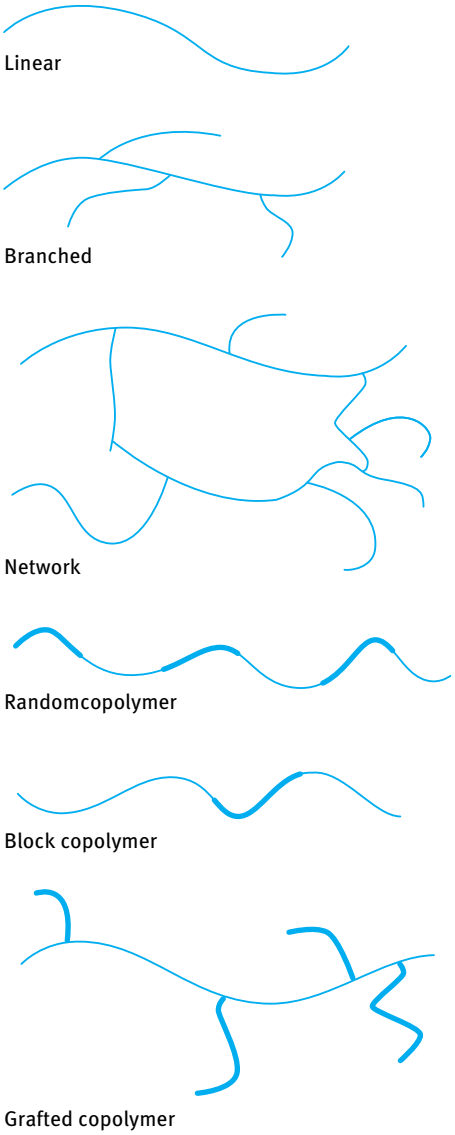

Fig. 11.12: Schematic representation of polymer structures.

The polymer properties are governed by the choice of monomers. The latter in the polymerization process constitute the repeat units, for example, acrylic acid is polymerized into poly(acrylic acid). A polymer can be linear, branched or crosslinked as is illustrated in Fig. 11.12 [5].

If the polymer is synthesized with more than one kind of polymer, it is called a copolymer (Fig. 11.12 (b)). The monomer units in a copolymer can be either

(i) randomly distributed;
(ii) distributed in blocks;
(iii) distributed such that one of the monomers is grafted in chains onto the backbone of the other monomer chain (graft copolymer) as illustrated in Fig. 11.12 (b).

The polarity of the monomer units is used to categorize the polymer:

(i) nonpolar polymers such as polystyrene and polyethylene;
(ii) polar, but water insoluble such as poly(methyl methacrylate);
(iii) water-soluble polymers such as polyethylene oxide and polyvinyl alcohol;
(iv) ionizable polymers, or polyelectrolytes, such as poly(acrylic acid).

The configuration of a polymer in solution depends on the balance between the interaction of the segments with the solvent and the interaction of the polymer segments with each other. As discussed above, a polymer can form a random coil or an extended configuration.

Dissolution of a polymer in a given solvent can be a problem, in particular at an industrial scale. Firstly, when the polymer is added to a solvent, the latter has to penetrate the polymer coil and finally the coil is swollen with the solvent forming a highly viscous and sticky mass (gel). The next step requires disentanglement of the chains from the gel resulting in the diffusion of the polymer chains into the solvent. This can be a slow process and it may take several hours or even days depending on the molar mass of the polymer and its chemical structure.

11.3.2 Free energy of mixing of polymer with solvent – the Flory–Huggins theory

The effect of solvency for the polymer chain has been considered in the thermodynamic treatment of Flory and Huggins [15–19], usually referred to as the Flory–Huggins theory. This theory considers the free energy of mixing of pure polymer with pure solvent, ΔG_{mix}, in terms of two contributions, namely the enthalpy of mixing, ΔH_{mix}, and the entropy of mixing, ΔS_{mix}, i.e. using the second law of thermodynamics,

$$\Delta G_{\text{mix}} = \Delta H_{\text{mix}} - T\Delta S_{\text{mix}}. \tag{11.11}$$

Assuming that the polymer chain adopts a configuration on a lattice (provided by solvent molecules) and considering that the mixing is "random", then the entropy

of mixing ΔS_{mix} is given by the following expression,

$$\Delta S_{\text{mix}} = -k[n_1 \ln \phi_1 + n_2 \ln \phi_2], \tag{11.12}$$

where k is the Boltzmann constant, n_1 is the number of solvent molecules with a volume fraction ϕ_1 and n_2 is the number of polymer molecules with a volume fraction ϕ_2.

The enthalpy of mixing, ΔH_{mix}, is given by the following expression,

$$\Delta H_{\text{mix}} = n_1 \phi_2 \chi kT, \tag{11.13}$$

where χ is a dimensionless interaction parameter and χkT expresses the difference in energy of a solvent molecule in pure solvent compared to its immersion in pure polymer. χ is usually referred to as the Flory–Huggins interaction parameter.

Combining equations (11.11)–(11.13), one obtains,

$$\Delta G_{\text{mix}} = kT[n_1 \ln \phi_1 + n_2 \ln \phi_2 + \chi n_1 \phi_2]. \tag{11.14}$$

The mixing of a pure solvent with a polymer solution creates an osmotic pressure, π, which can be expressed in terms of the polymer concentration c_2 and the volume fraction of the polymer,

$$\frac{\pi}{C_2} = RT\left[\frac{1}{M_2} + \left(\frac{v_2^2}{V_1}\right)\left(\frac{1}{2} - \chi\right)c_2 + \cdots\right], \tag{11.15}$$

where v_2 is the partial specific volume of the polymer ($v_2 = V_2/M_2$) and V_1 is the molar volume of the solvent.

The second term in equation (11.15) is the second virial coefficient B_2, i.e.,

$$\frac{\pi}{c_2} = RT\left[\frac{1}{M_2} + B_2 + \cdots\right], \tag{11.16}$$

$$B_2 = \left(\frac{v_2^2}{V_1}\right)\left(\frac{1}{2} - \chi\right). \tag{11.17}$$

Note that $B_2 = 0$ when $\chi = 1/2$, i.e. the polymer behaves as ideal in mixing with the solvent. This condition was termed by Flory [16] as the θ-point. Under these conditions, the polymer chains in solution have no repulsion or attraction or they adopt their unperturbed dimension. Clearly, when $\chi < 1/2$, B_2 is positive and mixing is non-ideal leading to positive deviation (repulsion); this occurs when the polymer chains are in "good" solvent conditions. In contrast, when $\chi > 1/2$, B_2 is negative and mixing is non-ideal leading to negative deviation (attraction); this occurs when the polymer chains are in "poor" solvent conditions (precipitation of the polymer may occur under these conditions). Since the polymer solvency depends on temperature, one can also define a theta temperature θ at which $\chi = 1/2$.

The function $[(1/2) - \chi]$ can also be expressed in terms of two mixing parameters, an enthalpy parameter κ_1 and an entropy parameter ψ_1, i.e.,

$$\left(\frac{1}{2} - \chi\right) = \kappa_1 - \psi_1. \tag{11.18}$$

The θ-temperature can also be defined in terms of κ_1 and ψ_1,

$$\theta = \frac{\kappa_1 T}{\psi_1}. \tag{11.19}$$

Alternatively, one can write,

$$\left(\frac{1}{2} - \chi\right) = \psi_1\left(1 - \frac{\theta}{T}\right). \tag{11.20}$$

The θ-temperature is an important parameter which describes a polymer-solvent system. At this temperature a polymer segment will not be able to tell whether it is in contact with another segment or a solvent molecule. The polymer will have the configuration it would have in its own liquid or it said to be in its "unperturbed dimension". In normal solvents the solvent quality increases as the temperature is raised (due to the larger thermal energy) and hence each polymer segment will have a tendency to be in contact with the solvent molecules rather in contact with the polymer's own segments. Thus, the polymer will expand its configuration. On the other hand, at temperatures below the θ-temperature, the polymer segments prefer to be in contact with other polymer segments rather than with the solvent molecules. Thus, the polymer will contract. The θ-temperature is also called the Flory temperature and the solvent or solvent mixture, at this temperature, is called a θ-solvent.

One can define an expansion or contraction parameter α that is given by,

$$\alpha = \frac{R_G}{R_G^0}, \tag{11.21}$$

where R_G^0 is the radius of gyration at the θ-temperature.

Although the Flory–Huggins theory is sound in principle, several experimental results cannot be accounted for. For example, it was found that the χ parameter depends on the polymer concentration in solution. Most serious is the fact that many polymer solutions (such as PEO) show phase separation on heating, when the theory predicts that it should happen only on cooling. Another complication arises from specific interaction with the solvent, e.g. hydrogen bonding between polymer and solvent molecules (e.g. with PEO and PVA in water). Also aggregation in solution (lack of complete dissolution) may present another problem.

The derivation of the Flory–Huggins equation was carried out under the assumption that volume changes occurring upon mixing of polymer and solvent are negligible. As discussed above, the free volume concept must be considered. This predicts that near the critical point, where phase separation occurs, there are no bonds between the molecules constraining the separation of solvent molecules. They are, however, present for the segments of polymer molecules. Hence, upon heating a polymer solution, the increase in free volume for the solvent is large, and much larger than that for the polymer. This difference in free volume creates a large difference in the coefficient of expansion between the polymer and solvent and this leads to phase separation on heating.

Prigogine et al. [17] introduced the concept of the effect of free volume dissimilarity by their theory of solutions and they questioned the association of the χ parameter with heat of mixing only. This led Flory and co-workers [15, 16] to introduce some additional concepts. They pointed out that although a solution of a polymer in a chemically similar solvent would have no contact dissimilarities, it would have them due to the differences in length and size of the polymer chains. This means that the volume changes taking place during mixing, V_M, could not be neglected.

The Flory–Huggins theory only applies for ideal linear polymers. It fails to describe the properties of polymers with a structure having high monomer density such as two- and three-dimensional branched polymers. It has been found that the theta temperature of star-branched polymers is generally lower than that of linear polymers and it also depends on the length of the arms [15, 16].

Another limitation of the Flory–Huggins theory is its applicability to polymers in aqueous solutions. Firstly, water produces strong specific interaction between the polymer and water molecules, mostly by hydrogen bonds. Secondly, complete dissolution of the polymer in water is questionable due to the aggregation of the molecules. For these reasons, the Flory–Huggins theory has been found not to be applicable for polymers such as poly(ethylene oxide) (PEO) or polyvinyl alcohol (PVA) which are known to form strong hydrogen bonds between the ethylene oxide or vinyl alcohol units and water. For example, colorimetric measurements showed that at low PEO concentrations each EO unit is hydrogen bonded to two water molecules, whereas at high PEO concentrations, the number of hydrogen bonds is significantly reduced to one water molecule per two EO units.

The solution properties of copolymers are much more complicated. This is due to the fact that the two copolymer components A and B behave differently in different solvents. Only when the two components are both soluble in the same solvent, then they exhibit similar solution properties. This is the case for example for a nonpolar copolymer in a nonpolar solvent. Dilute solutions of copolymers in solvents that are good for both components exhibit similar behaviour to homopolymer chains, resulting from interactions with solvent molecules and each other. Two possible models for copolymers have been proposed. The first one, called the segregated model, assumes that there are only a few hetero-contacts, and the two different polymer components behave like homopolymer chains. The second model, referred to as random structure model, takes into account some overlap between different blocks creating hetero-contacts between unlike segments. Several techniques can be applied to study the possible configurations of copolymer components in solution. Most studies have been carried out for block copolymers either in good solvents or θ-solvents for the blocks. For example, light scattering, viscosity and GPC studies were carried out for polystyrene-block-polyisoprene copolymers in methyl isobutylketone as the solvent. The solvent is a near θ-solvent for these polymers. The results showed segregated conformation for the block copolymer with a limited number of hetero-contacts. Small angle neutron scattering studies for polystyrene-block–poly(methylmethacrylate) in

toluene showed that the poly(methylmethacrylate) block is in a tightly coiled conformation, surrounded by a slightly expanded polystyrene shell.

In a selective solvent, whereby the medium is a good solvent for one component, say A, and a poor solvent for the second component B, one part of the amphipathic block or graft separate as a distinct phase, while the other stays in solution. The insoluble portion of the amphipathic copolymer will aggregate reversibly to form micelles. It is believed that the polymeric micelles are spherical and have a narrow particle size distribution. Thus micelle formation in block and graft copolymers is analogous to small molecule surface active materials. For graft copolymers in selective solvents, the formation of "molecular micelles" has been observed. These resembled particles with an insoluble swollen core surrounded by a sheath of soluble chains. Depending on the concentration of solution, the temperature and the nature of the solvent, multimolecular aggregates are observed. A schematic representation of monomolecular and multimolecular micelles is shown in Fig. 11.13.

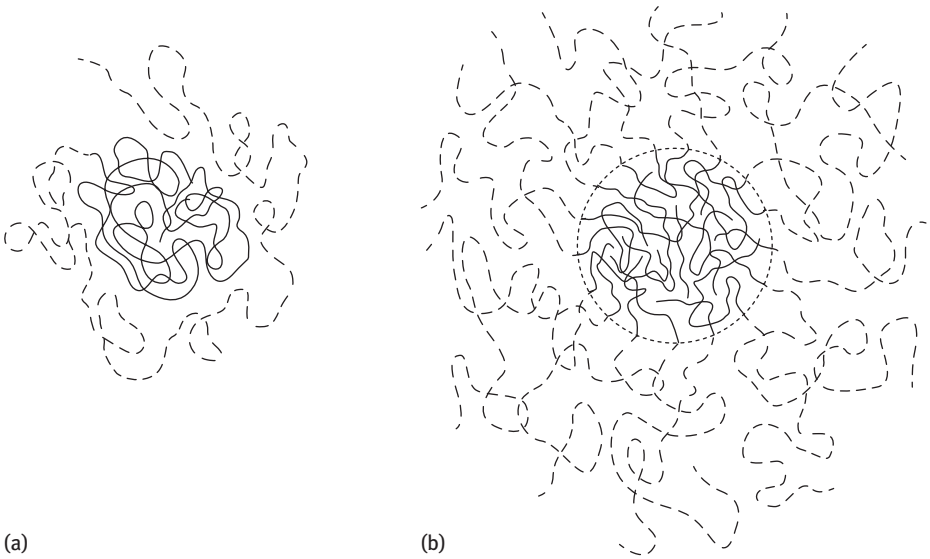

Fig. 11.13: Schematic representation of monomolecular (a) and multimolecular (b) micelles.

The critical micelle concentration (cmc) of these block and graft copolymers is usually very low. Because of the relatively high molecular weight of block and graft copolymers (when compared with simple surfactants), the concentrations of these materials have to be very low in order to precisely determine their cmc. Even at the cmc, the solution does not only contain micellar aggregates, but also single molecules over a very large range of concentrations. Similar to simple surfactants, the cmc can be determined using surface tension (γ) versus concentration measurements. From plots of

γ versus log C one can obtain the cmc. γ decreases with increasing log C until the cmc is reached and then γ remains constant. Since with most block and graft copolymers the molecular weight is not sufficiently narrow, calculation of C in mol dm^{-3} is not straightforward and hence C is usually expressed in wt%.

Several methods may be applied to obtain the micellar size and shape of block and graft copolymers, of which light scattering, small angle X-ray and neutron scattering are probably the most direct. Dynamic light scattering (photon correlation spectroscopy) can also be applied to obtain the hydrodynamic radius of the micelle. This technique is relatively easy to perform when compared with static light scattering, since it does not require rigorous preparation of the samples.

11.3.3 Viscosity measurements for characterization of a polymer in solution

A convenient way to characterize a polymer in solution at low concentrations is to measure the viscosity using capillary viscometry. The most widely used capillary viscometer is the Ostwald type shown schematically in Fig. 11.14. A variant of the Ostwald viscometer is the Cannon–Fenske type which is more convenient to use (Fig. 11.14).

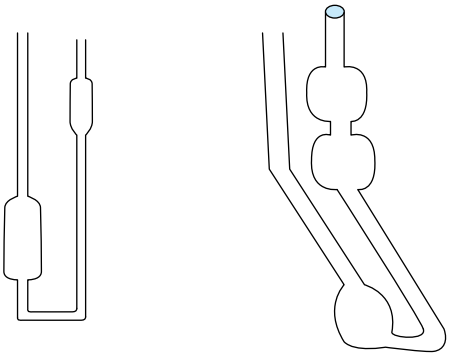

Ostwald viscometer Cannon–Fenske viscometer

Fig. 11.14: Schematic pictures of Ostwald and Cannon–Fenske viscometers.

In capillary viscometry, one measures the volumetric flow Q (m^3 s^{-1}) and the viscosity η is calculated using the Poiseulle equation [21],

$$\eta = \frac{\pi R^4 p}{8QL}. \tag{11.22}$$

R is the tube radius with length L; p is the pressure drop = $h\rho g$ (where h is the liquid height with density ρ and g is the acceleration due to gravity).

One usually compares the viscosity of the liquid in question η_2 with that of a liquid with known viscosity η_1. In this way, one can measure the flow rates of the two liquids using the same viscometer with a bulb of volume V (the flow rate is simply given by V divided by the time taken for the liquid to flow between the two marks on the viscometer t_1 and t_2 for the two liquids).

Using equation (11.22) one simply obtains,

$$\frac{\eta_1}{\eta_2} = \frac{t_1\rho_1}{t_2\rho_2}. \tag{11.23}$$

t_1 and t_2 are simply measured using a stopwatch (for automatic viscometers two fiber optics are used). Accurate temperature control is necessary (±0.01 °C). The flow time t must also be measured with an accuracy of ±0.01 s.

For measurement of the intrinsic viscosity $[\eta]$ of polymers which can be used to obtain the molecular weight and solvation of the polymer chains, one measures the relative viscosity η_r as a function of polymer concentration C (in the range 0.01–0.1 %).

$$\eta_r = \frac{\eta_s}{\eta_0}, \tag{11.24}$$

where η_s is the viscosity of the polymer solution and η_0 is that of the solvent.

From η_r one can obtain the reduced viscosity η_{red}

$$\eta_{red} = (\eta_r - 1). \tag{11.25}$$

From η_{red} one can obtain the specific viscosity η_{sp}

$$\eta_{sp} = \frac{\eta_{red}}{C}. \tag{11.26}$$

A plot of η_{sp} versus C gives a straight line that can be extrapolated to $C = 0$ to obtain the intrinsic viscosity $[\eta]$. This is illustrated in Fig. 11.15.

From $[\eta]$ one can obtain the molecular weight M using the Mark–Houwink equation

$$[\eta] = KM^{\alpha}, \tag{11.27}$$

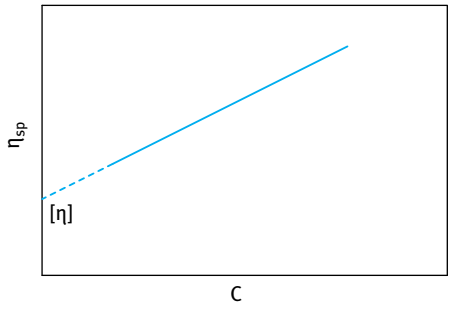

Fig. 11.15: Measurement of intrinsic viscosity of polymers.

where K and α are constants for a particular polymer and solvent (values for many polymer-solvent systems are tabulated in the Polymer Handbook). α is related to the solvency of the medium for the polymer chain. In a good solvent $\alpha > 0.5$; it has values in the range 0.5–0.8. The higher the value of α, the better the solvent for the chain.

11.3.4 Phase separation of polymer solutions

When dissolving two liquids, the molecules are free to move and hence the entropy for a liquid mixture is large. In contrast, when dissolving a polymer in a solvent, a segment of the polymer is attached to several other segments and hence the entropy of a single segment with a free solvent molecule is much less when compared with mixing two solvents [5]. Therefore, polymer solutions have lower total entropy and hence are less stable and more prone to phase separation when compared to mixtures of ordinary liquids. This was quantified by Flory and Huggins [15–19] as discussed above. The Flory–Huggins theory predicts that a solution with a higher molar mass is less stable towards phase when compared with a solution of the same polymer but with a lower molar mass. Hence, when a polymer phase separates in solution, the high molar mass species will separate out first, leaving the lower molar mass species in solution. This phenomenon is used for fractionation of polymer samples with respect to molar mass.

The temperature at which phase separation occurs for 1% solution is called the cloud point, due to the increased turbidity of the polymer solution as this temperature is reached. The highest, or lowest, temperature where a phase separation occurs is called the critical temperature and the corresponding polymer concentration is called the critical composition. The question of whether or not a polymer dissolves in a solvent is a matter of balance between the entropy and enthalpy of mixing. The entropy of mixing, which is low for polymers in solution, favours mixing. The enthalpy of mixing, which is a measure of the interaction energy between a segment and solvent molecule when compared with the interaction energy between segments and solvent molecule alone, is positive and it opposes mixing of the two components. In ordinary polymer/solvent systems, the stability with regard to phase separation will decrease with decreasing temperature. In this case, phase separation occurs when the temperature is sufficiently lowered and a concentrated polymer phase will be in equilibrium with a dilute polymer solution. Phase separation in this case can also occur by adding a nonsolvent to the polymer-solvent system.

However, some aqueous polymer solutions, whereby the polymer chain contains a polyoxyethylene oxide (PEO) chain, show phase separation when the temperature is increased. At very high temperatures, the two-phase region diminishes and the system is homogeneous again. This is due to the increased thermal energy that counteracts other forces at play. Thus, these polymer solutions show a low and upper critical solution temperature.

11.3.5 Solubility parameter concept for selecting the right solvent for a polymer

The solubility parameter is based on the assumption that "like dissolves like". A polymer is not soluble in certain liquids due to a large difference in the interaction between segments of the polymer and solvent molecules when compared to the interaction energy between segment-segment and solvent-solvent molecules. To achieve some solubility the segment-solvent interaction energy should be as close as possible to the interaction energy between the segment-segment and solvent-solvent molecules. One method for measuring the interaction energies is to obtain the enthalpy of vapourization, ΔH_{vap}, which reflects the cohesive forces in the liquid. This concept was introduced by Hildebrand [22] who defined the cohesive energy ratio or solubility parameter δ by dividing ΔH_{vap} by the molar volume V,

$$\delta^2 = \frac{\Delta H_{vap}}{V}. \tag{11.28}$$

The units for the solubility parameter are $cal^{1/2}\,cm^{-3/2}$ or $J^{1/2}\,m^{-3/2}$ (= $MPa^{1/2}$). Values of solubility parameters for various polymer-solvent systems are given in the book by Barton [23]. In order to find a suitable solvent for a polymer one should first find the solubility parameter of the polymer and then select solvents that have solubility parameters that are close to that of the polymer. For example, polystyrene has a solubility parameter of 9.1 $cal^{1/2}\,cm^{-3/2}$ and suitable solvents are cyclohexane ($\delta = 8.2$), benzene ($\delta = 9.2$) and methyl ethyl ketone ($\delta = 9.3$). In contrast n-hexane ($\delta = 7.3$) and ethanol ($\delta = 12.7$) are nonsolvents, i.e. they do not dissolve polystyrene.

Hansen [24] subdivided δ^2 into three contributions: δ_d^2 (dispersion), δ_p^2 (polar) and δ_p^2 (hydrogen bonding),

$$\delta^2 = \delta_d^2 + \delta_p^2 + \delta_h^2. \tag{11.29}$$

Several theories and computations are available for calculating the above contributions for various polymer and solvent systems.

References

[1] Tadros T. Applied surfactants. Weinheim: Wiley-VCH; 2005.
[2] Tadros TF. In: Goddard ED, Gruber JV, editors. Principles of polymer science and technology in cosmetics and personal care. New York: Marcel Dekker; 1999.
[3] Tadros T. In: Holmberg K, editor. Novel Surfactants, New York: Marcel Dekker; 2003.
[4] Piirma I. Polymeric surfactants. Surfactant Science Series, No. 42. New York: Marcel Dekker; 1992.
[5] Holmberg K, Jonsson B, Kronberg B, Lindman B. Surfactants and polymers in aqueous solution. Chichester: John Wiley & Sons Ltd.; 2003.
[6] von Rybinski W, Hill K. Alkyl polyglucosides. In: Holmberg K, editor. Novel Surfactants. New York: Marcel Dekker; 2003.
[7] Stevens CV, Meriggi A, Peristerpoulou M, Christov PP, Booten K, Levecke B, Vandamme A, Pittevils N, Tadros TF. Biomacromolecules. 2001;2:1256.

[8] Hirst EL, McGilvary DI, Percival EG. J Chem Soc. 1950:1297.
[9] Suzuki M. In: Suzuki M, Chatterton NJ, editors. Science and technology of fructans. Boca Raton: CRC Press; 1993. p. 21.
[10] Tadros TF, Vandamme A, Levecke B, Booten K, Stevens CV. Advances Colloid Interface Sci. 2004;108–109:207.
[11] McClements DJ, Gumus CE. Advances Colloid and Interface Sci. 2016;234:3.
[12] Fleute-Schlachter I, Feldman-Krane G. Silicone surfactants. In: Holmberg K, editor. Novel Surfactants. New York: Marcel Dekker; 2003.
[13] Barrett KEJ and Thomas HR. J Polym Sci Part A1. 1969;7:2627.
[14] Guyot A. Polymerizable surfactants. In: Holmberg K, editor. Novel Surfactants. New York: Marcel Dekker; 2003.
[15] Flory PJ. Statistical mechanics of chain molecules. New York: Interscience; 1969.
[16] Flory PJ. Principles of polymer chemistry. New York: Cornell University Press; 1953.
[17] Prigogine I, Trappeniers N, Mathos V. Discussions Faraday Soc. 1953;15:93.
[18] Eichinger BE, Flory PJ. Trans Faraday Soc. 1968;64:2035, 2053, 2061, 2066.
[19] Flory PJ, Ellenson JL, Eichinger E. Macromolecules. 1968;1:279.
[20] Strobel G. The physics of polymers. 3rd edition. Berlin: Springer; 2007.
[21] Tadros T. Rheology of Dispersions. Weinheim: Wiley-VCH; 2010.
[22] Hildebrand JH. Solubility of non-electrolytes. 2nd edition. New York: Reinhold; 1936.
[23] Barton AFM. Handbook of solubility prameters and other cohesive parameters. New York: CRC Press; 1983.
[24] Hansen CM. J Paint Technol. 1967;39:505.

12 Adsorption and conformation of polymeric surfactants at interfaces

12.1 Introduction

Nonionic and polymeric surfactants are essential materials for preparation of many colloidal dispersions, of which we mention dyestuffs, paper coatings, inks, agrochemicals, pharmaceuticals, personal care products, ceramics and detergents [1–3]. One of the most important applications of nonionic polymeric surfactants is in the preparation of oil-in-water (O/W) and water-in-oil (W/O) emulsions as well as solid/liquid dispersions [1–3]. In this case, the hydrophobic portion of the surfactant molecule should adsorb "strongly" at the O/W interface or become dissolved in the oil phase, leaving the hydrophilic components in the aqueous medium, whereby they become strongly solvated by the water molecules.

Since surfactant adsorption is reversible, the molecules are seldom strongly adsorbed at the interface and this may result in limited stability of the colloidal dispersion. The most effective stabilizers are polymeric surfactants of the A–B, A–B–A block and BA_n (or AB_n) graft copolymer types. In these polymeric surfactants, the chain B (referred to as the "anchor" chain) is chosen to be highly insoluble in the medium and to have a strong affinity to the surface. The chain(s) A (referred to as the "stabilizing chains") are chosen to be highly soluble in the medium and strongly solvated by its molecules. To understand the role of polymeric surfactants, it is necessary to consider the adsorption and conformation of the molecules at the interface and this is the main subject of the present chapter. Besides knowledge of the parameters that determine the adsorption process, namely chain-surface, chain-solvent and surface-solvent interactions, one of the most important effects is the conformation of the polymeric surfactant molecules at the interface. This is key to understanding how polymeric surfactants can be applied as stabilizers for disperse systems as will be discussed in Chapter 13.

For stabilization of emulsions and suspensions against flocculation, coalescence and Ostwald ripening the following criteria must be satisfied:

(i) Complete coverage of the droplets or particles by the polymeric surfactant. Any bare patches may result in flocculation as a result of van der Waals attraction or bridging.
(ii) Strong adsorption (or "anchoring") of the surfactant molecule to the surface of the droplet or particle.
(iii) Strong solvation (hydration) of the stabilizing chain to provide effective steric stabilization.
(iv) Reasonably thick adsorbed layer to prevent weak flocculation [1–3].

https://doi.org/10.1515/9783110540895-013

As mentioned above, most of the above criteria for stability are best served by using polymeric surfactants of the A–B, A–B–A block and BA_n (or AB_n) graft types, that were described in detail in Chapter 11, as they are the most efficient for stabilization of emulsions and suspensions. These block and graft copolymers are ideal for preparation of concentrated emulsions and suspensions, which are needed in many industrial applications.

In this chapter, I will discuss in detail the adsorption of polymeric surfactants at interfaces and their conformation. The theories of polymer adsorption will be discussed highlighting the most important parameters that affect polymer adsorption. The experimental techniques that can be applied to determine the various adsorption parameters will be described. This is then followed by a section on examples of polymeric surfactant adsorption at interfaces.

12.2 Polymers at interfaces

As mentioned above, understanding the adsorption and conformation of polymeric surfactants at interfaces is key to knowing how these molecules act as stabilizers. Most basic ideas on adsorption and conformation of polymers have been developed for the solid/liquid interface [4]. The first theories on polymer adsorption were developed in the 1950s and 1960s, with extensive developments in the 1970s. The process of polymer adsorption is fairly complicated. In addition to the usual adsorption considerations such as polymer/surface, polymer/solvent and surface/solvent interactions, one of the principal problems to be resolved is the configuration (conformation) of the polymer at the solid/liquid interface. This was recognized by Jenkel and Rumbach in 1951 [5] who found that the amount of polymer adsorbed per unit area of the surface would correspond to a layer more than 10 molecules thick if all the segments of the chain are attached. They suggested a model in which each polymer molecule is attached in sequences separated by bridges which extend into solution. In other words, not all the segments of a macromolecule are in contact with the surface. The segments which are in direct contact with the surface are termed “trains”; those in between and extending into solution are termed “loops”; the free ends of the macromolecule also extending into solution are termed “tails”. This is illustrated in Fig. 12.1 (a) for a homopolymer. Examples of homopolymers that are formed from the same repeating units are poly(ethylene oxide) or poly(vinyl pyrrolidone). These homopolymers have little surface activity at the O/W interface, since the homopolymer segments (ethylene oxide or vinylpyrrolidone) are highly water soluble and have little affinity to the interface. However, such homopolymers may adsorb significantly at the S/L interface. Even if the adsorption energy per monomer segment to the surface is small (fraction of kT, where k is the Boltzmann constant and T is the absolute temperature), the total adsorption energy per molecule may be sufficient to overcome the unfavourable entropy loss of the molecule at the S/L interface.

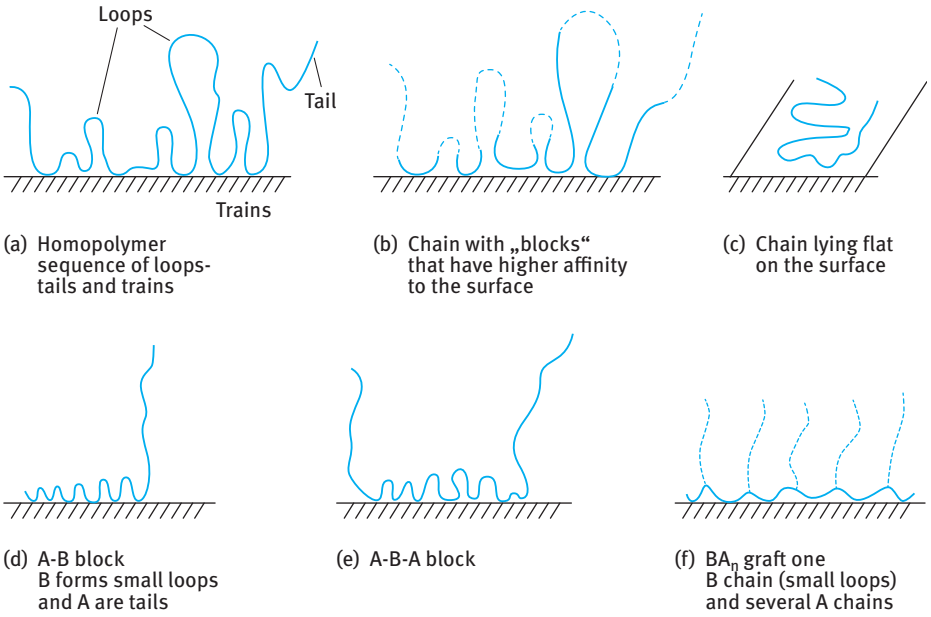

Fig. 12.1: Various conformations of macromolecules on a plane surface.

Clearly, homopolymers are not the most suitable emulsifiers or dispersants. A small variant is to use polymers that contain specific groups that have high affinity to the surface. This is exemplified by partially hydrolysed poly(vinyl acetate) (PVAc), technically referred to as poly(vinyl alcohol) (PVA). The polymer is prepared by partial hydrolysis of PVAc, leaving some residual vinyl acetate groups. Most commercially available PVA molecules contain 4–12 % acetate groups. These acetate groups, which are hydrophobic, give the molecule its amphipathic character. On a hydrophobic surface such as polystyrene, the polymer adsorbs with preferential attachment of the acetate groups on the surface, leaving the more hydrophilic vinyl alcohol segments dangling in the aqueous medium. The configuration of such "blocky" copolymers is illustrated in Fig. 12.1 (b). Clearly, if the molecule is made fully from hydrophobic segments, the chain will adopt a flat configuration as illustrated in Fig. 12.1 (c).

The most convenient polymeric surfactants are those of the block and graft copolymer type. A block copolymer is a linear arrangement of blocks of variable monomer composition. The nomenclature for a diblock is poly-A-block–poly-B and for a triblock is poly-A-block–poly-B–poly-A. An example of an A–B diblock is polystyrene block–polyethylene oxide and its conformation is represented in Fig. 12.1 (d). One of the most widely used triblock polymeric surfactants are the "Pluronics" (BASF, Germany) which consists of two poly-A blocks of poly(ethylene oxide) (PEO) and one block of poly(propylene oxide) (PPO). Several chain lengths of PEO and PPO are available. More recently, triblocks of PPO–PEO–PPO (inverse Pluronics) became available for

some specific applications. These polymeric triblocks can be applied as emulsifiers or dispersants, whereby the assumption is made that the hydrophobic PPO chain resides at the hydrophobic surface, leaving the two PEO chains dangling in aqueous solution and hence providing steric repulsion. Several other triblock copolymers have been synthesized, although these are of limited commercial availability. Typical examples are triblocks of poly(methyl methacrylate)–block poly(ethylene oxide)–block poly(methyl methacrylate). The conformation of these triblock copolymers is illustrated in Fig. 12.1 (e). An alternative (and perhaps more efficient) polymeric surfactant is the amphipathic graft copolymer consisting of a polymeric backbone B (polystyrene or polymethyl methacrylate) and several A chains ("teeth") such as polyethylene oxide. This graft copolymer is sometimes referred to as a "comb" stabilizer. Its configuration is illustrated in Fig. 12.1 (f).

The polymer/surface interaction is described in terms of adsorption energy per segment χ^s. The polymer/solvent interaction is described in terms of the Flory–Huggins interaction parameter χ. For adsorption to occur, a minimum energy of adsorption per segment χ^s is required. When a polymer molecule adsorbs on a surface, it loses configurational entropy and this must be compensated by an adsorption energy χ^s per segment. This is schematically shown in Fig. 12.2, where the adsorbed amount Γ is plotted versus χ^s. The minimum value of χ^s can be very small ($< 0.1\,kT$) since a large number of segments per molecule are adsorbed. For a polymer with say 100 segments and 10 % of these are in trains, the adsorption energy per molecule now reaches $1\,kT$ (with $\chi^s = 0.1\,kT$). For 1000 segments, the adsorption energy per molecule is now $10\,kT$.

As mentioned above, homopolymers are not the most suitable for stabilization of dispersions. For strong adsorption, one needs the molecule to be "insoluble" in the medium and to have strong affinity ("anchoring") to the surface. For stabilization, one needs the molecule to be highly soluble in the medium and strongly solvated by its molecules; this requires a Flory–Huggins interaction parameter less than 0.5.

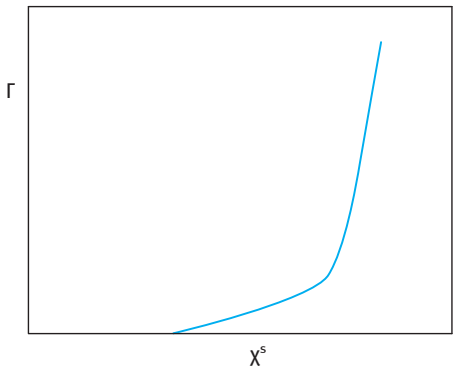

Fig. 12.2: Variation of adsorption amount Γ with adsorption energy per segment χ^s.

The above opposing effects can be resolved by introducing "short" blocks in the molecule which are insoluble in the medium and have a strong affinity to the surface, as for example partially hydrolysed polyvinyl acetate (88 % hydrolysed, i.e. with 12 % acetate groups), usually referred to as polyvinyl alcohol (PVA),

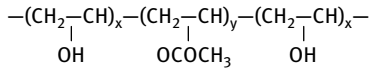

As mentioned above, these requirements are better satisfied using A–B, A–B–A and BA_n graft copolymers. B is chosen to be highly insoluble in the medium and it should have high affinity to the surface. This is essential to ensure strong "anchoring" to the surface (irreversible adsorption). A is chosen to be highly soluble in the medium and strongly solvated by its molecules. The Flory–Huggins χ parameter can be applied in this case. For a polymer in a good solvent, χ has to be lower than 0.5; the smaller the χ value the better the solvent for the polymer chains. Examples of B for hydrophobic particles in aqueous media are polystyrene, polymethylmethacrylate. Examples of A in aqueous media are polyethylene oxide, polyacrylic acid, polyvinyl pyrrolidone and polysaccharides. For nonaqueous media such as hydrocarbons, the A chain(s) could be poly(12-hydroxystearic acid).

For a full description of polymer adsorption one needs to obtain information on the following:

(i) The amount of polymer adsorbed Γ (in mg or mol) per unit area of the particles. It is essential to know the surface area of the particles in the suspension. Nitrogen adsorption on the powder surface may give such information (by application of the BET equation) provided there will be no change in area on dispersing the particles in the medium. For many practical systems, a change in surface area may occur on dispersing the powder, in which case one has to use dye adsorption to measure the surface area (some assumptions have to be made in this case).

(ii) The fraction of segments in direct contact with the surface, i.e. the fraction of segments in trains p (p = (number of segments in direct contact with the surface)/total number).

(iii) The distribution of segments in loops and tails, $\rho(z)$, which extend in several layers from the surface. $\rho(z)$ is usually difficult to obtain experimentally although recently application of small angle neutron scattering could obtain such information.

An alternative and useful parameter for assessing "steric stabilization" is the hydrodynamic thickness, δ_h (thickness of the adsorbed or grafted polymer layer plus any contribution from the hydration layer). Several methods can be applied to measure δ_h as will be discussed below.

12.3 Theories of polymer adsorption

Two main approaches have been developed to treat the problem of polymer adsorption:

(i) Random walk approach. This is based on Flory's treatment of the polymer chain in solution; the surface was considered as a reflecting barrier.
(ii) Statistical mechanical approach. The polymer configuration was treated as being made of three types of structures, trains, loops and tails, each having a different energy state.

The random walk approach is based on the random walk concept which was originally applied to the problem of diffusion and later adopted by Flory to deduce the conformations of macromolecules in solution. The earliest analysis was by Simha, Frisch and Eirich [6] who neglected excluded volume effects and treated the polymer as a random walk. Basically, the solution was represented by a three-dimensional lattice and the surface by a two-dimensional lattice. The polymer was represented by a realization of a random walk on the lattice. The probabilities of performing steps in different directions were considered to be the same except at the interface which acts as a reflecting barrier. The polymer molecules were, therefore, effectively assumed to be adsorbed with large loops protruding into the solvent and with few segments actually attached to the surface, unless the segment-surface attractive forces were very high. This theory predicts an isotherm for flexible macromolecules that is considerably different from the Langmuir-type isotherm. The number of attached segments per chain is proportional to $n^{1/2}$, where n is the total number of segments. Increasing the molecular weight results in increased adsorption, except for strong chain interaction with the surface.

This approach has been criticized by Silberberg [7] and by Di Marzio [8]. One of the major problems was the use of a reflecting barrier as the boundary condition, which meant over counting the number of distinguishable conformations. To overcome this problem, Di Marzio and McCrackin [9] used a Monte Carlo method to calculate the average number of contacts of the chain with the surface, the end-to-end length and distribution of segments $\rho(z)$ with respect to the distance z from the surface, as a function of chain length of the polymer and the attractive energy of the surface. The same method was also used by Clayfield and Lumb [10, 11].

The statistical mechanical approach is a more realistic model for the problem of polymer adsorption since it takes into account the various interactions involved. This approach was first used by Silberberg [12] who treated separately the surface layer, which contains adsorbed units (trains), and the adjacent layer in solution (loops or tails). The units in each layer were considered to be in two different energy states and partition functions were used to describe the system. The units close to the surface are adsorbed with an internal partition function determined by the short-range forces between the segments and the surface, whereas the units in loops and tails were con-

sidered to have an internal partition function equivalent to the segments in the bulk. By equating the chemical potential of macromolecules in the adsorbed state and in bulk solution, the adsorption isotherm could be determined. In this treatment, Silberberg [12] assumed a narrow distribution of loop sizes and predicted small loops for all values of the adsorption energy. Later, the loop size distribution was introduced by Hoeve et al. [13–15] and this theory predicted large loops for small adsorption free energies and small loops and more units adsorbed for larger adsorption free energies when the chains are sufficiently flexible. Most of these theories considered the case of an isolated polymer molecule at an interface, i.e. under conditions of low surface coverage, θ. These theories were extended by Silberberg [16] and Hoeve [17, 18] to take into account the lateral interaction between the molecules on the surface, i.e. high surface coverage. These theories also considered the excluded volume effect, which reduces the number of configurations available for interacting chains near the surface. Excluded volume effects are strongly dependent on the solvent, as is the case for chains in solution. Some progress has been made in the analysis of the problem of multilayer adsorption [17, 18].

One feature of an adsorbed layer that is important in the theory of steric stabilization is the actual segment distribution normal to the interface. Hoeve [17, 18] was the first to calculate this quantity for an adsorbed homopolymer of loops and tails, using random flight statistics. He showed that at a distance from the interface corresponding to the thickness of the trains, there was a discontinuity in the distribution. Beyond this the segment density falls exponentially with distance, as shown schematically in Fig. 12.3.

Similarly, Meier [19] developed an equation for the segment density distribution of a single terminally adsorbed tail. Hesselink [20, 21] has developed Meier's theory and given the segment density distribution for single tails, single loops, homopolymers and random copolymers, as illustrated in Fig. 12.4.

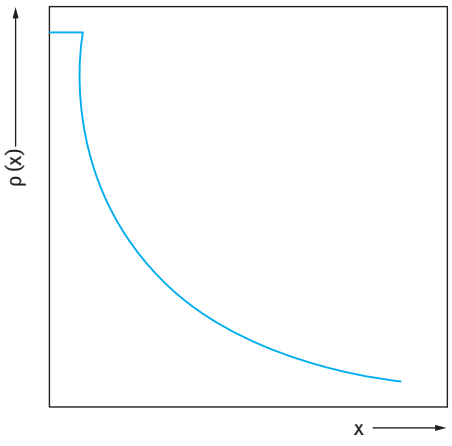

Fig. 12.3: Segment density–distance distribution.

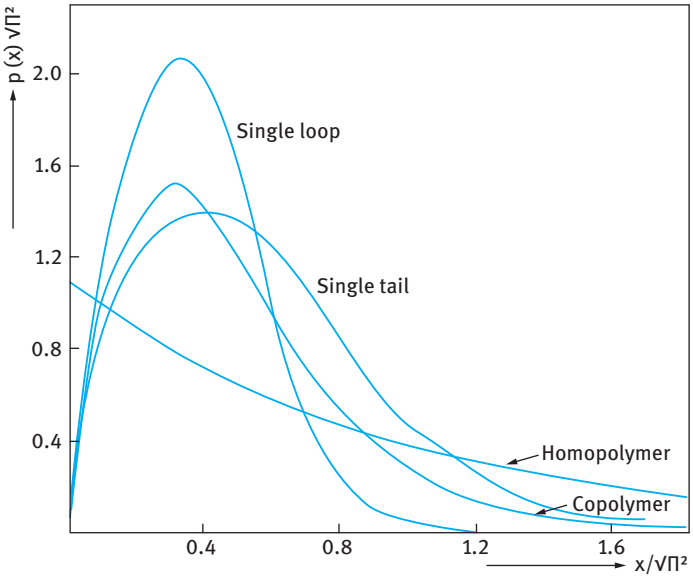

Fig. 12.4: Segment density distribution for single tails, single loops, homopolymers and random copolymers.

A useful model for treating polymer adsorption and configuration was suggested by Roe [22] Scheutjens and Fleer (SF theory) [23–26] that is referred to as the step weighted random walk approach. In order to be able to describe all possible chain conformations, Scheutjens and Fleer [23–26] used a model of a quasi-crystalline lattice with lattice layers parallel to the surface. Starting from the surface the layers are numbered $I = 1, 2, 3, \ldots, M$, where M is a layer in bulk solution. All the lattice sites within one layer were considered to be energetically equivalent. The probability of finding any lattice site in layer I occupied by a segment was assumed to be equal to the volume fraction ϕ_I in this layer. The conformation probability and the free energy of mixing were calculated with the assumption of random mixing within each layer (the Brag–Williams or mean field approximation). The energy for any segment is only determined by the layer number, and each segment can be assigned a weighting or Boltzmann factor, p_i, which depends only on the layer number. The partition functions were derived for the mixture of free and adsorbed polymer molecules, as well as for the solvent molecules. As mentioned before, all chain conformations were described as step weighted random walks on a quasi-crystalline lattice which extends in parallel layers from the surface; this is schematically shown in Fig. 12.5.

The partition function is written in terms of a number of configurations. These were treated as connected sequences of segments. In each layer, random mixing between segments and solvent molecules was assumed (mean field approximation).

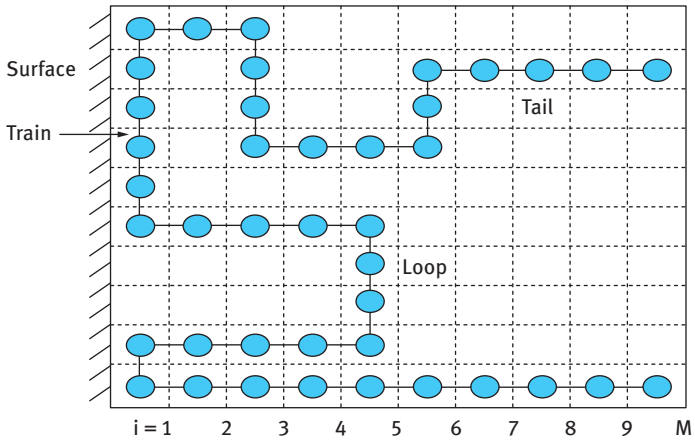

Fig. 12.5: Schematic representation of a polymer molecule adsorbing on a flat surface – quasi-crystalline lattice with segments filling layers that are parallel to the surface (random mixing of segments and solvent molecules in each layer is assumed).

Each step in the random walk was assigned a weighting factor p_i that consists of three contributions:

(i) An adsorption energy χ^s (which exists only for the segments that are near the surface).
(ii) Configurational entropy of mixing (that exists in each layer).
(iii) Segment-solvent interaction parameter χ (the Flory–Huggins interaction parameter; note that $\chi = 0$ for an athermal solvent; $\chi = 0.5$ for a θ-solvent).

The adsorption energy gives rise to a Boltzmann factor $\exp \chi^s$ in the weighting factor for the first layer, provided χ^s is interpreted as the adsorption energy difference (in units of kT) between a segment and a solvent molecule. The configurational entropy for the segment, as a part of the chain, is accounted for in the matrix procedure in which all possible chain conformations are considered. However, the configurational entropy loss of the solvent molecule, going from a layer i with low solvent concentration to the bulk solution with a higher solvent concentration, has to be introduced in p_i. This entropy loss can be written as $\Delta s^0 = k \ln \phi_*^0/\phi_i^0$ per solvent molecule, where ϕ_i^0 and ϕ_*^0 are the solvent volume fractions in layer I and in bulk solution respectively. This change is equivalent to introducing a Boltzmann factor $\exp(-\Delta s^0/k) = \phi_i^0/\phi_*^0$ in the weighting factor p_i. The last contribution stems from the mixing energy of the exchange process. The transfer of a segment from the bulk solution to layer i is accompanied by an energy change (in units of kT) $\chi(\phi_i^0 - \phi_*^0)$, where χ is the Flory–Huggins segment solvent interaction parameter.

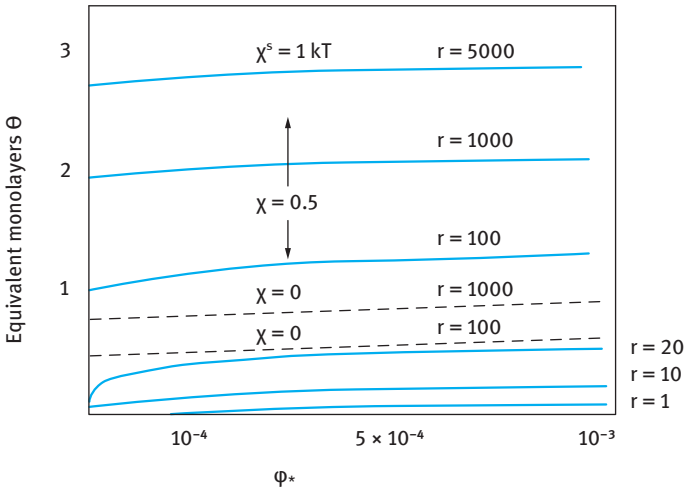

Fig. 12.6: Adsorption isotherms for oligomers and polymers in the dilute region based on the SF theory. Full curves $\chi = 0.5$; dashed curves $\chi = 0$.

Fig. 12.6 shows typical adsorption isotherms plotted as surface coverage (in equivalent monolayers) versus polymer volume fraction ϕ_* in bulk solution (ϕ_* was taken to vary between 0 and 10^{-3}, which is the normal experimental range).

The results in Fig. 12.6 show the effect of increasing the chain length r and effect of solvency (athermal solvent with $\chi = 0$ and theta solvent with $\chi = 0.5$). The adsorption energy χ^s was taken to be the same and equal to $1\,kT$. When $r = 1$, θ is very small and the adsorption increases linearly with increasing ϕ^* (Henry's type isotherm). On the other hand, when $r = 10$, the isotherm deviates strongly from a straight line and approaches a Langmuirian type. However, when $r \geq 20$ high affinity isotherms are obtained. This implies that the first polymer chains added are completely adsorbed resulting in extremely low polymer concentration in solution (approaching zero). This explains the irreversibility of adsorption of polymeric surfactants with $r > 100$. The adsorption isotherms with $r = 100$ and above are typical of those observed experimentally for most polymers that are not too polydisperse, i.e. showing a steep rise followed by a nearly horizontal plateau (which only increases few percent per decade increase of ϕ^*). In these dilute solutions, the effect of solvency is most clearly seen, with poor solvents giving the highest adsorbed amounts. In good solvents, θ is much smaller and levels off for long chains to attain an adsorption plateau, which is essentially independent of molecular weight.

Some general features of the adsorption isotherms over a wide concentration range can be illustrated by using logarithmic scales for both θ and ϕ_* which highlight the behaviour in extremely dilute solutions. Such a presentation [25–27] is shown in Fig. 12.7.

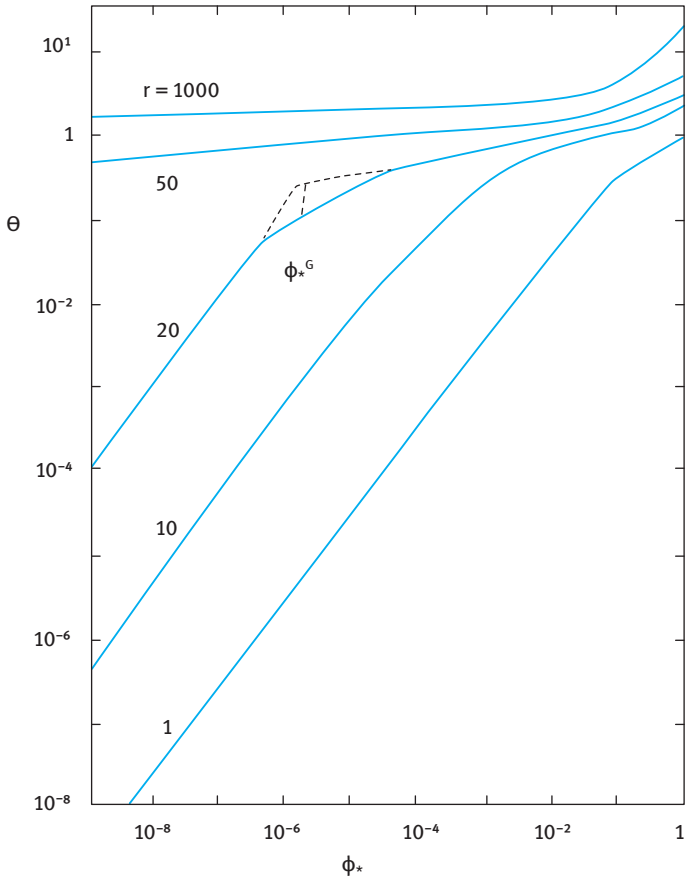

Fig. 12.7: Log-log presentation of adsorption isotherms of various r values, $\chi^s = 1; \chi = 0.5$; hexagonal lattice.

These results show a linear Henry region followed by a pseudoplateau region. A transition concentration, ϕ_*^{1c}, can be defined by extrapolation of the two linear parts. ϕ_*^c decreases exponentially with increasing chain length and when $r = 50$, ϕ_*^c is so small (10^{-12}) that it does not appear within the scale shown in Fig. 12.7. With $r = 1000$, ϕ_*^c reaches the ridiculously low value of 10^{-235}. The region below ϕ_*^c is the Henry region where the adsorbed polymer molecules behave essentially as isolated molecules. The representation in Fig. 12.7 also answers the question of reversibility versus irreversibility for polymer adsorption. When $r > 50$, the pseudoplateau region extends down to very low concentration ($\phi_*^c = 10^{-12}$) and this explains why one cannot easily detect any desorption upon dilution. Clearly, if such extremely low concentration can be reached, desorption of the polymer may take place. Thus, the lack of desorption (sometimes referred to as irreversible adsorption) is due to the fact that the equilibrium

between adsorbed and free polymer is shifted far in favour of the surface because of the high possible number of possible attachments per chain.

Another point that emerges from the SF theory is the difference in shape between the experimental and the theoretical adsorption isotherms in the low concentration region. The experimental isotherms are usually rounded, whereas those predicted from theory are flat. This is accounted for in terms of the molecular weight distribution (polydispersity) which is encountered with most practical polymers. This effect has been explained by Cohen-Stuart et al. [27]. With polydisperse polymers, the larger molecular weight fractions adsorb preferentially over the smaller ones. At low polymer concentrations, nearly all polymer fractions are adsorbed leaving a small fraction of the polymer with the lowest molecular weights in solution. As the polymer concentration is increased, the higher molecular weight fractions displace the lower ones on the surface, which are now released in solution, thus shifting the molecular weight distribution in solution to lower values. This process continues with a further increase in polymer concentration leading to fractionation whereby the higher molecular weight fractions are adsorbed at the expense of the lower molecular weight fractions which are released to the bulk solution. However, in very concentrated solutions, monomers adsorb preferentially with respect to polymers and short chains with respect to larger ones. This is due to the fact that in this region, the conformational entropy term predominates over the free energy, disfavouring the adsorption of long chains.

According to the SF theory, the bound fraction p and the direct surface coverage θ_1 depend on the chain length for the same volume fraction. This is illustrated in Fig. 12.8 which shows the adsorbed amount Γ (Fig. 12.8 (a)), surface coverage θ (Fig. 12.8 (b)) and fraction of adsorbed segments $p = \theta/\Gamma$ (Fig. 12.8 (c)) as a function of volume fraction ϕ_*.

In the Henry region ($\phi_* < \phi_*^c$), p is rather high and independent of chain length for $r \geq 20$. In this region the molecules lie nearly flat on the surface, with 87 % of segments in trains. At the other end of the concentration range ($\phi_* = 1$), p is proportional to $r^{-1/2}$. At intermediate concentrations, p is within these two extremes. With increasing polymer concentration, the adsorbed molecules become gradually more extended (lower p) until at very high ϕ_* values they become Gaussian at the interface. In better solvents the direct surface coverage is lower due to the stronger repulsion between the segments. This effect is more pronounced if the surface concentration differs strongly from the solution concentration. If the adsorption is small, the effect of the excluded volume effect (and therefore of χ) is rather weak; the same applies if both the concentrations in the bulk solution and near the surface are high. Both θ_1 and θ decrease with increasing solvent power (decreasing χ) but the effect is stronger for θ than for θ_1, resulting in a higher bound fraction (thus flatter chains) from better solvents at the same solution concentration.

The structure of the adsorbed layer is described in terms of the segment density distribution. As an illustration, Fig. 12.9 shows some calculations using the SF theory for loops and tails with $r = 1000$, $\phi^* = 10^{-6}$ and $\chi = 0.5$. In this example, 38 % of the

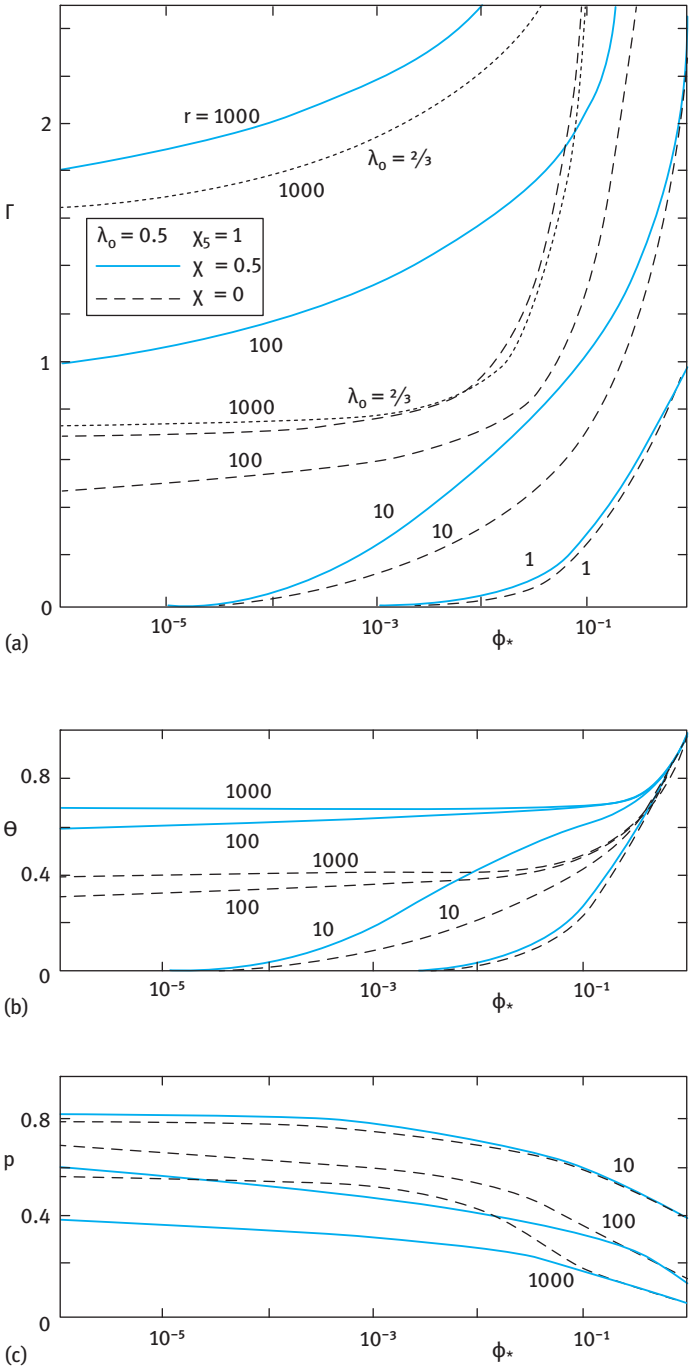

Fig. 12.8: Adsorbed amount Γ (a), surface coverage θ (b) and fraction of adsorbed segments $p = \theta/\Gamma$ (c) as a function of volume fraction ϕ_*. Full lines for a θ-solvent ($\chi = 0.5$), broken line for an athermal solvent ($\chi = 0$).

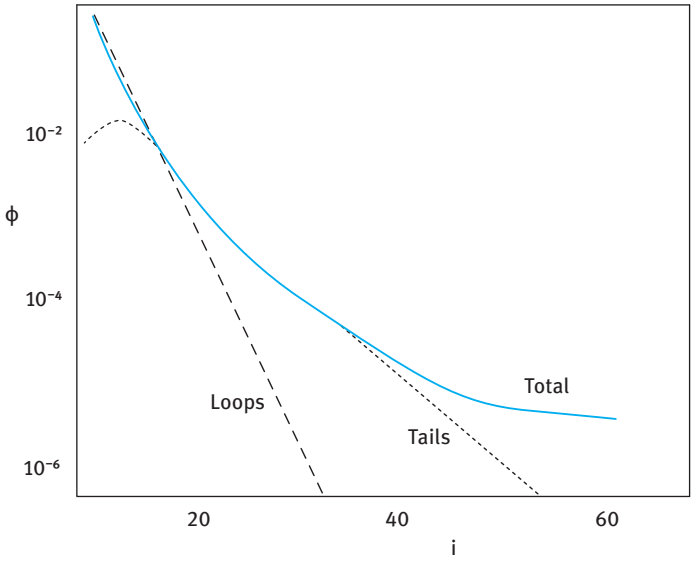

Fig. 12.9: Loop, tail and total segment profile according to the SF theory.

segments are in trains, 55.5 % in loops and 6.5 % in tails. This theory demonstrates the importance of tails, which dominate the total distribution in the outer region.

12.4 Scaling theory for polymer adsorption

De Gennes [28] introduced a simple theory for terminally attached polymer chains on a flat surface [29]. He considered the chain to be broken up into "blobs" as illustrated in Fig. 12.10.

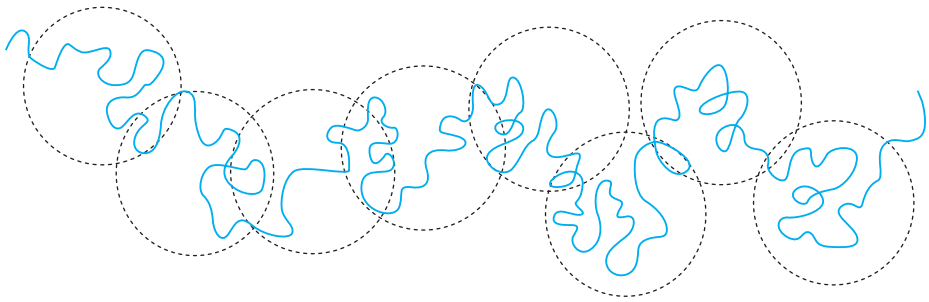

Fig. 12.10: Schematic representation of the blob model according to de Gennes [28].

Inside the blob, the chain is self-avoiding but the blobs themselves can overlap and are essentially ideal. For g monomers per blob, the blob size $\xi \approx g^{\nu/2} \approx g^{2/3}$. If the blobs can overlap, then $R \approx \xi^{0.5}$ and,

$$R \approx n^{0.5} g^{0.1}. \tag{12.1}$$

For an ideal chain, $g = 1$ and for a chain with full excluded volume $n = g$, which corresponds to the two extreme cases of an ideal and a swollen chain.

A schematic representation of the blob presentation of terminally attached chains is given in Fig. 12.11.

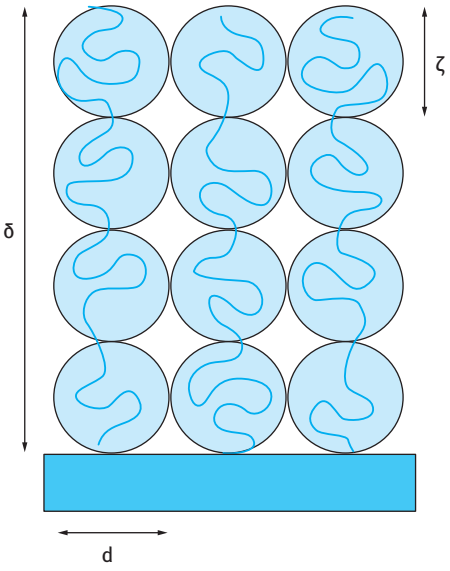

Fig. 12.11: Schematic representation of a terminally attached chain d by blobs of size ξ.

If each blob contains a self-avoiding walk of g monomers, then the blob size is given by,

$$\xi = g^{1/3} \tag{12.2}$$

For N monomers the brush length δ is given by,

$$\delta = \left(\frac{N}{g}\right)\xi. \tag{12.3}$$

The assumption is made that the blob size is directly related to the grafted amount σ so that,

$$\sigma = \frac{1}{\xi^2}. \tag{12.4}$$

Combining equations (12.3) and (12.4),

$$\delta = N\sigma^{1/3}. \tag{12.5}$$

The above analysis predicts that the brush length is linear in chain length. This is clearly true for a rod normal to the surface, but suggests that chains closely grafted together on a surface are very strongly stretched. A more sophisticated approach which confirms this result predicts that the brush volume fraction profile is parabolic [30].

12.5 Experimental techniques for studying polymeric surfactant adsorption

As mentioned above, for full characterization of polymeric surfactant adsorption one needs to determine three parameters:

(i) The adsorbed amount Γ (mg m^{-2} or mol m^{-2}) as a function of equilibrium concentration C_{eq}, i.e. the adsorption isotherm.
(ii) The fraction of segments in direct contact with the surface p (number of segments in trains relative to the total number of segments).
(iii) The segment density distribution $\rho(z)$ or the hydrodynamic adsorbed layer thickness δ_h.

It is important to obtain the adsorption parameters as a function of the important variables of the system:

(i) Solvency of the medium for the chain which can be affected by temperature, addition of salt or a nonsolvent. The Flory–Huggins interaction parameter χ could be measured separately.
(ii) The molecular weight of the adsorbed polymer.
(iii) The affinity of the polymer to the surface as measured by the value of χ^s, the segment-surface adsorption energy.
(iv) The structure of the polymer; this is particularly important for block and graft copolymers.

12.5.1 Measurement of the adsorption isotherm

This is by far the easiest to obtain. One measures the polymeric surfactant concentration before ($C_{initial}$, C_1) and after ($C_{equilibrium}$, C_2)

$$\Gamma = \frac{(C_1 - C_2)V}{A}, \tag{12.6}$$

where V is the total volume of the solution and A is the specific surface area (m^2 g^{-1}). It is necessary in this case to separate the particles from the polymer solution after adsorption. This could be carried out by centrifugation and/or filtration. One should make sure that all particles are removed. To obtain this isotherm, one must develop a

sensitive analytical technique for determination of the polymeric surfactant concentration in the ppm range. It is essential to follow the adsorption as a function of time to determine the time required to reach equilibrium. For some polymer molecules such as polyvinyl alcohol, PVA, and polyethylene oxide, PEO, (or blocks containing PEO), analytical methods based on complexation with iodine/potassium iodide or iodine/boric acid potassium iodide have been established. For some polymers with specific functional groups, spectroscopic methods may be applied, e.g. UV, IR or fluorescence spectroscopy. A possible method is to measure the change in refractive index of the polymer solution before and after adsorption. This requires very sensitive refractometers. High resolution NMR has been recently applied since the polymer molecules in the adsorbed state are in a different environment than those in the bulk. The chemical shift of functional groups within the chain is different in these two environments. This has the attraction of measuring the amount of adsorption without separating the particles.

12.5.2 Measurement of the fraction of segments p

The fraction of segments in direct contact with the surface can be directly measured using spectroscopic techniques:

(i) IR if there is specific interaction between the segments in trains and the surface, e.g. polyethylene oxide on silica from nonaqueous solutions [31, 32].
(ii) Electron spin resonance (ESR); this requires labelling of the molecule [33].
(iii) NMR, pulse gradient or spin-echo NMR. This method is based on the fact that the segments in trains are "immobilized" and hence they have lower mobility than those in loops and tails [34].

An indirect method for determining p is to measure the heat of adsorption ΔH using microcalorimetry [35]. One should then determine the heat of adsorption of a monomer H_m (or molecule representing the monomer, e.g. ethylene glycol for PEO); p is then given by the equation,

$$p = \frac{\Delta H}{H_m n}, \tag{12.7}$$

where n is the total number of segments in the molecule.

The above indirect method is not very accurate and can only be used in a qualitative sense. It also requires very sensitive enthalpy measurements (e.g. using an LKB microcalorimeter).

12.5.3 Determination of the segment density distribution $\rho(z)$ and adsorbed layer thickness δ_h

The segment density distribution $\rho(z)$ is given by the number of segments parallel to the surface in the z-direction. Three direct methods can be applied for determining the

adsorbed layer thickness: ellipsometry, attenuated total reflection (ATR) and neutron scattering. Both ellipsometry and ATR [36] depend on the difference between refractive indices between the substrate, the adsorbed layer and bulk solution and they require a flat reflecting surface. Ellipsometry [36] is based on the principle that light undergoes a change in polarizability when it is reflected at a flat surface (whether covered or uncovered with a polymer layer.

The above limitations when using ellipsometry or ATR are overcome by the application technique of neutron scattering, which can be applied to both flat surfaces as well as particulate dispersions. The basic principle of neutron scattering is to measure the scattering due to the adsorbed layer, when the scattering length density of the particle is matched to that of the medium (the so-called "contrast-matching" method). Contrast matching of particles and medium can be achieved by changing the isotopic composition of the system (using deuterated particles and mixture of D_2O and H_2O). It was used for measurement of the adsorbed layer thickness of polymers, e.g. PVA or poly(ethylene oxide) (PEO) on polystyrene latex [37]. Apart from obtaining δ, one can also determine the segment density distribution $\rho(z)$.

The above technique of neutron scattering clearly gives a quantitative picture of the adsorbed polymer layer. However, its application in practice is limited since one needs to prepare deuterated particles or polymers for the contrast matching procedure. The practical methods for determining the adsorbed layer thickness are mostly based on hydrodynamic methods. Several methods may be applied to determine the hydrodynamic thickness of adsorbed polymer layers of which viscosity, sedimentation coefficient (using an ultracentrifuge) and dynamic light scattering measurements are the most convenient. A less accurate method is from zeta potential measurements.

The viscosity method [38] depends on measuring the increase in the volume fraction of the particles as a result of the presence of an adsorbed layer of thickness δ_h. The volume fraction of the particles ϕ plus the contribution of the adsorbed layers is usually referred to as the effective volume fraction ϕ_{eff}. Assuming the particles behave as hard spheres, then the measured relative viscosity η_r is related to the effective volume fraction by the Einstein equation, i.e.,

$$\eta_r = 1 + 2.5\phi_{eff}. \tag{12.8}$$

ϕ_{eff} and ϕ are related from simple geometry by,

$$\phi_{eff} = \phi\left[1 + \left(\frac{\delta_h}{R}\right)\right]^3, \tag{12.9}$$

where R is the particle radius. Thus, from a knowledge of η_r and ϕ one can obtain δ_h using the above equations.

The sedimentation method depends on measuring the sedimentation coefficient (using an ultracentrifuge) of the particles S_0' (extrapolated to zero concentration) in the presence of the polymer layer [39]. Assuming the particles obey Stokes' law, S_0' is

given by the expression,

$$S_0' = \frac{(4/3)\pi R^3(\rho - \rho_s) + (4/3)\pi[(R + \delta_h)^3 - R^3](\rho_s^{ads} - \rho_s)}{6\pi\eta(R + \delta_h)}, \tag{12.10}$$

where ρ and ρ_s are the mass density of the solid and solution phase respectively, and ρ^{ads} is the average mass density of the adsorbed layer, which may be obtained from the average mass concentration of the polymer in the adsorbed layer.

In order to apply the above methods one should use a dispersion with monodisperse particles with a radius that is not much larger than δ_h. Small model particles of polystyrene may be used.

A relatively simple sedimentation method for determining δ_h is the slow speed centrifugation applied by Garvey et al. [39]. Basically, a stable monodisperse dispersion is slowly centrifuged at low g values (< 50 g) to form a close-packed (hexagonal or cubic) lattice in the sediment. From a knowledge of ϕ and the packing fraction (0.74 for hexagonal packing), the distance of separation between the centre of two particles R_δ may be obtained, i.e.,

$$R_\delta = R + \delta_h = \left(\frac{0.74 V \rho_1 R^3}{W}\right), \tag{12.11}$$

where V is the sediment volume, ρ_1 is the density of the particles and W their weight.

The most rapid technique for measuring δ_h is photon correlation spectroscopy (PCS) (sometime referred to as quasi-elastic light scattering) which allows one to obtain the diffusion coefficient of the particles with and without the adsorbed layer (D_δ and D respectively). This is obtained from measurements of the intensity fluctuation of scattered light as the particles undergo Brownian diffusion [40]. When a light beam (e.g. monochromatic laser beam) passes through a dispersion, an oscillating dipole is induced in the particles, thus re-radiating the light. Due to the random arrangement of the particles (which are separated by a distance comparable to the wavelength of the light beam, i.e. the light is coherent with the interparticle distance), the intensity of the scattered light will, at any instant, appear as random diffraction or "speckle" pattern. As the particles undergo Brownian motion, the random configuration of the speckle pattern changes. The intensity at any one point in the pattern will, therefore, fluctuate such that the time taken for an intensity maximum to become a minimum (i.e. the coherence time) corresponds approximately to the time required for a particle to move one wavelength. Using a photomultiplier of active area about the size of a diffraction maximum, i.e. approximately one coherence area, this intensity fluctuation can be measured. A digital correlator is used to measure the photocount or intensity correlation function of the scattered light. The photocount correlation function can be used to obtain the diffusion coefficient D of the particles. For monodisperse non-interacting particles (i.e. at sufficient dilution), the normalized correlation function $[g^{(1)}(\tau)]$ of the scattered electric field is given by the equation,

$$[g^{(1)}(\tau)] = \exp -(\Gamma\tau), \tag{12.12}$$

where τ is the correlation delay time and Γ is the decay rate or inverse coherence time. Γ is related to D by the equation,

$$\Gamma = DK^2, \tag{12.13}$$

where K is the magnitude of the scattering vector that is given by,

$$K = \left(\frac{4n}{\lambda_0}\right)\sin\left(\frac{\theta}{2}\right), \tag{12.14}$$

where n is the refractive index of the solution, λ is the wavelength of light in vacuum and θ is the scattering angle.

From D, the particle radius R is calculated using the Stokes–Einstein equation,

$$D = \frac{kT}{6\pi\eta R}, \tag{12.15}$$

where k is the Boltzmann constant and T is the absolute temperature. For a polymer coated particle, R is denoted R_δ which is equal to $R + \delta_h$. Thus, by measuring D_δ and D, one can obtain δ_h. It should be mentioned that the accuracy of the PCS method depends on the ratio of δ_δ/R, since δ_h is determined by difference. Since the accuracy of the measurement is ±1 %, δ_h should be at least 10 % of the particle radius. This method can only be used with small particles and reasonably thick adsorbed layers.

Electrophoretic mobility, u, measurements can also be applied to measure δ_h [41]. From u, the zeta potential ζ, i.e. the potential at the slipping (shear) plane of the particles can be calculated. Adsorption of a polymer causes a shift in the shear plane from its value in the absence of a polymer layer (which is close to the Stern plane) to a value that depends on the thickness of the adsorbed layer. Thus by measuring ζ in the presence (ζ_δ) and absence (ζ) of a polymer layer one can estimate δ_h. Assuming that the thickness of the Stern plane is Δ, then ζ_δ may be related to the ζ (which may be assumed to be equal to the Stern potential ψ_d) by the equation,

$$\tanh\left(\frac{e\psi_\delta}{4kT}\right) = \tanh\left(\frac{e\zeta}{4kT}\right)\exp[-\kappa(\delta_h - \Delta)], \tag{12.16}$$

where κ is the Debye parameter that is related to electrolyte concentration and valency.

It should be mentioned that the value of δ_h calculated using the above simple equation shows a dependency on electrolyte concentration and hence the method cannot be used in a straightforward manner. Cohen-Stuart et al. [41] showed that the measured electrophoretic thickness δ_e approaches δ_h only at low electrolyte concentrations. Thus, to obtain δ_h from electrophoretic mobility measurements, results should be obtained at various electrolyte concentrations and δ_e should be plotted versus the Debye length $(1/\kappa)$ to obtain the limiting value at high $(1/\kappa)$ (i.e. low electrolyte concentration) which now corresponds to δ_h.

12.6 Examples of the adsorption isotherms of nonionic polymeric surfactants

Fig. 12.12 shows the adsorption isotherms for PEO with different molecular weights on PS (at room temperature). It can be seen that the amount adsorbed in mg m^{-2} increases with increasing polymer molecular weight [42]. Fig. 12.13 shows the variation of the hydrodynamic thickness δ_h with molecular weight M. δ_h shows a linear increase with log M. δ_h increases with n, the number of segments in the chain, according to,

$$\delta_h \approx n^{0.8}. \tag{12.17}$$

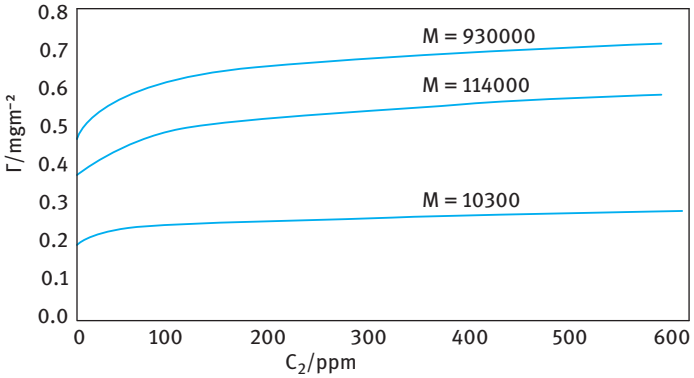

Fig. 12.12: Adsorption isotherms for PEO on PS.

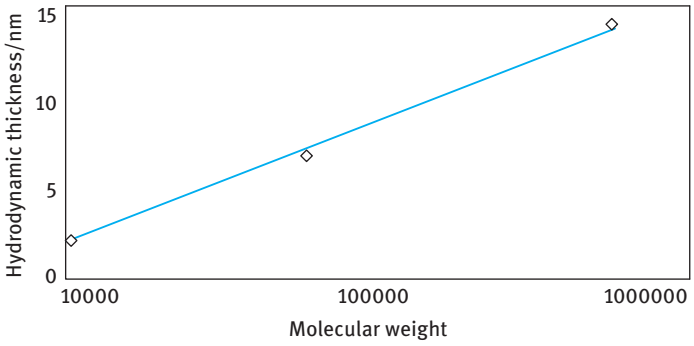

Fig. 12.13: Hydrodynamic thickness of PEO on PS as a function of the molecular weight.

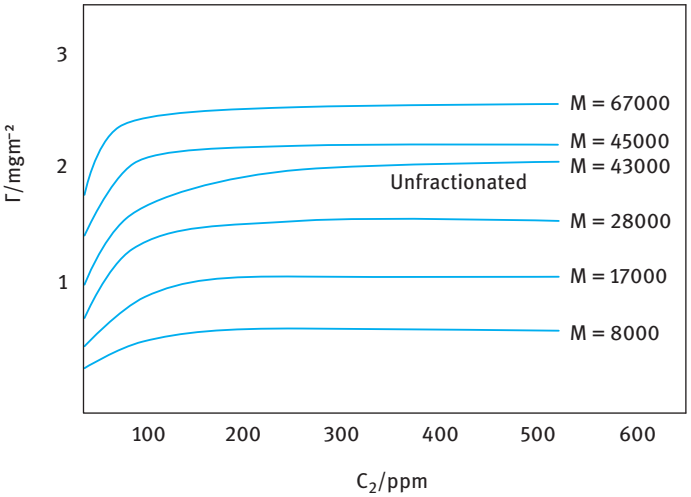

Fig. 12.14: Adsorption isotherms of PVA with different molecular weights on polystyrene latex at 25 °C.

Fig. 12.14 shows the adsorption isotherms of PVA with various molecular weights on PS latex (at 25 °C) [43]. The polymers were obtained by fractionation of a commercial sample of PVA with an average molecular weight of 45 000. The polymer also contained 12 % vinyl acetate groups. As with PEO, the amount of adsorption increases with increasing M. The isotherms are also of the high affinity type. Γ at the plateau increases linearly with $M^{1/2}$.

The hydrodynamic thickness was determined using PCS and the results are given below.

M	67000	43000	28000	17000	8000
δ_h (nm)	25.5	19.7	14.0	9.8	3.3

δ_h seems to increase linearly with increasing molecular weight.

The effect of solvency on adsorption was investigated by increasing the temperature (the PVA molecules are less soluble at higher temperature) or addition of electrolyte (KCl) [44, 45]. The results are shown in Fig. 12.15 and 12.16 for $M = 65100$.

The adsorption of block and graft copolymers is more complex since the intimate structure of the chain determines the extent of adsorption [42]. Random copolymers adsorb in an intermediate way to that of the corresponding homopolymers. Block copolymers retain the adsorption preference of the individual blocks. The hydrophilic block (e.g. PEO), the buoy, extends away from the particle surface into the bulk solution, whereas the hydrophobic anchor block (e.g. PS or PPO) provides firm attachment

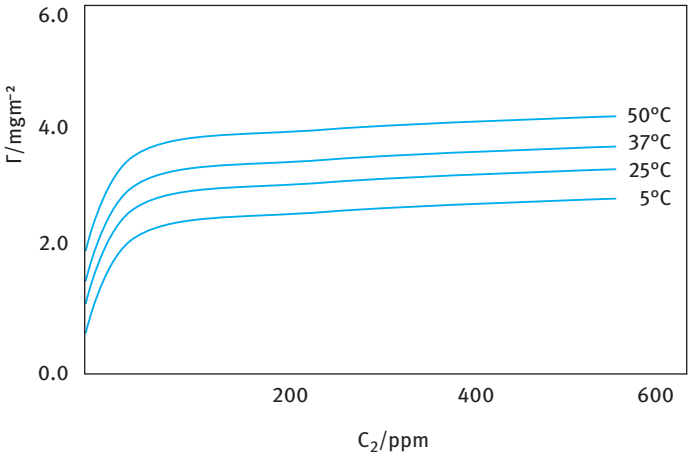

Fig. 12.15: Influence of temperature on adsorption.

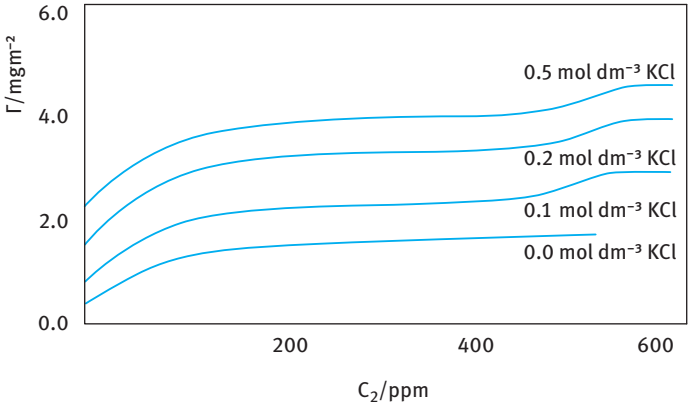

Fig. 12.16: Influence of addition of KCl on adsorption.

to the surface. Fig. 12.17 shows the theoretical prediction of diblock copolymer adsorption according to the Scheutjens and Fleer theory. The surface density σ is plotted versus the fraction of anchor segments ν_A. The adsorption depends on the anchor/buoy composition.

The amount of adsorption is higher than for homopolymers and the adsorbed layer thickness is more extended and dense. For a triblock copolymer A–B–A, with two buoy chains and one anchor chain, the behaviour is similar to that of diblock copolymers. This is shown in Fig. 12.18 for PEO–PPO–PEO block (Pluronic).

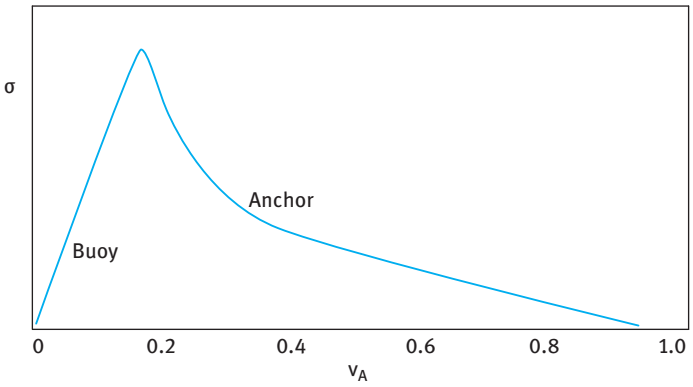

Fig. 12.17: Prediction of adsorption of diblock copolymer.

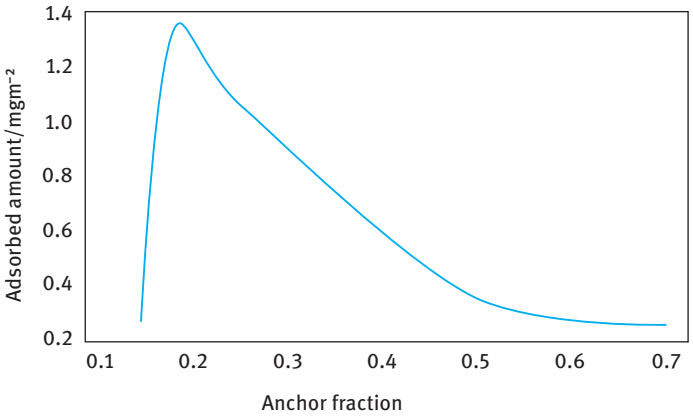

Fig. 12.18: Adsorbed amount (mg m^{-2}) versus fraction of anchor segment for an A–B–A triblock copolymer (PEO–PPO–PEO).

12.7 Adsorbed layer thickness results

Fig. 12.19 shows a plot of $\rho(z)$ against z for PVA ($M = 37000$) adsorbed on deuterated PS latex in D_2O/H^2O.

The results shows a monotonic decay of $\rho(z)$ with distance z from the surface and several regions may be distinguished. Close to the surface ($0 < z < 3$ nm), the decay in $\rho(z)$ is rapid and assuming a thickness of 1.3 nm for the bound layer, p was calculated to be 0.1, which is in close agreement with the results obtained using NMR measurements. In the middle region, $\rho(z)$ shows a shallow maximum followed by a slow decay which extends to 18 nm, i.e. close to the hydrodynamic layer thickness δ_h of the polymer chain (see below). δ_h is determined by the longest tails and is about 2.5 times the radius of gyration in bulk solution (≈ 7.2 nm). This slow decay of $\rho(z)$

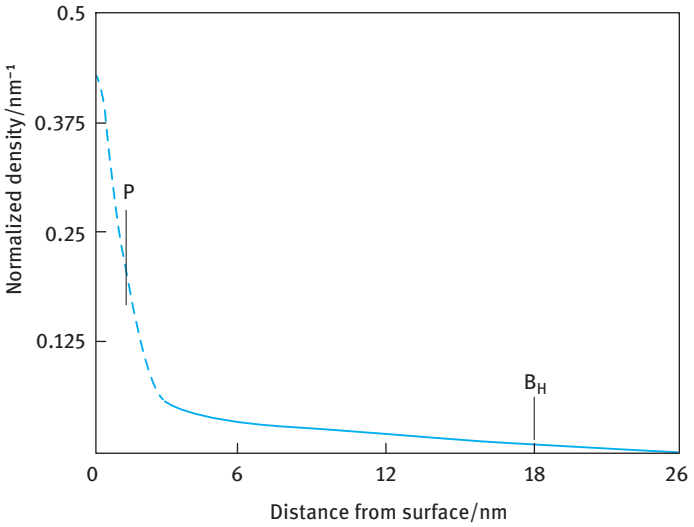

Fig. 12.19: Plot of $\rho(z)$ against z for PVA (M = 37000) adsorbed on deuterated PS latex in D_2O/H_2O.

with z at long distances is in qualitative agreement with Scheutjens and Fleers' theory [23], which predicts the presence of long tails. The shallow maximum at intermediate distances suggests that the observed segment density distribution is a summation of a fast monotonic decay due to loops and trains together with the segment density for tails with a maximum density away from the surface. The latter maximum was clearly observed for a sample which had PEO grafted to a deuterated polystyrene latex [37] (where the configuration is represented by tails only).

The hydrodynamic thickness of block copolymers shows different behaviour from that of homopolymers (or random copolymers). Fig. 12.20 shows the theoretical prediction for the adsorbed layer thickness δ which is plotted as a function of ν_A.

Fig. 12.21 shows the hydrodynamic thickness versus fraction of anchor segments for an ABA block copolymer of (polyethylene oxide)–poly(propylene oxide)–poly(ethylene oxide) (PEO–PPO–PEO) [42]. The theoretical (Scheutjens and Fleer) prediction of adsorbed amount and layer thickness versus fraction of anchor segments are shown in the inserts of Fig. 12.21. When there are two buoy blocks and a central anchor block, as in the above example, the A–B–A block shows similar behaviour to that of an A–B block. However, if there are two anchor blocks and a central buoy block, surface precipitation of the polymer molecule at the particle surface is observed and this is reflected in a continuous increase of adsorption with increasing polymer concentration as has been shown for an A–B–A block of PPO–PEO–PPO [42].

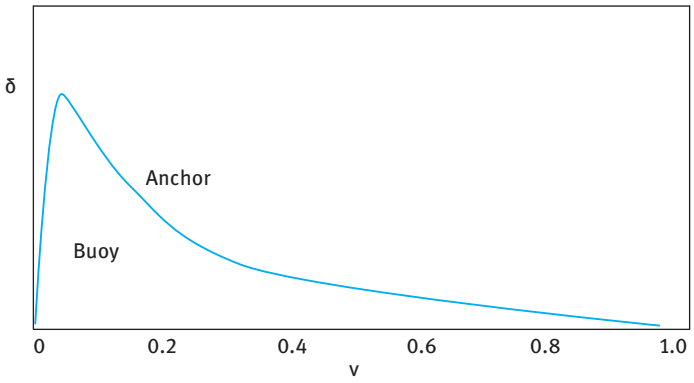

Fig. 12.20: Theoretical predictions of the adsorbed layer thickness for a diblock copolymer.

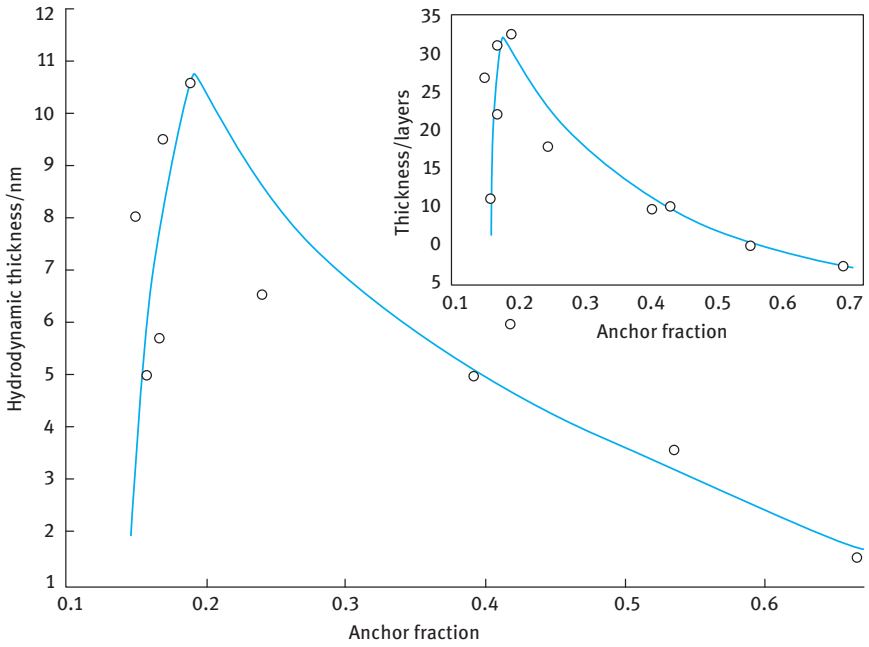

Fig. 12.21: Hydrodynamic thickness versus fraction of anchor segments v_A for PEO–PPO–PEO block copolymer onto polystyrene latex. Insert shows the mean field calculation of thickness versus anchor fraction using the SF theory.

12.8 Kinetics of polymer adsorption

The kinetics of polymer adsorption is a highly complex process. Several distinct processes can be distinguished, each with a characteristic timescale [42]. These processes may occur simultaneously and hence it is difficult to separate them. The first process is the mass transfer of the polymer to the surface, which may be either diffusion or convection. Having reached the surface, the polymer must then attach itself to a surface site, which depends on any local activation energy barrier. Finally, the polymer will undergo large-scale rearrangements as it changes from its solution conformation to a "tail-train-loop" conformation. Once the polymer has reached the surface, the amount of adsorption increases with time. The increase is rapid at the beginning but subsequently slows as the surface becomes saturated. The initial rate of adsorption is sensitive to the bulk polymer solution concentration and molecular weight as well as the solution viscosity. Nevertheless, all the polymer molecules arriving at the surface tend to adsorb immediately. The concentration of unadsorbed polymer around the periphery of the forming layer (the surface polymer solution) is zero and, therefore the concentration of polymer in the interfacial region is significantly greater than the bulk polymer concentration. Mass transport is found to dominate the kinetics of adsorption until 75 % of full surface coverage. At higher surface coverage, the rate of adsorption decreases since the polymer molecules arriving at the surface cannot immediately adsorb. Over time, equilibrium is set up between this interfacial concentration of polymer and the concentration of polymer in the bulk. Given that the adsorption isotherm is of the high affinity type, no significant change in adsorbed amount is expected, even over decades of polymer concentration. If the surface polymer concentration increases toward that of the bulk solution, the rate of adsorption decreases because the driving force for adsorption (the difference in concentration between the surface and bulk solutions) decreases. Adsorption processes tend to be very rapid and an equilibrated polymer layer can form within several 1000 s. However, desorption is a much slower process and this can take several years!

References

[1] Tadros T. Applied surfactants. Weinheim: Wiley-VCH; 2005.
[2] Tadros TF. In: Goddard ED, Gruber JV, editors. Principles of polymer science and technology in cosmetics and personal care. New York: Marcel Dekker; 1999.
[3] Tadros T. In: Holmberg K, editor. Novel Surfactants, New York: Marcel Dekker; 2003.
[4] Tadros TF. In: Buscall R, Corner T, Stageman JF, editors. Polymer colloids. London: Applied Sciences, Elsevier; 1985. p. 105.
[5] Jenkel E, Rumbach R. Z Elekrochem. 1951;55:612.
[6] Simha R, Frisch L, Eirich FR. J Phys Chem. 1953;57:584.
[7] Silberberg A. J Phys Chem. 1962;66:1872.
[8] Di Marzio EA. J Chem Phys. 1965;42:2101.

[9] Di Marzio EA, McCrakin FL. J Chem Phys. 1965;43:539.
[10] Clayfield EJ, Lumb EC. J Colloid Interface Sci. 1966;22:269, 285.
[11] Clayfield EJ, Lumb EC. Macromolecules. 1968;1:133.
[12] Silberberg A. J Chem Phys. 1968;48:2835.
[13] Hoeve CA, Di Marzio EA, Peyser P. J Chem Phys. 1965;42:2558.
[14] Hoeve CA. J Chem Phys. 1965;44:1505; 1966;47:3007.
[15] Hoeve CA. J Polym Sci. 1970;30:361; 1971;34:1.
[16] Silberberg A. J Colloid Interface Sci. 1972;38:217.
[17] Hoeve CAJ. J Chem Phys. 1965;44:1505.
[18] Hoeve CAJ. J Chem Phys. 1966;47:3007.
[19] Meier DJ. J Phys Chem. 1965;71:1861.
[20] Hesselink FT. J Phys Chem. 1969;73:3488.
[21] Hesselink FT. J Phys Chem. 1971;75:65.
[22] Roe RJ. J Chem Phys. 1974;60:4192.
[23] Scheutjens JMHM, Fleer GJ. J Phys Chem. 1979;83:1919.
[24] Scheutjens JMHM, Fleer GJ. J Phys Chem. 1980;84:178.
[25] Scheutjens JMHM, Fleer GJ. Adv Colloid Interface Sci. 1982;16:341.
[26] Fleer GJ, Cohen-Stuart MA, Scheutjens JMHM, Cosgrove T, Vincent B. Polymers at interfaces. London: Chapman and Hall; 1993.
[27] Cohen-Stuart MA, Scheutjens JMHM, Fleer GJ. J Polym Sci Polym Phys Ed. 1980;18:559.
[28] de Gennes PG. Scaling concepts of polymer physics. Ithaca: Cornell University Press; 1979.
[29] Cosgrove T. Polymers at interfaces. Oxford: Blackwell; 2005. Chapter 7.
[30] Milner ST. Science. 1991;251:905.
[31] Killmann E, Eisenlauer E, Horn MJ. Polymer Sci. Polymer Symposium. 1977;61:413.
[32] Fontana BJ, Thomas JR. J Phys Chem. 1961;65:480.
[33] Robb ID, Smith R. Eur Polym J. 1974;10:1005.
[34] Barnett KG, Cosgrove T, Vincent B, Burgess A, Crowley TL, Kims J, Turner JD, Tadros TF. Disc Faraday Soc. 1981;22:283.
[35] Cohen-Stuart MA, Fleer GJ, Bijesterbosch B. J Colloid Interface Sci. 1982;90:321.
[36] Abeles F. In: Passaglia E, Stromberg RR, Kruger J, editors. Ellipsometry in the measurement of surfaces and thin films. Nat. Bur. Stand. Misc. Publ. 256; 1964. p. 41.
[37] Cosgrove T, Crowley TL, Ryan T. Macromolecules. 1987;20:2879.
[38] Einstein A. Investigations on the theory of the Brownian movement. New York: Dover; 1906.
[39] Garvey MJ, Tadros TF, Vincent B. J Colloid Interface Sci. 1976;55:440.
[40] Pusey PN. In: Green JHS, Dietz R, editors. Industrial polymers: Characterisation by molecular weights. London: Transcripta Books; 1973.
[41] Cohen-Stuart MA, Mulder JW. Colloids and Surfaces. 1985;15:49.
[42] Obey TM, Griffiths PC. In: Goddard ED, Gruber JV, editors. Principles of polymer science and technology in cosmetics and personal care. New York: Marcel Dekker; 1999. Chapter 2.
[43] Garvey MJ, Tadros TF, Vincent B. J Colloid Interface Sci. 1974;49:57.
[44] van den Boomgaard T, King TA, Tadros TF, Tang H, Vincent B. J Colloid Interface Sci. 1978;61:68.
[45] Tadros TF, Vincent B. J Colloid Interface Sci. 1978:72:505.

13 Steric stabilization

13.1 Introduction

As mentioned in Chapter 12, many colloidal dispersions are stabilized against flocculation (and coalescence in the case of emulsions) by the use of polymeric surfactants. The latter, in particular, are very effective for stabilization due to their strong adsorption and formation of "thick" adsorbed layers (> 5 nm) which ensure effective steric stabilization. The use of natural and synthetic polymers (referred to as polymeric surfactants) for stabilization of colloidal dispersions plays an important role in industrial applications, such as in paints, cosmetics, pharmaceuticals, agrochemicals, ceramics, etc. Polymers are particularly important for preparation of concentrated dispersions, i.e. at high volume fraction ϕ of the disperse phase,

$$\phi = \frac{\text{volume of all particles}}{\text{total volume of dispersion}}. \tag{13.1}$$

Polymers are also essential for stabilization of nonaqueous dispersions, since in this case electrostatic stabilization is not possible (due to the low dielectric constant of the medium). To understand the role of polymers in dispersion stability, it is essential to consider the adsorption and conformation of the macromolecule at the solid/liquid interface and this was discussed in detail in Chapter 12. In this chapter, I will cover the topic of interaction between particles containing adsorbed polymeric surfactants and the theory of steric stabilization [1–3].

13.2 Interaction between particles or droplets containing adsorbed polymer layers

When two particles or droplets, each with a radius R and containing an adsorbed polymer layer with a hydrodynamic thickness δ_h, approach each other to a surface-surface separation distance h that is smaller than $2\delta_h$, the polymer layers interact with each other resulting in two main situations [1–3]:

(i) The polymer chains may overlap with each other.
(ii) The polymer layer may undergo some compression.

In both cases, there will be an increase in the local segment density of the polymer chains in the interaction region. This is schematically illustrated in Fig. 13.1. The real situation is perhaps in between the above two cases, i.e. the polymer chains may undergo some interpenetration and some compression.

https://doi.org/10.1515/9783110540895-014

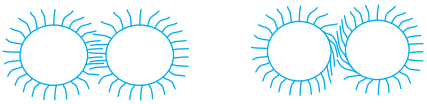

Interpenetration without compression

Compression without interpenetration

Fig. 13.1: Schematic representation of the interaction between particles containing adsorbed polymer layers.

Provided the dangling chains (the A chains in A–B, A–B–A block or BA_n graft copolymers) are in a good solvent, this local increase in segment density in the interaction zone will result in strong repulsion as a result of two main effects:

(i) Increase in the osmotic pressure in the overlap region as a result of the unfavourable mixing of the polymer chains, when these are in good solvent conditions. This is referred to as osmotic repulsion or mixing interaction and it is described by a free energy of interaction G_{mix}.

(ii) Reduction of the configurational entropy of the chains in the interaction zone; this entropy reduction results from the decrease in the volume available for the chains when these are either overlapped or compressed. This is referred to as volume restriction interaction, entropic or elastic interaction and it is described by a free energy of interaction G_{el}.

The combination of G_{mix} and G_{el} is usually referred to as the steric interaction free energy, G_{s}, i.e.,

$$G_{\text{s}} = G_{\text{mix}} + G_{\text{el}}. \tag{13.2}$$

The sign of G_{mix} depends on the solvency of the medium for the chains. If in a good solvent, i.e. the Flory–Huggins interaction parameter χ is less than 0.5, then G_{mix} is positive and the mixing interaction leads to repulsion (see below). In contrast, if $\chi >$ 0.5 (i.e. the chains are in a poor solvent condition), G_{mix} is negative and the mixing interaction becomes attractive. G_{el} is always positive and hence in some cases one can produce stable dispersions in a relatively poor solvent (enhanced steric stabilization).

13.2.1 Mixing interaction G_{mix}

This results from the unfavourable mixing of the polymer chains when these are in good solvent conditions. This is schematically shown in Fig. 13.2.

Consider two spherical particles with the same radius and each containing an adsorbed polymer layer with thickness δ. Before overlap, one can define in each polymer layer a chemical potential for the solvent μ_i^{α} and a volume fraction for the polymer in the layer ϕ_2^{α}. In the overlap region (volume element $\mathrm{d}V$), the chemical potential of the solvent is reduced to μ_i^{β}. This results from the increase in polymer segment concentration in this overlap region. In the latter, the volume fraction of the polymer is now ϕ_2^{β}, which is higher than ϕ_2^{α}. In other words, the chemical potential of the polymer

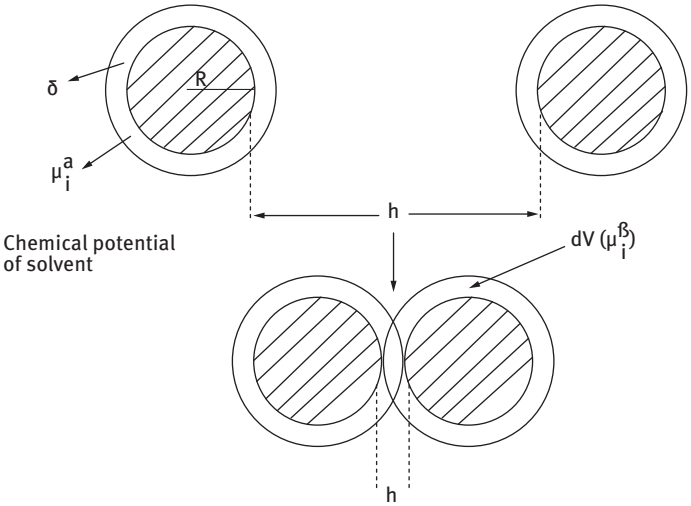

Fig. 13.2: Schematic representation of polymer layer overlap.

chains is now higher than in the rest of the layer (with no overlap). This amounts to an increase in the osmotic pressure in the overlap region; as a result solvent will diffuse from the bulk to the overlap region, thus separating the particles and hence a strong repulsive energy arises from this effect.

The above repulsive energy can be calculated by considering the free energy of mixing of two polymer solutions, as for example treated by Flory and Krigbaum [4]. The free energy of mixing is given by two terms:

(i) An entropy term that depends on the volume fraction of polymer and solvent.
(ii) An energy term that is determined by the Flory–Huggins interaction parameter χ,

$$\delta(G_{\text{mix}}) = kT(n_1 \ln \phi_1 + n_2 \ln \phi_2 + \chi n_1 \phi_2), \tag{13.3}$$

where n_1 and n_2 are the number of moles of solvent and polymer with volume fractions ϕ_1 and ϕ_2, k is the Boltzmann constant and T is the absolute temperature.

The total change in free energy of mixing for the whole interaction zone, V, is obtained by summing over all the elements in V,

$$G_{\text{mix}} = \frac{2kTV_2^2}{V_1} v_2 \left(\frac{1}{2} - \chi\right) R_{\text{mix}}(h), \tag{13.4}$$

where V_1 and V_2 are the molar volumes of solvent and polymer respectively, v_2 is the number of chains per unit area and $R_{\text{mix}}(h)$ is a geometric function which depends on the form of the segment density distribution of the chain normal to the surface, $\rho(z)$. k is the Boltzmann constant and T is the absolute temperature.

Using the above theory one can derive an expression for the free energy of mixing of two polymer layers (assuming a uniform segment density distribution in each layer) surrounding two spherical particles as a function of the separation distance h between the particles. The expression for G_{mix} is [5],

$$\frac{G_{mix}}{kT} = \left(\frac{2V_2^2}{V_1}\right)\nu_2^2\left(\frac{1}{2} - \chi\right)\left(\delta - \frac{h}{2}\right)^2\left(3R + 2\delta + \frac{h}{2}\right). \tag{13.5}$$

k is the Boltzmann constant, T is the absolute temperature, V_2 is the molar volume of polymer, V_1 is the molar volume of solvent and ν_2 is the number of polymer chains per unit area.

The sign of G_{mix} depends on the value of the Flory–Huggins interaction parameter χ: if $\chi < 0.5$, G_{mix} is positive and the interaction is repulsive; if $\chi > 0.5$, G_{mix} is negative and the interaction is attractive; if $\chi = 0.5$, $G_{mix} = 0$ and this defines the θ-condition.

13.2.2 Elastic interaction G_{el}

This arises from the loss in configurational entropy of the chains on the approach of a second particle. As a result of this approach, the volume available for the chains becomes restricted, resulting in loss of the number of configurations. This can be illustrated by considering a simple molecule, represented by a rod that rotates freely in a hemisphere across a surface (Fig. 13.3).

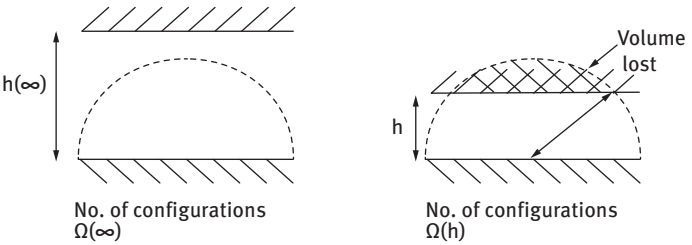

Fig. 13.3: Schematic representation of configurational entropy loss on approach of a second particle.

When the two surfaces are separated by an infinite distance, ∞, the number of configurations of the rod is $\Omega(\infty)$, which is proportional to the volume of the hemisphere. When a second particle approaches to a distance h such that it cuts the hemisphere (losing some volume), the volume available to the chains is reduced and the number of configurations become $\Omega(h)$ which is less than $\Omega(\infty)$. For two flat plates, G_{el} is given by the following expression [6],

$$\frac{G_{el}}{kT} = -2\nu_2 \ln\left[\frac{\Omega(h)}{\Omega(\infty)}\right] = -2\nu_2 R_{el}(h), \tag{13.6}$$

where $R_{el}(h)$ is a geometric function whose form depends on the segment density distribution. It should be stressed that G_{el} is always positive and could play a major role in steric stabilization. It becomes very strong when the separation distance between the particles becomes comparable to the adsorbed layer thickness δ.

13.2.3 Total energy of interaction

Combining G_{mix} and G_{el} with G_A gives the total energy of interaction G_T (assuming there is no contribution from any residual electrostatic interaction) [7], i.e.,

$$G_T = G_{mix} + G_{el} + G_A. \tag{13.7}$$

A schematic representation of the variation of G_{mix}, G_{el}, G_A and G_T with surface-surface separation distance h is shown in Fig. 13.4.

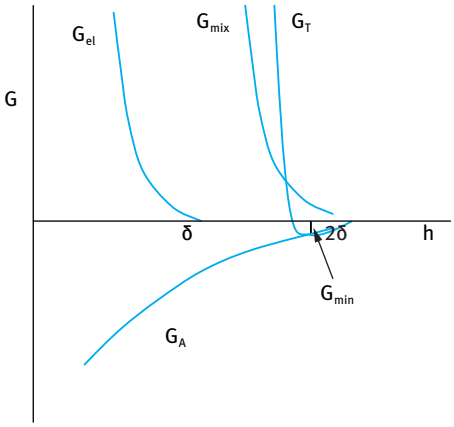

Fig. 13.4: Energy–distance curves for sterically stabilized systems.

G_{mix} increases very sharply with decreasing h, when $h < 2\delta$. G_{el} increases very sharply with decreasing h, when $h < \delta$. G_T versus h shows a minimum, G_{min}, at separation distances comparable to 2δ. When $h < 2\delta$, G_T shows a rapid increase with decreasing h. The depth of the minimum depends on the Hamaker constant A, the particle radius R and adsorbed layer thickness δ. G_{min} increases with increasing A and R. At a given A and R, G_{min} increases with decreasing δ (i.e. with decreasing molecular weight, M_w, of the stabilizer). This is illustrated in Fig. 13.5 which shows the energy–distance curves as a function of δ/R. The larger the value of δ/R, the smaller the value of G_{min}. In this case the system may approach thermodynamic stability as is the case with nanodispersions.

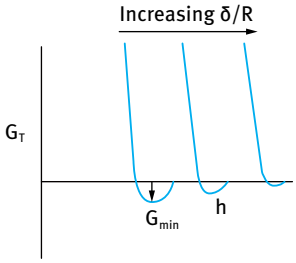

Fig. 13.5: Variation of G_{min} with δ/R.

13.2.4 Criteria for effective steric stabilization

(i) The particles should be completely covered by the polymer (the amount of polymer should correspond to the plateau value). Any bare patches may cause flocculation either by van der Waals attraction (between the bare patches) or by bridging flocculation (whereby a polymer molecule will become simultaneously adsorbed on two or more particles).
(ii) The polymer should be strongly "anchored" to the particle surfaces, to prevent any displacement during particle approach. This is particularly important for concentrated suspensions. For this purpose A–B, A–B–A block and BA_n graft copolymers are the most suitable where the chain B is chosen to be highly insoluble in the medium and has a strong affinity to the surface. Examples of B groups for hydrophobic particles in aqueous media are polystyrene and polymethylmethacrylate.
(iii) The stabilizing chain A should be highly soluble in the medium and strongly solvated by its molecules. Examples of A chains in aqueous media are poly(ethylene oxide) and poly(vinyl alcohol).
(iv) δ should be sufficiently large (> 5 nm) to prevent weak flocculation.

13.3 Measurement of steric repulsion between adsorbed layers of polymeric surfactants

Two techniques can be applied for direct measurement of interaction forces between macroscopic bodies containing adsorbed layers of polymeric surfactants and these are summarized below.

13.3.1 Surface force methods

In this method, the energy $E(D)$-distance curves for adsorbed layers of polymeric surfactants (that are physically adsorbed on smooth mica sheets) are obtained using the surface force apparatus originally described by Israelachvili [8–11]. It consists of measuring the forces between mica sheets with molecularly smooth surfaces with a

cross cylinder geometry. The mica sheets are partially silvered on the reverse side so that light interferometry can be used to measure the surface separation. The force between the surfaces is measured by monitoring the displacement of a leaf spring to which one of the sheets is attached. Initially measurements are made in the presence of electrolyte solution (10^{-2} mol dm^{-3} KNO^3) and then in the same electrolyte solution but with the mica sheets containing the adsorbed layers. In this manner one can subtract the double layer interaction from the total interaction to obtain the contribution from steric interaction. For this purpose a graft copolymer consisting of poly(methylmethacrylate) backbone to which several poly(ethylene oxide) are grafted, i.e. PMMA/MA(PEO)$_n$, is used.

The forces between the mica surfaces $F(D)$ bearing the copolymer layers are converted to the interaction potential energy $E(D)$ between flat surfaces using the Deryaguin approximation for cross cylinders [11],

$$E(D) = \frac{F(D)}{2\pi a}, \tag{13.8}$$

where D is the surface separation distance and a is the cylinder radius. Fig. 13.6 shows the energy–distance curve for mica sheets covered by the graft copolymer PMMA/MA(PEO)$_n$. The figure shows a monotonic and approximately exponential decrease of $E(D)$ with increasing separation distance D. The exponential decay makes it difficult to assess precisely the point at which the interaction begins. It falls below the detection limit of the instrument at ≈ 25 nm.

The energy of interaction between polymer layers can be calculated using de Gennes scaling theory [12],

$$E(D) = \frac{\beta kT}{s^3}\left[\frac{(2L)^{2.25}}{1.25(D)^{1.25}} + \frac{D^{1.75}}{1.75(2L)^{0.75}}\right] - \left[\frac{2L}{1.25} + \frac{2L}{1.75}\right], \tag{13.9}$$

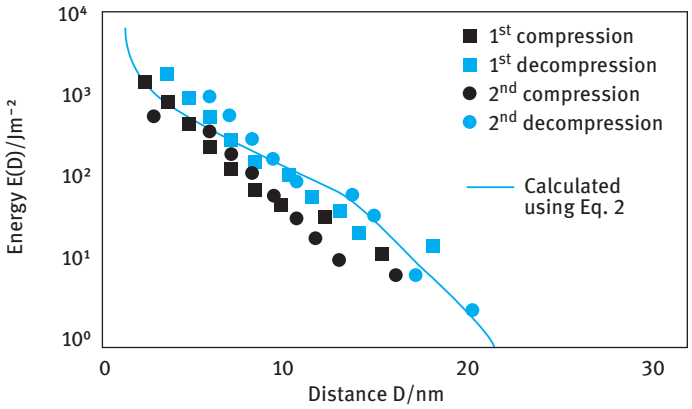

Fig. 13.6: Interaction energy $E(D)$ versus separation distance D.

where L is the stabilizer thickness on each surface (taken to be 12.5 nm, i.e. half the separation distance D at which $E(D)$ begins to increase with a further decrease in D). S is the distance between side chains, k is the Boltzmann constant and T is the absolute temperature The solid line in Fig. 13.6 shows the theoretical calculations based on equation (13.9). Agreement between theory and experiment is satisfactory.

The high frequency modulus of latex dispersions containing adsorbed layers of PMMA/MA(PEO)$_n$ graft copolymer was also measured. For this purpose latex dispersions were prepared using surfactant-free emulsion polymerization. The particle diameter was 330 ± 9 nm. Latex dispersions containing adsorbed PMMA/MA(PEO)$_n$ graft copolymer were prepared at various latex volume fractions.

The storage modulus G' of each dispersion was determined at low amplitudes (within the linear viscoelastic region) as a function of frequency. These measurements were obtained using dynamic (oscillatory) techniques (see Chapter 1, Vol. 2). A plot of G' versus frequency ω (rad s^{-1}) allows one to obtain the plateau value G'_∞ , i.e. the high frequency modulus which can be related to potential of mean force $V(R)$ as is illustrated below.

The relationship between G_∞ and $V(R)$ is given by the following expression [13–15],

$$G'_\infty = NkT + \frac{2\pi N^2}{15}\int_0^\infty g(R)\frac{\mathrm{d}}{\mathrm{d}r}\left[R^4\left(\frac{\mathrm{d}V(R)}{\mathrm{d}R}\right)\right]\mathrm{d}R. \tag{13.10}$$

N is the number density of particles and $g(R)$ is the radius distribution function. The assumption made in the derivation of the above expression that the particle interactions involve only central pair-wise additive potentials applies if the particles slip over each other without contact friction. Both short-range and long-range order have been observed in dispersions of monodisperse particles and it is likely that at least short-range order is retained where the system is under oscillatory shear with a low strain amplitude. If within the short-range domain a perfect lattice arrangement exists and $g(R)$ can be represented by a delta function centered at the nearest neighbour spacing, Evans and Lips showed that under these conditions, equation (13.10) reduces to [15],

$$G'_\infty = NkT + \frac{\phi_\mathrm{m} n}{5\pi R^2}\left[4\frac{\mathrm{d}V(R)}{\mathrm{d}R} + R\frac{\mathrm{d}^2V(R)}{\mathrm{d}R^2}\right], \tag{13.11}$$

where ϕ_m is the maximum packing fraction and n is the coordination number. Equation (13.8) can be expressed in terms of interaction force F,

$$F = -\frac{\mathrm{d}V(R)}{\mathrm{d}R}. \tag{13.12}$$

The data of Fig. 13.6 are given as interaction energy between flat plates. They can be converted to the force between two spheres $E(D)$ using the Deryaguin approximation. This leads to the following expression for G'_∞,

$$G'_\infty = NkT - \frac{\phi_\mathrm{m} n a}{5R^2}\left[4E(D) + R\frac{\mathrm{d}E(D)}{\mathrm{d}D}\right]. \tag{13.13}$$

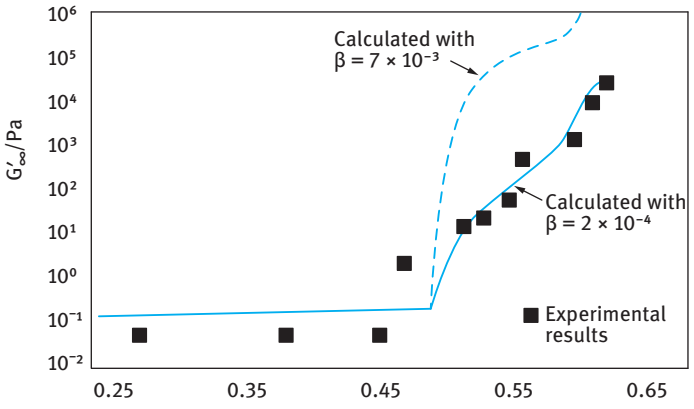

Fig. 13.7: G'_∞ versus ϕ.

Using equation (13.9) for $E(D)$ and assuming a reasonable value for L (12.5 nm) and β (7×10^{-3}, the value giving the best fit to equation (13.9)), it is possible to calculate G'_∞ as a function of the volume fraction ϕ of the latex from the energy–distance curve. The results of these calculations are shown in Fig. 13.7 together of the measured values of G'_∞.

It can be seen from Fig. 13.7 that the form of G'_∞ versus ϕ is correctly predicted. However, the calculated moduli values are about two orders of magnitude higher than the experimental values when the correct numerical prefactor β in the de Gennes expression has been used. By adjusting this numerical prefactor (solid line of Fig. 13.7) agreement between theoretical and experimental values of G'_∞ may be obtained.

13.3.2 Atomic Force Microscopy (AFM) measurements

In this case, the force between hydrophobic glass spheres and hydrophobic glass plate, both containing an adsorbed polymeric surfactant layer; is measured as a function of distance of separation both in water and in the presence of various electrolyte concentrations. The AFM is capable of measuring picoNewton surface forces at nanometre length scales. The interaction between glass spheres that were attached to the AFM cantilever and glass plates (both hydrophobized using dichlorodimethylsilane) and containing adsorbed layers of a graft copolymer of hydrophobically modified inulin (INUTEC® SP1, see Chapter 11) was measured as a function of INUTEC® SP1 concentration in water and at various Na_2SO_4 concentrations [16].

Measurements were initially carried out as a function of time (2, 5 and 24 hours) at 2×10^{-4} mol dm^{-3} INUTEC® SP1. The force–separation distance curves showed that after 2 and 5 hours equilibration time, the curve showed some residual attraction on withdrawal. By increasing the equilibration time (24 hours) this residual at-

traction on withdrawal disappeared and the approach and withdrawal curves were very close, indicating full coverage of the surfaces with polymer within this time. All subsequent measurements were carried out after 24 hours to ensure complete adsorption. Measurements were carried out at 5 different concentrations of INUTEC® SP1: 6.6×10^{-6}, 1×10^{-5}, 6×10^{-5}, 1.6×10^{-4} and 2×10^{-4} mol dm^{-3}. At concentrations $< 1.6 \times 10^{-4}$ mol dm^{-3} the withdrawal curve showed some residual attraction as is illustrated in Fig. 13.8 for 6×10^{-5} mol dm^{-3}. At concentrations $> 1.6 \times 10^{-4}$ mol dm^{-3} the approach and withdrawal curves were very close to each other as is illustrated in Fig. 13.9 for 2×10^{-4} mol dm^{-3}. These results indicate full coverage of the surfaces

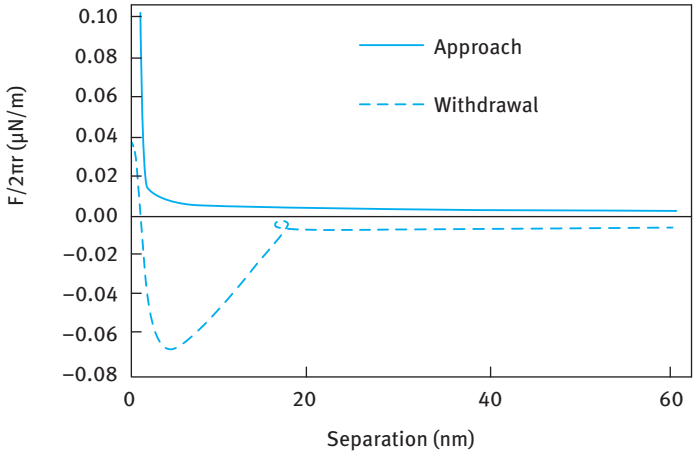

Fig. 13.8: Force–distance curves at 6×10^{-5} mol dm^{-3} INUTEC® SP1.

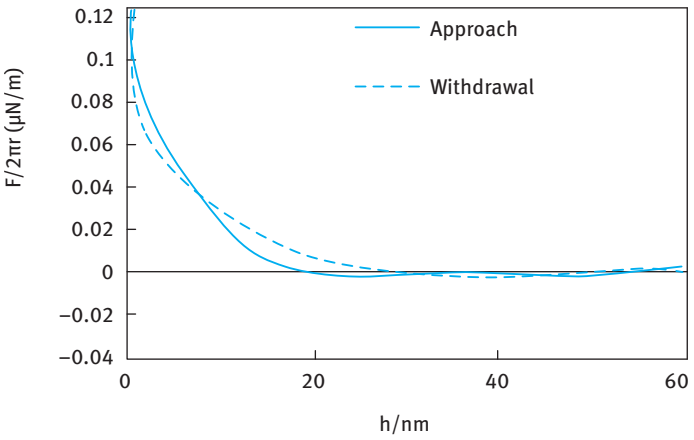

Fig. 13.9: Force–distance curves at 2×10^{-4} mol dm^{-3} INUTEC® SP1.

by the polymer when the INUTEC® SP1 concentration becomes equal or higher than 1.6×10^{-4} mol dm^{-3}. The results at full coverage give an adsorbed layer thickness of the order of 9 nm, which indicates strong hydration of the loops and tails of inulin [17].

Several investigations of the stability of emulsions and suspensions stabilized using INUTEC® SP1 showed absence of flocculation in the presence of high electrolyte concentrations (up to 4 mol dm^{-3} NaCl and 1.5 mol dm^{-3} $MgSO_4$) [17]. This high stability in the presence of high electrolyte concentrations is attributed to the strong hydration of inulin (polyfructose) loops and tails. This strong hydration was confirmed by measuring the cloud point of inulin in the presence of such high electrolyte concentrations (the cloud point exceeded 100 °C up to 4 mol dm^{-3} NaCl and 1.0 mol dm^{-3} $MgSO_4$). Evidence of such strong repulsion was obtained from the force-distance curves in the presence of different concentrations of Na_2SO_4 as shown in Fig. 13.10.

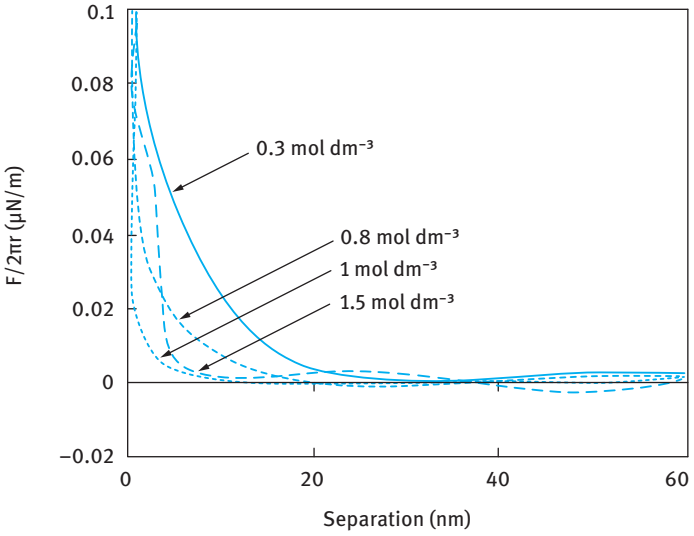

Fig. 13.10: Force–distance curves for hydrophobized glass surfaces containing adsorbed INUTEC® SP1 at various Na_2SO_4 concentrations.

The force–distance curves clearly show that the interaction remains repulsive up to the highest Na_2SO_4 concentration (1.5 mol dm^{-3}) studied. The adsorbed layer thickness decreases from approximately 9 nm at 0.3 mol dm^{-3} to about 3 nm at 1.5 mol dm^{-3} Na_2SO_4. This reduction in hydrodynamic thickness in the presence of high electrolyte concentrations is probably due to the change in the conformation of polyfructose loops and tails. It is highly unlikely that dehydration of the chains occurs since cloud point measurements have shown the absence of any cloud point up to 100 °C. Even at such low adsorbed layer thickness, strong repulsive interaction is observed indicating a high elastic repulsive term.

The interaction between INUTEC® SP1 adsorbed layers was investigated using rheological measurements. Steady state shear stress–shear rate curves (see Chapter 1, Vol. 2) were obtained at various volume fractions ϕ of polystyrene latex (PS) dispersions (in the range $\phi = 0.1–0.42$) that contained adsorbed layers of INUTEC® SP1. The results showed a shear thinning behaviour with the viscosity decreasing with applied shear rate and eventually reaching a plateau value when the shear rate exceeded 100 s^{-1}. Fig. 13.11 shows the variation of the relative viscosity η_r (measured at a shear rate of 1000 s^{-1}) as a function of the latex core volume fraction ϕ (with particle radius of 161 nm). It can be clearly seen that η_r increases gradually with increasing ϕ, but when the latter increases above 0.3 there is a rapid increase of η_r with any further increase of ϕ. This trend is typical for concentrated dispersions.

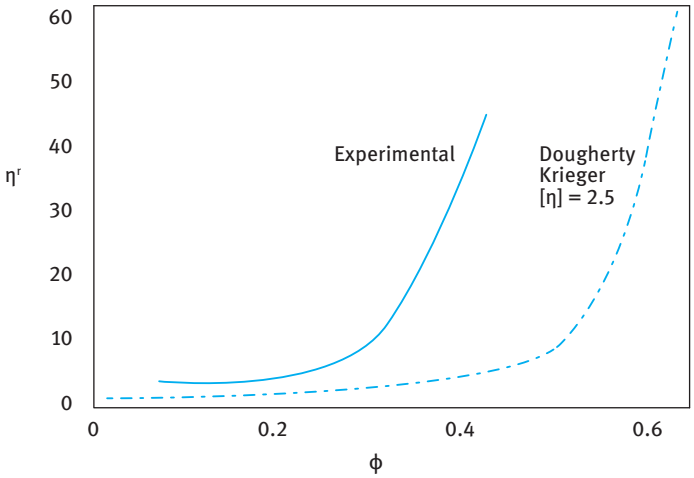

Fig. 13.11: Variation of η_r with core volume fraction of latex.

The η_r–ϕ curve was calculated on the basis of Dougherty–Krieger equation [18],

$$\eta_r = \left[1 - \frac{\phi}{\phi_p}\right]^{-[\eta]\phi_p}. \tag{13.14}$$

$[\eta]$ is the intrinsic viscosity and was taken to be equal to 2.5 (for hard spheres) and ϕ_p was obtained from a plot of $1/(\eta_r)^{1/2}$ versus ϕ (straight lines were obtained) and extrapolation of the results to $1/(\eta_r)^{1/2} = 0$. This gave a value of $\phi_p = 0.51$ for PS latex dispersions containing adsorbed INUTEC® SP1 layers.

It can be seen from Fig. 13.11 that the measured viscosity of the latex dispersions is significantly higher than the value calculated using the Dougherty–Krieger equation. This is due to the presence of adsorbed polymer layers on the latex particles.

From the measured η_r values one can obtain the effective volume fraction ϕ_{eff} of the latex dispersion, which can be used to obtain the adsorbed layer thickness δ,

$$\phi_{eff} = \phi\left[1 + \left(\frac{\delta}{R}\right)\right]^3. \tag{13.15}$$

This gave a value of $\delta = 9.6$ nm, which is close to the value obtained using the AFM measurements, again indicating the strong hydration of the polyfructose loops and tails.

Dynamic (oscillatory) measurements (see Chapter 1, Vol. 2) were obtained at various volume fractions ($\phi = 0.1$–0.42) of PS latex dispersions containing adsorbed layers of INUTEC® SP1. Initially, the frequency was fixed at 1 Hz (6.28 rad s^{-1}) and the storage modulus G' and the loss modulus G'' were measured as a function of applied stress (or strain) to obtain the linear viscoelastic region (where G' and G'' are independent of applied stress or strain). Measurements were then carried out as a function of frequency (0.01–10 Hz) while keeping the strain or stress in the linear region.

Fig. 13.12 shows the variation of G' and G'' with ϕ (at a stress amplitude in the linear region and frequency of 1 Hz). At $\phi < 0.2$, $G'' > G'$, whereas at $\phi > 0.2$, $G' > G''$ with $G' = G''$ at $\phi = 0.2$, corresponding to an effective volume fraction ϕ_{eff} of 0.24. This low value of ϕ_{eff} indicates very strong repulsive interaction beginning at long separation distance (long-range interaction) between the hydrated loops and tails of polyfructose chains.

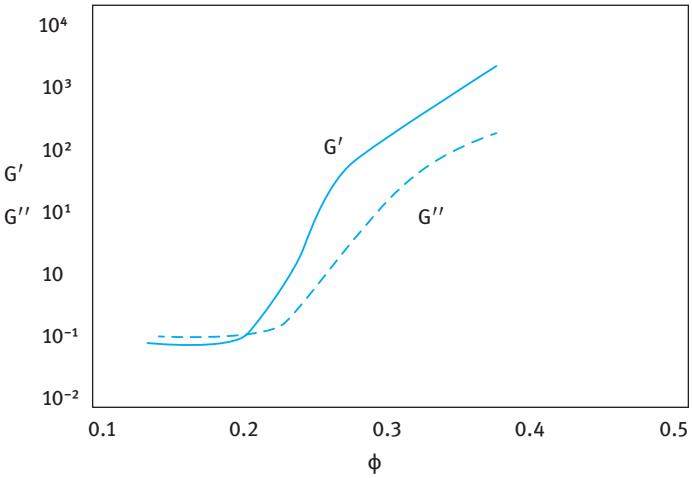

Fig. 13.12: Variation of G' and G'' (at 1 Hz) with volume fraction of PS latex containing adsorbed INUTEC® SP1 layers.

References

[1] Tadros TF. Polymer adsorption and dispersion stability. In: Tadros T, editor. The effect of polymers on dispersion properties. London: Academic Press; 1981.
[2] Napper DH. Polymeric stabilisation of colloidal dispersions. London: Academic Press; 1981.
[3] Tadros T. Polymeric surfactants. In: Tadros T, editor. Encyclopedia of colloid and interface science. Berlin: Springer; 2013.
[4] Flory PJ, Krigbaum WR. J Chem Phys. 1950;18:1086.
[5] Fischer EW. Kolloid Z. 1958;160:120.
[6] Mackor EL, van der Waals JH. J Colloid Sci. 1951;7:535.
[7] Hesselink FT, Vrij A, Overbeek JTG. J Phys Chem. 1971;75:2094.
[8] Israelachvili JN, Adams GE. J Chem Soc Faraday Trans. 1978;174:975.
[9] Luckham PF. Powder Technol. 1989;58:75.
[10] De L Costello BA, Luckham PF, Tadros TF. Colloids and Surfaces. 1988/1989;34:301.
[11] De L Costello BA, Luckham PF, Tadros TF. J Colloid Interface Sci. 1992;152:237.
[12] de Gennes PG. Advances Colloid Interface Sci. 1987;27:189.
[13] White LR. J Colloid Interface Sci. 1983;95:286.
[14] Zwanzig R, Mountain RD. J Chem Phys. 1965;43:4464.
[15] Evans ID, Lips A. J Chem Soc Faraday Trans. 1990;86:3413.
[16] Nestor J, Esquena J, Solans C, Luckham PF, Levecke B, Tadros TF. J Colloid Interface Sci. 2007;311:430.
[17] Nestor J, Esquena J, Solans C, Levecke B, Booten K, Tadros TF. Langmuir. 2005;21:4837.
[18] Krieger IM, Advances Colloid and Interface Sci. 1972;3:111.

14 Flocculation of sterically stabilized dispersions

14.1 Introduction

Colloidal dispersions that are stabilized by adsorbed polymers or polyelectrolytes undergo several flocculation mechanisms, depending on the conditions and/or addition of other materials [1–3]. The flocculation can be weak and reversible when for example the minimum in the energy–distance curves becomes deep enough (several kT units, where k is the Boltzmann constant and T is the absolute temperature) for sufficient attraction to occur [1–3]. As discussed in Chapter 13, the minimum depth increases as the ratio of adsorbed layer thickness to particle radius (δ/R) becomes smaller. When such a minimum reaches a critical value (that decreases with increasing volume fraction of the dispersion), flocculation occurs, forming a weak gel with the particles or droplets not touching each other. Such a weak gel can be fluidized by shaking the dispersion and on removal of shear the gel structure is reformed. This phenomenon is described as gel ↔ sol transformation and it results in thixotropy (reversible decrease of viscosity on application of shear and its recovery on removal of shear). In contrast, the flocculation can be strong and irreversible when the minimum becomes very deep. This irreversible flocculation occurs when the solvent for the chains becomes worse than a θ-solvent or the Flory–Huggins interaction parameter χ becomes higher than 0.5. In this case, the free energy of mixing, G_{mix}, become negative and when added to the van der Waals attraction, the net attraction becomes very large (several 100 kT units). Another mechanism of flocculation occurs when a "free", non-adsorbing polymer is added to the continuous medium. This phenomenon is referred to as depletion flocculation [1–3]. A fourth mechanism of flocculation occurs under conditions of incomplete coverage of the particle surface by the adsorbed polymer. Under these conditions, the polymer chain may become simultaneously adsorbed on two or more particles. This phenomenon is referred to as bridging flocculation [1–3]. A specific type of flocculation occurs in the presence of polyelectrolytes which are partially and strongly adsorbed on an oppositely charged surface (in the absence of complete coverage of the surface by the polyelectrolyte chains). Under these conditions the partially covered patches become attracted to the partially uncovered and oppositely charged surfaces [1–3]. Below a description of each flocculation mechanism is given.

14.2 weak (reversible) flocculation

This occurs when the thickness of the adsorbed layer is small (usually < 5 nm), particularly when the particle radius and Hamaker constant are large [1–3]. As mentioned above, the minimum depth may become sufficiently large for flocculation to take

https://doi.org/10.1515/9783110540895-015

place. For a given particle radius and Hamaker constant, the minimum depth can be controlled by controlling the adsorbed layer thickness. To illustrate this, polystyrene latex dispersions were prepared using different molar mass of partially hydrolysed poly(vinyl acetate), to be referred to as PVA. A commercial sample of PVA (88 % hydrolysed poly(vinyl acetate), i.e. containing 12 % acetate groups) was fractionated into narrow molar mass ranges using gel permeation chromatography [4]. The weight-average molar mass of each fraction was determined from measurements of the sedimentation coefficient using an ultracentrifuge [4]. The molecular dimensions in solution were also determined from intrinsic viscosity measurements. The latter were also used to determine the Flory–Huggins interaction parameter χ at 25, 37 and 50 °C. The χ values obtained were 0.464, 0.478 and 0.485 at 25, 37 and 50 °C respectively, indicating that water is a good solvent for PVA (note that χ increases slightly with the increase in temperature due to the possible dehydration of the polymer at higher temperature, but still $\chi < 0.5$ at all temperatures studied). The adsorption isotherms of the various molecular weight fractions were determined at 25 °C and the results are shown in Fig. 14.1.

The isotherms shown in Fig. 14.1 are of the high affinity type (irreversible adsorption) and, as predicted, the plateau adsorption Γ (mg m^{-2}) increases with increasing molar mass. The hydrodynamic adsorbed layer thickness, δ_h, was determined using three different techniques, namely, ultracentrifugation, photon correlation spectroscopy and slow-speed centrifugation [5]. The results obtained using the three methods agreed well with each other. A comparison was also made between δ_h and the hydrodynamic radius R_h. A summary of the adsorption, adsorbed layer thickness and hydrodynamic radius for the various PVA fractions is given in Tab. 14.1.

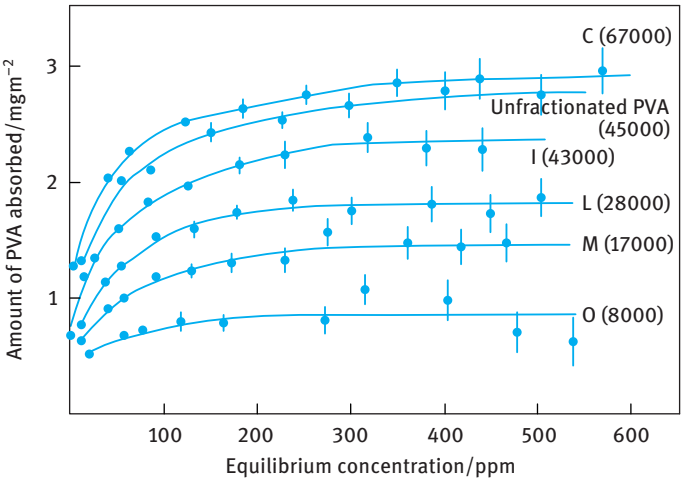

Fig. 14.1: Adsorption isotherms of PVA with various molar mass on polystyrene latex at 25 °C [4].

Tab. 14.1: Adsorption parameters for the various PVA fractions.

Fraction	M_w	Γ (mg m^{-2})	δ_h (nm)	R_h (nm)
Unfractionated	45000	2.79 ±0.15	22.6 ±2.6	5.5
C	67000	2.91 ±0.17	25.5 ±3.2	6.5
I	43000	2.38 ±0.10	19.7 ±2.2	5.4
L	28000	1.82 ±0.16	14.0 ±1.7	4.5
M	17000	1.47 ±0.14	9.8 ±2.4	3.6
O	8000	0.89 ±0.07	3.3 ±1.9	2.1

It can be seen from Tab. 14.1 that δ_h is significantly larger than $2R_h$. Since the volume occupied by the polymer chain at the surface is the same as the hydrodynamic volume of the chain in solution, the larger value of δ_h may be due to some deformation of the random coil on adsorption at the interface.

Using the above values of δ_h it is possible to calculate the energy–distance curves for polystyrene latex particles containing adsorbed PVA layers of various molecular weights, using for example the theory developed by Hesselink et al. [6]. The results of these calculations are shown in Fig. 14.2.

It is clear that for the high molecular weight fractions (M, L and I with molar mass 17 000, 28 000 and 43 000 respectively) δ_h is large (> 9.8 nm) and the energy minimum is too small for flocculation to occur. In contrast, with PVA with molar mass 8000, and $\delta_h \approx 3.3$ nm an appreciable attraction prevails at separation distance in the region of $2\delta_h$. In this case a weakly flocculated open structure could be produced. To illustrate this point, dispersions stabilized with PVA of various M_w were slowly centrifuged at 50 g, and the sediment was freeze-dried and examined by scanning electron microscopy [7]. The results are shown in Fig. 14.3 which clearly shows the close-packed

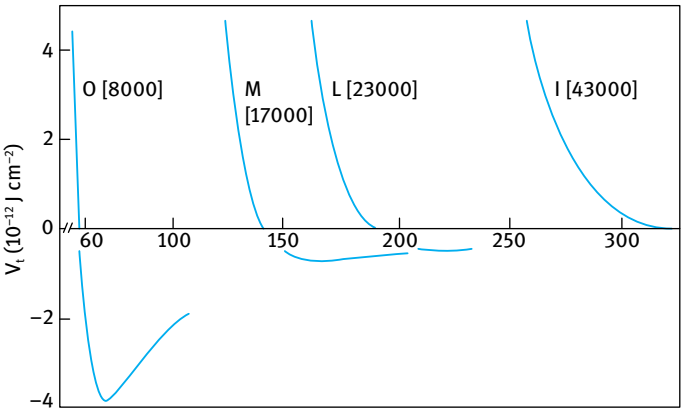

Fig. 14.2: Total energy of interaction versus separation distance for polystyrene latex with adsorbed layers of PVA of various molecular weights.

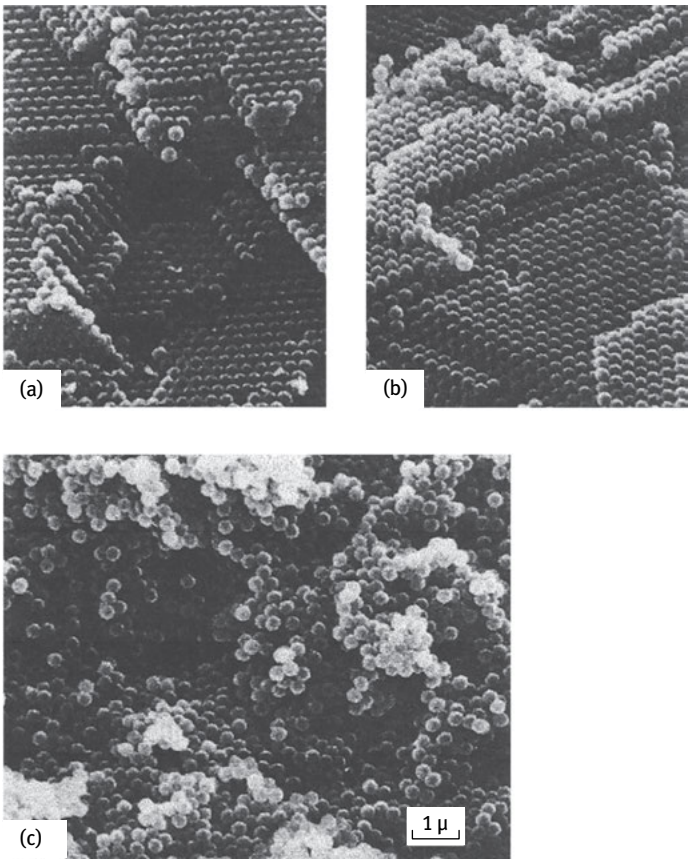

Fig. 14.3: Scanning electron micrographs of polystyrene sediments stabilized with PVA fractions: (a) $M_w = 43000$; (b) $M_w = 28000$; (c) $M_w = 8000$.

sediment (absence of flocculation) with the high molar mass fractions C and L and the weakly flocculated open structure obtained with the low molar mass fraction O.

The minimum depth required for causing weak flocculation depends on the volume fraction of the suspension. The higher the volume fraction, the lower the minimum depth required for weak flocculation. This can be understood if one considers the free energy of flocculation that consists of two terms, an energy term determined by the depth of the minimum (G_{min}) and an entropy term that is determined by reduction in configurational entropy on aggregation of particles,

$$\Delta G_{flocc} = \Delta H_{flocc} - T\Delta S_{flocc}. \tag{14.1}$$

With dilute suspensions, the entropy loss on flocculation is larger than with concentrated suspensions. Hence for flocculation of a dilute suspension, a higher energy minimum is required when compared to the case with concentrated suspensions.

The above flocculation is weak and reversible, i.e. on shaking the container redispersion of the suspension occurs. On standing, the dispersed particles aggregate to form a weak "gel". As mentioned above, this process (referred to as sol ↔ gel transformation) leads to reversible time dependence of viscosity (thixotropy) [8].

On shearing the suspension, the viscosity decreases and when the shear is removed, the viscosity is recovered. This phenomenon is applied in paints. On application of the paint (by a brush or roller), the gel is fluidized, allowing uniform coating of the paint. When shearing is stopped, the paint film recovers its viscosity and this avoids any dripping [9].

14.3 Incipient flocculation

This occurs when the solvency of the medium is reduced to become worse than θ-solvent (i.e. $\chi > 0.5$). This reduction in solvency can be induced by temperature changes [10, 11] or addition of a nonsolvent [10, 11] for the stabilizing chain. When the solvency is reduced, the dispersion often exhibits a sharp transition from long-term stability to fast flocculation. This process of incipient flocculation is, for example, observed when a dispersion stabilized by poly(ethylene oxide) moieties is heated. Over a few degrees temperature rise, the turbidity of the dispersion rises sharply indicating excessive flocculation. Flocculation can also occur by the addition of a nonsolvent, e.g. by addition of ethanol to a polymethylmethacrylate dispersion stabilized by poly(hydroxystearic) acid in a hydrocarbon solvent [12, 13]. The critical point at which flocculation is first observed is referred to as the critical flocculation temperature (CFT) or critical flocculation concentration of the added nonsolvent (CFV).

An illustration of incipient flocculation is given in Fig. 14.4 where χ was increased from < 0.5 (good solvent) to > 0.5 (poor solvent). One of the characteristic features of sterically stabilized systems, which distinguish them from electrostatically stabilized dispersions, is the temperature dependency of stability. Indeed, some dispersions flocculate on heating [14, 15]; others flocculate on cooling [14, 15]. Furthermore, in some cases dispersions can be produced which do not flocculate at any accessible temperature, whilst some sterically stabilized systems have been found to flocculate both on heating and cooling. This temperature dependency led Napper [10, 11] to describe stability in terms of the thermodynamic processes that govern stabilization. Thus, the temperature dependency of the Gibbs free energy of interaction (ΔG_R) for two sterically stabilized particles or droplets is given by,

$$\frac{\partial \Delta G_R}{\partial T} = -\Delta S_R, \tag{14.2}$$

where ΔS_R is the corresponding entropy change.

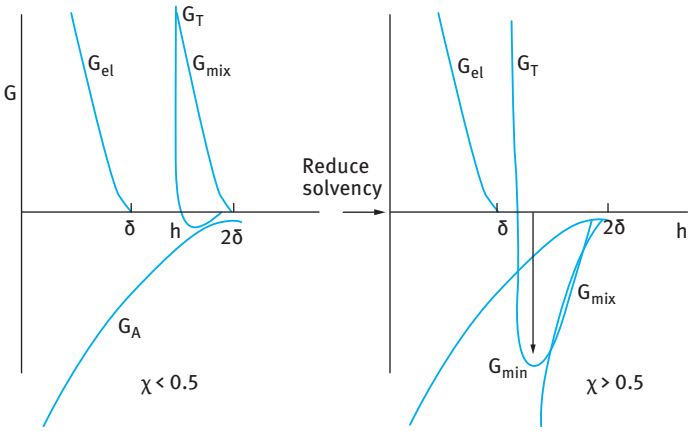

Fig. 14.4: Influence of reduction in solvency on the energy–distance curves.

In passing from the stability to the instability domain, ΔG_R must change sign, i.e. from being positive to being negative. It is convenient to split ΔG_R into its enthalpy and entropy contributions,

$$\Delta G_R = \Delta H_R - T\Delta S_R. \tag{14.3}$$

Thus the sign of ΔG_R will depend on the signs and relative magnitudes of ΔH_R and ΔS_R as summarized in Tab. 14.2.

Tab. 14.2: Types of steric stabilization.

ΔH_R	ΔS_R	$\Delta H_R / T\Delta S_R$	ΔG_R	Type	Flocculation
+	+	> 1	+	Enthalpic	On heating
–	–	< 1	+	Entropic	On cooling
+	–	≥	+	Combined	Not accessible
+	–	<	+	Enthalpic = Entropic	

As a result of extensive investigations on model sterically stabilized dispersions, it has been demonstrated that a strong correlation exists between the critical flocculation point and the θ-point of the stabilizing moieties in free solution. As mentioned before, the θ-point is that at which $\chi = 0.5$, i.e. the point at which the second virial coefficient of the polymer chain is equal to zero. The absolute methods for determining the θ-point include light scattering and osmotic pressure measurements. Less sound methods for determining the θ-point depend on establishing the phase diagrams of polymer solutions.

Using lattices with terminally-anchored polymer chains of various kinds, it has been established that the CFT is independent of the molar mass of the chain, the size of

the particle core and the nature of the disperse phase [12]. The CFT correlates strongly with the θ-temperature. Similar correlations have been found between the CFV and the θ-point [12]. However, such correlations are only obtained if the surface is fully covered by the polymer chains. Under conditions of incomplete coverage, flocculation occurs in dispersion media that are better than θ-solvents. This may be due to lateral movement of the stabilizer, desorption or even bridging flocculation (see below).

The correlation between the critical flocculation point and the θ-point implies that G_{mix} dominates the steric interaction. It has been argued that the contribution from G_{el} can be neglected until $h < \delta$, i.e. the polymer layer from one particle comes into direct contact with the second interface. With the high molar mass chains, the contribution from G_{A} to the total interaction is also negligible. This means that G_{T} is approximately equal to G_{mix} and it shows that χ is the main parameter controlling the stability. This is clearly illustrated in Fig. 14.4 which shows a significant value of G_{min} when $\chi > 0.5$.

Thus by measuring the θ-point (CFT or CFV) for the polymer chains (A) in the medium under investigation (which could be obtained from light scattering or viscosity measurements) one can establish the stability conditions for a dispersion, before its preparation. This procedure helps also in designing effective steric stabilizers such as block and graft copolymers.

14.4 Depletion flocculation

Depletion flocculation is produced by addition of "free" nonadsorbing polymer [16]. In this case, the polymer coils cannot approach the particles to a distance Δ (that is determined by the radius of gyration of free polymer R_{G}), since the reduction of entropy on close approach of the polymer coils is not compensated by an adsorption energy. The suspension particles will be surrounded by a depletion zone with thickness Δ. Above a critical volume fraction of the free polymer, ϕ_{p}^{+}, the polymer coils are "squeezed out" from between the particles and the depletion zones begin to interact. The interstices between the particles are now free from polymer coils and hence an osmotic pressure is exerted outside the particle surface (the osmotic pressure outside is higher than in between the particles) resulting in weak flocculation [16]. A schematic representation of depletion flocculation is shown in Fig. 14.5.

The magnitude of the depletion attraction free energy, G_{dep}, is proportional to the osmotic pressure of the polymer solution, which in turn is determined by ϕ_{p} and molecular weight M. The range of depletion attraction is proportional to the thickness of the depletion zone, Δ, which is roughly equal to the radius of gyration, R_{G}, of the free polymer. A simple expression for G_{dep} is [16],

$$G_{\text{dep}} = \frac{2\pi R\Delta^2}{V_1}(\mu_1 - \mu_1^0)\left(1 + \frac{2\Delta}{R}\right), \tag{14.4}$$

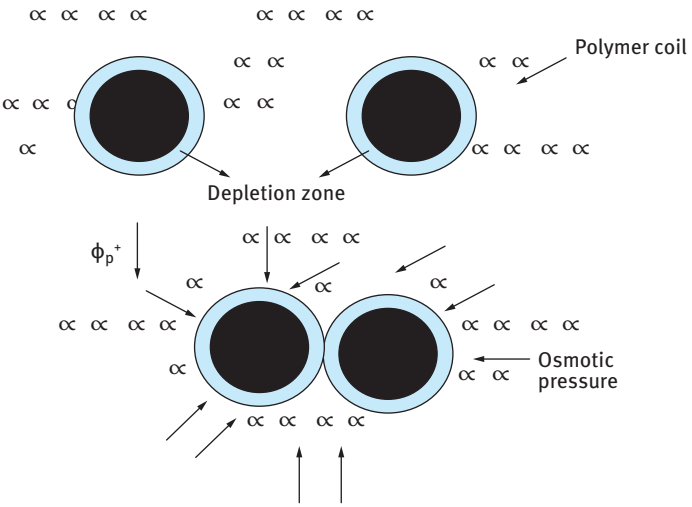

Fig. 14.5: Schematic representation of depletion flocculation.

where V_1 is the molar volume of the solvent, μ_1 is the chemical potential of the solvent in the presence of free polymer with volume fraction ϕ_p and μ_1^0 is the chemical potential of the solvent in the absence of free polymer. $(\mu_1 - \mu_1^0)$ is proportional to the osmotic pressure of the polymer solution.

14.5 Bridging flocculation by polymers and polyelectrolytes

Certain long chain polymers may adsorb in such a way that different segments of the same polymer chain are adsorbed on different particles, thus binding or "bridging" the particles together, despite the electrical repulsion [17, 18]. With polyelectrolytes of opposite charge to the particles, another possibility exists; the particle charge may be partly or completely neutralized by the adsorbed polyelectrolyte, thus reducing or eliminating the electrical repulsion and destabilizing the particles.

Effective flocculants are usually linear polymers, often of high molecular weight, which may be nonionic, anionic or cationic in character. Ionic polymers should be strictly referred to as polyelectrolytes. The most important properties are molecular weight and charge density. There are several polymeric flocculants that are based on natural products, e.g. starch and alginates, but the most commonly used flocculants are synthetic polymers and polyelectrolytes, e.g. polyacrylamide and copolymers of acrylamide and a suitable cationic monomer such as dimethylaminoethyl acrylate or methacrylate. Other synthetic polymeric flocculants are poly(vinyl alcohol), poly(ethylene oxide) (nonionic), sodium polystyrene sulphonate (anionic) and polyethyleneimine (cationic).

As mentioned above, bridging flocculation occurs because segments of a polymer chain adsorb simultaneously on different particles thus linking them together. Adsorption is an essential step and this requires favourable interaction between the polymer segments and the particles. Several types of interactions are responsible for adsorption that is irreversible in nature:

(i) Electrostatic interaction when a polyelectrolyte adsorbs on a surface bearing oppositely charged ionic groups, e.g. adsorption of a cationic polyelectrolyte on a negative oxide surface such as silica.
(ii) Hydrophobic bonding that is responsible for adsorption of nonpolar segments on a hydrophobic surface, e.g. partially hydrolysed poly(vinyl acetate) (PVA) on a hydrophobic surface such as polystyrene.
(iii) Hydrogen bonding, for example interaction of the amide group of polyacrylamide with hydroxyl groups on an oxide surface.
(iv) Ion binding, as is the case of adsorption of anionic polyacrylamide on a negatively charged surface in the presence of Ca^{2+}.

Effective bridging flocculation requires that the adsorbed polymer extends far enough from the particle surface to attach to other particles and that there is sufficient free surface available for adsorption of these segments of extended chains. When excess polymer is adsorbed, the particles can be restabilized, either because of surface saturation or by steric stabilization as discussed before. This is one explanation of the fact that an "optimum dosage" of flocculant is often found; at low concentration there is insufficient polymer to provide adequate links and with larger amounts restabilization may occur. A schematic picture of bridging flocculation and restabilization by adsorbed polymer is given in Fig. 14.6.

If the fraction of particle surface covered by polymer is θ, then the fraction of uncovered surface is $(1 - \theta)$ and the successful bridging encounters between the particles

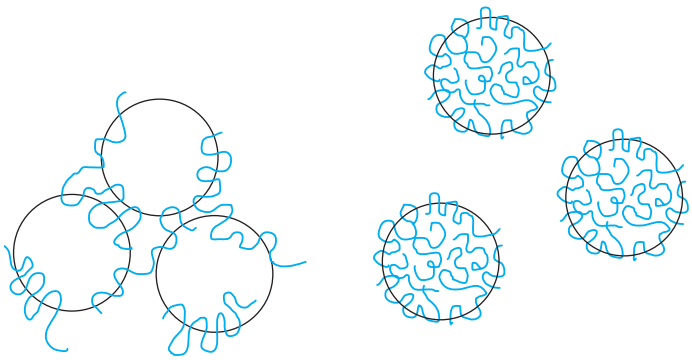

Fig. 14.6: Schematic illustration of bridging flocculation (left) and restabilization (right) by adsorbed polymer.

should be proportional to $\theta(1-\theta)$, which has its maximum when $\theta = 0.5$. This is the well-known condition of "half-surface coverage" that has been suggested as giving the optimum flocculation.

An important condition for bridging flocculation with charged particles is the role of electrolyte concentration. The latter determines the extension ("thickness") of the double layer which can reach values as high as 100 nm (in 10^{-5} mol dm^{-5} 1 : 1 electrolyte such as NaCl). For bridging flocculation to occur, the adsorbed polymer must extend far enough from the surface to a distance over which electrostatic repulsion occurs (> 100 nm in the above example).

This means that at low electrolyte concentrations quite high molecular weight polymers are needed for bridging to occur. As the ionic strength is increased, the range of electrical repulsion is reduced and lower molecular weight polymers should be effective.

In many practical applications, it has been found that the most effective flocculants are polyelectrolytes with a charge opposite to that of the particles. In aqueous media most particles are negatively charged, and cationic polyelectrolytes such as polyethyleneimine are often necessary. With oppositely charged polyelectrolytes it is likely that adsorption occurs to give a rather flat configuration of the adsorbed chain, due to the strong electrostatic attraction between the positive ionic groups on the polymer and the negative charged sites on the particle surface. This would probably reduce the probability of bridging contacts with other particles, especially with fairly low molecular weight polyelectrolytes with high charge density. However, the adsorption of a cationic polyelectrolyte on a negatively charged particle will reduce the surface charge of the latter, and this charge neutralization could be an important factor in destabilizing the particles. Another mechanism for destabilization has been suggested by Gregory [18] who proposed an "electrostatic patch" model. This applies to cases where the particles have a fairly low density of immobile charges and the polyelectrolyte has a fairly high charge density. Under these conditions, it is not physically possible for each surface site to be neutralized by a charged segment on the polymer chain, even though the particle may have sufficient adsorbed polyelectrolyte to achieve overall neutrality. There are then "patches" of excess positive charge, corresponding to the adsorbed polyelectrolyte chains (probably in a rather flat configuration), surrounded by areas of negative charge, representing the original particle surface. Particles which have this "patchy" or "mosaic" type of surface charge distribution may interact in such a way that the positive and negative "patches" come into contact, giving quite strong attraction (although not as strong as in the case of bridging flocculation). A schematic illustration of this type of interaction is given in Fig. 14.7. The electrostatic patch concept (which can be regarded as another form of "bridging") can explain a number of features of flocculation of negatively charged particles with positive polyelectrolytes. These include the rather small effect of increasing the molecular weight and the effect of ionic strength on the breadth of the flocculation dosage range and the rate of flocculation at optimum dosage.

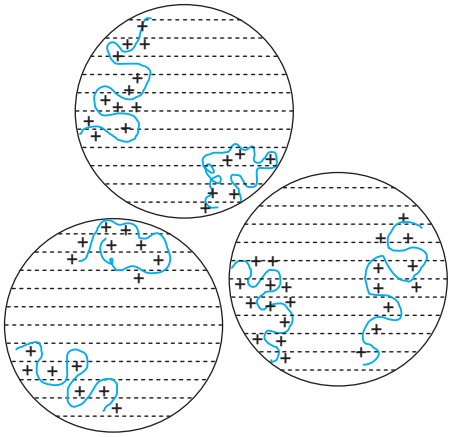

Fig. 14.7: "Electrostatic patch" model for the interaction of negatively charged particles with adsorbed cationic polyelectrolytes.

References

[1] Tadros T. Interfacial phenomena and colloid stability, Vol. 1. Berlin: De Gruyter; 2015.
[2] Tadros T. Formulation of disperse systems. Weinheim: Wiley-VCH; 2004.
[3] Tadros T. Applied surfactants. Weinheim: Wiley-VCH; 2005.
[4] Garvey MJ, Tadros TF, Vincent B. J Colloid Interface Sci. 1974;49:57.
[5] Garvey MJ, Tadros TF, Vincent B. J Colloid Interface Sci. 1976;55:440.
[6] Hesselink FT, Vrij A, Overbeek JTG. J Phys Chem. 1971;75:2094.
[7] Tadros TF. Advances Colloid and Interface Science. 1980;12:141.
[8] Tadros T. Rheology of Dispersions. Weinheim: Wiley-VCH; 2010.
[9] Tadros T. Colloids in paints. Weinheim: Wiley-VCH; 2010.
[10] Napper DH. Polymeric stabilisation of colloidal dispersions. London: Academic Press; 1983.
[11] Napper DH. Trans Faraday Soc. 1968;64:1701; J Colloid Sci. 1969;29:168.
[12] Napper DH. Kolloid Z, Z Polym. 1969;234:1149.
[13] Napper DH. Ind Eng Chem Prod Res Develop. 1970;9:467.
[14] Napper DH, Netschey A. J Colloid Interface Sci. 1971;37:528.
[15] Napper DH. J Colloid Interface Sci. 1977;58:390.
[16] Asakura A, Oosawa F. J Chem Phys. 1954;22:1235; J Polymer Sci. 1958;93:183.
[17] Gregory J. In: Tadros T, editor. Solid/liquid dispersions. London: Academic Press; 1987.
[18] Gregory J. Flocculation fundamentals. In: Tadros T, editor. Encyclopedia of colloid and interface science. Berlin: Springer; 2013.

Index